

UNCLASSIFIED

AD 298 671

*Reproduced
by the*

ARMED SERVICES TECHNICAL INFORMATION AGENCY
ARLINGTON HALL STATION
ARLINGTON 12, VIRGINIA



UNCLASSIFIED

NOTICE: When government or other drawings, specifications or other data are used for any purpose other than in connection with a definitely related government procurement operation, the U. S. Government thereby incurs no responsibility, nor any obligation whatsoever; and the fact that the Government may have formulated, furnished, or in any way supplied the said drawings, specifications, or other data is not to be regarded by implication or otherwise as in any manner licensing the holder or any other person or corporation, or conveying any rights or permission to manufacture, use or sell any patented invention that may in any way be related thereto.

298 671



THERMAL EFFECTS OF SHOCKWAVE
TURBULENT BOUNDARY LAYER INTERACTION AT
MACH NUMBERS 3 AND 5

12 November 1962

PREPARED BY

Victor Levin

V. Levin
Research Specialist
Fluid Dynamics &
Thermodynamics

Thomas J. Fabish

T. J. Fabish
Engineer
Fluid Dynamics &
Thermodynamics

APPROVED BY

P. L. Marshall

P. L. Marshall
Engineering Chief
Flight Sciences Research

R. M. Crone

R. M. Crone
Engineering Manager
Flight Sciences &
Systems Research

NORTH AMERICAN AVIATION , INC.

**COLUMBUS DIVISION
COLUMBUS 16, OHIO**

NA 62H-795

FOREWORD

The research reported herein was performed by the Flight Sciences and Systems Research Department, North American Aviation, Inc., Columbus, Ohio, for the Department of the Navy, Bureau of Naval Weapons, RAAD-34, under Contract N0w 61-0679-c. Mr. K. K. Skirpa of the Airframe Design Branch was the Bureau of Naval Weapons Project Engineer.

Acknowledgement is given to Mr. F. E. Whitesel and Mr. L. R. Alexander, who were the Contractor's representatives for the wind tunnel program, and Miss K. V. Layfield, who prepared the graphs and performed the numerical calculations. In addition, credit should be given to Mr. P. H. Davison, who read the manuscript and gave the authors many helpful suggestions.

ABSTRACT

A wind tunnel investigation was made at Mach numbers 3 and 5 of the heat transfer and pressure distribution on a flat plate in a region where an oblique shockwave impinges upon and interacts with a turbulent boundary layer. The strength of the shockwave was varied so that interaction regions both with and without separation were studied. Plots of the ratio of the local Stanton number through the interaction region to the zero pressure gradient Stanton number gave qualitatively similar distributions for both Mach numbers and all shock strengths. The data from the present tests plus the results of experiments reported in the literature were employed in the construction of a method which predicts the heat transfer distribution in an incident shockwave turbulent boundary layer interaction region over a fairly wide range of free-stream conditions.

SUMMARY

A wind tunnel investigation was made of the isothermal wall heat transfer rates and static pressure distributions associated with the interaction of an oblique shockwave with a turbulent boundary layer on a flat plate. The tests were conducted at nominal Mach numbers of 3 and 5 and free-stream Reynolds numbers per foot of 7.4×10^6 and 3.6×10^6 , respectively. All measurements were made on a flat test plate which contained instrumentation for determining heat transfer rates, wall temperature, and static pressure distribution.. In addition, two boundary layer probes were permanently installed on the test plate at separate stations. At Mach 3 natural transition of the test plate boundary layer occurred upstream of the area instrumented for heat transfer measurements. A system of injecting air into the boundary layer near the leading edge of the test plate was employed to thicken the boundary layer at Mach 3. At Mach 5 it was found necessary to employ both grit and air injection into the boundary layer in order to obtain turbulent flow upstream of the heat transfer instrumentation. Blowing an additional amount of air into the boundary layer above the minimum amount required to insure turbulence did not appreciably thicken the boundary layer at Mach 5.

The oblique shockwave which impinged upon the test plate was generated by a deflected flat plate placed above the test plate. The angle of the shock generator plate with respect to the wind tunnel centerline, α , could be varied from 0° to 15° . At both Mach 3 and 5 tunnel choking occurred at α somewhat greater than 12.0° .

Both the test plate and the shock generator plate spanned the wind tunnel test section. Observations of the streamline pattern on the test plate with flow paint indicated that the flow field was two-dimensional in the region in which heat transfer and pressure measurements were made.

The length, Δx , of the oblique shockwave turbulent boundary interaction region was determined from the static pressure distribution. It was found that the rise in the isothermal heat transfer coefficient, h_T , from the upstream undisturbed value, h_1 , to a peak value, h_2 , occurred well within the pressure interaction region and covered a length of approximately $0.60 \Delta x$. The decay in heat transfer coefficient downstream of the peak value was fairly slow when the aft end of the test plate was not unduly disturbed by the expansion from the trailing edge of the shock generator plate.

NORTH AMERICAN AVIATION , INC.

COLUMBUS DIVISION
COLUMBUS 16, OHIO

NA 62H-795

Attempts at correlating the data were made using the local Stanton number, St_e , and the transformed momentum thickness Θ_e as defined by Reshotko and Tucker in NACA TN 4154.

Plots of the Stanton number ratio, St_e/St_∞ , (subscript e refers to local conditions and ∞ to upstream undisturbed conditions) in terms of a non-dimensional length parameter revealed that an approximate similarity existed among all of the shockwave turbulent boundary layer data obtained in the present study. Results of other published experiments concerned with considerably different models, but still involving the interaction of a turbulent boundary layer with a shockwave, revealed distributions of St_e/St_∞ which were qualitatively similar to the present tests. All the suitable available data were used to derive a tentative relationship between the peak value of the Stanton number ratio and the static pressure ratio across an interaction region. This relationship was employed in the construction of a calculation design procedure which covers a fairly wide range of free-stream conditions.

Another correlation appeared feasible which involved the transformed momentum thickness ratio across the heat transfer interaction region. The values of the ratio fall into roughly three groups characterized by attached, incipient, and separated flow conditions. The correlation indicated that the Reynolds analogy factor decreases across the interaction region. This is in qualitative agreement with the observed decrease in the local recovery factor across the interaction.

A correlation of the pressure interaction length indicated that whenever air injection thickened the boundary layer, the results were equivalent to a boundary layer thickened by an extension of the boundary layer run. The heat transfer measurements were practically insensitive to air injection.

NORTH AMERICAN AVIATION , INC.COLUMBUS DIVISION
COLUMBUS 16, OHIO

NA 62H-795

TABLE OF CONTENTS

	<u>Page</u>
ABSTRACT	ii
SUMMARY	iii
LIST OF TABLES	vii
LIST OF FIGURES	viii
I INTRODUCTION	1
II EXPERIMENTAL PROGRAM	3
A. Experimental Apparatus	3
B. Experimental Program and Data Reduction	5
III EXPERIMENTAL RESULTS	11
A. Mach 3.0 Data	11
1. Static Pressure on the Test Plate	11
2. Boundary Layer Rakes	13
3. Heat Transfer Coefficient	13
4. Recovery Factor	15
B. Mach 5.0 Data	17
1. Static Pressures on the Test Plate	18
2. Boundary Layer Rakes	20
3. Heat Transfer Coefficient	20
4. Recovery Factor	21
IV DISCUSSION AND CORRELATION OF DATA	24
A. Effect of Boundary Layer Trips on Correlation of Pressure Interaction Length	24
B. Stanton Number Ratio Distribution	26
C. Momentum Thickness and Heat Transfer Comparisons for No Interaction	35
D. Correlation of Transformed Momentum Thickness Across the Interaction Region	38
V DESIGN PROCEDURE	43

NORTH AMERICAN AVIATION , INC.

**COLUMBUS DIVISION
COLUMBUS 16, OHIO**

NA 62H-795

	<u>Page</u>
VI	
CONCLUDING REMARKS	48
A. Review of Significant Results	48
B. Recommendations for Further Study	51
VII	
NOTATION	53
VIII	
REFERENCES	56
APPENDIX A	59

NORTH AMERICAN AVIATION , INC.

COLUMBUS DIVISION
COLUMBUS 16, OHIO

NA 62H-795

LIST OF TABLES

<u>Table No.</u>	<u>Title</u>	<u>Page</u>
I	List of Data Runs and Run Parameters	62
II	Data Used in the Interaction Lengths and Transformed Momentum Thickness Correlations	63
III	Comparison of Measured and Theoretical Values of θ_a and h_T	68

LIST OF FIGURES

<u>Figure No.</u>	<u>Title</u>	<u>Page</u>
1	Model Installation Diagram	69
2	Schematic of Heat Transfer Test Plate	70
3	Schematic of Boundary Layer Rake	71
4	Nichrome Element Diagram	72
5	Typical Heater Element Circuit	73
6	Nichrome Heater Element Arrangement at Mach 3.0	74
7	Nichrome Heater Element Arrangement at Mach 5.0	75
8	Test Plate and Shock Generator Mounted on Steel Plate Which Replaces Tunnel Schlieren Window	76
9	Test Plate Inserted in Wind Tunnel	77
10	Schlieren Photograph of Flow on Test Plate at $M_o = 2.95$ Employing a Boundary Layer Blowing Ratio, P_{re}/P_o , of 2.0 With the Shock Generator Plate Removed	78
11	Schlieren Photograph of Flow on Test Plate at $M_o = 2.95$ Employing a Boundary Layer Blowing Ratio, P_{re}/P_o , of 5.9 for a Shock Generator Plate Angle of 0°	79
12	Schlieren Photograph of Flow on Test Plate at $M_o = 2.95$ With No Boundary Layer Blowing For A Shock Generator Plate Angle of 6.0°	80
13	Schlieren Photograph of Flow on Test Plate at $M_o = 2.95$ With No Boundary Layer Blowing For A Shock Generator Plate Angle of 9.5°	81
14	Schlieren Photograph of Flow on Test Plate at $M_o = 2.95$ Employing a Boundary Layer Blowing Ratio, P_{re}/P_o , of 2.0 for a Shock Generator Plate Angle of 12.0°	82
15	Schlieren Photograph of Flow on Test Plate at $M_o = 5.02$ Employing a Boundary Layer Blowing Ratio, P_{re}/P_o , of 4.9 for a Shock Generator Plate Angle of 12.0°	83
16	Method of Obtaining Heat Transfer Coefficient and Recovery Temperature From Corrected Heat Flow Rates and Nichrome Temperature	84
17	Static Pressure Distribution on the Test Plate at $M_o = 2.95$ With No Boundary Layer Blowing for Four Values of the Shock Generator Plate Angle, α	85

<u>Figure No.</u>	<u>Title</u>	<u>Page</u>
18	Static Pressure Distribution on the Test Plate at $M_o = 2.95$ With Boundary Layer Blowing For Four Values of the Shock Generator Plate Angle, α	86
19	Effect of Boundary Layer Blowing on the Static Pressure Distribution at $M_o = 2.95$ for a Shock Generator Plate Angle of 12°	87
20	Boundary Layer Profiles at $M_o = 2.95$	88
21	Boundary Layer Profiles at $M_o = 2.95$	89
22	Heat Transfer Coefficient Distribution on the Test Plate at $M_o = 2.95$ With No Boundary Layer Blowing and With Shock Generator Plate Removed	90
23	Heat Transfer Coefficient Distribution on the Test Plate at $M_o = 2.95$ With A Blowing Ratio of 2.0 and With Shock Generator Plate Removed	91
24	Heat Transfer Coefficient Distribution on the Test Plate at $M_o = 2.95$ With No Boundary Layer Blowing for a Shock Generator Plate Angle of 0° ...	92
25	Heat Transfer Coefficient Distribution on the Test Plate at $M_o = 2.95$ With A Blowing Ratio of 5.9 for a Shock Generator Plate Angle of 0°	93
26	Heat Transfer Coefficient Distribution on the Test Plate at $M_o = 2.95$ With No Boundary Layer Blowing for a Shock Generator Plate Angle of 6° ...	94
27	Heat Transfer Coefficient Distribution on the Test Plate at $M_o = 2.95$ With A Blowing Ratio of 5.9 for a Shock Generator Plate Angle of 6°	95
28	Heat Transfer Coefficient Distribution on the Test Plate at $M_o = 2.95$ With No Boundary Layer Blowing for a Shock Generator Plate Angle of 9.5° .	96
29	Heat Transfer Coefficient Distribution on the Test Plate at $M_o = 2.95$ With A Blowing Ratio of 5.9 for a Shock Generator Plate Angle of 9.5° ..	97
30	Heat Transfer Coefficient Distribution on the Test Plate at $M_o = 2.95$ With No Boundary Layer Blowing for a Shock Generator Plate Angle of 12° ..	98
31	Heat Transfer Coefficient Distribution on the Test Plate at $M_o = 2.95$ With A Blowing Ratio of 2.0 for a Shock Generator Plate Angle of 12°	99
32	Heat Transfer Coefficient Distribution on the Test Plate at $M_o = 2.95$ With A Blowing Ratio of 5.9 for a Shock Generator Plate Angle of 12° ...	100

NORTH AMERICAN AVIATION , INC.

COLUMBUS DIVISION
COLUMBUS 16, OHIO

NA 62H-795

<u>Figure No.</u>	<u>Title</u>	<u>Page</u>
33	Effect of Boundary Layer Blowing on the Heat Transfer Coefficient Distribution at $M_o = 2.95$ for a Shock Generator Plate Angle of 12°	101
34	Recovery Factor Distribution at $M_o = 2.95$ For Various Blowing Ratios With A Shock Generator Plate Angle of 0°	102
35	Distribution of Effective Recovery Factor at $M_o = 2.95$ With The Shock Generator Plate Removed	103
36	Distribution of Effective Recovery Factor at $M_o = 2.95$ for a Shock Generator Plate Angle of 0°	104
37	Comparison of Recovery Factor (η) and Effective Recovery Factor (η_e) at $M_o = 2.95$ With and Without Boundary Layer Blowing for a Shock Generator Plate Angle of 0°	105
38	Distribution of Effective Recovery Factor at $M_o = 2.95$ for Shock Generator Plate Angle of 6°	106
39	Distribution of Effective Recovery Factor at $M_o = 2.95$ for a Shock Generator Plate Angle of 9.5°	107
40	Distribution of Effective Recovery Factor at $M_o = 2.95$ for a Shock Generator Plate Angle of 12°	108
41	Static Pressure Distribution on the Test Plate at $M_o = 5.02$ with Approximately the Same Degree of Boundary Layer Blowing for Five Values of the Shock Generator Plate Angle, α	109
42	Static Pressure Distribution at $M_o = 5.02$ for Values of the Blowing Ratio and Shock Generator Plate Angle, α	110
43	Effect of Boundary Blowing on the Static Pressure Distribution at $M_o = 5.02$ for a Shock Generator Plate Angle of 11°	111
44	Boundary Layer Profiles at $M_o = 5.02$	112
45	Boundary Layer Profiles at $M_o = 5.02$	113
46	Boundary Layer Profiles at $M_o = 5.02$	114
47	Heat Transfer Coefficient Distribution on the Test Plate at $M_o = 5.02$ With a Blowing Ratio of 3.9 and With Shock Generator Plate Removed	115

NORTH AMERICAN AVIATION, INC.

COLUMBUS DIVISION
COLUMBUS 10, OHIO

NA 62H-795

<u>Figure No.</u>	<u>Title</u>	<u>Page</u>
48	Heat Transfer Coefficient Distribution on the Test Plate at $M_o = 5.02$ With a Blowing Ratio of 3.8 for a Shock Generator Plate Angle of 0°	116
49	Heat Transfer Coefficient Distribution on the Test Plate at $M_o = 5.02$ With a Blowing Ratio of 4.2 for a Shock Generator Plate Angle of 0°	117
50	Heat Transfer Coefficient Distribution on the Test Plate at $M_o = 5.02$ With a Blowing Ratio of 4.1 for a Shock Generator Plate Angle of 7.4°	118
51	Heat Transfer Coefficient Distribution on the Test Plate at $M_o = 5.02$ With a Blowing Ratio of 3.8 for a Shock Generator Plate Angle of 9.7°	119
52	Heat Transfer Coefficient Distribution on the Test Plate at $M_o = 5.02$ With a Blowing Ratio of 8.4 for a Shock Generator Plate Angle of 9.7°	120
53	Heat Transfer Coefficient Distribution on the Test Plate at $M_o = 5.02$ With a Blowing Ratio of 4.1 for a Shock Generator Plate Angle of 11°	121
54	Heat Transfer Coefficient Distribution on the Test Plate at $M_o = 5.02$ With a Blowing Ratio of 7.0 for a Shock Generator Plate Angle of 11°	122
55	Heat Transfer Coefficient Distribution on the Test Plate at $M_o = 5.02$ With a Blowing Ratio of 9.5 for a Shock Generator Plate Angle of 11°	123
56	Heat Transfer Coefficient Distribution on the Test Plate at $M_o = 5.02$ With a Blowing Ratio of 4.9 for a Shock Generator Plate Angle of 12°	124
57	Heat Transfer Coefficient Distribution on the Test Plate at $M_o = 5.02$ With a Blowing Ratio of 9.6 for a Shock Generator Plate Angle of 12°	125
58	Heat Transfer Coefficient Distribution on the Test Plate at $M_o = 5.02$ With No Boundary Layer Blowing for a Shock Generator Plate Angle of 10°	126

NORTH AMERICAN AVIATION , INC.

COLUMBUS DIVISION
COLUMBUS 14, OHIO

NA 62H-795

<u>Figure No.</u>	<u>Title</u>	<u>Page</u>
59	Heat Transfer Coefficient Distribution on the Test Plate at $M_o = 5.02$ With No Boundary Layer Blowing for a Shock Generator Plate Angle of 11° .	127
60	Effect of Boundary Layer Blowing on the Heat Transfer Coefficient Distribution at $M_o = 5.02$ for a Shock Generator Plate Angle of 11°	128
61	Recovery Factor Distribution at $M_o = 5.02$ for A Shock Generator Plate Angle of 0°	129
62	Recovery Factor Distribution at $M_o = 5.02$ for Shock Generator Plate Angles of 7.4° and 10°	130
63	Recovery Factor Distribution at $M_o = 5.02$ for A Shock Generator Plate Angle of 12°	131
64	Distribution of Effective Recovery Factor at $M_o = 5.02$ for a Shock Generator Plate Angle of 0° and Also With the Plate Removed	132
65	Distribution of Effective Recovery Factor at $M_o = 5.02$ for a Shock Generator Plate Angle of 7.4°	133
66	Distribution of Effective Recovery Factor at $M_o = 5.02$ for a Shock Generator Plate Angle of Approximately 10°	134
67	Distribution of Effective Recovery Factor at $M_o = 5.02$ for a Shock Generator Plate Angle of 11°	135
68	Distribution of Effective Recovery Factor at $M_o = 5.02$ for a Shock Generator Plate Angle of 12°	136
69	Comparison of Recovery Factor (η) and Effective Recovery Factor (η_e) at $M_o = 5.02$ with Moderate Boundary Layer Blowing for a Shock Generator Plate Angle of 12°	137
70	Qualitative Effect of Shockwave Boundary Layer Interaction on Recovery Factor Distribution At $M_o = 5.02$	138
71	Correlation of Interaction Length Which Indicates A Distinction Between Forced and Natural Transition	139
72	Correlation of Interaction Length Which Indicates A Distinction Among Two Types of Forced Transition and Natural Transition	140
73	Pressure Distributions from Reference (1), Appendix III, For Those Data Runs Which Were Used in This Report	141

NORTH AMERICAN AVIATION , INC.

COLUMBUS DIVISION
COLUMBUS 16, OHIO

NA 62H-795

<u>Figure No.</u>	<u>Title</u>	<u>Page</u>
74	Pressure Distributions From Reference (1), Appendix III, For Those Data Runs Which Were Used in this Report	142
75	Mach Number, Mass Flow Ratio and Shock Generator Plate Angle Versus Static Pressure Ratio Across A Reflected Shock For Two-Dimensional Inviscid Flow With An Upstream Mach Number of 2.98	143
76	Mach Number, Mass Flow Ratio and Shock Generator Plate Angle Versus Static Pressure Ratio Across A Reflected Shock For Two-Dimensional Inviscid Flow With An Upstream Mach Number of 4.77	144
77	Effect of the Shockwave Boundary Layer Interaction on the Local Stanton Number Ratio at $M_o = 2.95$ With No Boundary Layer Blowing	145
78	Effect of the Shockwave Boundary Layer Interaction on the Local Stanton Number Ratio at $M_o = 2.95$ With Boundary Layer Blowing	146
79	Effect of the Shockwave Boundary Layer Interaction on the Local Stanton Number Ratio at $M_o = 5.02$ For Boundary Layer Blowing Ratios From 3.9 to 4.9	147
80	Effect of the Shockwave Boundary Layer Interaction on the Local Stanton Number Ratio at $M_o = 5.02$ For Boundary Layer Blowing Ratios From 7.0 to 9.6	148
81	Overall Variation of Stanton Number Ratio Obtained in the Present Tests	149
82	Stanton Number Ratio Distribution Found in Other Two-Dimensional Turbulent Flow Investigations	150
83	Inviscid Static Pressure Ratio Across a Reflected Shock	151
84	Effect of Shockwave Boundary Layer Interaction at $M_o = 2.95$ on Local Recovery Factor	152
85	Effect of Shockwave Boundary Layer Interaction at $M_o = 5.02$ on Local Recovery Factor	153
86	Stagnation Pressure Ratio and Static Temperature Ratio Versus Static Pressure Ratio Across a Reflected Shock for Two-Dimensional Inviscid Flow With An Upstream Mach Number of 2.98	154
87	Stagnation Pressure Ratio and Static Temperature Ratio Versus Static Pressure Ratio Across a Reflected Shock for Two-Dimensional Inviscid Flow with an Upstream Mach Number of 4.77	155

NORTH AMERICAN AVIATION , INC.

COLUMBUS DIVISION
COLUMBUS 16, OHIO

NA 62H-795

<u>Figure No.</u>	<u>Title</u>	<u>Page</u>
88	Variation of the Transformed Momentum Thickness Ratio (Θ_A at Peak Heat Transfer Location to Θ_A at the Beginning of the Pressure Interaction) With Mach Number	156
89	Pressure Ratio Across A Reflected Shock Pattern as a Function of the Initial Flow Deflection Angle ...	157
90	Correlation of Pressure Interaction Length to be Used in Design Procedure if Method of Inducing Transition is Known	158
91	Correlation of Pressure Interaction Length to be Used in Design Procedure if Method of Inducing Transition is not Known	159
92	Correlation of Location of Beginning of Pressure Interaction Region in Terms of Known Parameters ...	160
93	Inviscid Mass Flow Ratio Across a Reflected Shock ...	161
94	Distribution of Heat Transfer Coefficient Employed in Design Procedure	162
95	Suggested Variation in Stanton Number Downstream of End of Pressure Interaction	163
96	Comparison of Experimental Heat Transfer Coefficient Distribution with that Calculated According to the Design Procedure	164

I. INTRODUCTION

On a vehicle traveling at supersonic speeds there will usually be found one or more shockwaves which impinge upon or emanate from a region in which a boundary layer has developed. In cases of supersonic air-breathing propulsion systems the occurrence of shockwave impingement on the inlet diffuser boundary layer is unavoidable. The interaction of a shockwave with a boundary layer will modify both the viscous and inviscid flow field. Inviscid shockwave theory specifies a step function pressure distribution across the shock front. However, experimental evidence shows that the rise in pressure across the shockwave is obtained over a finite length in the region of interaction with the boundary layer. Of greater significance are the results of a few tests which indicate that the heat transfer rates in the aft portion of the interaction are higher than would be computed from undisturbed local flow conditions. Since the temperatures encountered at flight speeds in excess of Mach 3 may seriously affect a vehicle's structural integrity it is clear that an accurate prediction of heat transfer rates in an area influenced by shockwave boundary layer interaction is important.

Of course, the interaction of a shockwave with a boundary layer is a highly complex phenomenon. No theory has been devised, even for restricted conditions, which correctly predicts the effect of the interaction on all of the fluid mechanical properties. Therefore, the necessity of obtaining experimental data in this field is obvious. It was found by Chapman (Reference 9) and others that it is meaningful to divide all shockwave boundary interactions into three basic types, viz., (1) the boundary layer is laminar throughout the interaction, (2) the boundary layer is laminar at the beginning of the interaction but transition occurs before the end of the interaction, and (3) the boundary layer is turbulent upstream of the interaction and remains turbulent throughout the interaction. The present study is primarily concerned with the heat transfer rates associated with the third type of interaction. Unfortunately, almost all of the shockwave turbulent boundary layer interaction experiments found in the literature in which a useful range of parameters were tested contain only pressure measurement data (e.g. see References 1, 2 and 9). The limited amount of available experimental heat transfer data which pertains to the present problem falls into two classes. First, the tests were made on specific vehicle configurations, with the resulting flow field so complex, that analysis or correlations with basic variables is virtually impossible. In the second class of experiments, tests

NORTH AMERICAN AVIATION , INC.

COLUMBUS DIVISION
COLUMBUS 16, OHIO

NA 62H-795

have been made in a two-dimensional flow field, but with only one Mach number and one or two shock strengths so that although the flow field can be defined the data range is insufficient for correlation. In this latter category are the experiments described in References (12), (15), (16) and (17). In these tests the shockwave is generated by the surface along which the boundary layer has developed. No case was found in which the heat transfer data were obtained in the region of an oblique shockwave impinging upon a turbulent boundary layer.

The present tests were conducted in order to partially fill the considerably large gap in knowledge concerning the experimental heat transfer associated with shockwave turbulent boundary layer interaction. In particular, a two-dimensional experimental heat transfer investigation was made at Mach numbers 3 and 5 on a flat plate with a turbulent boundary layer and with an impinging oblique shockwave of variable strength. An attempt was made to increase the boundary layer thickness utilizing an air injection system. A sufficient amount of data was sought so that the heat transfer rates could be predicted in the interaction region over a useful Mach number and Reynolds number range.

II. EXPERIMENTAL PROGRAM

A. EXPERIMENTAL APPARATUS

The model was designed to provide the following:

- (a) Two-dimensional flow on a plane surface (the heat transfer test plate).
- (b) An oblique shock of variable strength impinging on the boundary layer on the test plate.
- (c) A boundary layer on the test plate which becomes turbulent upstream of the influence of the impinging shock.
- (d) Instrumentation on the test plate for determining both the heat transfer coefficient and the static pressure distribution in the shockwave boundary layer interaction region and the boundary layer velocity profiles upstream and downstream of the interaction.

Schematics of the model and certain details of the instrumentation are shown in Figures 1 through 7. Photographs of the model are shown in Figures 8 and 9.

The results of the experiments described in References (1) and (2) indicate that two-dimensional flow and shock systems can be obtained only if the test plate and the shock generator plate are essentially free of aspect ratio effects. In the present case this was accomplished by designing the model so that it completely spanned the tunnel test section. Both the test plate and the shock generator plate were supported from circular steel plates which replaced the existing Schlieren windows in the tunnel (Figure 1). The test plate attitude could be adjusted within the limits of $\pm 2^\circ$ in order to permit alignment with the free stream. The shock generator plate attitude could be varied from 0° to 15° . The generator plate had a different pivot point for each free-stream Mach number which allowed the shock to impinge approximately 11.75" from the leading edge of the test plate (i.e., the window centerline) for generator plate angles from 0 to 12° . Angles above 12° caused tunnel choking.

The test plate was provided with a boundary layer air injection system which was used for either thickening an already turbulent boundary layer or helping to induce full turbulence in a transitional boundary layer. The air injection system (see Figure 2) consisted of a row of holes 2.58 inches downstream of the leading edge of the test plate, a plenum chamber underneath the plate, and the necessary plumbing and control valves to provide a controllable amount of airflow injected normal to the free-stream airflow. For the Mach 5.0 run a $\frac{1}{4}$ " wide fixed transition strip of .033" grit was located 1.5" (model station 1.5) from the leading edge of the test plate.

The static pressure distribution on the test plate was measured with a row of twenty-three, .051" inside diameter, flush, pressure taps located 2.5" off the model centerline and placed $\frac{1}{2}$ " apart with the first tap located at model station 3.5 (see Figure 4). Pitot rakes were permanently installed to measure the boundary layer velocity profiles at model stations 9.0 and 15.0. Pressure measurements were made in the boundary layer air injection system to permit duplication of blowing rates. One pressure was measured in the air supply tube between a needle valve and a restrictor located outside of the tunnel. A second pressure, P_c , was measured in the plenum chamber under the leading edge of the test plate.

The heat transfer instrumentation on the test plate is similar to that used in References (3) and (4). A single heat transfer gage consists of a nichrome ribbon heating element cemented to an insulating surface (melamine fiber glass composite) plus a thermocouple which measures the element temperature. The thermocouple was inserted in the fiber glass approximately .003" below the center of the element. Since fiber glass is an electrical as well as a thermal insulating plastic, the thermocouple was electrically isolated from the nichrome ribbon. The electrical current flow path in the heating elements was made by milling slots (.002" to .003" wide) in the metal as shown in Figure 2. Originally the slots were filled with Krylon in order to obtain a smooth surface. During the initial phase of the wind tunnel tests, however, it was found that the Krylon was bubbling and peeling off. Attempts to use other insulating filler material had the same undesirable results. After a discussion with an experimenter who had tested a similar heat transfer model, it was concluded that the thickness of the nichrome ribbon (about .002") would have a negligible effect on the results since this dimension represented less than 2% of the boundary layer thickness. Consequently, the slots were left unfilled for the remaining runs.

Figure 5 is a schematic of a typical heater element circuit. It is seen that a variable resistor was used to control the current

in the heater element. The current was supplied by a constant voltage, direct current power supply.

Spanwise heat loss from the transverse heater elements was minimized by guard heater elements located along the sides of the heat transfer area (see Figure 4). Four thermocouples were located on the back of the fiber glass slab to aid in determining the conductive heat loss through the fiber glass slab. Also, a thermocouple was inserted in the lower surface of the shock generator plate to measure the recovery temperature for use in calculating the radiation heat loss. In all, 38 heating elements including the guard elements and 35 thermocouples were installed on the test plate, with an additional thermocouple on the shock generator.

At least one Schlieren photograph was taken for each run employing the windows located in the steel plates which supported the model. These windows were only three inches in diameter and thus, only a small portion of the flow field could be viewed. Larger windows were not used because of various design considerations. The Schlieren system at the test facility was designed to employ a collimated light beam approximately 18 inches in diameter. Since the system was basically incompatible with the three inch window diameter, it is not too surprising that the photographs suffer from poor definition. Schlieren photographs at Mach 3.0 corresponding to each angle of the shock generator plate tested are shown in Figures 10 through 14. Only one photograph, Figure 15, taken at Mach 5.0 is shown. At Mach 5.0 almost all the interaction occurred upstream of the region viewed by the photographs.

B. EXPERIMENTAL PROGRAM AND DATA REDUCTION

The experimental program was conducted at the USN Missile and Astronautics Test Center, Point Mugu, California, in the time period from 7 May through 25 May 1962. The tests were conducted at free-stream Mach numbers of 2.95 and 5.02 (nominally 3.0 and 5.0) and at free-stream Reynolds numbers per foot of 7.4×10^6 and 3.6×10^6 , respectively. A summary of the test conditions at each Mach number is given in Table I.

The heat transfer measurements on the test plate were limited to 24 data channels by the equipment available at the test facility. That is, only the temperature and electrical power dissipation of 24 heater elements could be monitored for a given heat transfer test. The side guard heater elements had to be included in the 24 heater element limitation. Therefore, several preliminary

test runs were made at each Mach number in order to establish the shockwave boundary layer interaction length which in turn set a lower limit on the allowable length of the instrumented section to be used. The heater element patterns selected for Mach numbers 3 and 5 are shown in Figures 6 and 7, respectively. It may be noted by comparing Figures 6 and 7 with Figure 4 that some of the $\frac{1}{4}$ " wide nichrome ribbons are connected in series to operate effectively as a $\frac{1}{2}$ " wide element. Although the output of all thirty-six thermocouples were read into the data system for each data point, only selected thermocouples were used for heat transfer data reduction.

A heat transfer test run consisted of data points taken at three or four different temperatures with the shock strength and the condition of the boundary layer upstream of the interaction held constant. A data point was obtained by adjusting the current flow in each heater element (including the guard elements) so that all thermocouples used for monitoring the elements read essentially the same temperature. The heat transfer coefficient, h , measured by a given element was obtained by plotting the convective heat loss per unit area per second, $(Q/A)_c$, versus the temperature of the nichrome ribbon, T_N (see Figure 16). The slope of the straight line (determined by a least square fit) through these points yields the heat transfer coefficient through the relationship,

$$(Q/A)_c = h (T_N - T_R)$$

where, as shown in Figure 16, the effective recovery temperature, T_R , is defined as the intercept of the straight line on the $(Q/A)_c$ versus T_N plot with the line $(Q/A)_c = 0$. The values of $(Q/A)_c$ and T_N are the result of corrections to the actual measurements. The corrected convective heat loss is given as

$$\left(\frac{Q}{A}\right)_c = \frac{(\text{electrical power dissipated by the element}) - \left(\begin{array}{l} \text{power conducted} \\ \text{and radiated} \\ \text{away from the element} \end{array}\right)}{\text{planform area of the element}}$$

The heat loss by conduction was calculated by assuming a one-dimensional heat flow to the back of the fiber glass. The thermocouples beneath the guard elements indicated that this assumption was accurate. However, when a shock impinged on the test plate, at least one pair of side

guard elements was in a region of strongly varying heat transfer. With the aid of a digital computer program calculations were made of the spanwise heat loss from the heat transfer elements through the guard elements in a region of varying heat transfer. It was found that for the worst case at Mach 5 the conduction losses through the guard elements represented less than 4% of the heat input to a heat transfer element. At Mach 3 the effect would be even less significant. The radiation correction was obtained with the aid of the measured temperatures of the wind tunnel wall and shock generator plate and employed the following assumptions:

- (a) The emissivity of the nichrome ribbon was 0.7.
- (b) The view factor from a heater element to the shock generator plate was 0.87.
- (c) The view factor from a heater element to the wind tunnel walls was 0.13.

For the undisturbed flat plate the combination of conduction and radiation losses represented approximately 10% of the electrical energy dissipated in an element at Mach 3.0 and 40% at Mach 5.0.

Although the thermocouple employed for monitoring the temperature of a particular heater element was located only .003" beneath the element, it is not correct to equate the temperature of the element, T_w , with the thermocouple temperature, T . This is because of the large difference in thermal conductivity of the thermocouple as compared with the surrounding fiber glass and the resulting distortion of the heat flow field. An investigation was made employing a digital computer program to determine the value of T_w for a given value of T . It was found that T_w could be expressed approximately in the form $T_w = aT - bT_s$ where a and b are constants and T_s is the temperature recorded on the back of the fiber glass slab. The highest value of T used for most of the runs was about 160°F which yields a value of 165°F for T_w .

This test was conducted so that the heat transfer coefficients could be determined for the case of an isothermal wall. Thus, the effect of deviations from this ideal condition must be evaluated in order that proper corrections can be made to the experimental results. Within the area instrumented for heat transfer measurements and surrounded by heater guard elements, the variation in temperature was small enough so that, in general, no correction was necessary. However, since the heated portion of the test plate did not extend to the leading edge, an important correction had to be made due to

the step function rise in temperature and its consequential effect on the experimentally determined heat transfer rates. In Reference (5) the effect of a step-temperature distribution on the heat transfer coefficient for turbulent flow over a flat plate with zero pressure gradient is given as

$$\frac{h_{step}}{h_T} = \left[1 - K \left(\frac{L}{x} \right)^{\frac{4}{5} \frac{N+2}{N+1}} \right]^{-\frac{1}{N+2}}$$

where

h_{step} = heat transfer coefficient for step temperature distribution

h_T = heat transfer coefficient for a true isothermal wall

N = reciprocal of exponent in power law for boundary layer velocity profile

L = distance from leading edge of the plate to the temperature step

x = distance from leading edge

K is a function of L/x , Mach number, and T_w/T_{aw} ; however, for values of T_w/T_{aw} near unity (as in this test) a value of $K=1$ is correct. For the present experiments $N=7$ can be considered as a typical value valid for both the Mach 3 and 5 tests. For the case of shockwave boundary layer interaction the correction was assumed to be the same as for a flat plate with zero pressure gradient. Therefore, all the heat transfer data were corrected to isothermal wall conditions by the equation,

$$h_T = \left[1 - \left(\frac{L}{x} \right)^{\frac{2}{10}} \right]^{\frac{1}{4}} h_c$$

where h_c is the heat transfer coefficient with the corrections made for conduction, radiation, and thermocouple reading.

It is to be noted that at each Mach number almost all the runs were made at one of two values of the boundary layer air injection plenum chamber pressure ratio, P_{in}/P_{∞} . At Mach 3 the two values were $P_{in}/P_{\infty} = 1.0$ and 5.9 . $P_{in}/P_{\infty} = 1.0$, which corresponds to no boundary

layer blowing, was normally used at Mach 3 since the boundary layer was turbulent upstream of the heat transfer instrumentation. For $P_{in}/P_{\infty} > 6$ it was found that the boundary layer velocity profiles became distorted and thus blowing was producing an undesirable effect. Since the runs at $P_{in}/P_{\infty} = 5.9$ did not produce large changes in the static pressure and heat transfer distribution through an interaction region, just two exploratory runs at an intermediate value ($P_{in}/P_{\infty} = 2.0$) were made.

At Mach 5.0 it was necessary to employ boundary layer blowing, in addition to the $\frac{1}{4}$ " wide strip of grit, merely to insure turbulence in the boundary layer. The minimum value of P_{in}/P_{∞} which gave turbulent flow was approximately 3.5. It is to be noted that $P_{in}/P_{\infty} \approx 1.4$ corresponds to no boundary layer blowing at Mach 5 because the static pressure on the undisturbed test plate was about 1.4 times the tabulated free-stream pressure. For $P_{in}/P_{\infty} > 10.0$ the velocity profiles became distorted. In general, blowing had a smaller effect at Mach 5 than at Mach 3, therefore, almost all the turbulent data were obtained at blowing rates in the vicinity of the two allowable extremes of P_{in}/P_{∞} .

Several difficulties arose in interpreting the Mach 5 tabulated data. During the Mach 5 tests it was noticed that thermocouple #18 (see Figure 4) beneath the $\frac{1}{2}$ " heater element #13 (see Figure 7) recorded a temperature considerably lower than the thermocouples placed directly below the other nichrome elements. At the time, this anomaly was thought to be due to a malfunction in the thermocouple. It was not considered serious because another thermocouple (#17) was used to monitor the temperature of heater element #13. After the tests were completed, it was found that the thermocouple #18 had not malfunctioned. Upon disassembling the test plate instrumentation it was found that the $\frac{1}{4}$ " wide nichrome strip-placed directly above thermocouple #18 (this nichrome strip was the downstream half of the $\frac{1}{2}$ " element #13) was subjected to a partial electrical short. That is, a portion of the recorded electrical current found a path through the steel plate rather than through the nichrome strip. Calculations were made utilizing the recorded temperatures in the vicinity of the partial electrical short in order to obtain an

NORTH AMERICAN AVIATION , INC.

COLUMBUS DIVISION
COLUMBUS 16, OHIO

NA 62H-795

upper bound on its effect on the calculated heat transfer coefficients. It was found that a sizeable error in h_r due to the electrical short could have occurred only for heater elements #13 and #14. This error is no larger than 30% (and probably much less) for a zero pressure gradient. With $\alpha > 0^\circ$ elements #13 and #14 are in the interaction region, therefore, the error is not as significant, being less than 8% for $\alpha = 7.4^\circ$. Since the actual percentage correction cannot be determined and since conclusions drawn from the data are not seriously affected, h_r was not corrected for the error arising from the partial electrical short.

A further difficulty arose with respect to interpreting the Mach 5 data and by coincidence heater elements #13 and #14 were involved. The tabulated data from Pt. Mugu indicated that for $\alpha > 0^\circ$ the value of h_r measured with heater elements #13 and #14 (the center of each element is at model stations 12.75 and 13.75, respectively) was consistently about 50% higher than h_r measured with heater elements #12, #15, and #16. This "blip" in the distribution of the tabulated h_r could not be attributed to the expansion wave emanating from the trailing edge of the shock generator plate since the "blip" occurred even when the pressure distribution was relatively flat downstream of heater element #12. It is felt that the "blip" is not the result of anomalous behavior of the flow, but rather it is due to an error in the data reduction procedure. Specifically, the error consisted of assigning the measured electrical current in the guard elements #23 and #24 to #13 and #14 and vice versa. Whether the misarrangement was in the electrical connections to the data reduction system or was within the data reduction program itself is not known. Neither possibility can be checked since the model has been dismantled and the Pt. Mugu facilities have been closed. Nevertheless, self-consistency of the Mach 5 data strongly implied that the error actually occurred and the data were corrected with this in mind. Figures 47 through 60 which give the Mach 5 heat transfer coefficient distributions also contain the data points (flagged symbols) that are felt to be erroneous. These "incorrect" data are shown because, (1) they are contained in the original data reduction and tabulation made at Pt. Mugu and (2) it is not possible to assign a 100% certainty to the belief that the flagged data points are truly incorrect.

III. EXPERIMENTAL RESULTS

In this section the Mach 3.0 and Mach 5.0 data are presented separately. At each Mach number the most significant results are the distributions of static pressure on the test plate, corrected heat transfer coefficient, and recovery temperature. Also, the velocity profiles obtained at model stations 9.0 and 15.0 are shown. Although this report is only concerned with turbulent interactions (i.e., the boundary layer is turbulent upstream of the influence of the impinging shock), supplemental data are presented which were acquired during tests in which the boundary layer became turbulent in the interaction region.

A. MACH 3.0 DATA

A free-stream Mach number of 2.95 was calculated from the tunnel settling chamber pressure, P_t , and the pressure measured with a pitot tube placed below and forward of the test plate. The static taps on the test plate, however, indicated pressures somewhat less than the free-stream value in a region unaffected by the interaction. If the test plate static pressure is assumed to be the result of an isentropic expansion from free-stream conditions, then the Mach number in the undisturbed region over the test plate is 2.98. Thus, 2.98 is considered to be the free-stream Mach number of the shock-wave boundary layer interaction.

1. Static Pressures on the Test Plate

The static pressure distribution on the test plate for the various shock generator plate angles, α , and for the various boundary layer blowing ratios, P_0/ρ_0 , are shown in Figures 17 through 19. Noted on the graphs are three significant quantities, namely,

- (a) The point at which the shock would strike the boundary layer if there were no interaction.
(Determined graphically from scale drawings of the test apparatus.)

- (b) The point at which the expansion from the trailing edge of the shock generator plate impinges on the boundary layer downstream of the interaction. (Determined in same manner as (a)).
- (c) The inviscid pressure rise which results from a reflected shock generated by a wedge at angle α and upstream Mach number of 2.98.

In all cases the static pressure rose above the inviscid value and then appeared to decrease before the expansion from the aft end of the generator plate influenced the pressure. At $\alpha = 12^\circ$ the generator plate expansion impinged at $x = 15.3$ and, thus, may have affected the last two pressure taps. For $\alpha < 12^\circ$ the expansion impinged downstream of $x = 16$ and should not have influenced the pressure measurements. In similar experiments where an incident oblique shock interacted with a boundary layer, it was found that the pressure in the reattachment region will occasionally exceed the inviscid value. However, in the present case, the consistency and the size of the pressure "blip" implies that either a small, additional, unexplained compression and then expansion were generated somewhere in the flow field or else the reattaching flow overcompressed and then expanded to the proper downstream pressure. It may be noted that a small pressure "blip" occurred for $\alpha = 0^\circ$ in the region where a Mach line emanating from the leading edge of the shock generator plate struck the test plate boundary layer. This "blip" probably arose from either the pressure field associated with the slight bluntness of the leading edge of the shock generator plate (diameter $\approx .01$) or the pressure field generated above the generator plate which was then fed upstream through the sidewall boundary layer.

The generator plate angles $\alpha = 6^\circ$, 9.5° , and 12° were chosen to correspond to the conditions of fully attached flow, incipient separation, and separated flow, respectively. Incipient separation may be defined to occur, for increasing shock strength, at the value of α which corresponds to a change in the static pressure distribution from one with one inflection point to a distribution with three inflection points. Kuehn in Reference (6) developed this criterion. For the present tests the pressure taps were spaced $\frac{1}{2}$ " apart and did not yield a sufficient definition of the pressure distribution to determine the occurrence of incipient separation. However, the Schlieren photograph for $\alpha = 9.5^\circ$ (see Figure 13) did indicate a small region of separated flow. For $\alpha = 12^\circ$ the pressure distribution showed three distinct inflection points which definitely indicated separated and reattached flow. The Schlieren photograph in Figure 14 verifies this observation.

Air injection (i.e., blowing) into the boundary layer has a comparatively small effect on the pressure distribution. As shown in Figure 19 the length of the interaction region does increase slightly with blowing and the peak pressure appears to decrease slightly. Within the accuracy of the instrumentation blowing has no influence on the static pressure upstream of the interaction.

2. Boundary Layer Rakes

Although the boundary layer rakes at model stations 9.0 and 15.0 did not contain a sufficient number of pitot tubes for obtaining an accurate velocity profile, they were useful in indicating certain gross effects. The profiles obtained at Mach 2.95 are shown in Figures 20 and 21. The thickness of the boundary layer, δ , was determined from log-log plots of distance, y , above the test plate versus velocity ratio, U/U_∞ . The results appear to be accurate to ± 0.02 inches. With no blowing and no shock, δ was approximately 0.13" and 0.19" at model stations 9.0 and 15.0, respectively. It was found that for $P_t/P_\infty > 6$ the velocity profiles became distorted at station 9.0 without increasing δ . For $P_t/P_\infty = 2.0$, δ increased to 0.16" and 0.23" at the upstream and downstream probes, respectively. With a blowing ratio of 5.9, $\delta = 0.19$ " at the forward probe.

Values of the momentum thickness, Θ , were calculated from the velocity (or Mach number) profiles in several cases by assuming constant total temperature throughout the boundary layer and integrating the appropriate function by plotting the integrand against distance above the plate and using a planimeter to find the area under the curve.

3. Heat Transfer Coefficient

The heat transfer coefficient distributions (corrected to an isothermal wall) for Mach 3 are shown in Figures 22 through 33. On each graph three theoretical lines are drawn which were determined for zero pressure gradient (i.e., no shock) turbulent flow. These lines are the results of calculations of the Reshotko and Tucker theory (Reference 7) assuming the boundary layer turbulent at the leading edge of the test plate. The three lines correspond to the following:

NORTH AMERICAN AVIATION , INC.

COLUMBUS DIVISION
COLUMBUS 16, OHIO

NA 62H-795

- (a) Heat transfer distribution calculated strictly by the method of Reference (7).
- (b) Heat transfer distribution as given by Reference (7) but incorporating the experimentally determined momentum thickness at the upstream boundary layer probe for $P_c/P_o = 1.0$.
- (c) Heat transfer distribution as given by Reference (7) but incorporating the experimentally determined momentum thickness at the upstream boundary layer probe for $P_c/P_o = 5.9$.

It is interesting to note that the line corresponding to the strict use of the theory lies between the two that employ the measured momentum thickness, θ . The measured θ 's at station 9.0 are 5.7×10^{-3} and 13.7×10^{-3} inches for $P_c/P_o = 1.0$ and 5.9, respectively.

The change is about a factor of 2.4 in θ but this infers only a 20% variation in heat transfer according to Reshotko's theory. Thus, it is not too surprising to find that for the undisturbed boundary layer the difference in the experimental heat transfer between blowing and no blowing is essentially hidden by the experimental scatter.

It may be seen that a bump occurs in the isothermal heat transfer coefficient, h_r , distribution between stations 12.5 and 13.5 when the shock generator plate is removed and when the generator is installed at $\alpha = 0^\circ$ (see Figures 22 through 25). The reason for this rise in h_r is not understood. When the shock generator is installed at $\alpha = 0^\circ$ there is a small pressure disturbance emanating from the leading edge of the plate (this was discussed in Section III A 1), but this increase in pressure does not warrant the fairly sizeable increase in h_r . However, with the generator plate removed no pressure disturbance is found and the area under the bump is reduced. Thus, this anomaly in the h_r distribution may be due to causes not easily detected, such as cross flow due to asymmetric disturbance of the sidewall boundary layer. It is believed that when strong disturbances are introduced in the flow by deflecting the generator plate, this phenomenon will not introduce any important errors in the results. One indirect verification of the argument is shown in Figure 71 where good correlation of pressure interaction length, is found with the present data and the results of other experiments.

The length of the pressure interaction region ascertained from the static pressure distribution is shown on each of the heat transfer graphs for $\alpha > 0^\circ$. It is seen that the length of the heat transfer interaction region (from the station at which h_r first rises above the zero pressure gradient value to where h_r peaks) is consistently less than Δx (the pressure interaction length). In general, h_r increases linearly to the peak and then decays until the end of the heat transfer instrumentation is reached.

The effect of various blowing rates on the distribution of h_r for $\alpha = 12^\circ$ is shown in Figure 33. Increased blowing appears to slightly decrease h_r at the peak. The same comment applies to the $\alpha = 6^\circ$ data, but essentially no effect is found at $\alpha = 9.5^\circ$. However, since the influence of blowing is small any trend will be partially masked by the natural scatter in the data.

4. Recovery Factor

In this report the usual definition of recovery factor, η , is employed:

$$\eta = \frac{T_{aw} - T_i}{T_r - T_i}$$

where T_{aw} is the adiabatic wall temperature, T_r is the stagnation temperature of the free-stream, and T_i is the static temperature outside the boundary layer on the test plate with no impinging shock. For adiabatic flow external to the boundary layer, η , can be written as

$$\eta = \frac{(1 + 0.2 M_i^2) \frac{T_{aw}}{T_r} - 1}{0.2 M_i^2}$$

where $M_i = 2.98$ for the nominal Mach 3 data. The distribution of η along the test plate for various blowing rates and with $\alpha = 0$ is shown in Figure 34. It is seen that boundary layer blowing has a small, but explicit, effect on η with increasing h_o/p_o , yielding lower values of recovery factor. A definite "wiggle" in the curves is found downstream of station 12.0 which implies that a disturbance exists which influences the boundary layer.

In many engineering applications η for turbulent flow is considered to be equal to the cube root of the Prandtl number, Pr . T_{aw} is about 525°R for the data of Figure 34, and the corresponding Prandtl number is 0.71; therefore, $\eta = \sqrt[3]{Pr} = 0.894$. In Figure 34 this value of η is a reasonable approximation to the experimental recovery factor, especially for the lower blowing rates.

The adiabatic wall temperatures were obtained with the power to the heater elements turned off and with the tunnel operating continuously for more than one-half hour. Thus, it is felt that steady state temperatures had been reached and the thermocouple outputs were truly indicative of the correct T_{aw} . Unfortunately, no runs of this nature were made for $\alpha > 0^\circ$. If it is desired to gain further information regarding η , then it must be done indirectly by investigating the effective recovery factor, η_R , distribution which is defined by the relationship,

$$\eta_R = \frac{T_R - T_i}{T_r - T_i}$$

The effective recovery temperature, T_R , was defined in Section II B with the aid of Figure 16. Since the value of T_R at a given station denotes the isothermal wall temperature which corresponds to zero heat transfer, it is a more significant quantity in calculating heat flow than T_{aw} . Apparently, the tacit assumption has been made by most investigators that $T_{aw} = T_R$, although they are not necessarily the same as pointed out by Gadd in Reference (8). However, a large difference between the two temperatures (and hence between η and η_R) is not to be expected. In fact, Gadd reports that Thomann in Sweden found T_{aw} and T_R to be virtually the same for experiments performed at Mach 1.8*. Distributions of η_R on the test plate with the generator plate removed and with the generator at zero angle of attack are shown in Figures 35 and 36. A comparison between η and η_R for $\alpha = 0$ is illustrated in Figure 37. For $P_o/P_o = 1.0$, η and η_R are practically identical

*It should be noted a larger experimental error is to be expected in T_R than in T_{aw} . T_R at a particular station is the result of extrapolating a straight line determined by four experimental sets of values of heat transfer and temperature, whereas, T_{aw} at the same station is obtained directly from a single thermocouple reading.

NORTH AMERICAN AVIATION , INC.

COLUMBUS DIVISION
COLUMBUS 16, OHIO

NA 62H-795

except in the region between stations 12.0 and 14.0 where a difference as large as 0.03 is found. The data in Figure 37 obtained with boundary layer blowing indicate a fairly consistent but small difference between η and η_A . η_A has the same general distribution and is about 0.01 less than η . Thus, it is seen that although η and η_A are not identical they both illustrate similar distributions along the test plate. Therefore, any qualitative trends found true for η_A should also be valid for η .

The effective recovery factor distributions on the test plate for generator plate deflections of 6.0° , 9.5° and 12.0° are shown in Figures 38 through 40. From all three figures it may be seen that the influence of blowing diminishes with distance such that beyond station 12.0 the differences are within experimental accuracy (about ± 0.008). This effect is not due to the impinging shock since the data with the shock generator plate removed (Figure 35) indicate the same general trend. There is a small, consistent increase in η_A downstream of station 12.0 for increasing shock strength from $\eta_A \approx 0.88$ for $\alpha = 0^\circ$ to $\eta_A \approx 0.91$ for $\alpha = 12.0^\circ$. The low values of η_A upstream of station 12.0 for $\alpha = 9.5^\circ$ (see Figure 39) apparently resulted from recording data before the heat flow had reached equilibrium conditions in the insulating plastic laminate. The effect of not quite obtaining steady state heat flow will produce only a small error in the heat transfer and recovery temperature measurements in the interaction region, i.e., downstream of station 12.0.

B. MACH 5.0 DATA

A free-stream Mach number of 5.02 was determined from the settling chamber pressure, P_t , and from the pitot tube placed below the test plate. However, the static pressure, P_{st} , measured on the wind tunnel wall with a tap placed below and slightly forward of the test plate indicated values about 30% higher than P_t (the static pressure calculated by allowing an isentropic expansion from P_t until a Mach number of 5.02 is attained). The static pressure on the test plate, P_i , was slightly higher than P_{st} . An unrealistic Mach number of about 4.5 was obtained from the Rayleigh pitot formula by using the values of P_{st} and the pitot tube pressure. A Mach number slightly greater than 4.8 was calculated by assuming an isentropic expansion from the stagnation pressure P_t to a free-stream static pressure equal to P_{st} . Of course, one possible reason for the lack of correlation of the various calculated Mach numbers is a pressure reading error. Since P_i and P_{st} were

fairly close in value it is reasonable to suspect the accuracy of the pitot tube. However, another explanation may be based on the possible angularity of the flow (apparently, the Mach 5 nozzle was never checked for flow angularity). That is, the nozzle flow possibly had not completed its expansion before reaching the leading edge of the test plate, and thus, the flow was compressed by the top of the test plate, producing the increase of P_t over P_o . If it is assumed that the flow was symmetrical, then the generator plate was also subjected to an under expanded flow field, and as a result, the generator surface facing the test plate compressed the flow. There are several reasons for accepting this latter explanation. First, it was found that with the generator plate at zero angle-of-attack (i.e., parallel to the tunnel centerline) there was a positive pressure rise on the test plate between model stations 10.0 and 11.0 (see Figures 41 and 42). This is the region where a weak shock emanating from the leading edge of the generator plate would impinge on the test plate. Second, it is generally accepted that the pitot tube pressure is insensitive to small changes in angle-of-attack; consequently, the pitot tube beneath the test plate would have measured the correct local Mach number in a slightly expanding flow field if the pitot pressure was determined accurately. Therefore, the reason for the discrepancy between the measured values of P_{tr} and P_t as compared with the value of P_o determined indirectly from a pitot tube measurement is either that the pitot tube pressure was inaccurate or that the flow field was expanding in the region of the test plate and generator plate leading edges, thereby creating an effective positive angle-of-attack (about 2°) for both surfaces. Fortunately, both explanations yield essentially the same Mach number ($M_1 = 4.77$) on the upstream portion of the test plate and very nearly the same value of the calculated reflected shock inviscid pressure rise on the test plate for a given angle-of-attack. For the sake of simplicity all calculations for the nominal Mach 5 data assume that the flow upstream of the test and generator plates is parallel to the tunnel centerline and at a Mach number of 4.77. However, the titles of the graphs refer to a free-stream Mach number of 5.02 since this is consistent with the tabulated data obtained from the Pt. Mugu data reduction facilities.

1. Static Pressures on the Test Plate

The Mach 5 static pressure distributions are shown in Figures 41, 42 and 43 for the various combinations of α and P_o/P_o tested in the wind tunnel. The increase in P/P_o through the interaction is generally less than the inviscid value shown on the graphs for

a simple reflected shock. Part of the difference, as noted previously, may be due to the inviscid pressure increase not being quite correct because of the uncertainty in determining the true free-stream conditions. However, for $\alpha = 11^\circ$ and 12° , this uncertainty cannot completely explain why a greater inviscid pressure rise was attained. The actual reason is that for the two highest values of α the expansion emanating from the generator plate trailing edge impinged on the test plate in a region of increasing pressure and did not allow any further increase. Instead, the pressure decayed quite rapidly. From the results of Bogdonoff, Reference (2), it is believed that the boundary layer on the test plate upstream of the expansion impingement point was not influenced by the expansion.

During all Mach 5 tests a $\frac{1}{4}$ " wide strip of .033" grit was placed 1.5" from the leading edge of the test plate. Apparently when no boundary layer blowing was applied (note: $P_{t2}/P_\infty \approx 1.4$ implies no blowing

since $P_{t1}/P_\infty \approx 1.4$), the flow was laminar despite the effect of the grit. The pressure distributions with no blowing for $\alpha = 10^\circ$ and 11° indicate a comparatively slow rise and then a flattening out before the pressure increases rapidly to its peak value. This type of curve is indicative of flow which separated while laminar and then became turbulent, e.g., see Reference (9). That the flow was laminar for $P_{t2}/P_\infty \approx 1.4$ is further verified by the heat transfer

data discussed later. Air injection into the boundary layer produced transition on the upstream portion of the plate as evidenced by the shorter interaction length at $\alpha = 11^\circ$ and the increase in heat transfer upstream of the interaction. Increased blowing beyond that necessary to obtain turbulent flow had a negligible effect (within the accuracy of the data) on the interaction length for a given α .

With boundary layer blowing, the three generator angles, $\alpha = 9.7^\circ$, 11° , 12° , yield attached, incipiently separated, and separated flow, respectively. Incipient separation is considered to occur at $\alpha \approx 11^\circ$ because a slight inflection in the pressure distribution is found within the interaction region. It is probable that if the pressure taps were more closely spaced, incipient separation would have been determined at a few tenths of a degree less than 11° . At $\alpha = 12^\circ$ a distinct inflection in the pressure distribution in the interaction region infers that the flow was separated.

2. Boundary Layer Rakes

The Mach 5 velocity profiles at stations 9.0 and 15.0 determined from the pitot tube boundary layer rake pressures are shown in Figures 44, 45 and 46. With no boundary layer blowing, $P_{rc}/P_o \approx 1.4$,

the profiles at station 9.0 indicate a region within the boundary layer for which the slope of the profile, du/dy , is practically zero.

In addition, the data points within a run (i.e., keeping all conditions the same but changing the wall temperature) gave different profiles, which implies either an unusual sensitivity to temperature or, more likely, unsteady flow. With blowing the shape of the velocity profiles appear normal for $\alpha = 0^\circ$ and with the generator plate removed. The profiles at stations 9.0 and 15.0, however, are almost identical, indicating a constant thickness of 0.34". It would seem that the only straightforward reason for the boundary layer not thickening with distance is the result of a favorable pressure gradient or a three-dimensional relieving effect. Neither explanation appears to be applicable in this case since the pressure distribution is flat and the oil flow studies of the streamlines showed a two-dimensional pattern.

For $\alpha > 0^\circ$ the upstream probe was unaffected by the interaction except at $\alpha = 12^\circ$. At $\alpha = 12^\circ$ the interaction started near station 8.5 and the forward velocity profile was somewhat distorted, which indicates an increase in the velocity defect as compared to the profiles for $\alpha < 12^\circ$. For $\alpha > 0^\circ$ all velocity profiles obtained with the downstream probe were similar in shape. The velocity defect was less than the defect at station 9.0 (the converse effect was found at Mach 3) and $du/dy \approx 0$ between $y = 0.05"$ and $y = 0.085"$.

The value of the velocity ratio, u/u_e , at which $du/dy \approx 0$, increased with increasing shock strength.

Increasing blowing from $P_{rc}/P_o \approx 4$ to $P_{rc}/P_o \approx 9.5$ had no consistent effect on the shape of the velocity profiles, and the boundary layer thickness remained at about 0.34".

3. Heat Transfer Coefficient

The heat transfer coefficient distributions for Mach 5 are shown in Figures 47 through 60. Two theoretical lines corresponding to zero pressure gradient heat transfer coefficient are drawn on each graph. One line was derived from the straightforward use of the

turbulent heat transfer theory of Reference (7) assuming the boundary layer becomes turbulent at the leading edge of the test plate. The second line was also calculated from the theory of Reference (7), but was adjusted to account for the experimentally determined momentum thickness. Unlike the Mach 3 case, the momentum thickness was not altered significantly by varying ρ_e/ρ above the minimum value

necessary to obtain turbulent flow. Consequently, only one line was needed to show the theoretical heat transfer distribution based on measured Θ . It may be seen that the strict use of the theory yields better agreement with the data than the theory adjusted to account for measured Θ .

The length of the pressure interaction region, Δx , is noted on the heat transfer graphs for $\alpha > 0^\circ$. Consistent with the trend found at Mach 3, the heat transfer interaction length is less than Δx . Also, in agreement with the Mach 3 results, an increase in blowing rate will either have no effect or will increase the heat transfer interaction length and slightly decrease the peak heat transfer coefficient. Any definite trend is hidden by scatter in the data. Upstream of the interaction with no boundary layer blowing (see Figures 58 and 59) the value of h_T is quite low which is indicative of laminar or the initial phase of transitional flow. Apparently transition to turbulence occurs rapidly in the interaction region as implied by the h_T distribution.

4. Recovery Factor

The Mach 5 adiabatic wall temperature distribution on the test plate was determined for $\alpha = 0^\circ, 7.4^\circ, 10^\circ$ and 12° by recording the thermocouple outputs after the tunnel had been operating for at least 30 minutes. The results in terms of recovery factor, η , are shown in Figures 61, 62 and 63. In Figure 61 it is seen that for $\alpha = 0^\circ$ and no boundary layer blowing η increases slowly with increasing distance from the leading edge and then peaks and begins to decrease near station 10.5. A similar variation of η with distance is found in the data obtained by Brinich (see Reference 10) with a hollow blunted cylinder at Mach 5. Brinich showed that for a transitional boundary layer η goes through a peak with the peak in η corresponding to the end of transition (this was verified with Schlieren photographs). Bluntness also raised the entire level of the η distribution and delayed transition when compared with the results obtained with a sharp leading edge cylinder. The value of the peak η in Figure 61 is 0.92 which compares favorably with $\eta = .912$ found by Brinich when the semi-width of the bluntness was .030". (It is recalled that the height of the grit employed in

the present test was .033".) Also, the rate of change of η with distance agrees well with the hollow cylinder tests up to the peak, but Brinich's data indicate a slower decay in η downstream of the maximum η . Thus, in the present tests it appears that without boundary layer blowing, grit produces the same qualitative effect on the boundary layer as a blunted leading edge.

As was mentioned previously, the combined effects of grit and boundary layer blowing produced transition upstream of the instrumented portion of the test plate. This was evidenced by the pressure and heat transfer data. For $\alpha = 0^\circ$, η decreased slowly with distance as would be expected by analogy with the hollow cylinder data of Reference (10). Increasing the blowing rate from $\dot{m}/\rho_\infty = 3.9$ to $\dot{m}/\rho_\infty = 8.9$ had practically no effect on η .

In Figures 62 and 63 an unexpected distribution of η is found for $\alpha > 0^\circ$. η suddenly increases and then decreases within a space of two inches or less. Near the end of the instrumented region (between stations 14.0 and 16.0) approximately the same value, $\eta = 0.883$, is attained whether or not blowing is applied. In the same region $\eta \approx 0.892$ for $\alpha = 0^\circ$. The qualitative effect of shockwave boundary layer interaction on η at Mach 5 is sketched in Figure 70. At Mach 3 this unusual variation in η did not occur; however, the effect was found at Mach 3.1 by Brinich (Reference 11) when two-dimensional roughness elements were placed on a hollow cylinder. As noted at the bottom of Figure 70, a wedge type roughness element with the flat surface facing the oncoming flow produces the same type of variation in η as found with the present Mach 5 data for $\alpha > 0^\circ$. Brinich also found that comparatively large variations in η occur in the vicinity of a roughness element placed downstream of one or more (the maximum tested was four) similar elements. That is, the effect may be induced in the same boundary layer more than once. It is also interesting to note that in an experiment conducted by Gadd at Mach 2.44 a result similar to Brinich's and the present Mach 5 data was found. In Gadd's experiment (Reference 12) a slab was placed in the turbulent boundary layer on a wind tunnel wall. The height of the slab was about 2.5 times the undisturbed boundary layer thickness, δ , whereas in Brinich's test the roughness elements were probably less than one-half δ . Gadd found that the recovery factor increased and peaked upstream of the slab and decreased downstream of the rearward facing step to a value below the undisturbed boundary layer recovery factor. Why no large change in η was observed for the present Mach 3 tests is not understood, but it may be related to the absence of grit. It would have been interesting to see if this phenomenon would have occurred at Mach 5 if the test plate were long enough to allow transition without the aid of grit.

It may be that grit produces a change in the turbulent mechanism such that further disturbances to the boundary layer yield a somewhat different result than would be found for a boundary layer which underwent natural transition. This point is discussed further with regard to the length of the interaction region in Section IV A.

The effective recovery factor, η_r , was defined in Section III A 4 as a function of the effective recovery temperature, T_r . The distribution of η_r on the test plate for various values of h_w/p and α is shown in Figures 64 through 69. Unfortunately, the method of obtaining T_r (see Figure 16) was rather inaccurate, especially in regions of low heat transfer. Thus, for $\alpha = 0^\circ$ or upstream of the interaction for $\alpha > 0^\circ$ a large amount of scatter is expected in η_r . Inspection of Figure 64 reveals that considerable scatter does exist in η_r for the undisturbed boundary layer (about $\pm .02$). In the region of comparatively high heat transfer more accurate results are obtained. In Figures 65 through 68 this is evidenced by the data downstream of station 11.0. The relationship between η and η_r as illustrated in Figure 69, is the same as that found at Mach 3, i.e., η_r yields a distribution similar to η but the variation is between wider limits.

IV. DISCUSSION AND CORRELATION OF DATA

A. EFFECT OF BOUNDARY LAYER TRIPS ON CORRELATION OF PRESSURE INTERACTION LENGTH

In addition to the present data, pressure data from References (1), (2) and (6) were used in the correlation of the pressure interaction length, $\Delta\kappa$. (The applicable pressure data from Reference (1) are presented in Figures 73 and 74.) In the present tests, the pressure taps and the boundary layer rakes were not located on the heated portion of the test plate. The pressure data from the foregoing references were from tests employing adiabatic walls. As shown in References (8) and (13); however, flow properties are fairly insensitive to small differences between T_w and T_{aw} . Therefore it is assumed that small rates of heat transfer have negligible effects on S_f , θ , P_t/ρ , and $\Delta\kappa$. Also, since the heat transfer elements in this test were located in a small section centered on the test plate, it is assumed that the heat transfer did not introduce significant three-dimensional effects into the flow.

Two correlations of $\Delta\kappa$ were made and are shown in Figures 71 and 72. The data used in making these plots are listed in Table II. As noted previously, the boundary layer thicknesses were obtained from velocity profiles by extrapolation of the straight line portion of the log-log plots of y versus u/u_e through $u/u_e = 1$. These values of δ were then adjusted to account for the length of boundary layer run from the point where the measurements were taken to the point where the pressure interaction began. To make this adjustment it was assumed that δ varied as $\kappa^{0.825}$ where κ is measured from the leading edge of the plate. Since the flow did not become turbulent at the leading edge in this or the experiments of References (1) and (6), this adjustment was somewhat in error even if the κ dependence assumed was accurate. The momentum thicknesses were obtained from the probe measurements and adjusted for distance as previously described using the same κ dependence to the beginning of the interaction. The pressure interaction length, $\Delta\kappa$, was defined to be the distance from the station where the pressure first began to rise above P_1 to the pressure peak, P_3 . The quantity $(P_3/P_1 - 1)/R_f$ may be used to characterize the pressure interaction.

The variations of $\Delta x/\delta_i$ and $\Delta x/\theta_i$ with this parameter are shown in Figures 71 and 72. It is seen that $\Delta x/\delta_i$ and $\Delta x/\theta_i$ vary almost linearly with the interaction parameter.

Figure 71 shows two pressure interaction correlation lines. On the lower line lie the present $M_1 = 2.98$ results and the experimental data of Bogdonoff (Reference 2) and Simon (Reference 1). On the upper line are found the present $M_1 = 4.77$ data and Kuehn's data (Reference 6). From Table II it may be seen that in comparing the present $M_1 = 4.77$ data and Kuehn's data, R_{δ} and M_1 differ by about a factor of 2 and 1.6, respectively, and although these two sets of data correlate well, they do not correlate with the remaining data which define the lower line in Figure 71. Since the data on the lower line were obtained from experiments covering a range of values of R_{δ} and M_1 it appears that the separation of all data points into two separate correlation lines must be attributed to the method of inducing transition. For the $M_1 = 4.77$ data of this test and Kuehn's experiments, leading edge boundary layer trips were used. In the present case transition was affected by a combination of grit plus boundary layer blowing, whereas Kuehn forced transition by placing a rearward facing step near the leading edge of an otherwise flat plate. It should be noted that Bogdonoff's measurements were conducted along a wind tunnel wall where natural transition occurred. Figure 71 shows that the two methods of artificially tripping the boundary layer have the same effect on $\Delta x/\delta_i$, however, a gross difference is indicated between the cases where transition is induced as compared with the flows that experience natural transition.

The second interaction length correlation, Figure 72, represents a plot of $\Delta x/\theta_i$ versus $(P/P_i - 1)/R_{\delta}$. It is seen that in this case three distinct lines are determined by the data. Employing the reasoning given above, it is plausible to attribute the grouping of the points to the method of inducing transition. It is not too surprising that the parameter $\Delta x/\theta_i$ is more sensitive to the details of the boundary layer than $\Delta x/\delta_i$, since θ is certainly more sensitive than δ to the past history of the boundary layer and any significant changes in the turbulent mechanism. It should be noted that attempts to correlate the interaction length using parameters involving local skin friction upstream of the interaction yielded the same type of results as those discussed previously. A correlation which is useful in predicting interaction length for a given set of upstream conditions is considered in Section V.

The most significant fact to be gained from the foregoing discussion is that the method of inducing transition may have a noticeable effect on the subsequent behavior of the turbulent boundary layer. This was evidenced by the two correlations of $\Delta\%$ shown in Figures 71 and 72. In addition, it is also important to note that increasing the boundary layer blowing ratio, R_w/ρ , above the minimum value needed to induce turbulence does not alter the correlation. That is, a particular correlation cannot differentiate between changes in δ_i or Θ_i produced by (1) varying the free-stream conditions (including the length of boundary layer run) or (2) merely varying the rate of air injection in the boundary layer. Thus, it appears (although it certainly has not been proven) that if the boundary layer can be thickened with blowing without producing a distorted velocity profile, then it will interact with a shock wave in exactly the same manner as a boundary layer thickened the same amount by either decreasing the Reynolds number per unit length or increasing the length of run. This implies that leading edge blowing may be used to simulate Reynolds number effects.

B. STANTON NUMBER RATIO DISTRIBUTION

In order to correlate the heat transfer data of the present test in terms of non-dimensional quantities, one reasonable parameter to choose is the local Stanton number,

$$St_e = \frac{h}{C_p(\rho u)_e}$$

where $(\rho u)_e$ is the local mass flow external to the boundary layer. Increasing shock strength (i.e., α going from 0° to 12°) infers higher values of $(\rho u)_e$ in the shockwave boundary layer interaction region. However, if the viscous flow maintains itself as a zero pressure gradient boundary layer and merely adjusts to the change in the external inviscid flow produced by the reflected shock, then despite the increase in $(\rho u)_e$, St_e would also increase (but only slightly). The increase is primarily due to the change in Mach number through a shock and the attendant effect on the zero pressure gradient boundary layer (see Reference 22). Therefore, an appreciable change in St_e in the interaction region is an indication of a corresponding change in the boundary layer. To determine St_e certain assumptions must be made in the $(\rho u)_e$ calculations.

The flow properties external to the boundary layer are known only indirectly from the static pressure distribution on the test plate. The invariance of static pressure in the y direction through a boundary layer, derived from an order of magnitude argument, is no longer valid in the interaction region. The large streamwise gradients of static pressure on the wall are associated with streamwise curvature in the flow which, in turn, infers the existence of vertical pressure gradients. Thus, there will be some discrepancy between the test plate static pressure, p , and the static pressure, p_e , in the inviscid flow external to the boundary layer. Nevertheless, p is a reasonable approximation to p_e and no significant differences of a qualitative nature are to be expected. An additional assumption is made that at each point in the inviscid external flow, the local flow properties including the static pressure are the result of the undisturbed flow on the test plate going through a reflected, oblique, inviscid shock*. In Figures 75 and 76 Mach number, mass flow, ratio, and initial flow deflection angle are plotted versus pressure ratio across a reflected oblique shock-wave in inviscid flow for upstream Mach numbers of 2.98 and 4.77. These two graphs were employed in the calculation of St_e from the heat transfer and pressure data. For each experimental value of pressure ratio a mass flow ratio was determined from Figure 75 or 76. The local Stanton number ratio was calculated using this mass flow ratio and the local experimental value of h_r . The results of the calculations are given in Figures 77 through 80. In these figures St_e/St_i is plotted versus $(x-x_i)/\Delta x$ where the zero pressure gradient Stanton number St_i , the pressure interaction length Δx , and the station at which the interaction begins x_i , are also experimentally determined. Each point in the graphs corresponds to the location of a static pressure tap or the center of a heat transfer element. Since in no case are the two locations coincident it was necessary to fair the pressure data to obtain a pressure at the center of a heat transfer element and conversely to obtain the heat transfer coefficient at a pressure tap location. In all cases the fairings were made through the actual data points even when the data appeared somewhat erratic. However, a certain amount of arbitrariness remained while fairing in a region where large pressure or heat transfer gradients occurred. It is seen that a certain rough similarity exists among all four graphs. The Stanton number ratio is

*This assumption, of course, is never quite true except at the end of the pressure interaction. However, since the flow external to the boundary layer will undoubtedly experience an increase in entropy, even near the beginning of the interaction, it is probably more valid to relate the measured static pressures to a reflected shock system than to use the simple isentropic relationships (as Gadd did in Reference 8).

less than unity in the upstream portion of the interaction region, it rises steeply and peaks at $(\alpha - \alpha_1)/\Delta\alpha < 1$, and then decays at a comparatively slow rate. The lowest value of St_c/St_t is less than 0.4 and the peak is between 1.5 and 1.8. The overall variation in St_c/St_t is given in Figure 81. Certainly, the area covered by the shading in Figure 81 is too great to claim that the particular set of parameters St_c/St_t and $(\alpha - \alpha_1)/\Delta\alpha$ chosen uniquely describe

the heat transfer phenomenon downstream of α_1 . However, there is a considerable amount of unavoidable error in determining the correlation parameters which may be responsible for almost all of the spread in the data. At $M_o = 2.95$ the inability to accurately determine α_1 and $\Delta\alpha$ (due to the $\frac{1}{2}$ " spacing of the pressure taps) and at $M_o = 5.02$ the errors associated in calculating h_r (primarily due to the low heat transfer rates caused by low tunnel densities) are the most probable sources of scatter.

Since a literature survey did not reveal any turbulent boundary layer heat transfer investigations involving an impinging oblique shock, no direct comparison with other experiments can be made. However, it is of interest to see if the heat transfer associated with a turbulent boundary layer disturbed by means other than an impinging shock can be related to the present data. In Figure 82 two-dimensional turbulent flow heat transfer distributions obtained from three separate tests are shown in terms of Stanton number ratio. A few comments concerning the data in the figure are warranted. In certain respects, Gadd's data (References 8 and 12), which were obtained by disturbing the flow on a wind tunnel wall with a rectangular slab, display a similarity to the present results. Upstream of the slab, St_c/St_t decreases to a value less than unity in the separated region and then increases sharply. Again, downstream of the slab it is found that $St_c/St_t < 1.0$ and as the flow reattaches to the wind tunnel wall, St_c/St_t rapidly approaches a peak value of 1.7 before it begins to decay. Seban's low speed data (Reference 18) in Figure 82 show the result of disturbing a flat plate flow with an $1/8$ " diameter rod placed spanwise on a plate. It is observed that the upstream influence of the rod produced a small oscillation in the St_c/St_t curve which is also found in Gadd's data. The peak value of St_c/St_t is approximately 1.5 and downstream decay from this value is quite slow, decreasing to a value of 1.2 at a distance of 95 rod diameters downstream of the rod. (Note that in the case of the rod, the quantity H , which non-dimensionalizes distance, was chosen arbitrarily to be 0.60" so that the data would fit on the graph.) The heat transfer data

obtained by Naysmith (Reference 15) on a wind tunnel wall downstream of a ramp indicates qualitative but not quantitative agreement with the data discussed previously. The St_e/St_i distribution from Reference (15) in Figure 82 does not contain the data taken upstream of the boundary layer reattachment point because the measurements in the separated region directly behind the ramp were reported to be unreliable. It appears that a peak value of $St_e/St_i > 3.0$ may occur in the flow reattachment zone. This maximum value of St_e/St_i is considerably higher than what was found in the other Stanton number ratio distributions (Figures 81 and 82). It is difficult to determine if the high values of St_e/St_i found by Naysmith are to be expected since no other heat transfer experiments involving shockwave turbulent boundary layer interaction on a flat plate have been discovered in the literature. However, use may be made of body of revolution data under certain conditions. If the Mach number is fairly high and the boundary layer dimensions are small compared with the local body diameter, the flow field in the vicinity of a body of revolution is approximately two-dimensional (in the planar sense). This is especially true at the juncture of a cylindrical mid-body and a conical flare. Two suitable heat transfer experiments conducted in a wind tunnel on pointed-nosed bodies of revolution are reported in References (16) and (17). In Reference (16) the tests were performed at $M_o = 6.8$ on bodies with 10° and 30° conical flares. Natural transition of the boundary layer occurred on the cylinder upstream of the flare for the high Reynolds number runs. Peak values of St_e/St_i reported in Reference (16) are 3.5 and 1.25* for the 30° and 10° conical flares, respectively. In Reference (17) turbulent heat transfer tests were performed at $M_o = 4.98$ on bodies with 10° and 24° conical flares. A boundary layer trip on the nose induced turbulent flow well upstream of the influence of the cylinder flare juncture. The peak values of St_e/St_i are approximately 2.2 and 1.4 for the 24° and 10° flares. It is to be noted that in both References (16) and (17) the turbulent data indicated little or no separation in the vicinity of the cylinder flare juncture.

*For the 10° flare the peak value of St_e/St_i was found to be approximately 1.35 if the measured pressures are employed in determining the local mass flow, $(\rho u)_e$, external to the boundary layer. In Reference (16) $(\rho u)_e$ was determined assuming the flow external to the boundary layer identical to inviscid planar flow deflected through a wedge angle equal to the flare angle.

Peak values of $St_2/St_1 > 1.8$ have been found in three different cases. Whereas, the remaining data gave $St_2/St_1 \leq 1.8$ (note: the subscript "2" applied to Stanton number denotes the peak value). It was noticed that $St_2/St_1 > 1.8$ occurred whenever the mass flow ratio in the flow external to the boundary layer was approximately invariant with pressure ratio, i.e., whenever

$$\left. \frac{d[(\rho u)_2/(\rho u)_1]}{d(P_2/P_1)} \right|_{x=x_2} \approx 0$$

A graph of the mass flow ratio versus the pressure ratio across a reflected shock at various Mach numbers is shown in Figure 83. Similar shaped curves are also determined if a single oblique shock is considered as, for example, at the juncture of a cylinder and a conical flare. In the figure $(P_2/P_1)_B$ is defined as the value of pressure

ratio at the "elbow" of the mass flow ratio versus pressure ratio curve. Where the elbow actually occurs is somewhat arbitrary.

In all cases mentioned previously for which $St_2/St_1 \leq 1.8$ in a

supersonic flow field, the pressure ratio at the peak Stanton number location is less than $(P_2/P_1)_B$. From the foregoing considerations

a tentative expression for the peak Stanton number ratio may be given as

$$\frac{St_2}{St_1} = \frac{h_2/h_1}{(\rho u)_2/(\rho u)_1} \approx \frac{f(P_2/P_1)}{g(P_2/P_1)}$$

where $h_2/h_1 \approx f(P_2/P_1)$, $g = (\rho u)_2/(\rho u)_1$, and the tacit assumption is made that the inviscid flow properties at the end of

the pressure interaction (subscript "3") are approximately equal to those at the point where the Stanton number peaks (subscript "2"). From the sketch below it is seen that $f(P_3/P_1)$ may be expressed as

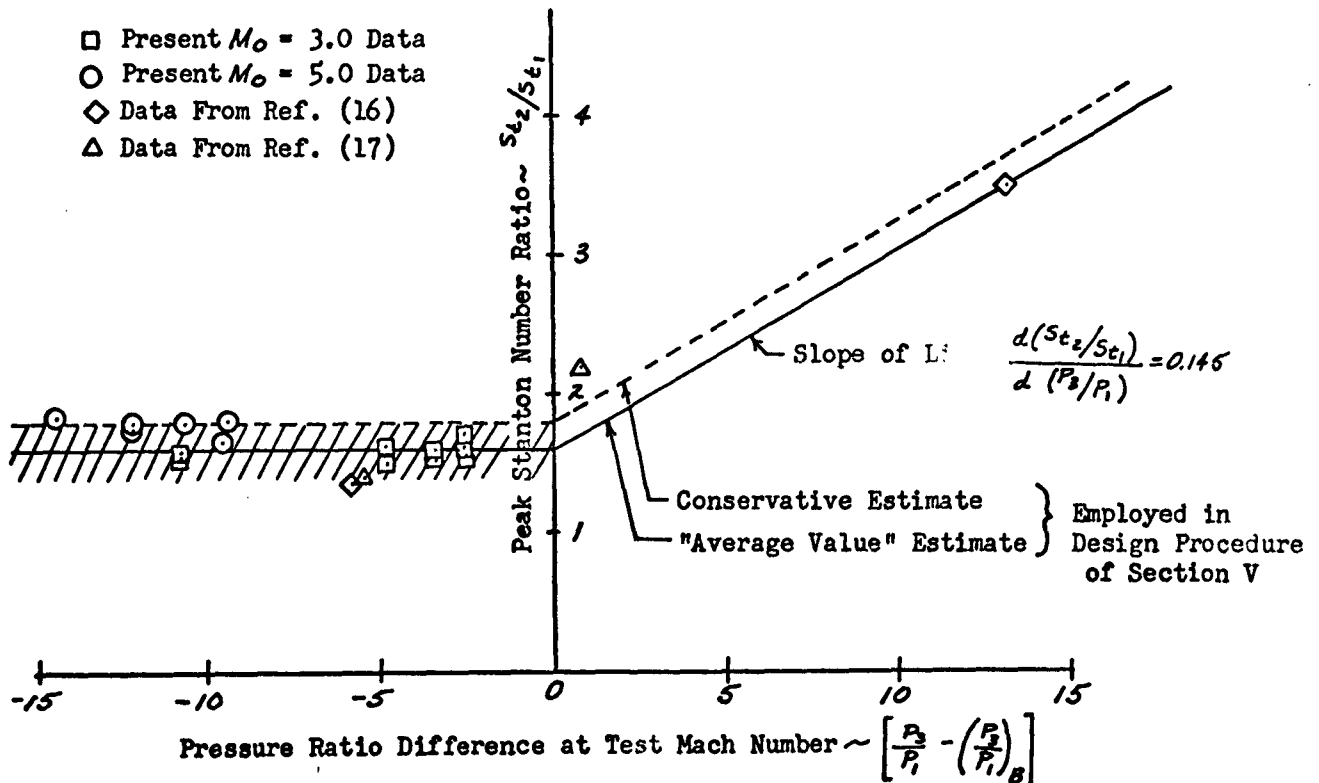
$$f(P_3/P_1) = \begin{cases} K_1 g(P_3/P_1) & \text{for } P_3/P_1 < (P_3/P_1)_B \\ K_1 + K_2 [P_3/P_1 - (P_3/P_1)_B] & \text{for } P_3/P_1 > (P_3/P_1)_B \end{cases}$$

where $1.4 < K_1 < 1.8$ (except for values of $P_3/P_1 \approx 1.0$) and

$K_2 \approx 0.145$. The expression for $f(P_3/P_1)$ was obtained from the

Experimental Peak Stanton Number Ratio Versus a Theoretical

Inviscid Pressure Ratio Increment



assumption that for $P_2/P_1 > (P_2/P_1)_c$ (note: $g(P_2/P_1)$ is

approximately constant under this condition) the peak Stanton number ratio varies linearly with pressure ratio. The constant K_2 was determined primarily from the 30° conical flare data of Reference (16). The foregoing equations for St_w/μ , are purely speculative, but it is felt that they represent the most simple, and yet physically reasonable, formulation that could be derived from the available data. In order to obtain more accurate expressions additional heat transfer tests are required.

The problem of relating the increase in Stanton number ratio within the shockwave boundary layer interaction region to a corresponding change in the boundary layer heat transfer mechanism utilizing the available information can only be attacked indirectly. It has been conjectured by Naysmith (Reference 15) and others that a reattaching separated boundary layer acts as if it contained a thin "inner boundary layer" which is initiated at the reattachment point. This concept is in qualitative agreement with experiments (References 9, 15 and 18) in which high heat transfer rates (supposedly due to the thinness of the "inner boundary layer") and low shearing stress at the wall (supposedly due to the low velocity external to the "inner boundary layer") were found. Further verification of the "inner boundary layer" notion for unseparated flow is found in References (16) and (17) where experimental supersonic turbulent heat transfer data on axisymmetric bodies with conical flare afterbodies are presented. In both references it was found that reasonably good agreement of theory with data was obtained on the flare if the boundary layer upstream of the flare is neglected and a new zero pressure gradient boundary layer beginning at the cylinder-flare juncture is assumed.

If the "inner boundary layer" concept is a valid representation of the structure of the disturbed boundary layer, then an increase in η_e (the recovery factor based on local flow conditions external to the entire boundary layer) above the value found for zero pressure gradient flow is to be expected downstream of the beginning of the "inner boundary layer". The reason that an "inner boundary layer" implies an increased η_e is as follows: It can be shown (e.g., see References 10 and 20) that for a turbulent boundary layer the true local recovery factor, η_L , is essentially invariant for moderate changes in Reynolds number and Mach number as long as it is based on conditions which are local from the "viewpoint" of the boundary layer. For the usual boundary layer $\eta_L = \eta_e$. Since the "inner boundary layer" is immersed in a thicker viscous shear layer the true local Mach number, M_L , seen by the "inner boundary layer" will

NORTH AMERICAN AVIATION , INC.

COLUMBUS DIVISION
COLUMBUS 16, OHIO

NA 62H-795

be less than the local Mach number, M_L , external to the entire boundary layer. The adiabatic wall temperature for the case of an "inner boundary layer" is found from the relation

$$\frac{T_{aw}}{T_f} = \frac{1 + 0.2 \eta_L M_L^2}{1 + 0.2 M_L^2}$$

If the fundamental change in the turbulent viscous flow due to its interaction with a shockwave is the creation of an "inner boundary layer" (i.e., no important changes in the transport properties), then η_L at a given point in the flow field should remain unaffected by the interaction. Therefore, T_{aw}/T_f should increase downstream of

the interaction since the local Mach number, M_L , seen by the "inner boundary layer" is certainly less than the upstream Mach number, M_1 . Even neglecting the "inner boundary layer", T_{aw}/T_f

should increase downstream of a shockwave because the Mach number external to the boundary layer, M_e , is less than M_1 . However, the existence of an "inner boundary layer" creates an additional increase in T_{aw}/T_f (since $M_L < M_e$) and hence an increase in η_e

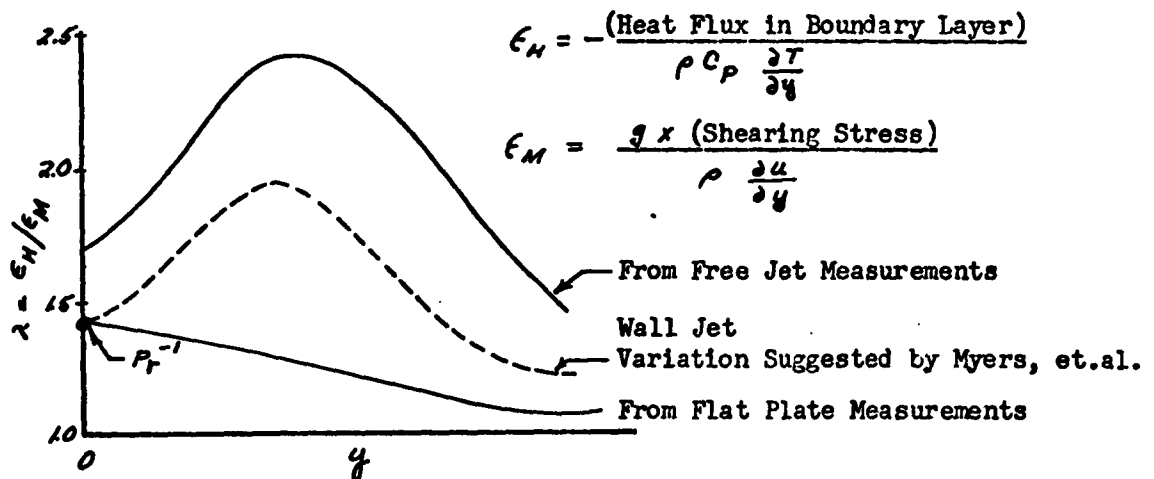
as seen from the equation

$$\eta_e = \frac{(1 + 0.2 M_e^2) \frac{T_{aw}}{T_f} - 1}{0.2 M_e^2}$$

A serious doubt is cast on the "inner boundary layer" concept since all the data investigated, including the results of the present tests, show no indication of an increase in η_e downstream of the peak Stanton number ratio. Figures 84 and 85 are typical of the local recovery factor distributions found in this study. It is seen that η_e downstream of station 12.0 for the case of an impinging shock is consistently lower than the zero pressure gradient η_e . However, in Figure 85 a quite pronounced peak in η_e is found near station 9.5. This rise in η_e , which starts at the beginning of the pressure interaction and then ends a short distance later, may be due to the creation of an "inner boundary layer" which is then destroyed before the end of the interaction region is reached. It is to be noted that

on page 22 this "blip" in η_c is compared with similar results obtained by Brinich employing two-dimensional roughness strips.

The results of certain low speed experiments suggest an alternative to the "inner boundary layer" concept which gives a qualitative explanation to the observed Stanton number ratio rise downstream of a shockwave. In the present case the use of subsonic experiments to gain insight into the interaction of a supersonic flow field with a turbulent boundary layer appears valid. For example, there is definite similarity with respect to local Stanton number ratio, St_x/St_1 , distribution between the low speed flow disturbed by a rod and the $M_\infty = 2.44$ flow disturbed by a slab (see Figure 82). A fairly obvious approach that may be used in an investigation of the properties of a reattaching separated flow is to consider the flow as being equivalent to a wall jet. Although the analogy may not be exact, it is difficult not to believe that the two phenomena are basically comparable. It is pointed out by Meyers (Reference 19) that the tests of Reference (21) show that low speed wall jet turbulence levels* at the point of maximum jet velocity are almost four times the maximum turbulence level found in a zero pressure gradient boundary layer. Also in Reference (19), Meyers suggests that the ratio of eddy diffusivity for heat, ϵ_H , and eddy diffusivity for momentum, ϵ_M , varies in the manner shown in the sketch below.



Variation of Eddy Diffusivity Ratio (Taken From Reference 19)

*The term "turbulence level" is defined here to be equal to $\frac{u'}{U_\infty}$, where u' is the root-mean-square of the x component of the turbulent velocity fluctuations and U_∞ is a reference velocity outside the boundary layer.

NORTH AMERICAN AVIATION , INC.

COLUMBUS DIVISION
COLUMBUS 16, OHIO

NA 62H-795

Therefore, not only a high level of turbulence is found within a wall jet, but apparently the turbulent mechanism has been modified so that there is a large increase in the ability to transport heat as compared with the transport of momentum. If the wall jet is truly equivalent to a reattaching separated flow, then it may be seen from the sketch that high heat transfer rates, and yet low values of wall shearing stress, are obtained downstream of the reattachment point. In the laminar sublayer at the wall where the turbulence disappears, it can be shown that the eddy diffusivity ratio, λ , is equal to the reciprocal of the Prandtl number. Since the recovery factor was found to decrease downstream of the shockwave for almost all supersonic experiments, it is implied that the Prandtl number also decreased. Thus, if in the foregoing sketch the appropriate line for flow downstream of a shockwave were drawn it would probably intersect the λ axis at a slightly higher value than the flat plate line.

C. MOMENTUM THICKNESS AND HEAT TRANSFER COMPARISONS FOR NO INTERACTION

The theory of Reshotko and Tucker (Reference 7) was employed to calculate a theoretical momentum thickness, Θ , and heat transfer coefficient, h_r , for comparison with the present experimental data in the cases where no interaction was present.

The theory of Reference (7) applies to a body with a smooth leading edge. Also, the transition point in the flow must be known for accurate application of the theory. In the present calculations turbulent flow was assumed to begin at the leading edge and the surface was assumed to be isothermal from the leading edge (the heat transfer data presented herein are corrected to an isothermal surface). Leading edge blowing was used in some of the $M_1 = 2.98$ tests and blowing plus grit were used in the $M_1 = 4.77$ tests. Also, the origin of turbulent flow was not known though it is certain that the origin was not at the leading edge. Therefore, conditions were present in some of the tests which cannot be theoretically accounted for.

The most important aspects of the theory that can be checked from the present data are the theoretical prediction of the magnitudes of h_r and Θ and the α dependence of h_r . In the present case the instrumentation did not allow a detailed survey of the boundary layer. Therefore, the measurements of boundary layer thickness, δ , and Θ are considered to be quite approximate. However, they are sufficiently accurate to give results in the pressure interaction length correlations

(Figures 71 and 72) which are consistent with those of other tests wherein the boundary layer was carefully probed.

Zero pressure gradient values of Θ_h were calculated from the theory of Reference (7) for the present $M_i = 2.98$ and $M_i = 4.77$ data and for the tests from Reference (1) which are used in this report. The equations from Reference (7) for flat plate flow over a smooth isothermal flat plate, turbulent from the leading edge are as follows.

$$\Theta_h = \frac{0.0259}{\left(\frac{a_T}{v_T} M_o\right)^{0.177} \left(\frac{T_T}{T_e}\right)^{0.267} \left(\frac{T_{ref}}{T_e}\right)^{0.602}} x^{0.123} \quad (1)$$

$$St = \frac{h_T}{g_{c_p}(q_u)_e} = \frac{0.123 \text{ exp}[-1.561 H_{i,fp}]}{\left(\frac{T_{ref}}{T_e}\right)^{0.732} \left(\frac{T_T}{T_e}\right)^{0.268} \left(\frac{M_o a_T}{v_T}\right)^{0.267} (Pr)^{\frac{1}{3}} (\Theta_h)^{0.268}} \quad (2)$$

$$\text{where } \frac{T_{ref}}{T_e} = \frac{1}{2} \left(\frac{T_w}{T_e} + 1 \right) + 0.22 \left(\frac{T_{aw}}{T_e} - 1 \right)$$

$$T_{aw} = T_e (1 + 0.2 Pr^{\frac{1}{3}} M_o^2)$$

$H_{i,fp}$ = "Incompressible" form factor for a flat plate

x = Distance from leading edge.

The values $H_{i,fp} = 1.28$, $Pr^{\frac{1}{3}} = 0.89$ and appropriate values for

T_w (see Table III) were used in the calculations of $h_T(x)$. In Table III the values of Θ , M_o and the resulting Θ_h from the experimental measurements are compared with the theoretical values of Θ_h . Also appearing in Table III are the values of h_T for the

present tests calculated from the theory using both the values of Θ_h from the rake measurements and the theoretical values. The theoretical $h_r(x)$ using the measured and theoretical Θ_h 's and employing the theoretical χ dependence of $\chi^{0.75}$ for both the measured and theoretical Θ_h 's are shown on all of the heat transfer coefficient figures for the purpose of comparing the theoretical magnitudes and χ dependence of h_r with the experimental results.

Table III shows that for the present tests the theoretical Θ_h overestimates the experimental Θ_h for $M_1 = 2.98$ and $P_{rc}/P_o = 1$, and underestimates it for $M_1 = 2.98$ and $P_{rc}/P_o = 5.9$. This is to be expected since the delay in transition would cause the measured Θ_h to be smaller than the theoretical for the case of no blowing. With boundary layer blowing ($P_{rc}/P_o = 5.9$) Θ_h more than doubled and transition occurred further upstream than in the case of no blowing. Because the measured Θ_h for $P_{rc}/P_o = 1$ and $P_{rc}/P_o = 5.9$ lie above and below

the respective theoretical Θ_h , the converse is found for the h_r values calculated from Equation (2). Since Θ_h varies as the 0.268 power in the h_r formula, the differences in h_r using the different values of Θ_h are small and all heat transfer calculations agree well with the experimental zero pressure gradient data for $M_1 = 2.98$.

For $M_1 = 4.77$ the grit and leading edge blowing which were used in every turbulent run caused the measured Θ_h to be over twice as high as the theoretical value. The increase in blowing from 4.0 to 9.1 had little effect on changing δ and Θ at this Mach number. It is surprising that the theoretical value of Θ_h gave results for h_r which produced better agreement with the experimental values than did the measured value of Θ_h used in the h_r formula.

Figures 22 through 25 and 47 through 49 compare the theoretical h_r 's (using theoretical Θ_h and measured Θ_h 's) with the experimental values. It is seen that the theory of Reference (7) predicts the magnitudes of h_r and the χ dependence of h_r fairly well even if Θ_h is off by more than a factor of 2. The heat transfer coefficient appears to be insensitive to leading edge effects, such as grit, unlike the pressure interaction length parameters.

The best agreement between theoretical and measured Θ_h found in Table III was obtained from the data of Reference (1). From Mach number and Reynolds number considerations it is probable that transition occurred closer to the leading edge in the Reference (1) tests than in the present tests, and since the boundary layer probe

measurements were thorough, fairly accurate values for Θ_h should have been obtained. Thus, the theory of Reference (7) is partially verified by the agreement with the measured Θ_h 's of Reference (1).

It appears from the foregoing comparisons that the insensitivity of the heat transfer coefficient to the boundary layer parameter Θ_h allows an estimation of h_r to be made fairly accurately by a theory such as that of Reference (7) even though the boundary layer parameters may be poorly estimated.

In the preparation of this report, whenever δ or θ in a zero pressure gradient field were required at an κ location upstream or downstream of where the boundary layer was probed, they were adjusted from their measured values by using the theoretical κ dependence of $\kappa^{0.713}$ from Reference (7). In Table III the values of δ and θ obtained in the present tests from rake measurements at model stations 9.0 and 15.0 are shown for four cases in which the generator plate was removed. As mentioned previously the values of δ and θ obtained from the fixed rakes are not as accurate as those obtained from movable probes but they may be used to give an approximate value of the κ dependence obtained in these tests. It may be seen in Table III that the theoretical $\kappa^{0.713}$ dependence for δ and θ is fairly close to the average value of $\kappa^{0.72}$ found from the $M_1 = 2.98$ data. However, the measurements at $M_1 = 4.77$ show an almost negligible variation of δ and θ with distance. This result is not understood. The rake measurements of local Mach number near the edge of the boundary layer indicated an expansion large enough to show up on the pressure distributions; however, the recorded pressures do not indicate such an expansion.

Many calculations based on δ_1 and θ_1 , which were determined from the measured values by using the theoretical $\kappa^{0.713}$ dependence, were completed before the negligible κ dependence of these quantities at $M_1 = 4.77$ was noticed. Since the distances that the measured δ and θ were moved to obtain δ_1 and θ_1 were always small (less than 9% of the value of κ at which the measurements were made in all cases) the calculations were not changed.

D. CORRELATION OF TRANSFORMED MOMENTUM THICKNESS ACROSS THE INTERACTION REGION

In order to calculate the heat transfer coefficient from theories such as that of Reference (7), knowledge of the variation of θ with κ is required. This is because θ is the only varying boundary layer parameter involved in the simplified Reynold's analogy and skin friction formula. In the region where the shock interacts with the

boundary layer, however, large gradients in the thermal and fluid boundary layer parameters occur even for weak shocks as evidenced by the present data and the data of References (1) and (2). Thus, the gradient terms in the modified Reynold's analogy of Cohen, Reference (14), become sufficiently important such that the heat transfer depends on more than Θ alone. Intuitively, it would seem that at some distance downstream of this high gradient region the heat transfer coefficient would again be given in terms of the one parameter, Θ . The distance downstream of the shock at which the simplified Reynold's analogy and skin friction formula can again be used to give the heat transfer coefficient is not known. One reason for the uncertainty is that downstream of the interaction the velocity profile is filling out from the distorted form, which was caused by the interaction with the shockwave, so that Θ is changed at an unknown rate with κ . Also, the present recovery factor, \mathcal{R} , data indicate that \mathcal{R} and the Reynolds analogy factor, S , decrease (assuming $\mathcal{R} = Pr^{1/3}$ and $S = Pr^{2/3}$ for this argument) to a value downstream of the shock which is lower than expected from the change in Pr due to the change in static temperature. This indicates a change in the transport properties of the boundary layer caused by the interaction. The effects of this change would also (intuitively) be expected to disappear somewhere downstream. Effects such as these prohibit the calculation of the heat transfer coefficient downstream of the interaction using the simple Reynold's analogy and skin friction formulae with downstream conditions determined from the shock relations.

Due to the lack of experimental data and theoretical guidelines, it is difficult to arrive at any definite statements concerning the downstream heat transfer decay. However, an attempt was made employing an indirect approach. Under the assumption that the theory of Reference (7) applies at and downstream of a "reattachment" point (defined below), approximate values of Θ_h and S at the reattachment point may be determined by utilizing the present heat transfer data and the boundary layer profile data from References (1) and (2). These values may serve as initial values for calculations of heat transfer downstream of the reattachment point if the κ dependence of Θ_h and S can be estimated in the theoretical formula for Stanton number.

The correlation of the transformed momentum thickness ratio, Θ_{h2}/Θ_{h1} , across the interaction will now be described.

The present data show that the peak heat transfer coefficient occurred slightly upstream of the end of the pressure interaction. Therefore, even in cases where a separation bubble existed, the peak heating occurred well into the reattachment region so that the ordinary

boundary layer equations can be applied. For both attached and separated flows it is assumed that the theory of Reference (7) applies at the point where the peak in the h_r distribution occurs. This assumption implies that any effects on h_r due to significant gradients in the flow field existing at the peak h_r location will be combined into the values of $\Theta_{a,2}$ and S_2 obtained by means of the method described below. It is implicitly assumed, therefore, that the skin friction formula developed in Reference (7) applies near reattachment.

The formula for Stanton number from Reference (7) is

$$St = \frac{h}{g C_T (q_w)_e} = \frac{0.123 \exp [-1.561 H_{i,fp}]}{\left(\frac{T_f}{T_e}\right)^{0.268} \left(\frac{M_e a_T}{V_T}\right)^{0.261} \left(\frac{T_{ref}}{T_e}\right)^{0.732}} \frac{1}{S(\Theta_{\frac{1}{2}})^{0.268}} \quad (3)$$

$$\text{where } \frac{T_{ref}}{T_e} = \frac{1}{2} \left(\frac{T_w}{T_e} + 1 \right) + 0.22 \left(\frac{T_{hw}}{T_e} - 1 \right)$$

$H_{i,fp}$ = "Incompressible" form factor for flat plate = constant

Applying Equation (3) at the beginning of the pressure interaction, x_1 , and at x_2 where the peak heat transfer coefficient, h_2 , occurs gives the following equation for $\Theta_{a,2}/\Theta_{a,1}$, the ratio of the transformed momentum thickness across the heat transfer interaction region.

$$\frac{\Theta_{a,2}}{\Theta_{a,1}} = \left[\frac{S_1}{S_2} \right]^{0.73} \left[\frac{\left(\frac{T_{ref}}{T_e} \right)_1}{\left(\frac{T_{ref}}{T_e} \right)_2} \right]^{2.73} \left[\frac{T_{e,2}}{T_{e,1}} \frac{M_{e,1}}{M_{e,2}} \frac{P_{T,1}}{P_{T,2}} \right] \left[\frac{(q_w)_{e,2}}{(q_w)_{e,1}} \frac{h_1}{h_2} \right]^{0.73} \quad (4)$$

NORTH AMERICAN AVIATION, INC.

COLUMBUS DIVISION
COLUMBUS 16, OHIO

NA 62H-795

Using reflected shock relationships, the external conditions at the peak heat transfer location were determined from plots of M_a and

$$T_e/T_{e1} \times P_{Te}/P_{T1} \times (q_w)_e/(q_w)_1 \quad \text{versus pressure ratio } P/P_1 \quad \text{with}$$

the upstream Mach number M_1 as parameter (see Figures 75, 76, 86 and 87). The wall static pressure ratio measured at the peak heat transfer location was used in finding these external conditions in each case. All values used in the calculations appear in Table II. With h_1 and h_e known from the data, Equation (4) may be used to

calculate the product, $\Theta_{w2}/\Theta_{w1} \times \left[\frac{S_2}{S_1} \right]^{3.73}$. Since S_2 is not

known, use was made of shock wave boundary layer interaction data from other sources. That is, boundary layers were probed through the interaction region in References (1) and (2); the first using a flat plate and covering a range of Mach numbers, R_δ , and flow deflection angles; the second using the tunnel wall boundary layer and one Mach number, one R_δ , and various shockwave angles.

Seven values of Θ_{w2}/Θ_{w1} were obtained from the data of Reference (1) and one value from Reference (2). The position in the interaction region at which Θ_{w2} was taken in these two experiments was chosen to correspond as closely as possible to where the peak heat transfer coefficient would be expected to occur in the present tests. This position was, for $\alpha > 6^\circ$, approximately 25% of Δx measured upstream from x_3 . Since the probes were not always positioned where desired, an additional approximation to Θ_{w2} was introduced. By comparing the Θ_{w2}/Θ_{w1} ratios obtained from the direct measurements

with the values of $\Theta_{w2}/\Theta_{w1} \left[\frac{S_2}{S_1} \right]^{3.73}$ obtained indirectly from the

present heat transfer data, it was noticed that the two sets of values could be brought into general agreement if the value of

$$\left[\frac{S_2}{S_1} \right]^{3.73} \quad \text{was taken as 4 in all cases. This means that}$$

$S_2 = 0.690 S_1$, where $S_1 \approx (Pr)^{2/3} = 0.791$. This decrease in S from S_1 to S_2 is in line with the observed decrease in the experimental recovery factors from η_1 to η_2 . No comparison with directly measured values was available for the Θ_{w2}/Θ_{w1} ratios calculated from the present $M_1 = 4.77$ data.

NORTH AMERICAN AVIATION , INC.

COLUMBUS DIVISION
COLUMBUS 16, OHIO

NA 62H-795

The values of θ_{n2}/θ_{n1} are listed in Table II and are plotted as functions of M_1 with the parameters α and R_{δ}/p_0 in Figure 88.

It is seen in Figure 88 that the θ_{n2}/θ_{n1} values fall into three rather distinct bands even though the error involved in determining the ratio from the heat transfer data is quite large (due to the fact

$\theta_{n2}/\theta_{n1} \propto [h_1/h_2]^{3.73}$ and the error in h_1 and h_2 are by nature

large). Table II also indicates whether the flow is attached, incipient, or separated for each of the tests. It may be seen from Figure 88 that Mach number and boundary layer blowing have a small effect on θ_{n2}/θ_{n1} but there is no discernable trend due to R_{δ} .

The condition of the flow, whether separated, incipient or attached, was determined by applying Kuehn's criterion (Reference 6) which was discussed in Section III A 1. Kuehn's results were used to define the condition of the flow for the data of References (1), (2) and (6) and the present $M_1 = 2.98$ data. Since Kuehn's data did not extend to $M_1 = 4.77$, this case had to be judged from the pressure data taken. In the present experiment the spacing of the pressure taps allowed the incipient separation condition to be determined only to within about $\alpha = \pm 1^\circ$. It is concluded that the $\alpha = 9.7^\circ$ and $\alpha = 11^\circ$ tests at $M_1 = 4.77$ correspond to just below incipient and just above incipient separation respectively.

V. DESIGN PROCEDURE

In this section a step-by-step procedure is outlined for calculating the isothermal heat transfer coefficient distribution which result from an impinging oblique shockwave interacting with a turbulent boundary layer on a flat plate. The flow field is considered to be two-dimensional in the planar sense. The essential features of the calculation are the estimation of: (1) the length of the pressure interaction region, Δx , as determined by the static pressure distribution on the flat plate and (2) the isothermal heat transfer coefficient, h_T , distribution from the beginning of the pressure interaction to a point a short distance downstream of the end of the interaction. Correlations of the interaction length were discussed in Section IV-A which indicated that the method of inducing transition had a strong influence on the correlation. However, in this section Δx is determined from correlations which are more appropriate for use in a design calculation. The calculation of the heat transfer coefficient distribution resulting from the shockwave turbulent boundary layer interaction was obtained primarily from the tentative relationships discussed in Section IV-B.

The calculation procedure requires that the following quantities are known:

1. The Mach number upstream of the interaction, M ,
2. The boundary layer thickness immediately upstream of the interaction, δ_i . An equation for estimating δ_i can be obtained from Reference (1):

$$\delta_i = 0.047 (N+1) \left(\frac{\nu_i}{U_i} \right) \left(\frac{U_i L}{\nu_i} \right)^{0.7}$$

where U_i and ν_i are the velocity and the kinematic viscosity, respectively, in the inviscid flow upstream of the interaction.

L is the distance from the point of boundary layer transition to the beginning of the interaction, and N is the reciprocal of the

NORTH AMERICAN AVIATION, INC.

COLUMBUS DIVISION
COLUMBUS 16, OHIO

NA 62H-795

exponent in the boundary layer power profile law,

$$\frac{U}{U_1} = \left(\frac{x}{x_1} \right)^{\frac{1}{n}}$$

3. The point on the flat plate, x_{sh} , which corresponds to the intersection of the oblique shockwave with the edge of the boundary layer if there were no interaction. This is illustrated in Figure 92.
4. The Reynolds number per unit length upstream of the interaction, Re .
5. The static pressure ratio across the oblique reflected shockwave in an inviscid flow field, P_2/P_1 (see Figure 89).
6. The isothermal heat transfer coefficient upstream of the interaction, h_i . A theoretical prediction of h_i by the theory of Reference (7) can be obtained by employing Equations (1) and (2) (which are valid for an isothermal wall) in Section IV-C.

The calculation procedure given below pertains only to a wall which is isothermal far upstream of the interaction.

Step-by-Step Calculation Procedure

- Step 1: Calculate the pressure interaction length, $\Delta x = x_2 - x_1$ from either Figure 90 or 91. Figure 90 will give greater accuracy if it is known whether the boundary layer transition is natural or forced.
- Step 2: Locate the interaction length in relation to x_{sh} by calculating x_i from Figure 92.
- Step 3: From the known value of α and M_1 find the mass flow ratio, $(\rho u)_2/(\rho u)_1$, across the reflected oblique shock from Figure 93 or 83.

NORTH AMERICAN AVIATION, INC.

COLUMBUS DIVISION
COLUMBUS 16, OHIO

NA 62H-795

Step 4: The peak value of the Stanton number ratio, St_2/St_1 , can also be determined with the aid of Figure 93. If the combination of α and M_1 gives a point on the curve for a given M_1 to the left of the dashed curve in Figure 93, then $St_2/St_1 = K$, = 1.6 or 1.8

(Note: $K_1 = 1.8$ is the highest value of St_2/St_1 found experimentally for all $(P_3/P_1) < (P_3/P_1)_B$ and 1.6 is an average peak value of all the present data, see Sketch on page 31). If α and M_1 locate a point to the right of the dashed curve in Figure 93, then

$$\frac{St_2}{St_1} = K_1 + 0.145 \left[\left(\frac{P_3}{P_1} \right) - \left(\frac{P_3}{P_1} \right)_B \right]$$

For a given Mach number, M_1 , the pressure ratio $(P_3/P_1)_B$ corresponds to the value of $\alpha (= \alpha_B)$ at the intersection of the dashed line with a solid line. $(P_3/P_1)_B$ can be found directly from Figure 83 or by determining the pressure ratio in Figure 89 which corresponds to α_B and M_1 .

Step 5: Calculate h_2 from:

$$h_2 = h_1 \left(\frac{St_2}{St_1} \right) \left(\frac{(\rho u)_2}{(\rho u)_1} \right) \left[\frac{BTU}{ft^2 \sec^{\circ}R} \right]$$

Step 6: Sketch the h_T distribution from κ_1 to the peak value h_2 at κ_2 according to Figure 94 as follows: Extend the upstream value of h 15% of $\Delta \kappa$ downstream of κ_1 ; locate κ_2 25% of $\Delta \kappa$ upstream of κ_3 ; connect the two points, (κ_1, h_1) and (κ_2, h_2) , by a straight line. Then extend the peak value, h_2 , downstream to κ_3 where the downstream decay will begin.

NORTH AMERICAN AVIATION, INC.

COLUMBUS DIVISION
COLUMBUS 16, OHIO

NA 62H-795

Step 7: From Figure 95 determine the downstream decay of the heat transfer coefficient beginning at X_3 . The rate of decay was determined from Figure 81. The isothermal heat transfer coefficient downstream of X_3 is calculated from the formula,

$$h_T = h_2 \left(\frac{St_e}{St_2} \right) \sim \frac{BTU}{Ft^2 \times Sec \times ^\circ R}.$$

Append the downstream decay of h_T to the h_T distribution obtained in Step 6 beginning at X_3 .

Step 8: Calculate the recovery temperature $T_R/T_T = \frac{(1 + 0.2 \eta M_1^2)}{(1 + 0.2 M_1^2)}$ with $\eta = 0.89$ where T_T represents the freestream stagnation temperature. Use this T_R all the way through and downstream of the interaction.

Step 9: Calculate $Q/A = h_T (T_w - T_R) \sim BTU/Ft^2 \times sec$ using the h_T distribution obtained.

A. EXAMPLE CALCULATION

Known conditions: $M_1 = 4.77$, $\delta_1 = 0.34"$, $Re = 3.32 \times 10^5/in.$,

$X_{sh} = 10.7"$ from leading edge, $P_3/P_1 = 7.25$ (for $\alpha = 11^\circ$)

Step 1: From Figure 89 or 76, $\alpha = 11^\circ$ and $M_1 = 4.77$, it is inferred that $P_3/P_1 = 8.25$. However, due to the expansion from the shock generator trailing edge the peak pressure ratio is reduced to a value of 7.25 (see Figure 43). Use Figure 91 (assuming type of transition, forced or natural, is not known) to obtain ΔX .

With $\frac{P_3/P_1}{\sqrt{M_1^2 - 1} \sqrt{Re} \times 10^{-4}} = 1.22$ Figure 91 gives, $\frac{\Delta X}{\delta_1} = 14.4$

So, $\Delta X = 4.9$ in.

Step 2: With $\sqrt{R_{s_1}} \frac{p_{y_{p_1}} - 1}{\sqrt{M_1^2 - 1}} = 4.46$ Figure 92 gives,

$$\frac{X_{sh} - X_1}{\Delta X} = 0.325$$

So, $X_1 = 10.7 - (0.325 \times 4.9) = 9.1$ in. from leading edge.

$$X_3 = X_1 + \Delta X = 14.0 \text{ in.}$$

Steps 3 and 4: Figures 93 and 89 or 76 gives the peak value

$$\frac{St_2}{St_1} = \begin{cases} 1.8 & \text{conservative experimental value} \\ 1.6 & \text{average experimental value} \end{cases} \quad \text{and} \quad \frac{(pU)_3}{(pU)_1} = 3.5$$

Step 5: The theoretical value of h_1 (from Table III) for this test run at $X = 9.0$ " was $h_1 = 2.2 \times 10^{-3}$ (BTU/ft² x sec x °R).

$$\text{Therefore, } h_2 = h_1 \left(\frac{St_2}{St_1} \right) \left[\frac{(pU)_3}{(pU)_1} \right] = 2.2 \times 10^{-3} \times 1.8 \times 3.5$$

$$= 13.9 \times 10^{-3} \left(\frac{\text{BTU}}{\text{ft}^2 \times \text{sec} \times \text{OR}} \right) \text{ is a conservative estimate}$$

of the peak heat transfer coefficient and $h_2 = 2.2 \times 10^{-3} \times 1.6 \times 3.5 = 12.3 \times 10^{-3} \left(\frac{\text{BTU}}{\text{ft}^2 \times \text{sec} \times \text{OR}} \right)$ represents an average value which shows better agreement with the present data.

Step 6: See Figure 96 for the sketch of the h_T distribution and comparison with the experimental distribution.

Step 7: In Figure 96 h_T downstream of X_3 was calculated using Figure 95 from the formula,

$$h_T = h_2 \frac{St_e}{St_2} = \begin{cases} 13.9 \times 10^{-3} (St_e / St_2) \\ 12.3 \times 10^{-3} (St_e / St_2) \end{cases} \text{The coordinate } X \text{ was}$$

obtained from the dimensionless coordinate in Figure 95 by using the ΔX from Step 2 and X_1 from Step 3. Note that the impingement of the expansion wave from the trailing edge of the shock generator plate tends to reduce h_T at a faster rate than would occur if no expansion were present so that comparison of the experimental h_T to the estimated is not possible beyond the expansion wave impingement point.

NORTH AMERICAN AVIATION , INC.

COLUMBUS DIVISION
COLUMBUS 16, OHIO

NA 62H-795

VI. CONCLUDING REMARKS

A. REVIEW OF SIGNIFICANT RESULTS

The most significant results found in this study are:

1. The isothermal heat transfer coefficient, h_r , on the undisturbed test plate may be accurately predicted by the theory of Reference (7), even though the use of grit and air injection into the boundary layer gives measured values of momentum thickness, Θ , considerably different from Θ predicted by the theory of Reference (7). The insensitivity of h_r to Θ predicted by theory appears valid.
2. In Figures 71 and 72 plots are given of pressure interaction length, Δx , as a function of other parameters which characterize the flow. The data correlate along straight lines with each line indicative of the method of inducing transition. From these figures the following observations are noted:
 - (a) Artificial methods of inducing transition yield a boundary layer with a turbulent structure which is different from the mechanism in "naturally" turbulent flow.
 - (b) Moderate amounts of air injection into a boundary layer do not alter its turbulent structure. Thus, if air injection or blowing thickens a turbulent boundary layer, then its subsequent behavior will be as if the thickening was the result of a longer run of an undisturbed, zero pressure gradient, turbulent flow.
3. The adiabatic wall temperature, T_{AW} , and the effective recovery temperature, T_R , are approximately, but not exactly, the same quantity. (Note: T_R is the temperature at which the local heat transfer rate is zero.) The average value of T_R and T_{AW} in a shockwave boundary layer interaction region are nearly equal but the variations in T_R are between wider limits than is found for T_{AW} .

NORTH AMERICAN AVIATION , INC.

COLUMBUS DIVISION
COLUMBUS 16, OHIO

NA 62H-795

4. At Mach 5 for the cases of shock impingement on the test plate, a "blip" was found in the recovery factor, η , distribution. (Note: η is proportional to T_{aw}). This blip is similar to the results obtained in Reference (11) with two-dimensional roughness elements.
5. The peak in the heat transfer coefficient occurs upstream of the end of the pressure interaction region. The zero pressure gradient value of heat transfer coefficient is maintained a short distance downstream of the beginning of the pressure interaction. The heat transfer coefficient then rises monotonically (except perhaps over a very small distance) to the peak value.
6. The Stanton number ratio, St_e/St_i , is defined as the ratio of the Stanton number based on local flow conditions external to the boundary layer to the zero pressure gradient Stanton number. The local conditions external to the boundary layer may be estimated from the static pressure distribution on the test plate. Plots have been made of St_e/St_i versus $\frac{\kappa - \kappa_i}{\Delta \kappa}$, where κ_i is the station at which the pressure interaction begins and $\Delta \kappa$ is the length of the pressure interaction. All of the appropriate data obtained in the present tests show qualitatively similar distributions downstream of κ_i . Immediately downstream of κ_i , St_e/St_i decreases to a value less than unity. Then the Stanton number ratio increases rapidly and usually reaches a peak in the vicinity of $\frac{\kappa - \kappa_i}{\Delta \kappa} = .75$. For all of the present data the peak in St_e/St_i is between 1.5 and 1.8. The decay of St_e/St_i downstream of the peak is fairly slow with St_e/St_i remaining well above unity for those tests in which the expansion from the trailing edge of the shock generator plate did not have a strong influence on the test plate static pressure distribution.

NORTH AMERICAN AVIATION, INC.

COLUMBUS DIVISION
COLUMBUS 16, OHIO

NA 62H-795

7. The results reported in the literature of heat transfer tests on reattaching separated boundary layers in a two-dimensional flow field reveal an interesting qualitative similarity to the present experiments; viz., (1) in the separated zone the Stanton number ratio is below unity and then peaks in the region of reattachment, and (2) the recovery factor based on local conditions, η_a , in and downstream of the separated region is less than the zero pressure gradient value.
8. Based on the present data and the few published heat transfer measurements in the interaction region of a shockwave and a turbulent boundary layer, it is suggested that the Stanton number ratio at the peak, $\overline{St}_2/\overline{St}_1$, has the following form,

$$\frac{\overline{St}_2}{\overline{St}_1} = \begin{cases} K_1 & \text{for } P_2/P_1 < (P_2/P_1)_B \\ K_1 + K_2 \left(\frac{P_2}{P_1} - (P_2/P_1)_B \right) & \text{for } \frac{P_2}{P_1} > (P_2/P_1)_B \end{cases}$$

where P_2/P_1 is the static pressure ratio across the interaction for a given Mach number, and $(P_2/P_1)_B$ is the pressure ratio which corresponds to the "elbow" in the curve of mass flow ratio versus pressure ratio (e.g., see Figure 83). K_1 and K_2 are approximately constant with $K_1 \approx 1.4$ to 1.8 and $K_2 \approx 0.145$.

9. A correlation of the ratio of the transformed momentum thickness across the heat transfer interaction region, Θ_{n2}/Θ_{n1} , appears feasible. The values of the ratio fall into roughly three groups characterized by attached, incipient and separated flow conditions. The indirect calculation of Θ_{n2}/Θ_{n1} from the present data utilizing many assumptions indicates a decrease in the Reynold's analogy factor across the interaction region. This is in qualitative agreement with the observed decrease in the experimental local recovery factor across the interaction region.

B. RECOMMENDATIONS FOR FURTHER STUDY

The discussion in the preceding sections indicate that certain aspects concerning the interaction of a turbulent boundary layer with a shockwave require further study. First, in Section IV-A it was pointed out that gross effects on the pressure interaction length correlations are due to the method of inducing transition (natural or artificial) and that different boundary layer tripping techniques may induce diverse results. However, boundary layer blowing seemed to effectively increase the boundary layer and momentum thicknesses without introducing spurious effects into the correlations. The pressures obtained with the pitot rakes showed that no gross distortions of the velocity profile were created by employing grit and/or blowing. This implies that the time-average pressures through the boundary layer are not strongly affected. Since the boundary layer rake could not measure the laminar sublayer, the foregoing observations might be an indication that the grit introduced a long lasting disturbance into the sublayer which in turn exerted a large influence on the development of the boundary layer when disturbed by the incident shock. Therefore, it would be desirable to conduct a shockwave turbulent boundary layer test in which various trips are employed under identical conditions. Accurate measurements should be made of the interaction length and the boundary layer velocity profiles, especially the subsonic portion, at various stations beginning immediately downstream of the trip.

In the present tests a qualitative difference in the local recovery factor distributions between Mach numbers 3 and 5 was found. At Mach 3 the recovery factor decreased somewhat through and downstream of the interaction region, but at $M_o = 5$ the local recovery factor increased to a high value near the beginning of the interaction region and then decreased to a value downstream of the interaction which was lower than the upstream value. The reasons for this rather profound difference between the $M_o = 3$ and $M_o = 5$ data are not understood. Additional experiments should be conducted in which adiabatic wall temperatures are measured. Perhaps temperature measurements made in conjunction with the tests suggested in the preceding paragraph would isolate the factors which are the primary cause of the effect.

The present data showed that the Stanton number is high at and downstream of the point where a separated turbulent boundary layer reattaches. However, Gadd in Reference (8) and Seban in Reference (18) indicate that the skin friction is low in this region. It is probable that low values of skin friction would also be found downstream of a shock-wave turbulent boundary layer interaction even if no boundary layer separation occurred. As discussed in Section IV-B the physical reason underlying the increase in Stanton number and decrease in skin friction

coefficient across the interaction region may be the result of a change in the κ distribution of the ratio of the heat to momentum eddy diffusivity, $\lambda(y)$. It was also suggested in Section IV-B that accompanying the change in $\lambda(y)$ is an overall increase in the level of turbulence in the boundary layer through the interaction. It has been shown experimentally that for increasing distance in the downstream direction, the skin friction coefficient increases and the Stanton number decreases slowly from their values at the end of the interaction. Therefore, it is expected that both the level of turbulence and $\lambda(y)$ will eventually return to the usual zero pressure gradient values. Although the measurements would be tedious and expensive, it is felt that it would be worthwhile to determine the variation in turbulence and $\lambda(y)$ in the streamwise direction through and far downstream of a shock-wave turbulent boundary layer interaction. The physical insight gained from such detailed measurements would probably allow a theoretical model of the interaction to be constructed which would have quite general application.

Certain interesting properties of the boundary layer downstream of the interaction region could be determined from measurements which are considerably simpler and less expensive to obtain than those suggested in the preceding paragraph. In particular the measurements would consist of accurately determining the heat transfer rates and the boundary layer velocity profile at numerous stations downstream of the interaction region. From this information it would be possible to determine under what conditions, if any, that the comparatively simple relationships between heat transfer coefficient, momentum thickness, Reynolds analogy factor, and distance in the streamwise direction given by Reshotko and Tucker in Reference (7) are valid downstream of a shockwave turbulent boundary layer interaction.

Of course, it would be useful to extend the range of the present types of measurements to other Mach numbers and higher pressure ratios along with variations in Reynolds number. Extending the range of pressure ratio across the interaction region is important for the verification or invalidation of the assumption utilized in the peak Stanton number formula in Section IV-B which considers the peak Stanton number to be a function of shock strength at a given Mach number.

VII. NOTATION

a	speed of sound
C_p	specific heat at constant pressure, $0.24 \frac{\text{BTU}}{\text{lb}^\circ\text{R}}$ for air
g	acceleration due to gravity, 32.2 ft/sec^2
H	boundary layer form factor (δ^*/θ) except where otherwise defined
h	heat transfer coefficient
h_T	heat transfer coefficient on a wall which is isothermal along the entire run of the boundary layer
M	Mach number
P	pressure
P_c	pressure in test plate plenum chamber
Pr	Prandtl number
Q/A	heat transfer rate per unit area
Re	Reynolds number per inch of free stream flow
Re_δ	Reynolds number based on δ
Re_θ	Reynolds number based on θ
St	Stanton number
S	Reynold's analogy factor
T	temperature
T_e	local static temperature external to the boundary layer,
T_R	"effective" recovery temperature, see Figure 16

NORTH AMERICAN AVIATION , INC.

COLUMBUS DIVISION
COLUMBUS 16, OHIO

NA 62H-795

T_w	average temperature of nichrome heater elements with power turned on, i.e., $T_w = \frac{1}{n} \sum_{i=1}^n T_{wi}$
T_i	static temperature upstream of the interaction, $\frac{T_r}{(1+0.2M_i^2)}$
U	velocity in the free-stream direction
x	distance along test plate measured from leading edge
y	vertical distance above surface of test plate
α	flow turning angle - angle of shock generator plate
δ	boundary layer thickness
ϵ_H	eddy diffusivity for heat
ϵ_M	eddy diffusivity for momentum
η	recovery factor based on local adiabatic wall temperature and T_i , $\frac{T_{aw} - T_i}{T_r - T_i}$
η_e	local recovery factor, $\frac{T_{aw} - T_e}{T_r - T_e}$
η_R	recovery factor based on T_R and T_i , $\frac{T_R - T_i}{T_r - T_i}$
θ	momentum thickness
θ_h	transformed momentum thickness, $\frac{\theta}{(1 + \frac{\gamma-1}{2} M_\infty^2)^3}$
λ	ratio of eddy diffusivities, ϵ_H/ϵ_M
μ	coefficient of viscosity
ν	coefficient of kinematic viscosity
ρ	density

NORTH AMERICAN AVIATION , INC.

COLUMBUS DIVISION
COLUMBUS 16, OHIO

NA 62H-795

SUBSCRIPTS

T	stagnation conditions
e	condition at edge of boundary layer
t_e	transformed to incompressible plane
i	related incompressible value
$_{ref}$	evaluated at reference condition
o	free-stream value upstream of test plate
P	x location at which boundary layer was probed
sh	refers to incident shock
AW	adiabatic wall
1	condition at beginning of pressure interaction region or the condition for the case of no interaction
2	condition at x location where peak heat transfer coefficient or peak Stanton number ratio occurs
3	In referring to experimentally determined values, the subscript represents quantities evaluated at the location of the experimental peak in the static pressure distribution on the test plate. In cases pertaining to a reflected shockwave in inviscid flow the subscript refers to the theoretical static conditions downstream of the reflection.

NORTH AMERICAN AVIATION, INC.

COLUMBUS DIVISION
COLUMBUS 16, OHIO

NA 62H-795

VIII. REFERENCES

1. Simon, W. E., "An Experimental Investigation and Correlation of the Effects of Boundary Layer Bleed on Shockwave-Turbulent Boundary Layer Interaction", North American Aviation, Inc., Report NA 60H-401, Appendix III, 1960
2. Bogdonoff, S. M., Kepler, C. E., Sanlorenzo, E., "A Study of Shock Wave Turbulent Boundary Layer Interaction at $M = 3$," Princeton Univ., Dept. Aero. Engr. Report No. 22, July 1953
3. Larson, H. K., "Heat Transfer In Separated Flows," Jour. of the Aero. Sci., Vol. 26, No. 11, Nov. 59
4. Seban, R. A., Doughty, D. L., "Heat Transfer to Turbulent Boundary Layers With Variable Free Stream Velocity", Trans. ASME, Vol. 78, No. 1, Jan. 56.
5. Conti, R. J., "Heat Transfer Measurements at a Mach Number of 2 In The Turbulent Boundary Layer on a Flat Plate Having a Stepwise Temperature Distribution", NASA TN D-159, Nov. 1959
6. Kuehn, D. M., "Experimental Investigation of the Pressure Rise Required For The Incipient Separation of Turbulent Boundary Layers In Two-Dimensional Supersonic Flow", NASA MEMO 1-21-59A, Feb. 1959
7. Reshotko, E. and Tucker, M., "Approximate Calculation of the Compressible Turbulent Boundary Layer With Heat Transfer and Arbitrary Pressure Gradient", NACA TN 4154, Dec. 1957.
8. Gadd, G. E. and Holder, D. W., "The Behaviour of Supersonic Boundary Layers In The Presence of Shock Waves", I.A.S. Preprint No. 59-138, Presented at the Seventh Anglo-American Aeronautical Conference, New York, New York, 1959.
9. Chapman, D. R., Kuehn, D. M. and Larson, H. K., "Investigation of Separated Flows In Supersonic and Subsonic Streams With Emphasis on the Effect of Transition", NACA TN 3869, March 1957
10. Brinich, P. F., "Recovery Temperature, Transition, and Heat Transfer Measurements at Mach 5", NASA TN D-1047, August 1961.

NORTH AMERICAN AVIATION , INC.

COLUMBUS DIVISION
COLUMBUS 18, OHIO

NA 62H-795

11. Brinich, P. F., "Recovery Temperatures and Heat Transfer Near Two-Dimensional Roughness Elements at Mach 3.1", NACA TN 4213, Feb. 1958.
12. Gadd, G. E. and Cope, W. F. and Attridge, J. L., "Heat Transfer and Skin Friction Measurements at a Mach Number of 2.44 For a Turbulent Boundary Layer on a Flat Surface and In Regions of Separated Flow", British A.R.C. 20, 472, Oct. 1958.
13. Erdos, J., Pallone, A., "Shock-Boundary Layer Interaction and Flow Separation", Proceedings of the 1962 Heat Transfer and Fluid Mech. Inst., June 1962.
14. Cohen, N. B., "A Method For Computing Turbulent Heat Transfer In the Presence of a Streamwise Pressure Gradient For Bodies In High Speed Flow", NASA Memo 1-2-59L, March 1959.
15. Naysmith, A., "Heat Transfer and Boundary Layer Measurements In A Region of Supersonic Flow Separation and Reattachment", British R.A.E. Tech Note No. Aero. 2558, May 1958.
16. Becker, J. V. and Korycinski, P. F., "Heat Transfer and Pressure Distribution at a Mach Number of 6.8 On Bodies With Conical Flares and Extensive Flow Separation", NASA TN D-1260, April 1962.
17. Schaefer, J. W. and Ferguson, H., "Investigation of Separation and Associated Heat Transfer and Pressure Distribution on Cone-Cylinder-Flare Configurations at Mach Five", A.R.S. Journal, Vol. 32, No. 5, May 1962.
18. Seban, R. A., "Heat Transfer and Flow With Separated and Reattached Boundary Layers as Produced by Surface Irregularities", WADC Tech. Report 56-217, Astia Document No. AD-110447, May 1956.
19. Myers, G. E., Schauer, J. J. and Eustis, R. H., "The Plane Turbulent Wall Jet, Part II Heat Transfer", Thermosciences Division, Dept. of Mech. Engr., Stanford Univ., Report No. 2 Dec. 1961.
20. Brinich, P. F. and Sands, N., "Effect of Bluntness on Transition for a Cone and Hollow Cylinder at Mach 3.1", NACA TN 3979, May 1957.
21. Bradshaw, P. and Gee, M. T., "Turbulent Wall Jets with and without an External Stream", British ARC 22008, F.M. 2971, 1960.

NORTH AMERICAN AVIATION , INC.

COLUMBUS DIVISION
COLUMBUS 16, OHIO

NA 62H-795

22. Van Driest, E. R., "Turbulent Boundary Layers In Compressible Fluids", Jour. of Aero. Sci., Vol. 18, No. 3, March 1951.

NORTH AMERICAN AVIATION, INC.

COLUMBUS DIVISION
COLUMBUS 16, OHIO

NA 62H-795

APPENDIX A

NOTES ON THE Θ_{a1}/Θ_{a1} CORRELATION OF SECTION IV-D

If it is assumed that the Stanton number, St_1 , corresponding to the peak heat transfer coefficient, and the location of the peak, κ_1 , can be estimated by a method such as the procedure outlined in Section V, then the transformed momentum thickness, Θ_{a1} , at κ_1 can be obtained from the correlation shown in Figure 88. According to the assumptions stated in Section IV-D the Stanton number variation downstream of κ_1 can be calculated from a knowledge of Θ_{a1} as long as the κ dependence of Θ_a and the Reynolds analogy factor, S , can be obtained. Equation (3) in Section IV-D evaluated at $\kappa = \kappa_1$ is

$$St_1 = \frac{f(T_r, M_{a1}, T_w, T_{aw1})}{[S_1 \Theta_{a1}^{0.268}]} \quad (5)$$

where $f = \frac{0.123 \exp. [-1.561 H_{1,SP}]}{\left(\frac{T_r}{T_a}\right)^{0.268} \left(\frac{M_a a_r}{V_r}\right)^{0.268} \left(\frac{T_{ref}}{T_a}\right)^{0.732}}$

In general, conditions external to the boundary layer at κ_1 will not be known since the present data shows that the peak heating occurs somewhat before the wall pressure gradient vanishes at κ_1 .

Calculations employing Equation (5) (using theoretical downstream conditions for f , $S_1 = 0.690 \times 0.791 = 0.546$, and Θ_{a1} determined by the correlation in Figure 88) gave values for h_1 which were within 20% of the experimental values obtained in the present tests for all data runs except the $\alpha = 60^\circ$, $M_1 = 2.98$, and $h_w/p_w = 1$ run where the calculated h_1 was 52% higher than the experimental value. Although the estimate of h_1 from Equation (5) using the theoretical downstream conditions gave a poor estimate only in the one case mentioned above, it is felt that the simpler Stanton number correlation of Section IV-B should yield more consistent results in estimating h_1 . Equation (5) can then be

NORTH AMERICAN AVIATION, INC.

COLUMBUS DIVISION
COLUMBUS 16, OHIO

NA 62H-795

used in the following way to obtain Stanton number or heat transfer coefficient downstream of the peak heating point. Rewriting Equation (5) as;

$$\frac{h_T}{g C_p (\rho u)_e} = St(x) = \frac{\tau f(T_r, M_{e3}, T_w, T_{aw3})}{[S(x) \Theta_h(x)]} \quad \text{for } x > x_2 \quad (6)$$

where τ is a constant evaluated in Step 5 below and f is evaluated using the theoretical conditions in the inviscid flow downstream of the interaction, and $T_{aw3} \approx T_{aw1}$

The proposed method is as follows:

1. Find St_2 and x_2 by the procedures given in Section V.
2. For the given incident shock strength and M_1 , find Θ_{h2}/Θ_{h1} from the Θ_h correlation in Figure 88.
3. Calculate Θ_{h1} from a theory such as that of Reference (7).
4. Calculate $\Theta_{h2} = \left(\frac{\Theta_{h2}}{\Theta_{h1}} \right) \times \Theta_{h1}$.
5. Evaluate Equation (6) at $x = x_2$ using $S_2 = 0.690 S_1 \approx 0.546$ Θ_{h2} , $f(T_r, M_{e3}, T_w, T_{aw1})$ and St_2 to obtain τ . τ is the constant which brings both sides of Equation (6) into agreement at $x = x_2$.
6. With τ known, use Equation (6) with $S(x)$, $\Theta_h(x)$ to calculate $St(x)$ for $x \geq x_2$.

At present $S(x)$, $\Theta_h(x)$ for $x \geq x_2$ are not known. One would intuitively expect $S(x)$ to change from the value S_2 to its value for a normal turbulent boundary layer ($\approx \rho r^{2/3}$) at some distance downstream where the velocity profiles have filled out to normal turbulent profiles. Concerning $\Theta_h(x)$, the present boundary layer rake data at $M_1 = 2.98$ and the probe data from Reference (1) used in this report were examined briefly to determine the order of magnitude of the x dependence of Θ_h . The distance in the

NORTH AMERICAN AVIATION , INC.

COLUMBUS DIVISION
COLUMBUS 16, OHIO

NA 62H-795

streamwise direction between κ_1 and the nearest point at which the boundary layer was probed was approximately 2" in the present tests and 1.2" in Reference (1). The data indicated that for an equation of the form

$$\theta_h = \theta_{h2} \left(\frac{\kappa}{\kappa_1} \right)^N \text{ for } \kappa > \kappa_1$$

N was within the limits $1 < N < 3$. Since the κ separation used was of the order of $\Delta\kappa$, N could be greater than 3 near κ_1 . It is expected that $N(\kappa)$ will decrease with increasing κ from its large initial value at κ_1 as the velocity profile is restored. If $N(\kappa)$ could be determined, $S(\kappa)$ could probably be given an average value and $S(\kappa)$ for $\kappa > \kappa_1$ could be calculated from Equation (6) for comparison with experimental values. The present data give only limited information concerning the downstream decay of heat transfer since expansion waves from the trailing edge of the generator plate usually interfered with the heat transfer measurements a short distance downstream from κ_1 . In the present tests the greatest distance between κ_1 and the point where the expansion wave from the generator plate struck the boundary layer was about 10 upstream boundary layer thicknesses.

NORTH AMERICAN AVIATION, INC.

COLUMBUS DIVISION
COLUMBUS 16, OHIO

NA 62H-795

Table I

LIST OF DATA RUNS AND RUN PARAMETERS

Number	M_0	M_1	P_n/ρ_e	α (Degrees)
1	2.95	2.98	1.0	6
2	↓	↓	5.9	6
3			1.0	9.5
4			5.9	9.5
5			1.0	12
6			2.0	12
7			5.9	12
8	5.02	4.77	4.05	7.4
9	↓	↓	3.9	9.7
10			8.4	9.7
11			4.05	11
12			6.96	11
13			9.5	11
14			4.9	12
15			9.6	12
16	2.95	2.98	1.0	0
17	↓	↓	5.9	0
18			1.0	generator out
19			2.0	generator out
20	5.02	4.77	3.7	0
21	↓	↓	4.2	0
22			4.0	generator out
23			9.1	generator out
24			1.5	10
25			1.4	11

Table II
DATA USED IN THE INTERACTION LENGTHS AND TRANSFORMED MOMENTUM THICKNESS CORRELATIONS

Present Data	α (Deg.)	M_i	ρ_m/ρ_c	P_T (lbs/in ²)	T_T (°R)	R_a (Per in.)	x_i (Inches)	Δx (Inches)	P_3/P_1	δ (*) (Inches)	$\Theta \times 10^3$ (*) (Inches)	δ_i (†) (Inches)
1	6	2.98	1.0	50	573	6.04×10^5	12	1	2.39	0.13	5.26-5.66	0.16
2	6	↓	5.9	50	570	↓	12	1	2.35	0.19	12.7-13.7	0.24
3	9.5	↓	1.0	49.8	570	↓	11.4	2.4	3.46	0.13	5.26-5.66	0.16
4	9.5	↓	5.9	49.9	575	↓	11	2.75	3.56	0.19	12.7-13.7	0.22
5	12	↓	1.0	48.6	573	↓	10	4.0	5.50	0.13	5.26-5.66	0.14
6	12	↓	2.0	50	575	↓	9.7	4.3	5.25	0.16	10.0-7.0	0.17
7	12	↓	5.9	50.6	570	↓	9.9	4.1	5.25	0.19	12.7-13.7	0.21
8	7.4	4.77	4.05	64	570	3.32×10^5	10.75	2.25	4.15	0.33	15 → 16.2	0.38
9	9.7	↓	3.9	63.8	565	↓	10.25	3.75	5.86	0.33	15 → 16.2	0.37
10	9.7	↓	8.4	63.8	568	↓	10.25	3.75	6.16	0.35	15.3-16.9	0.39
11	11	↓	4.05	64	565	↓	9.25	4.75	7.22	0.33	15 → 16.2	0.34
12	11	↓	6.96	64.2	565	↓	9.25	4.75	7.25	0.34	15 → 16.7	0.35
13	11	↓	9.5	63.9	566	↓	9.5	4.5	6.81	0.35	15.3-17.0	0.37
14	12	↓	4.9	63.8	560	↓	8.5	5.0	8.41	0.33	15 → 16.2	0.32
15	12	↓	9.6	63.7	568	↓	8.25	5.25	8.47	0.35	15.3-17.0	0.33

(*) Found from measurements from forward rake located at $x = 9$ inches - the last values of Θ were used in the calculations.

(†) $\delta_i = \delta$ adjusted for distance from $x = 9$ inches to x_i , using an x dependence of $x^{0.2}$ for δ .

NORTH AMERICAN AVIATION , INC.

COLUMBUS DIVISION
COLUMBUS 10, OHIO

NA 62H-795

Table II - CONTINUED

Present Data	(*) $\Theta, \times 10^3$ (Inches)	(*) $R_e \times 10^{-4}$	(Inches) κ_2	(*) $h_1 \times 10^3$ $\frac{\text{BTU}}{\text{ft}^2 \text{sec}^0 \text{R}}$	(*) $h_2 \times 10^3$ $\frac{\text{BTU}}{\text{ft}^2 \text{sec}^0 \text{R}}$	P_2/P_1	α_2 (Deg.)	M_2	T_2/T_1	$\frac{(g u)_2}{(g u)_1}$	P_{T2}/P_{T1}	(*) ST_2/ST_1
1	7.17	9.94	12.9	9.0	25	2.34	6.0	2.42	1.284	1.67	0.983	1.66
2	17.3	14.5	12.9	9.0	22	2.29	5.8	2.43	1.277	1.65	0.985	1.48
3	6.88	9.55	13.3	9.4	30	3.40	9.0	2.16	1.442	2.05	0.951	1.56
4	16.1	13.5	13.3	9.8	31	3.48	9.2	2.14	1.450	2.08	0.948	1.53
5	6.19	8.57	13.4	9.5	39	4.74	11.95	1.91	1.610	2.41	0.905	1.71
6	7.45	10.3	13.4	9.5	36	4.50	11.50	1.95	1.580	2.35	0.914	1.61
7	14.3	12.4	13.4	10	36	4.46	11.42	1.96	1.579	2.34	0.915	1.54
8	18.7	12.7	13.0	2	9.4	4.15	6.9	3.62	1.560	2.52	0.979	1.86
9	18.1	12.2	12.8	1.9	10.7	5.46	8.4	3.40	1.711	2.97	0.884	1.85
10	18.8	12.9	12.8	2.0	10.7	5.70	8.67	3.36	1.740	3.05	0.875	1.85
11	16.6	11.2	12.8	2.0	12.1	6.76	9.68	3.22	1.842	3.39	0.837	1.79
12	17.1	11.6	12.8	1.8	10.9	6.78	9.7	3.21	1.846	3.40	0.836	1.78
13	17.8	12.1	13.0	1.8	10.2	6.21	9.1	3.29	1.790	3.22	0.857	1.76
14	15.5	10.5	12.8	1.8	13.3	8.22	10.95	3.04	1.980	3.77	0.789	1.96
15	15.8	10.8	12.8	1.7	12.3	8.14	10.90	3.05	1.971	3.75	0.790	1.93

(*) $\Theta_1 = \Theta$ adjusted for distance from $\kappa = 9$ inches to κ_1 using an κ dependence of $\kappa^{1.75}$ for Θ .

(†) Experimentally determined values utilizing a faired curve in the h versus κ plots when data scatter was erratic.

(‡) These values of peak Stanton number ratio differ somewhat from those found in Figures 77-80. This is due to a somewhat arbitrary method of fairing the pressure and heat transfer data to obtain the numbers used in this table.

NORTH AMERICAN AVIATION, INC.

COLUMBUS DIVISION
COLUMBUS 16, OHIO

NA 62H-795

Table II - CONTINUED

Present Data	T_w Used In Calculations (°R)	T_{aw1} (°R)	T_{aw2} (°R)	$\theta_{h1} \times 10^4$ (Inches)	θ_{h2}/θ_w <small>with $T_{w1} = T_{w2}$ $[\frac{T_{w1}}{T_{w2}}] = 4$</small>	Flow Attached, Incipient, or Separated
1	577	527	527	3.36	1.74	Att.
2			527	8.10	2.50	Att.
3				3.22	3.73	Just Below Inc.
4				7.53	4.16	Inc.
5				2.90	4.84	Sep.
6				4.26	5.12	Sep.
7				6.91	5.92	Sep.
8		525	520	1.10	2.56	Att.
9		525		1.05	4.12	Just Below Inc.
10		525		1.10	4.56	Just Below Inc.
11		526		0.970	6.84	Just Above Inc.
12		526		0.990	6.92	Just Above Inc.
13		526		1.04	6.40	Just Above Inc.
14		528		0.905	7.08	Sep.
15		529		0.926	7.32	Sep.

(*) At $M_1 = 4.77$, directly measured with thermocouples; at $M_1 = 2.98$, found approximately from extrapolated plot of heat flux versus T_w .

(†) Calculated from θ , and M_1 .

(††) Calculated from h_1, h_2 , and Equation (4).

NORTH AMERICAN AVIATION, INC.

COLUMBUS DIVISION
COLUMBUS 16, OHIO

NA 62H-795

Table II - CONTINUED

	α (Deg.)	M_i	P_T Lb/in ²	T_T (Approx.) (°R)	$Re \times 10^{-5}$ (Per in.)	x_i (Inches)	Δx (Inches)	β/p_i	δ (Inches)	$\theta \times 10^3$ (Inches)	x_p (Inches)
Data From Reference (1)	1	3.06	57.9	590	6.00	13.90	0.75	2.08	0.152	9.88	13.00
	2	3.07	58.0	590	6.00	13.60	1.30	2.91	0.159	10.0	13.00
	3	2.27	43.3	577	6.89	13.25	1.65	2.56	0.155	11.2	13.00
	4	2.72	57.8	590	7.25	13.50	1.65	3.07	0.132	8.99	13.00
	5	2.27	42.8	577	6.89	13.25	1.90	2.91	0.142	10.2	13.00
	6	2.35	46.7	577	7.40	13.25	1.90	2.92	0.132	9.33	13.25
	7	2.33	46.7	577	7.40	12.75	2.90	3.54	0.125	9.10	12.50
Data From Reference (6)	8	2.93				4.40	0.77	3.02	0.097	6.20	5.23
	9	2.96				4.30	0.92	3.32			
	10	2.99				4.25	1.05	3.58			
	11	3.00				4.20	1.11	3.70			
	12	3.03				4.15	1.19	4.00			
	13	3.06				4.05	1.30	4.35			
	14	3.09				3.90	1.45	4.77			
Data From Reference (2)	15	2.97			12.4 (Approx.)	-0.30	0.75	2.73	0.16	8.62	-0.7
	16					-0.30	0.80	2.97			
	17					-0.40	0.85	3.22			
	18					-0.65	1.45	3.93			
	19					-0.70	1.56	4.07			

(*) Found from measurements by probe at x_p

(†) Distance from coordinate origin at which boundary layer upstream of interaction was probed: $x_i \neq x_p$ in general.

NORTH AMERICAN AVIATION, INC.

COLUMBUS DIVISION
COLUMBUS 16, OHIO

NA 62H-795

Table II - CONTINUED

	δ_1 (Inches)	$\theta_1 \times 10^3$ (Inches)	$R_{15} \times 10^{-4}$	κ_2 (Inches)	$\theta_2 \times 10^3$ (Inches)	$\theta_N \times 10^4$ (Inches)	$\theta_{N2} \times 10^4$ (Inches)	M_2 (Measured by Probe)	M_3 (Measured by Probe)	Flow Attached, Incipient, or Separated
Data From Reference (1)										
1	0.160	10.4	9.60	14.40	9.95	4.41	8.41	2.53	2.59	Att.
2	0.161	10.4	9.66	14.40	10.4	4.35	11.0	2.36	2.35	Att.
3	0.157	11.3	10.8	14.40	15.7	13.5	41.9	1.69	1.72	Att.
4	0.136	9.29	9.86	15.15	15.2	6.09	27.6	1.96	1.96	Inc.
5	0.144	10.3	9.92	14.40	20.0	12.3	59.9	1.66	1.63	Sep.
6	0.132	9.33	9.77	14.65	18.7	10.0	50.1	1.64	1.64	Sep.
7	0.127	9.25	9.40	14.65	20.5	10.2	63.3	1.55	1.57	Sep.
Data From Reference (2)										
8	0.084	5.38	5.2			2.87				Att.
9	0.083	5.29	5.1			2.82				Att.
10	0.082	5.23	5.1			2.79				Att.
11	0.081	5.19	5.0			2.76				Inc.
12	0.080	5.13	5.0			2.74				Sep.
13	0.079	5.03	4.9			2.68				Sep.
14	0.076	4.87	4.8			2.60				Sep.
Data From Reference (2)										
15	0.16	8.62	19.9 (Approx.)			4.09				Att.
16										Att.
17										Inc.
18				+0.4	10.3		20.1	1.90	2.00	Sep.
19										Sep.

(*) δ_1, θ_1 are δ and θ adjusted for distance from κ_p to κ_1 .

(†) Approximate distance from leading edge at which, as inferred from present data, heat transfer would be expected to peak. κ_2 had to be chosen at a location where a probe measurement of $\theta(-\theta_2)$ had been made so the approximation to κ_2 was further worsened.

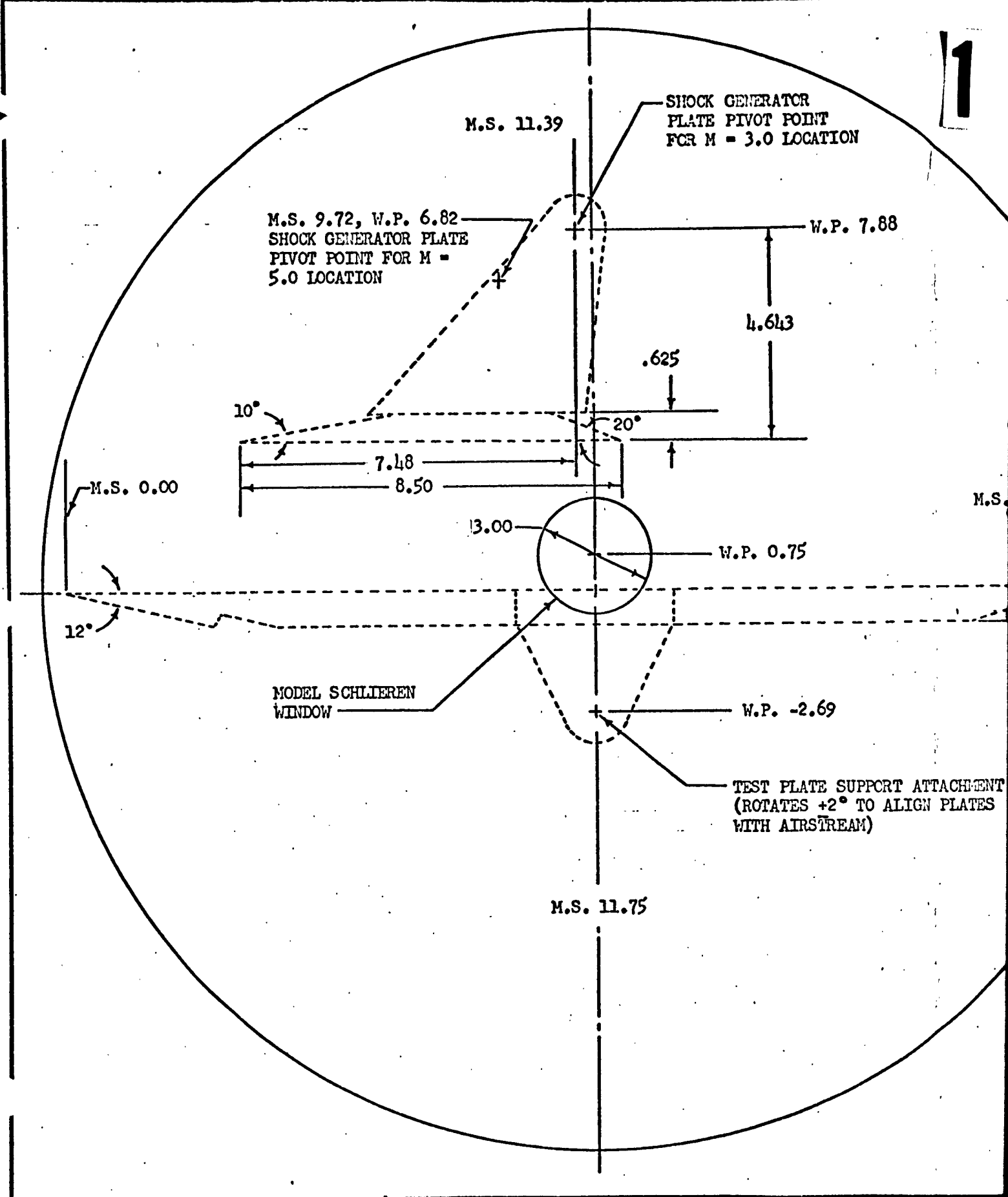
Table III

COMPARISON OF MEASURED AND THEORETICAL VALUES OF Θ_k AND h_f											
Leading Edge Condition	κ (Inches)	M_1	Measured $\Theta \times 10^3$ (Inches)	Measured $\Theta_{a,4} \times 10^4$ (Inches)	Theoretical $\Theta_{a,7} \times 10^4$ (Inches)	Theoretical $h_{f,10}^3 = \frac{C}{\Theta_{a,4}^3}$ BTU ft ² sec ³ R	$h_{f,10}^3 = \frac{C}{\Theta_{a,7}^3}$ BTU ft ² sec ³ R	Measured $h_f \times 10^3$ (Extrapolated)	T_w Used in Calculation (°R)	δ (Inches) (Per ft.)	$R \times 10^{-5}$
Present Data	9	2.98	5.26-5.66	2.65	3.84	11.5	10.4	10.1	625	0.13	6.04
			12.7	5.95	5.86	9.3	9.30	9.0		0.19	6.04
			10.0	4.68	3.84	9.9	10.4	10.0		0.16	6.04
			16.1	7.55	5.86	8.7	9.30	8.5		0.23	6.04
			12.7-13.7	6.39	3.84	9.1	10.4	10.0		0.19	6.04
$P_{re}/P_a = 3.9$ -Grit	9	4.77	15-16.2	0.947	0.355	1.66	2.15	2.0	↓	0.33	3.32
	15	4.77	16.7	0.975	0.544	1.64	1.92	1.8		0.34	3.32
$P_{re}/P_a = 9.4$ -Grit	9	4.77	15.3-17.0	0.995	0.355	1.63	2.15	2.0	↓	0.35	3.32
	15	4.77	17.3	1.01	0.544	1.63	1.92	1.8		0.36	3.32
Reference (1) No Blowing or Grit	13.00	3.06	9.88	4.41	4.79				549	0.152	6.00
	(1)										
	(2)	3.07	10.0	4.35	4.79				549	0.159	6.00
	(3)	2.27	11.2	13.52	16.4				545	0.155	6.89
	(4)	2.72	8.99	6.09	8.01				551	0.132	7.25
	(5)	2.27	10.2	12.3	16.4				545	0.142	6.89
	(6)	2.35	9.33	10.0	14.4				547	0.132	7.40
(7)	2.33	9.10	10.2	13.7				547	0.125	7.40	

Distance from leading edge of test plate at which rake or probe measurement was made.

(*)	Calculated from Θ	using M_1
1	0.0000	0.0000
2	0.0000	0.0000
3	0.0000	0.0000
4	0.0000	0.0000
5	0.0000	0.0000
6	0.0000	0.0000
7	0.0000	0.0000
8	0.0000	0.0000
9	0.0000	0.0000
10	0.0000	0.0000
11	0.0000	0.0000
12	0.0000	0.0000
13	0.0000	0.0000
14	0.0000	0.0000
15	0.0000	0.0000
16	0.0000	0.0000
17	0.0000	0.0000
18	0.0000	0.0000
19	0.0000	0.0000
20	0.0000	0.0000
21	0.0000	0.0000
22	0.0000	0.0000
23	0.0000	0.0000
24	0.0000	0.0000
25	0.0000	0.0000
26	0.0000	0.0000
27	0.0000	0.0000
28	0.0000	0.0000
29	0.0000	0.0000
30	0.0000	0.0000
31	0.0000	0.0000
32	0.0000	0.0000
33	0.0000	0.0000
34	0.0000	0.0000
35	0.0000	0.0000
36	0.0000	0.0000
37	0.0000	0.0000
38	0.0000	0.0000
39	0.0000	0.0000
40	0.0000	0.0000
41	0.0000	0.0000
42	0.0000	0.0000
43	0.0000	0.0000
44	0.0000	0.0000
45	0.0000	0.0000
46	0.0000	0.0000
47	0.0000	0.0000
48	0.0000	0.0000
49	0.0000	0.0000
50	0.0000	0.0000
51	0.0000	0.0000
52	0.0000	0.0000
53	0.0000	0.0000
54	0.0000	0.0000
55	0.0000	0.0000
56	0.0000	0.0000
57	0.0000	0.0000
58	0.0000	0.0000
59	0.0000	0.0000
60	0.0000	0.0000
61	0.0000	0.0000
62	0.0000	0.0000
63	0.0000	0.0000
64	0.0000	0.0000
65	0.0000	0.0000
66	0.0000	0.0000
67	0.0000	0.0000
68	0.0000	0.0000
69	0.0000	0.0000
70	0.0000	0.0000
71	0.0000	0.0000
72	0.0000	0.0000
73	0.0000	0.0000
74	0.0000	0.0000
75	0.0000	0.0000
76	0.0000	0.0000
77	0.0000	0.0000
78	0.0000	0.0000
79	0.0000	0.0000
80	0.0000	0.0000
81	0.0000	0.0000
82	0.0000	0.0000
83	0.0000	0.0000
84	0.0000	0.0000
85	0.0000	0.0000
86	0.0000	0.0000
87	0.0000	0.0000
88	0.0000	0.0000
89	0.0000	0.0000
90	0.0000	0.0000
91	0.0000	0.0000
92	0.0000	0.0000
93	0.0000	0.0000
94	0.0000	0.0000
95	0.0000	0.0000
96	0.0000	0.0000
97	0.0000	0.0000
98	0.0000	0.0000
99	0.0000	0.0000
100	0.0000	0.0000

(4) C and $\Theta_{4,7}$ are calculated from theory of Reference (7) using the P_T, T in Table II and $H_{c,fp} = 1.28, (P_T)^{1/3} = 0.89$.



PREPARED BY: VRP

CHECKED BY: FEW

DATE:

NORTH AMERICAN AVIATION, INC.
COLUMBUS DIVISION COLUMBUS 16, OHIO.

PAGE NO. 69 OF

REPORT NO. NA 62H-795

MODEL NO.

MODEL INSTALLATION DIAGRAM

Fig. 1

2

W.P. 7.88

MODEL END PLATES
(REPLACES TUNNEL SCHLIEREN WINDOW)

M.S. 21.38

W.P. 0.00 TUNNEL C

W.P. -0.75

,69

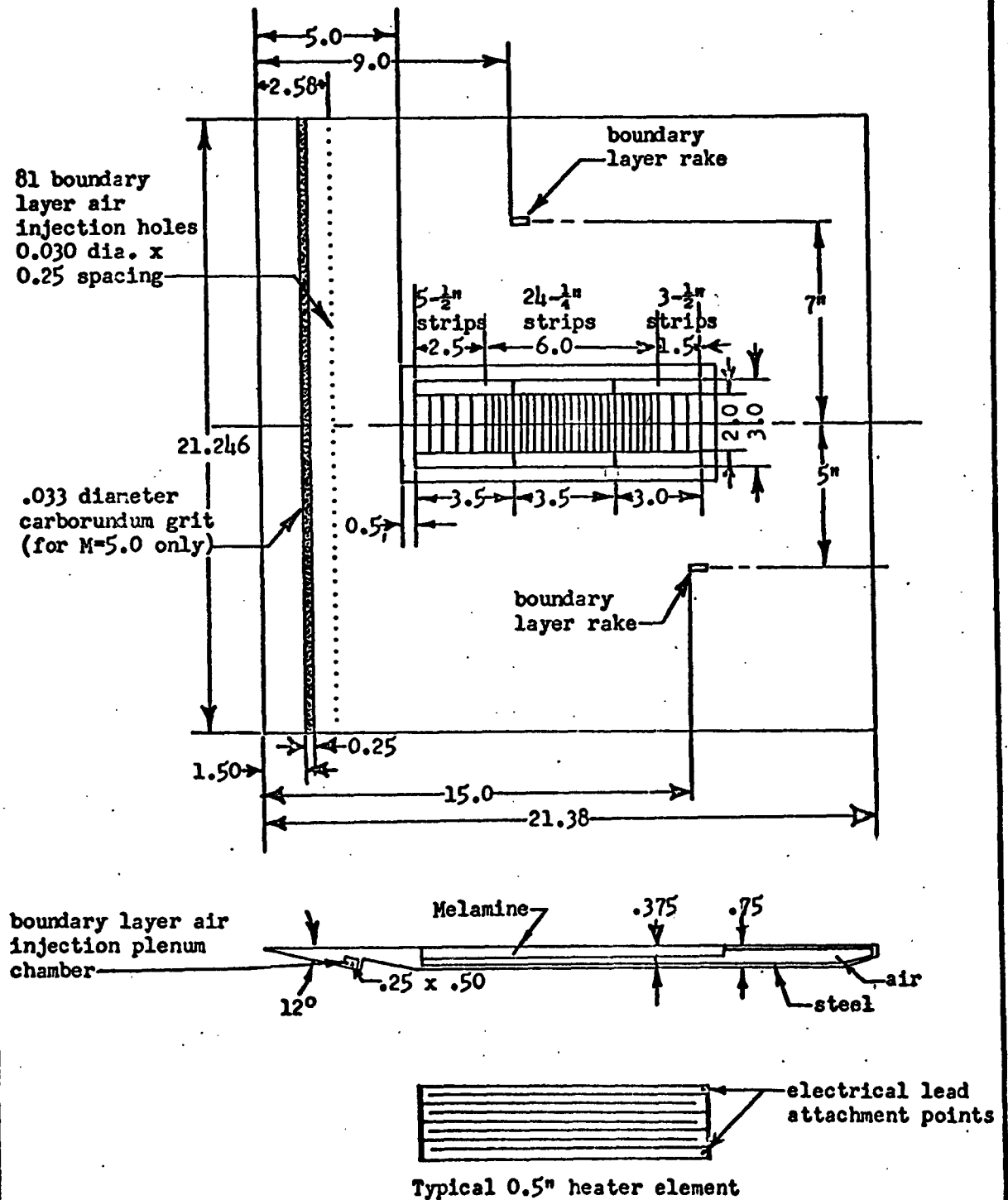
WE SUPPORT ATTACHMENT
+2° TO ALIGN PLATES
(STREAM)

NOTE: MODEL DIMENSIONS IN INCHES
UNLESS OTHERWISE NOTED.

PREPARED BY: NAW	NORTH AMERICAN AVIATION, INC. COLUMBUS DIVISION COLUMBUS 16, OHIO	PAGE NO. 70 OF
CHECKED BY: FEW		REPORT NO. NA 62H-795
DATE:		MODEL NO.

Fig. 2

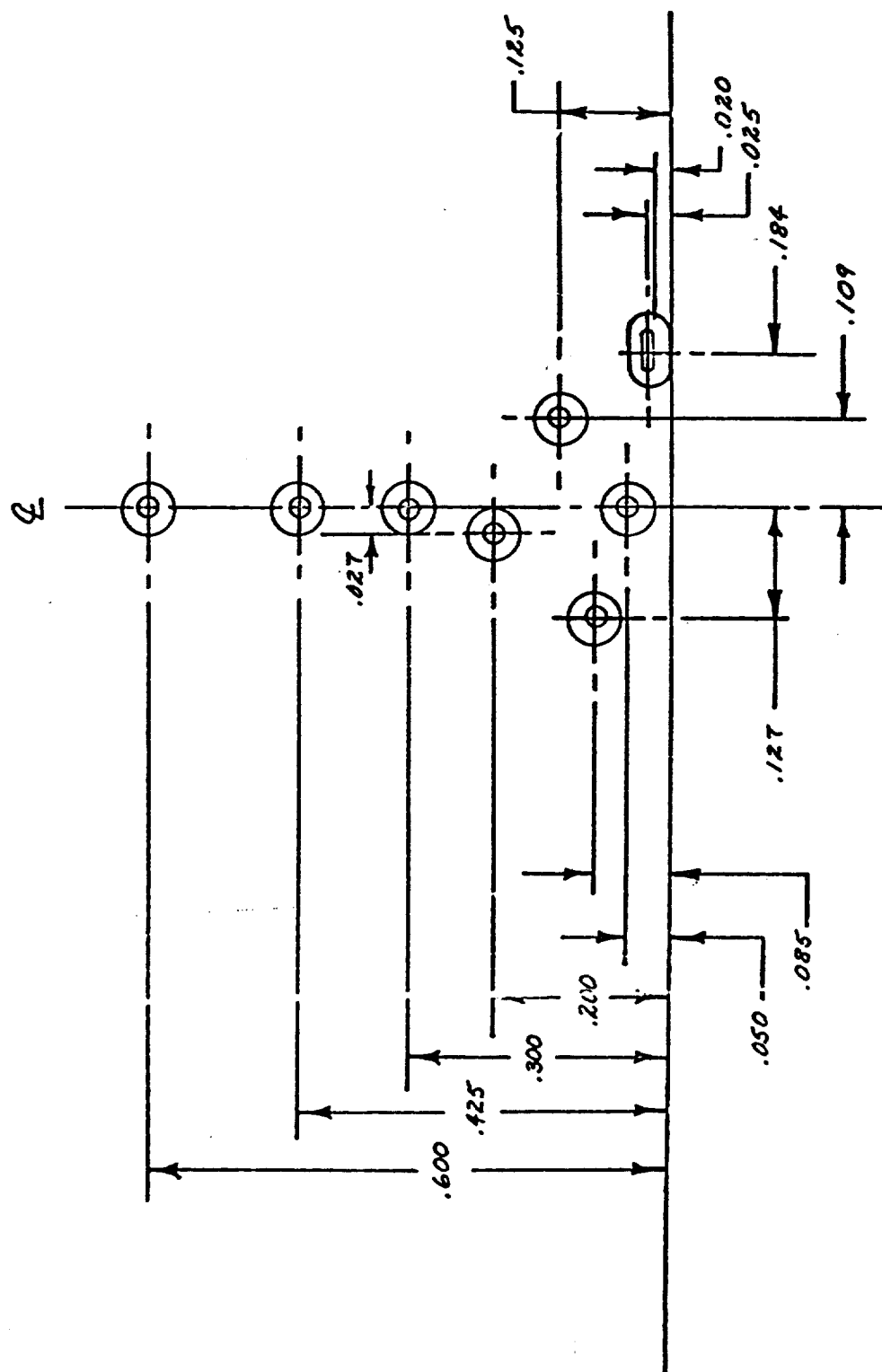
SCHEMATIC OF HEAT TRANSFER TEST PLATE



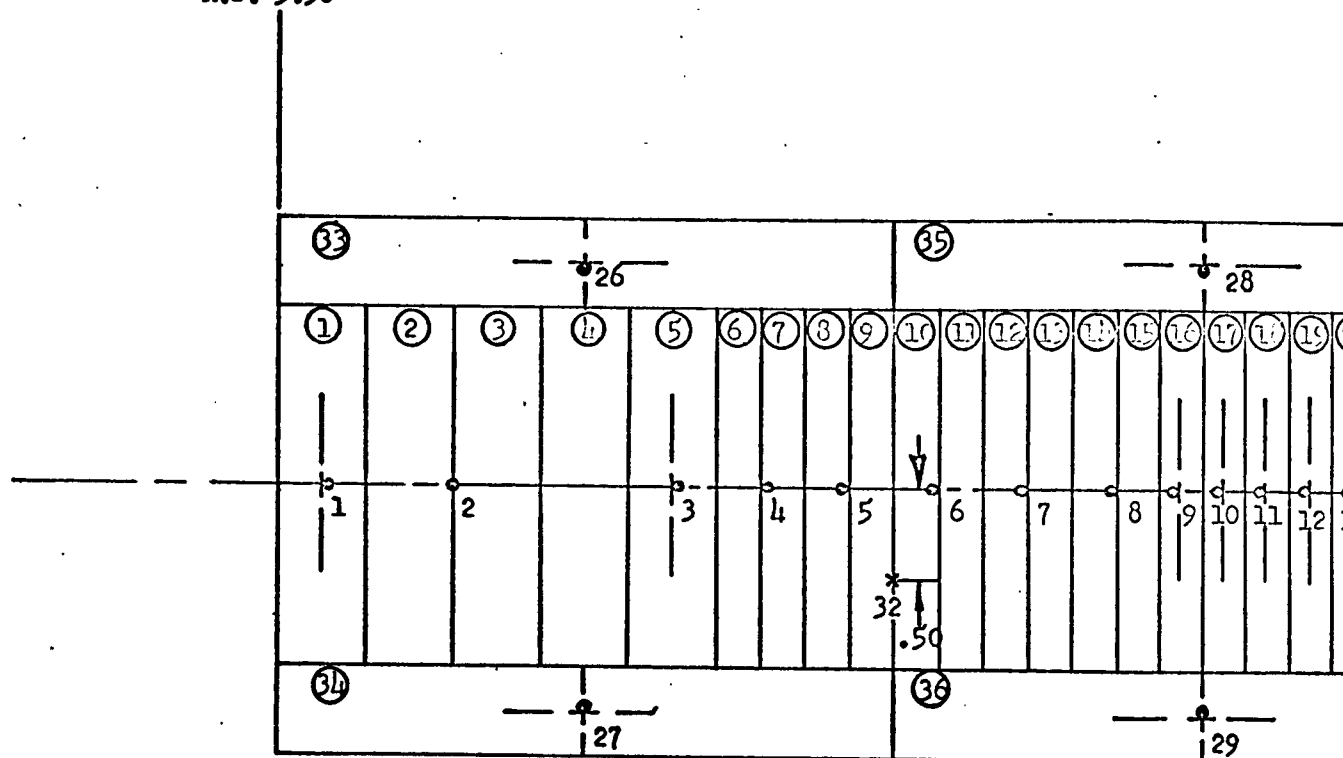
PREPARED BY:	NORTH AMERICAN AVIATION, INC. COLUMBUS DIVISION COLUMBUS 18, OHIO	PAGE NO. 71 OF
CHECKED BY:		REPORT NO. NA 62H-795
DATE:		MODEL NO.

FIG. 3

SCHEMATIC OF BOUNDARY LAYER RAKE



M.S. 5.50



○ Nichrome Element Number

● Thermocouples Under Heater Elements

✕ Thermocouples On Back Of Melamine Plate

T₃₆ is Thermocouple in Shock Generator Plate.

PREPARED BY: JAW

CHECKED BY: FEW

DATE:

NORTH AMERICAN AVIATION, INC.
COLUMBUS DIVISION COLUMBUS 16, OHIO.

PAGE NO. 72 OF

REPORT NO. NA 62H-795

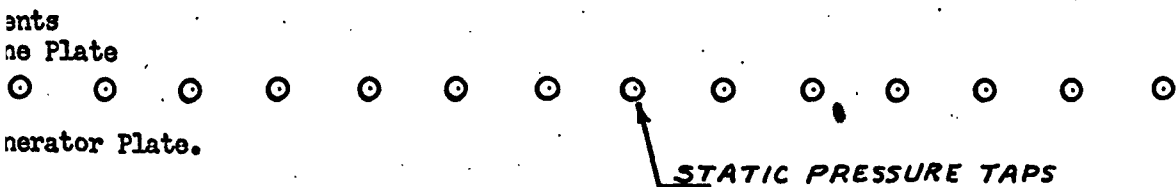
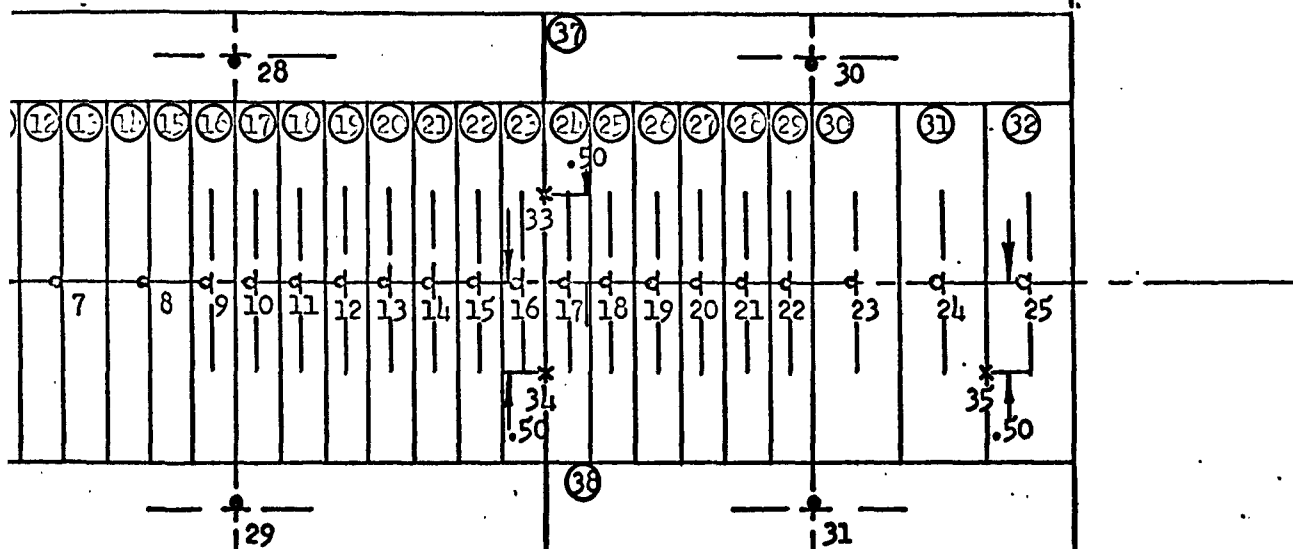
MODEL NO.

2

FIG. 4

NICHROME ELEMENT DIAGRAM

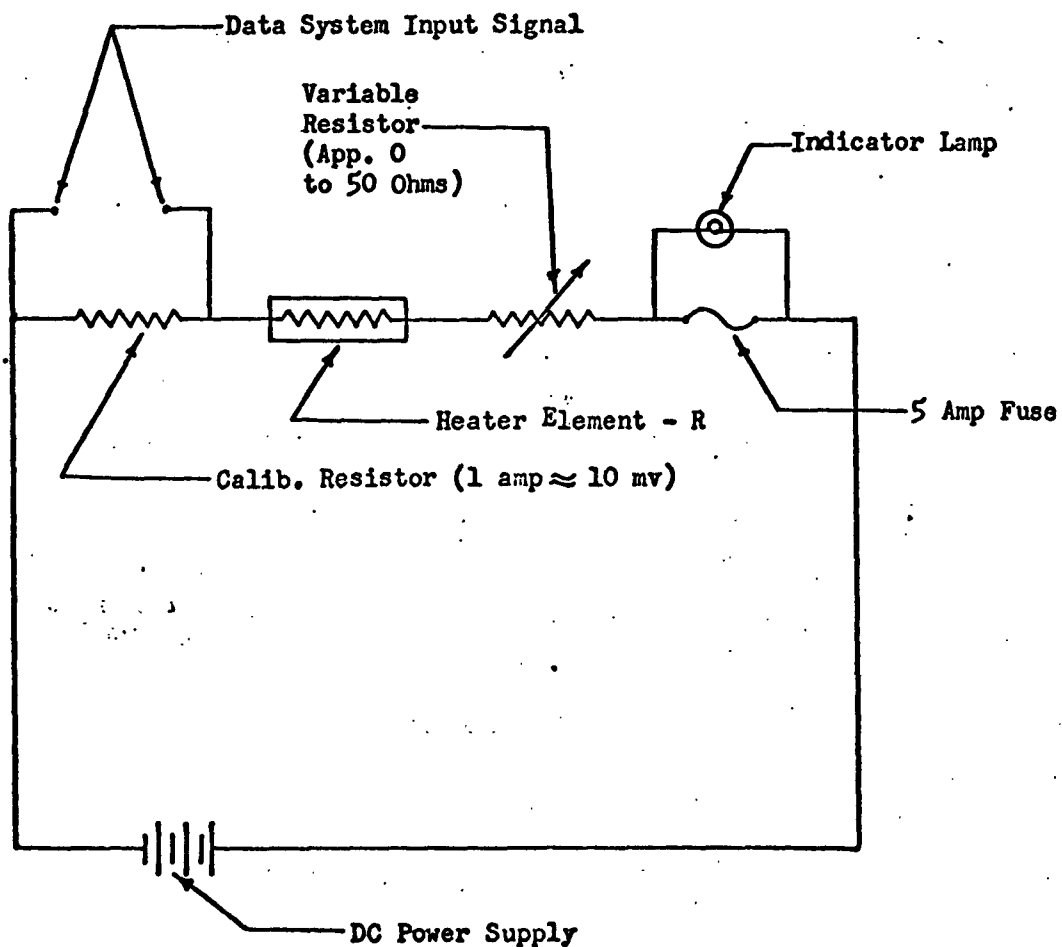
M.S. 15.50



PREPARED BY: VRP	NORTH AMERICAN AVIATION, INC. COLUMBUS DIVISION COLUMBUS 16, OHIO	PAGE NO. 73 OF
CHECKED BY: FEN		REPORT NO. NA 62H-79
DATE:		MODEL NO.

FIG. 5

TYPICAL HEATER ELEMENT CIRCUIT



PREPARED BY:	NORTH AMERICAN AVIATION, INC. COLUMBUS DIVISION COLUMBUS 16, OHIO	PAGE NO. 75 OF
CHECKED BY:		REPORT NO. NA 62H-795
DATE:		MODEL NO.

FIG. 7

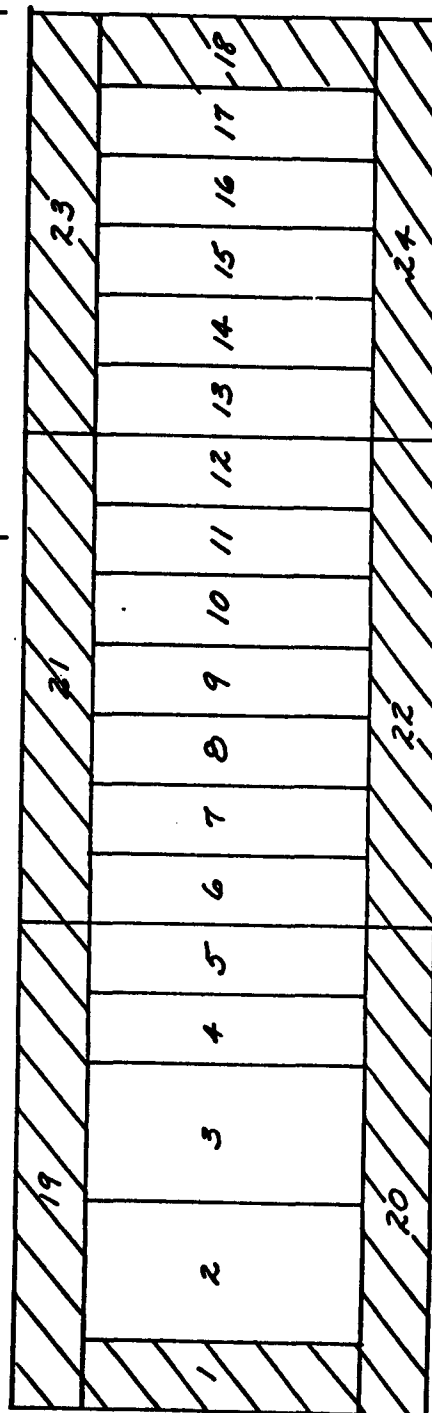
NICHROME HEATER ELEMENT ARRANGEMENT

AT MACH 5.0

M.S. 5.30

M.S. 11.75

M.S. 15.50



AIR FLOW

NOTE: HATCHING DENOTES
GUANO ELEMENT

WINDOW

TO SCALE → ONE INCH

PREPARED BY:	NORTH AMERICAN AVIATION, INC.		PAGE NO. 76 OF
CHECKED BY:	COLUMBUS DIVISION	COLUMBUS 18, OHIO	REPORT NO. NA 62H-795
DATE:			MODEL NO. FIG. 8

TEST PLATE AND SHOCK GENERATOR MOUNTED ON
STEEL PLATE WHICH REPLACES TUNNEL SCHLIEREN
WINDOW



PREPARED BY:	NORTH AMERICAN AVIATION, INC. COLUMBUS DIVISION COLUMBUS 18, OHIO	PAGE NO. 77 OF
CHECKED BY:		REPORT NO. NA 62H-795
DATE:		MODEL NO.

FIG. 9

TEST PLATE INSERTED IN WIND TUNNEL



PREPARED BY:	NORTH AMERICAN AVIATION, INC. COLUMBUS DIVISION COLUMBUS 18, OHIO	PAGE NO. 78 OF
CHECKED BY:		REPORT NO. NA 62H-795
DATE:		MODEL NO.

Fig. 10

SCHLIEREN PHOTOGRAPH OF FLOW ON TEST
PLATE AT $M_0 = 2.95$ EMPLOYING A BOUNDARY
LAYER BLOWING RATIO, P_{pc}/P_0 , OF 2.0 WITH
THE SHOCK GENERATOR PLATE REMOVED



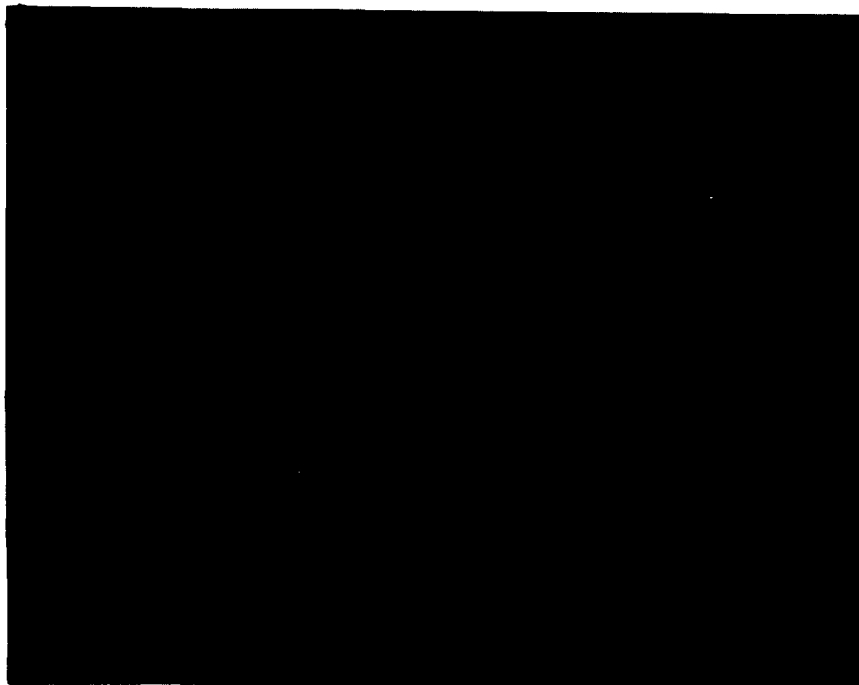
AIR FLOW



PREPARED BY:	NORTH AMERICAN AVIATION, INC.	PAGE NO. 79 OF
CHECKED BY:	COLUMBUS DIVISION COLUMBUS 16, OHIO	REPORT NO. NA 62H-795
DATE:		MODEL NO.

FIG. 11

SCHLIEREN PHOTOGRAPH OF FLOW ON TEST
PLATE AT $M_0 = 2.95$ EMPLOYING A BOUNDARY
LAYER BLOWING RATIO, P_{Pc}/P_0 , OF 5.9 FOR
A SHOCK GENERATOR PLATE ANGLE OF 0°



AIR FLOW



PREPARED BY:	NORTH AMERICAN AVIATION, INC. COLUMBUS DIVISION COLUMBUS 16, OHIO	PAGE NO. 80 OF
CHECKED BY:		REPORT NO. NA 62H-795
DATE:		MODEL NO.

Fig. 12

SCHLIEREN PHOTOGRAPH OF FLOW ON TEST
PLATE AT $M_0 = 2.95$ WITH NO BOUNDARY
LAYER BLOWING FOR A SHOCK GENERATOR
PLATE ANGLE OF 6.0°




AIR FLOW


PREPARED BY:	NORTH AMERICAN AVIATION, INC. COLUMBUS DIVISION COLUMBUS 18, OHIO	PAGE NO. 81 OF
CHECKED BY:		REPORT NO. NA 62H-795
DATE:		MODEL NO.

FIG. 13

SCHLIEREN PHOTOGRAPH OF FLOW ON TEST
PLATE AT $M_0 = 2.95$ WITH NO BOUNDARY
LAYER BLOWING FOR A SHOCK GENERATOR
PLATE ANGLE OF 9.5°



AIR FLOW


PREPARED BY:	NORTH AMERICAN AVIATION, INC. COLUMBUS DIVISION COLUMBUS 18, OHIO	PAGE NO. 82 OF
CHECKED BY:		REPORT NO. NA 62H-795
DATE:		MODEL NO.

Fig. 14

SCHLIEREN PHOTOGRAPH OF FLOW ON TEST
PLATE AT $M_0 = 2.95$ EMPLOYING A BOUNDARY
LAYER BLOWING RATIO, P_{w}/P_0 , OF 2.0 FOR A
SHOCK GENERATOR PLATE ANGLE OF 12.0°



AIR FLOW
←

PREPARED BY:	NORTH AMERICAN AVIATION, INC. COLUMBUS DIVISION COLUMBUS 18, OHIO	PAGE NO. 83 OF
CHECKED BY:		REPORT NO. NA 62R-795
DATE:		MODEL NO.

Fig. 15

SCHLIEREN PHOTOGRAPH OF FLOW ON TEST
PLATE AT $M_0 = 5.02$ EMPLOYING A BOUNDARY
LAYER BLOWING RATIO, P_{bc}/P_0 , OF 4.9 FOR A
SHOCK GENERATOR PLATE ANGLE OF 12.0°



AIR FLOW
 ←

PREPARED BY:	NORTH AMERICAN AVIATION, INC.		PAGE NO. 84 of
CHECKED BY:	COLUMBUS DIVISION	COLUMBUS 16, OHIO	REPORT NO. NA 62H-79
DATE:			MODEL NO.

METHOD OF OBTAINING HEAT TRANSFER COEFFICIENT
AND RECOVERY TEMPERATURE FROM CORRECTED
HEAT FLOW RATES AND NICHROME TEMPERATURE

$$h = \frac{d(\dot{Q}/A)_c}{dT_N} = \text{HEAT TRANSFER COEFFICIENT NOT CORRECTED FOR NON-ISOTHERMAL WALL EFFECTS.}$$

SINCE THE SLOPE IS CONSTANT:

$$(\dot{Q}/A)_c = h(T - T_R)$$

$$(\dot{Q}/A)_c = \frac{(\text{ELECTRICAL POWER DISSIPATED BY A HEATER ELEMENT}) - (\text{POWER CONDUCTED AND RADIATED AWAY FROM ELEMENT})}{\text{PLATFORM AREA OF ELEMENT}}$$

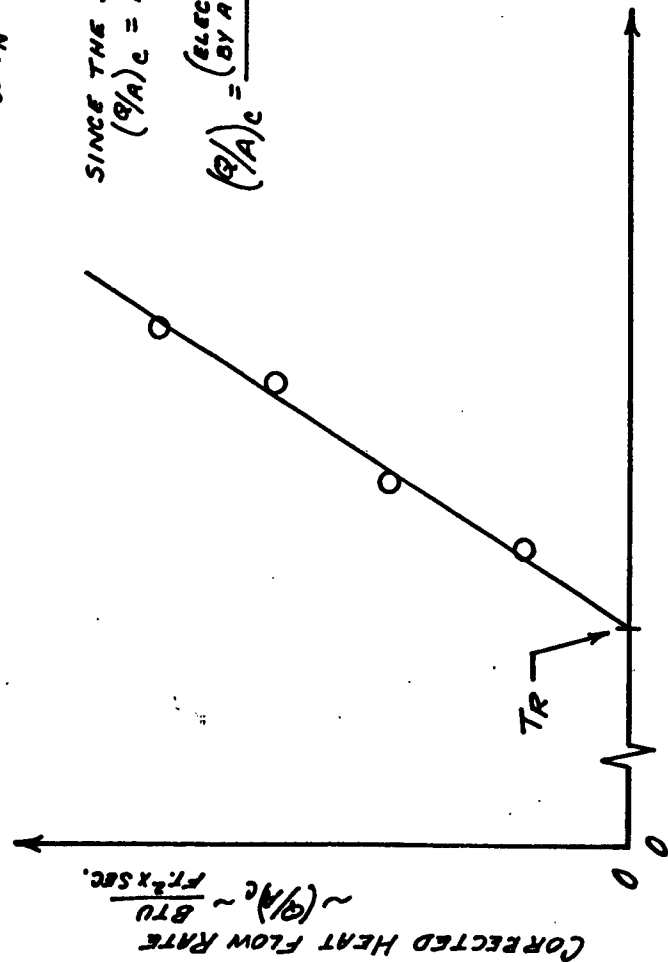


FIG. 16

PREPARED BY:

NORTH AMERICAN AVIATION, INC.

PAGE NO. 85 OF

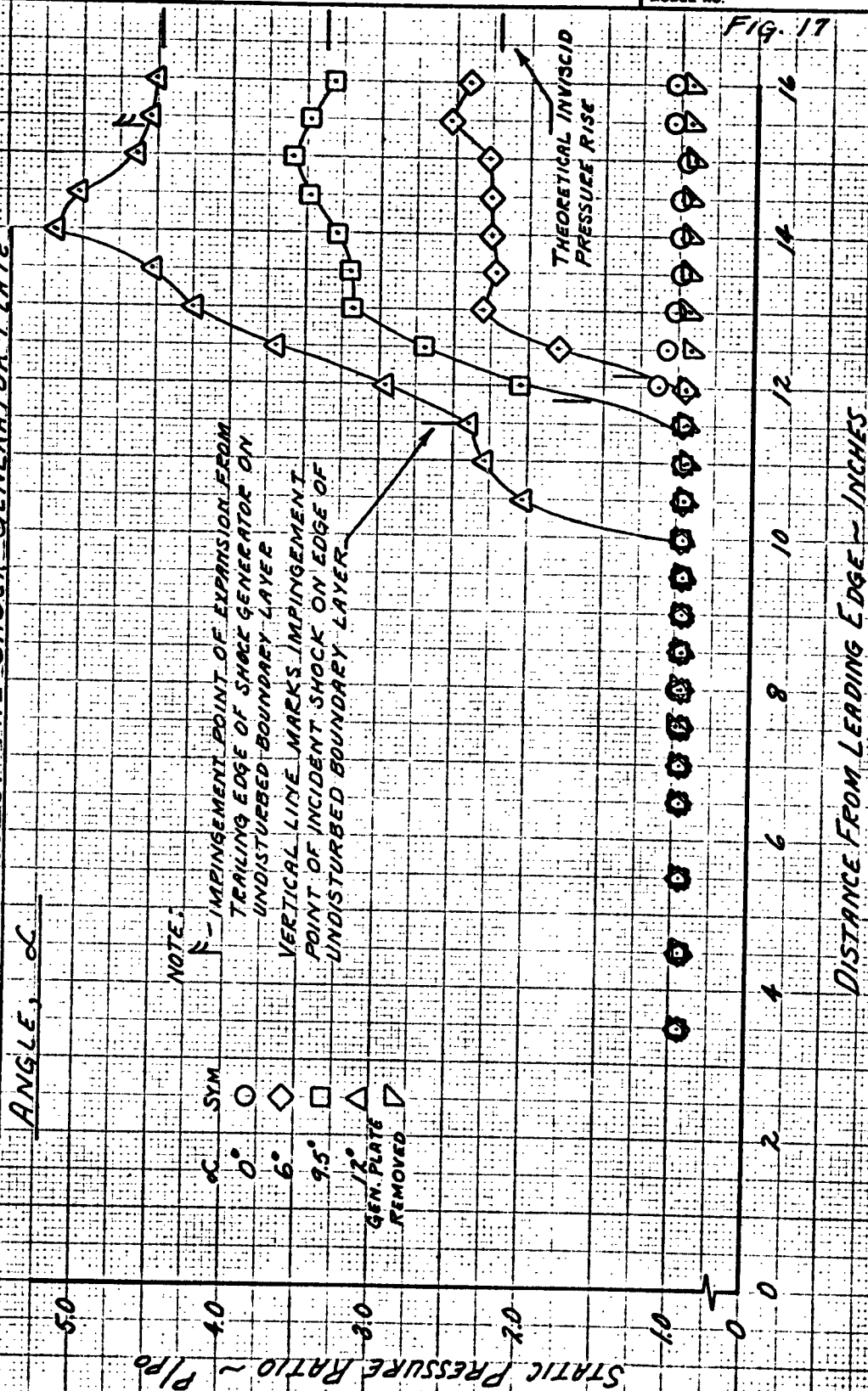
CHECKED BY:

REPORT NO. NA 62H-795

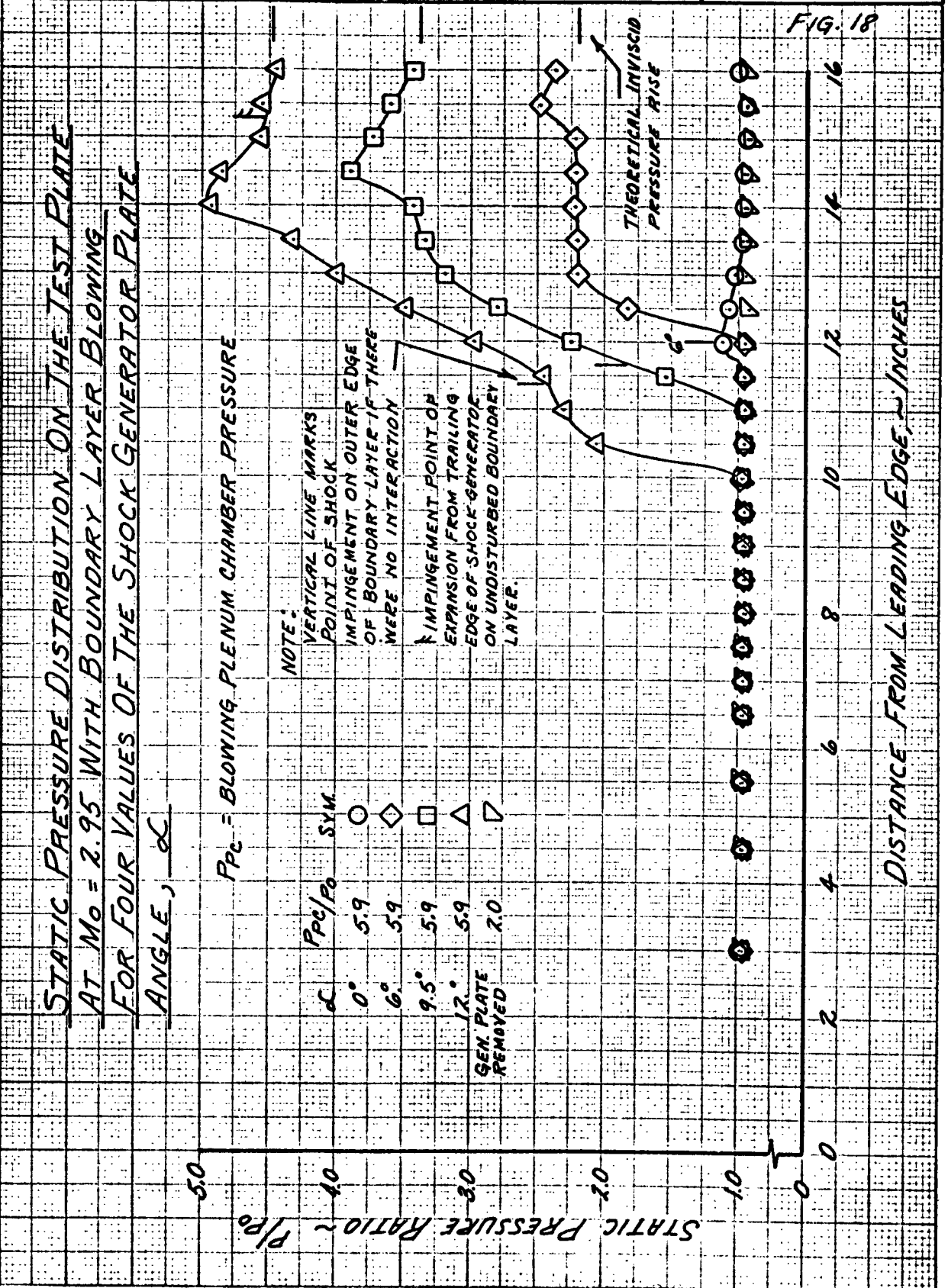
DATE:

MODEL NO.

STATIC PRESSURE DISTRIBUTION ON THE TEST PLATE
AT $M_o = 2.95$ WITH NO BOUNDARY LAYER BLOWING
FOR FOUR VALUES OF THE SHOCK GENERATOR PLATE
ANGLE, α



PREPARED BY:	NORTH AMERICAN AVIATION, INC.	PAGE NO. 86 OF
CHECKED BY:		REPORT NO. NA 62H-795
DATE:		MODEL NO.



NORTH AMERICAN AVIATION, INC.

PREPARED BY:

PAGE NO. 87 OF

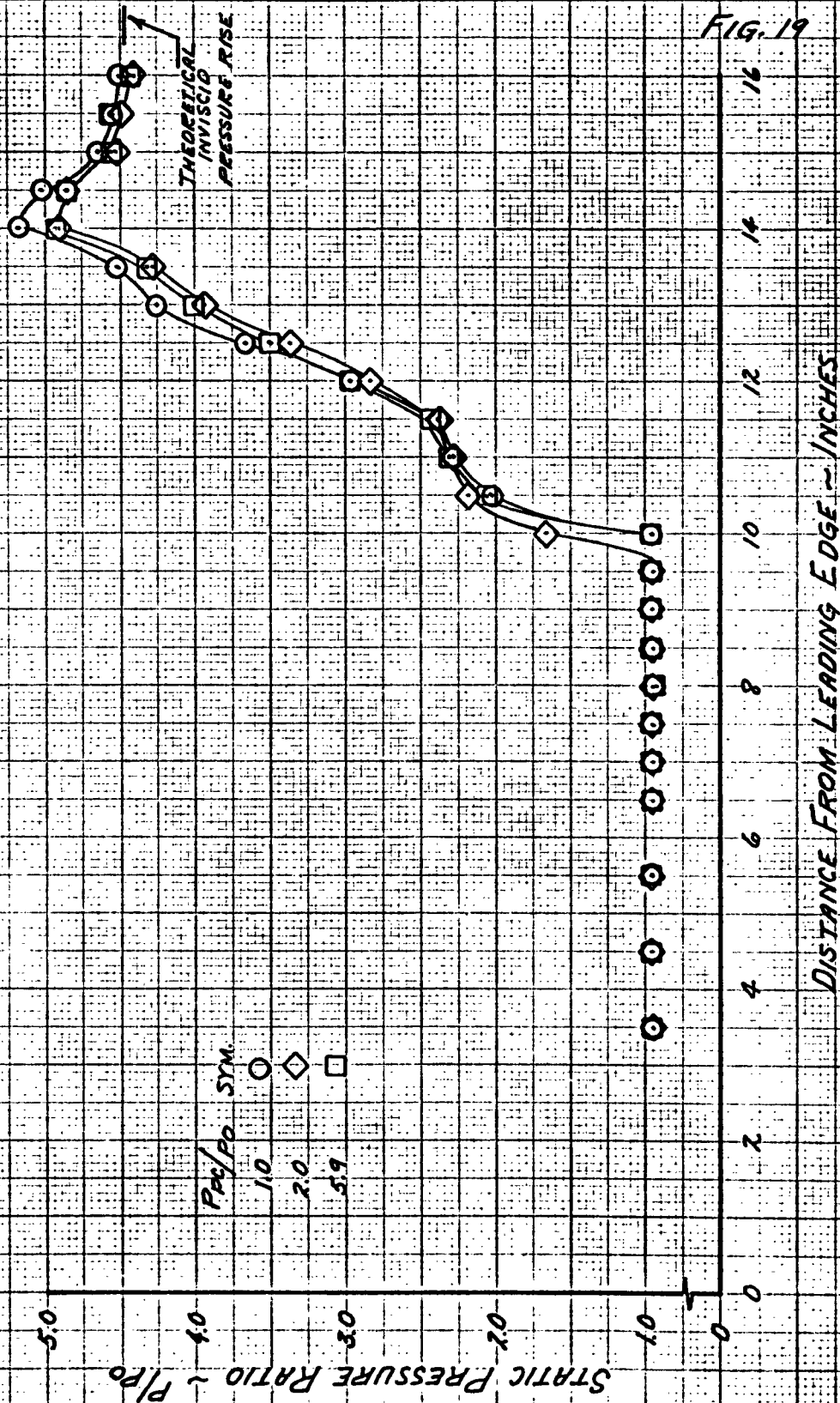
CHECKED BY:

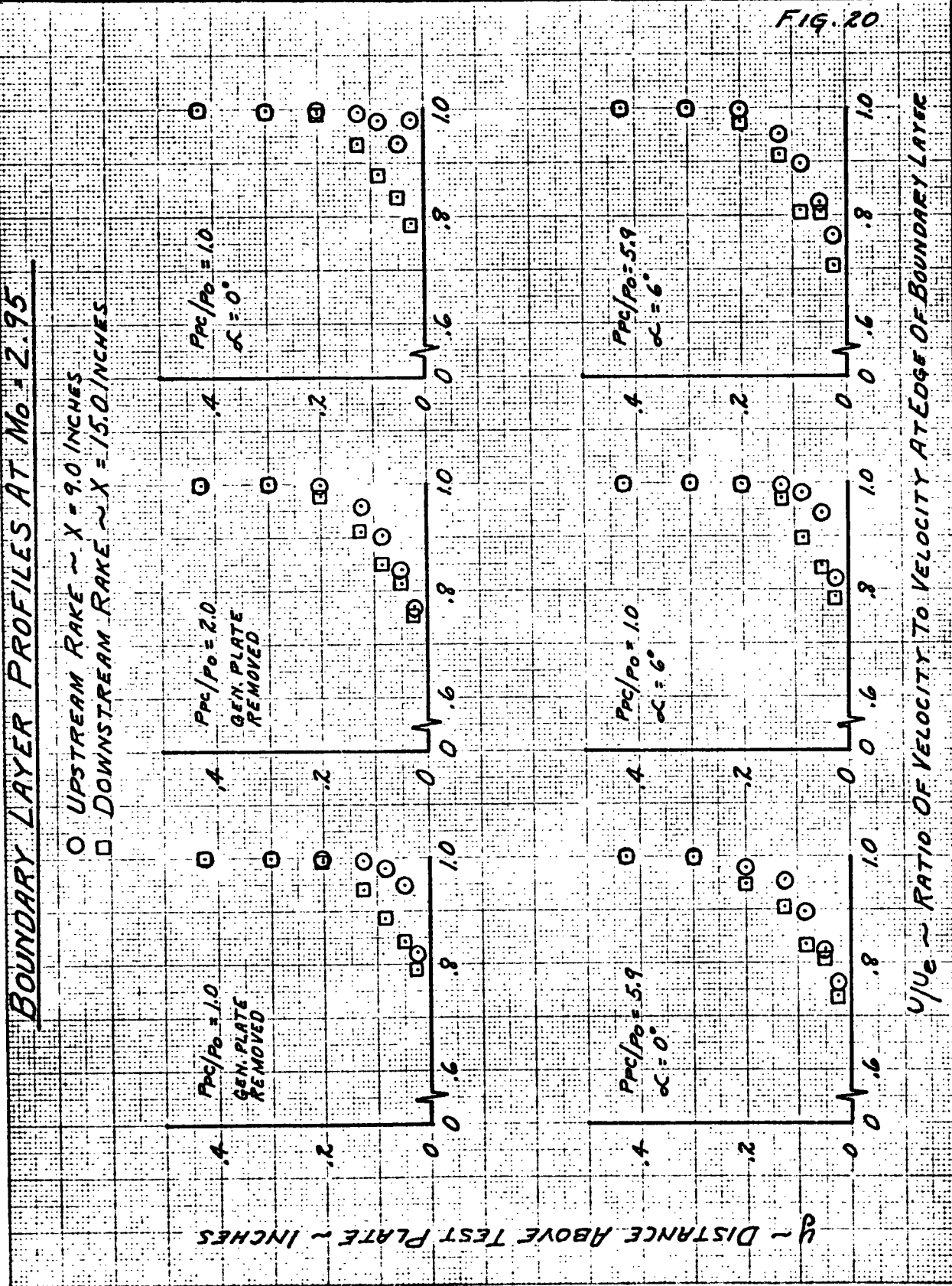
REPORT NO. NA 62H-795

DATE:

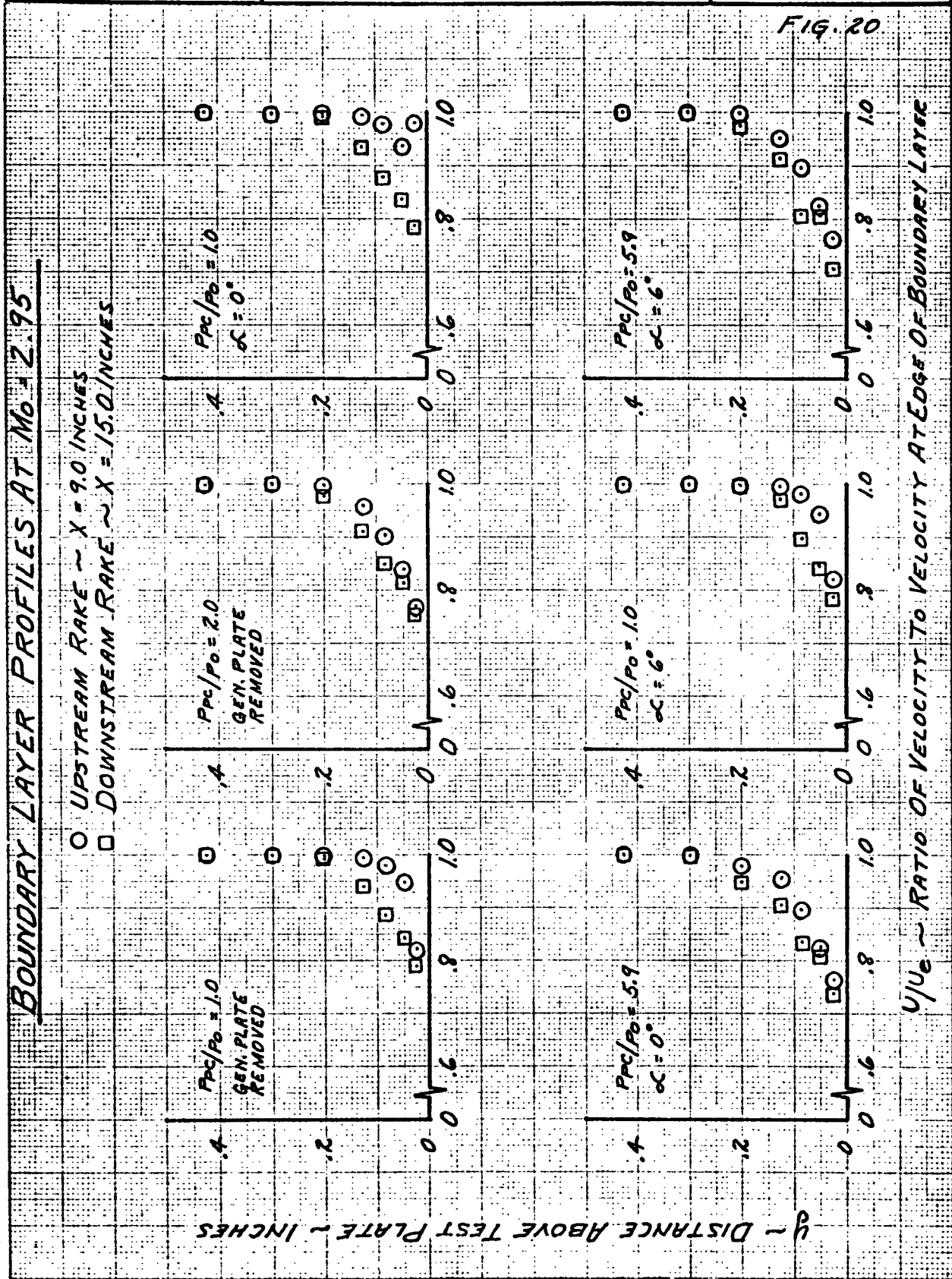
MODEL NO.

EFFECT OF BOUNDARY LAYER BLOWING ON THE STATIC
PRESSURE DISTRIBUTION AT $M_o = 2.95$ FOR A SHOCK
GENERATOR PLATE ANGLE OF 12°





PREPARED BY:	NORTH AMERICAN AVIATION, INC.	PAGE NO. 88 OF
CHECKED BY:		REPORT NO. NA 62H-795
DATE:		MODEL NO.



PREPARED BY:	NORTH AMERICAN AVIATION, INC.	PAGE NO. 89 OF
CHECKED BY:		REPORT NO. NA 62H-795
DATE:		MODEL NO.

BOUNDARY LAYER PROFILES AT $M_0 = 2.95$

○ UPSTREAM RAKE ~ $X = 9.0$ INCHES
□ DOWNSTREAM RAKE ~ $X = 15.0$ INCHES

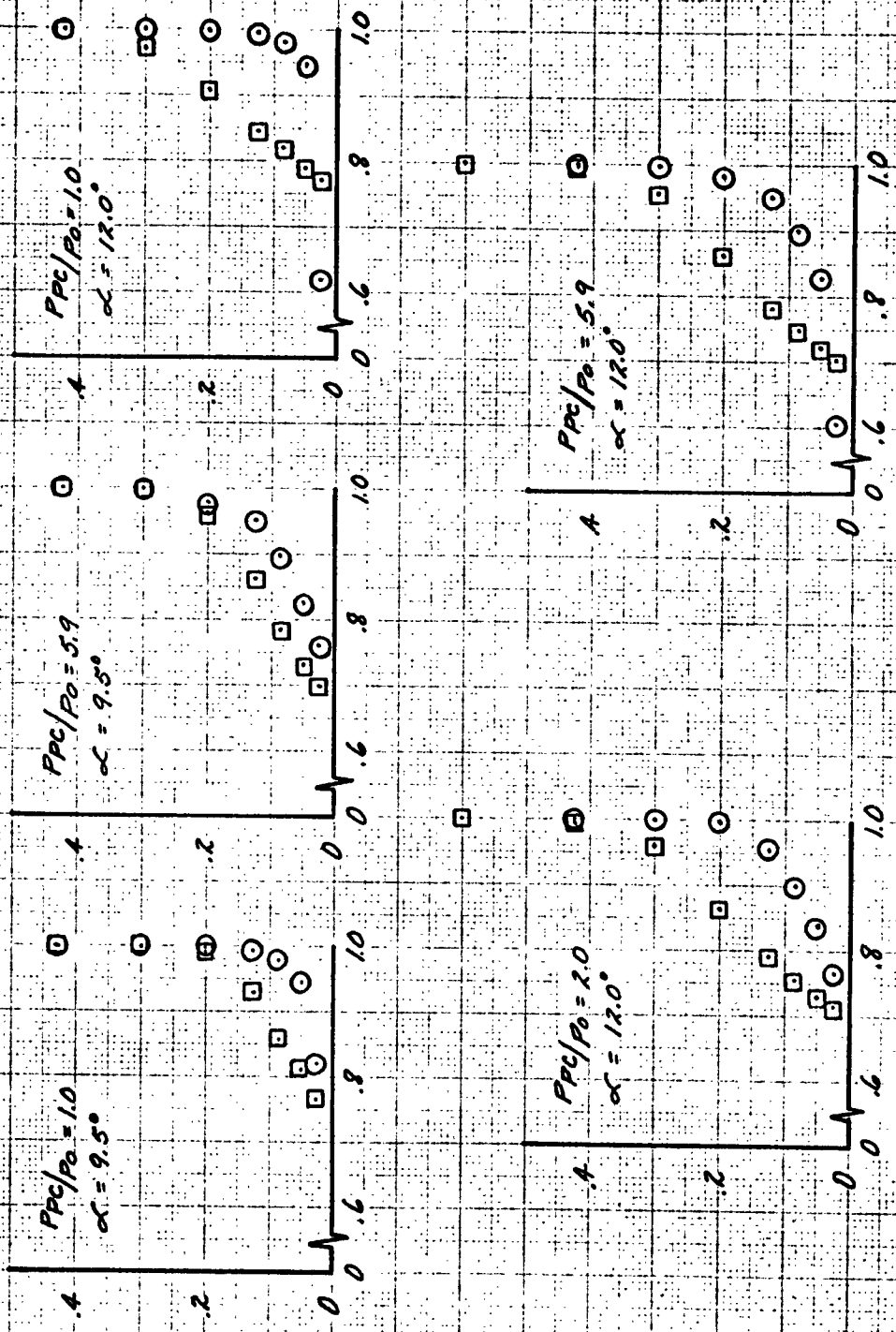
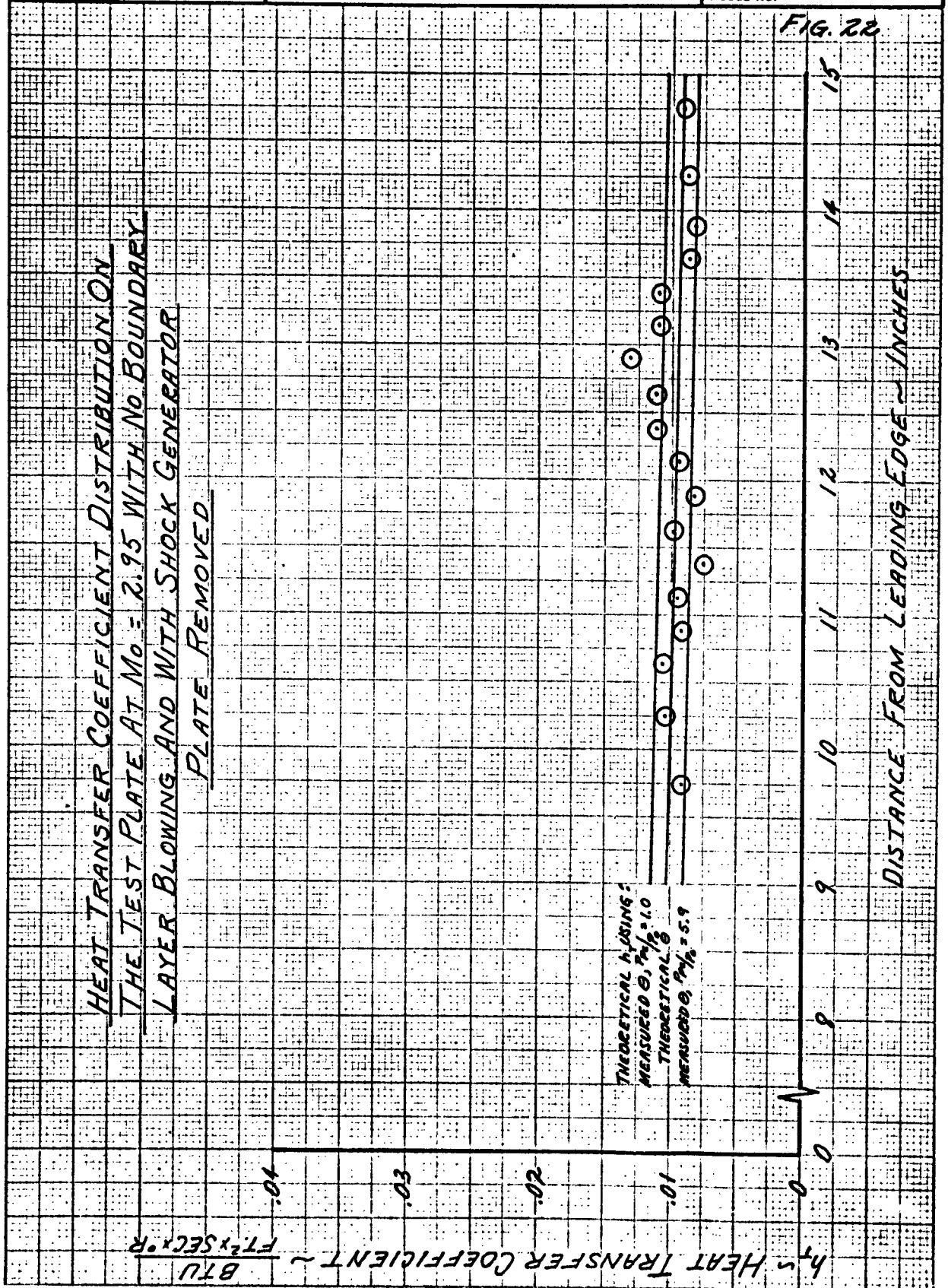


Fig. 21

U/U_e ~ RATIO OF VELOCITY TO VELOCITY AT EDGE OF BOUNDARY LAYER

y ~ DISTANCE ABOVE TEST PLATE ~ INCHES

PREPARED BY:	NORTH AMERICAN AVIATION, INC.	PAGE NO. 90 OF 97
CHECKED BY:		REPORT NO. NA 62H-795
DATE:		MODEL NO.



NORTH AMERICAN AVIATION, INC.

PREPARED BY:

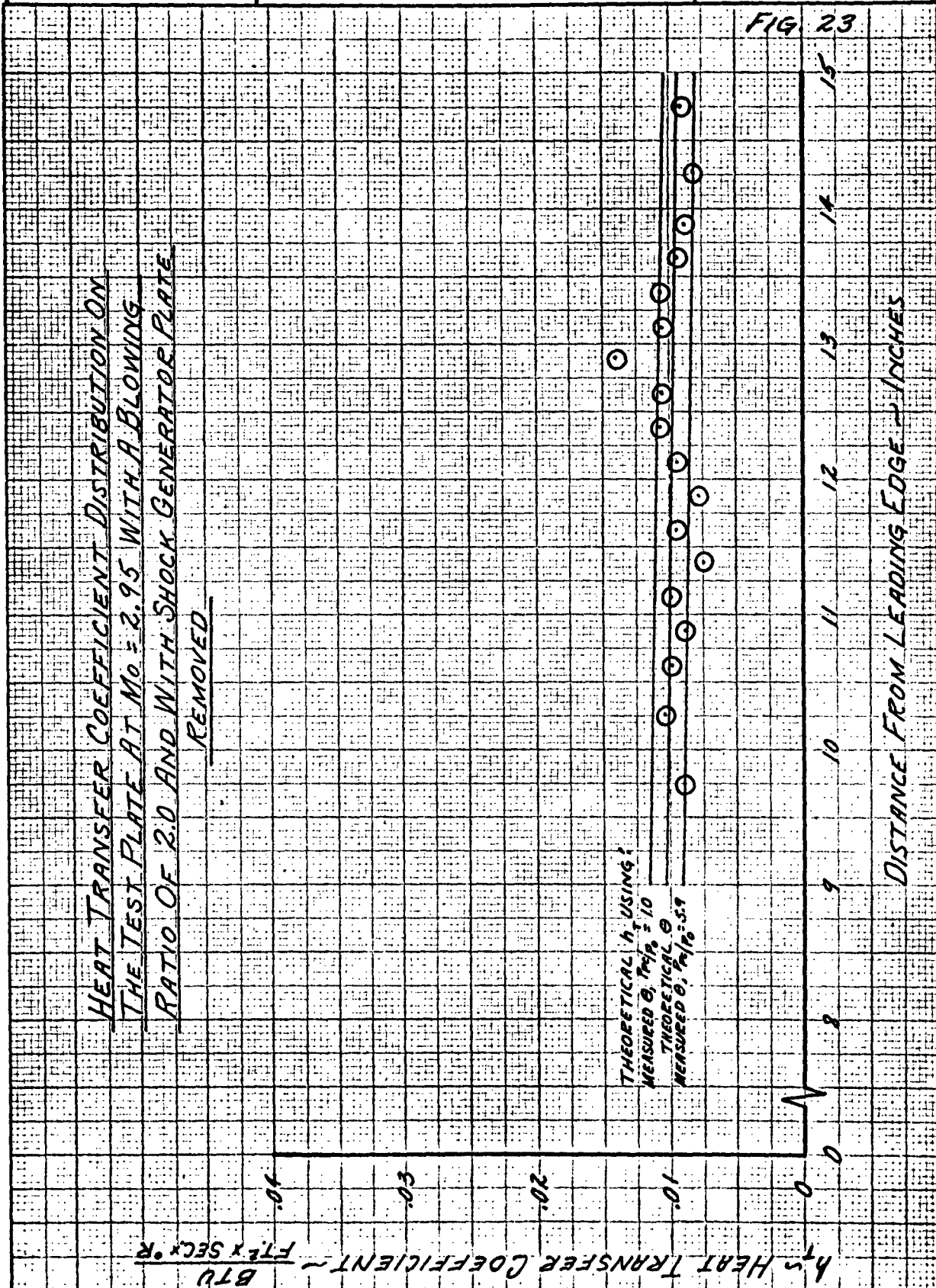
PAGE NO. 91 OF 97

CHECKED BY:

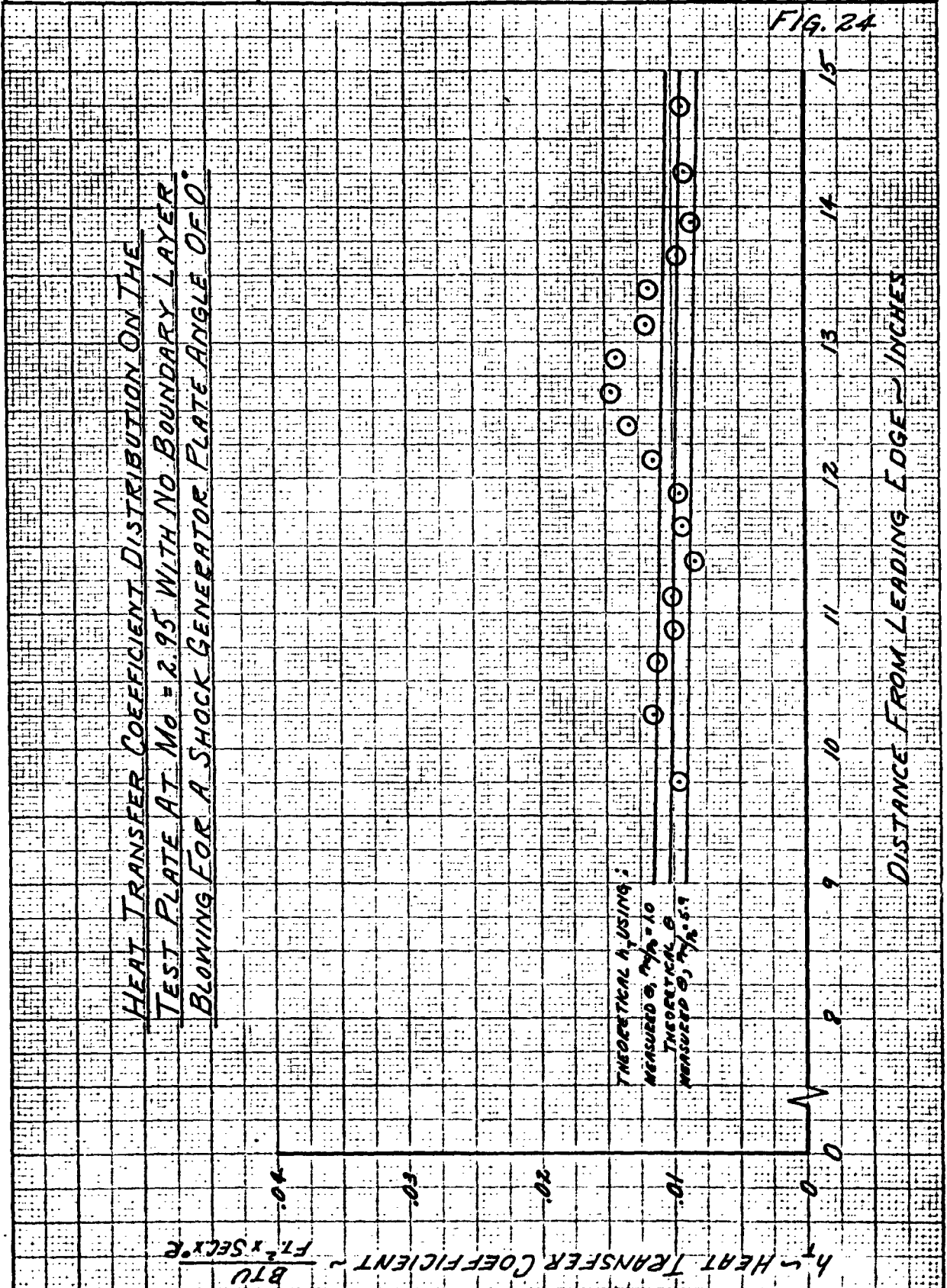
REPORT NO. NA 62H-795

DATE:

MODEL NO.



PREPARED BY:	NORTH AMERICAN AVIATION, INC.	PAGE NO. 92 OF
CHECKED BY:		REPORT NO. NA 62H-795
DATE:		MODEL NO.



PREPARED BY:

NORTH AMERICAN AVIATION, INC.

PAGE NO. 93 OF

CHECKED BY:

REPORT NO. NA 62H-795

DATE:

MODEL NO.

HEAT TRANSFER COEFFICIENT DISTRIBUTION ON
THE TEST PLATE AT $M_0 = 2.95$ WITH A BLOWING
RATIO OF 5.9 FOR A SHOCK GENERATOR PLATE
ANGLE OF 0°

h - HEAT TRANSFER COEFFICIENT $\sim \frac{BTU}{FT^2 \times SEC \times R}$

THEORETICAL h USING:
MEASURED θ , $P_{t1}/P_0 = 10$
THEORETICAL θ
MEASURED θ , $P_{t1}/P_0 = 5.9$

FIG. 25

DISTANCE FROM LEADING EDGE - INCHES

NORTH AMERICAN AVIATION, INC.

PREPARED BY:

PAGE NO. 94 OF

CHECKED BY:

REPORT NO. NA 62H-795

DATE:

MODEL NO.

HEAT TRANSFER COEFFICIENT DISTRIBUTION ON THE
TEST PLATE AT $M_0 = 2.95$ WITH NO BOUNDARY LAYER
BLOWING FOR A SHOCK GENERATOR PLATE ANGLE OF 6°

BTU
FT² SEC. °R

h_T HEAT TRANSFER COEFFICIENT

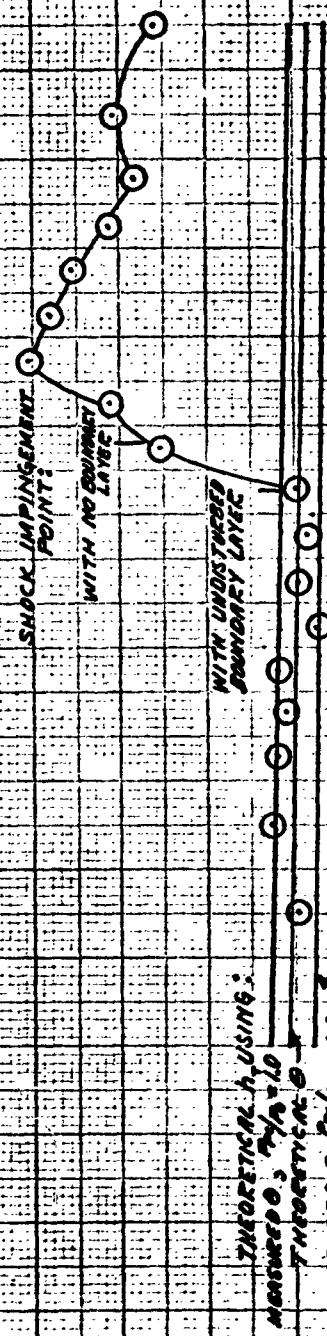


FIG 26

DISTANCE FROM LEADING EDGE - INCHES

PREPARED BY:

NORTH AMERICAN AVIATION, INC.

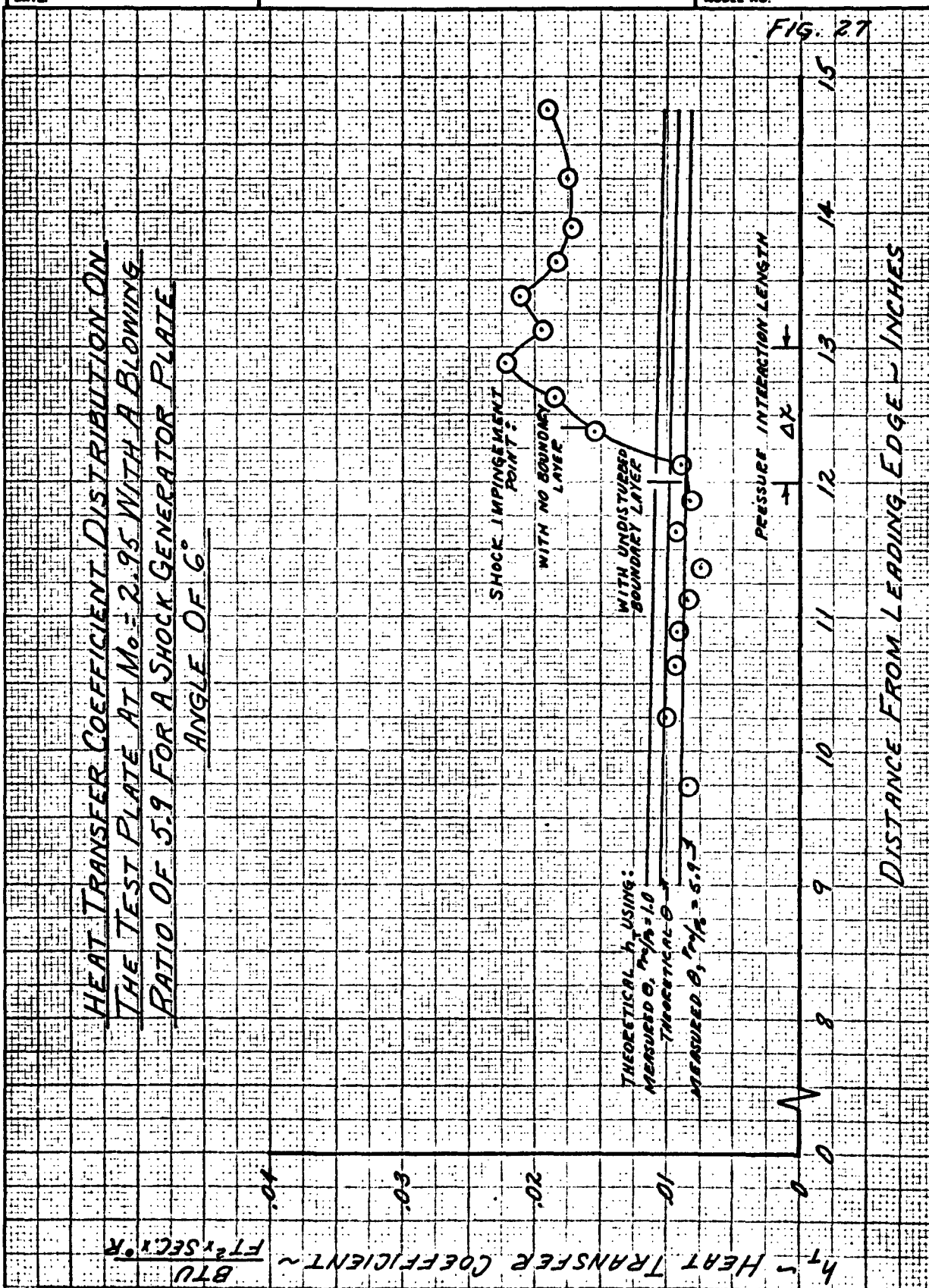
PAGE NO. 95 OF

CHECKED BY:

REPORT NO. NA 62H-795

DATE:

MODEL NO.



NORTH AMERICAN AVIATION, INC.

PAGE NO. 96 OF

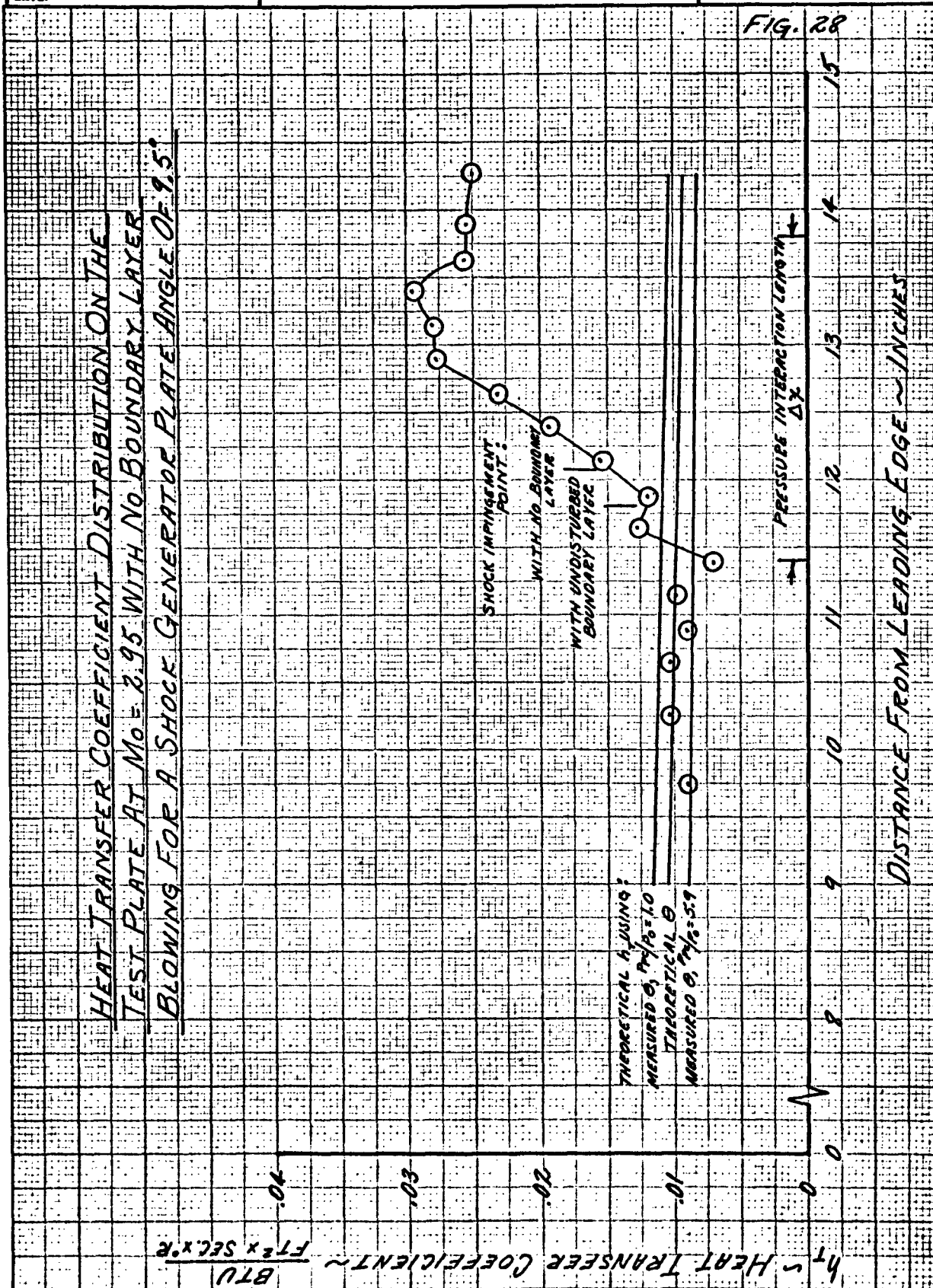
PREPARED BY:

REPORT NO. NA 62H-795

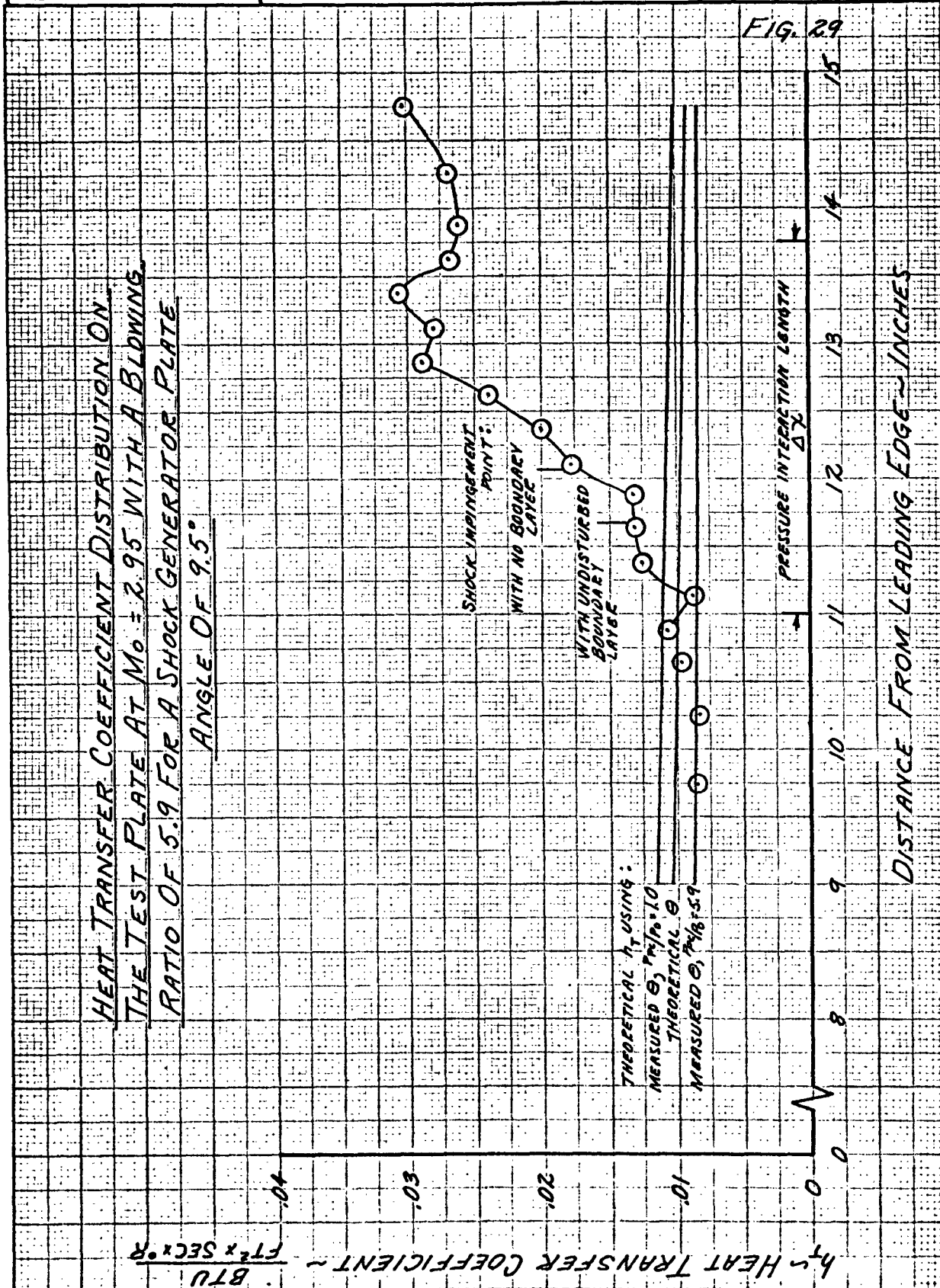
CHECKED BY:

DATE:

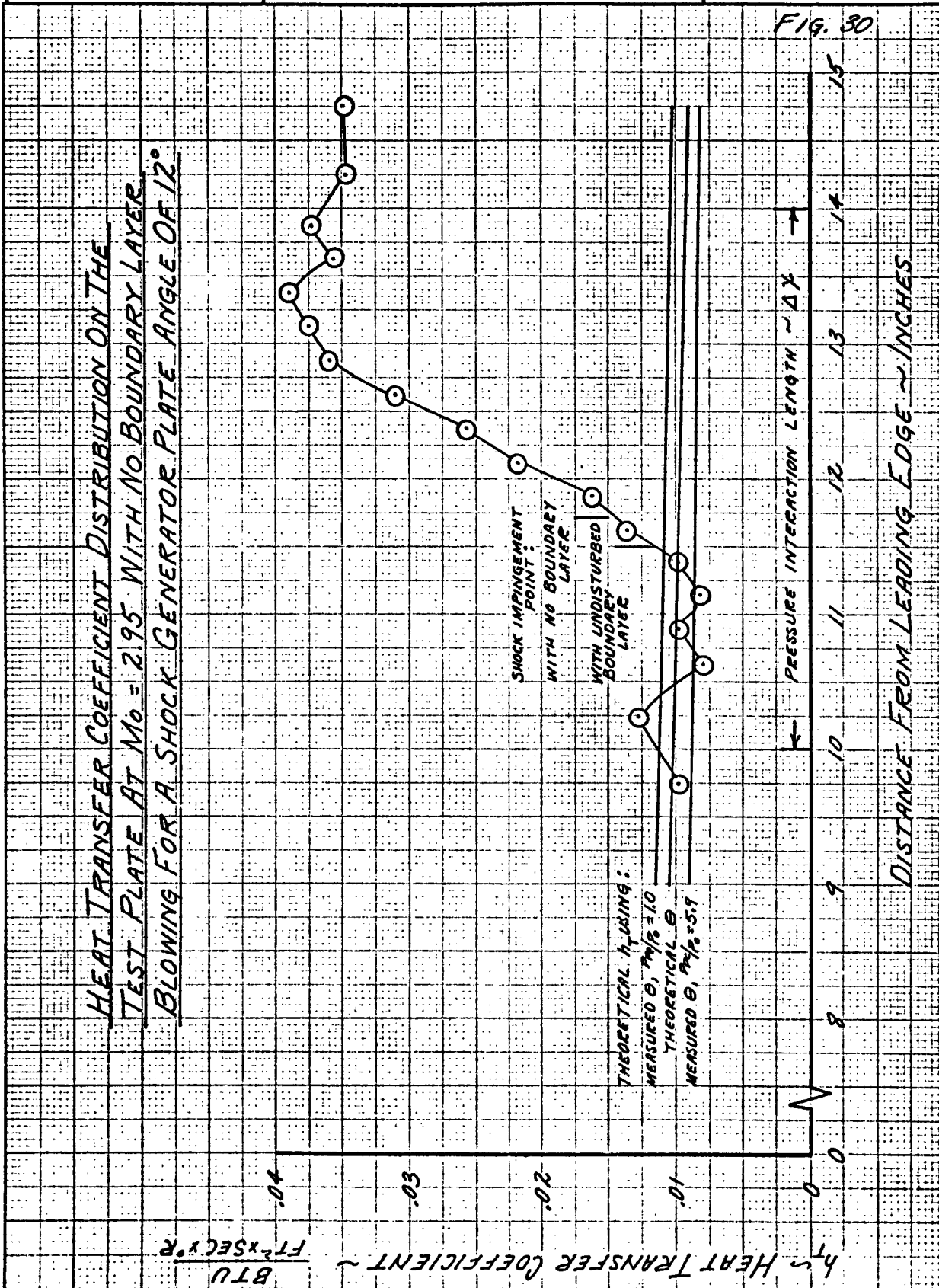
MODEL NO.



PREPARED BY:		NORTH AMERICAN AVIATION, INC.	PAGE NO. 97 OF
CHECKED BY:			REPORT NO. NA 62H-795
DATE:			MODEL NO.



PREPARED BY:		NORTH AMERICAN AVIATION, INC.	PAGE NO. 98 OF
CHECKED BY:			REPORT NO. NA 62H-795
DATE:			MODEL NO.



NORTH AMERICAN AVIATION, INC.

PREPARED BY:

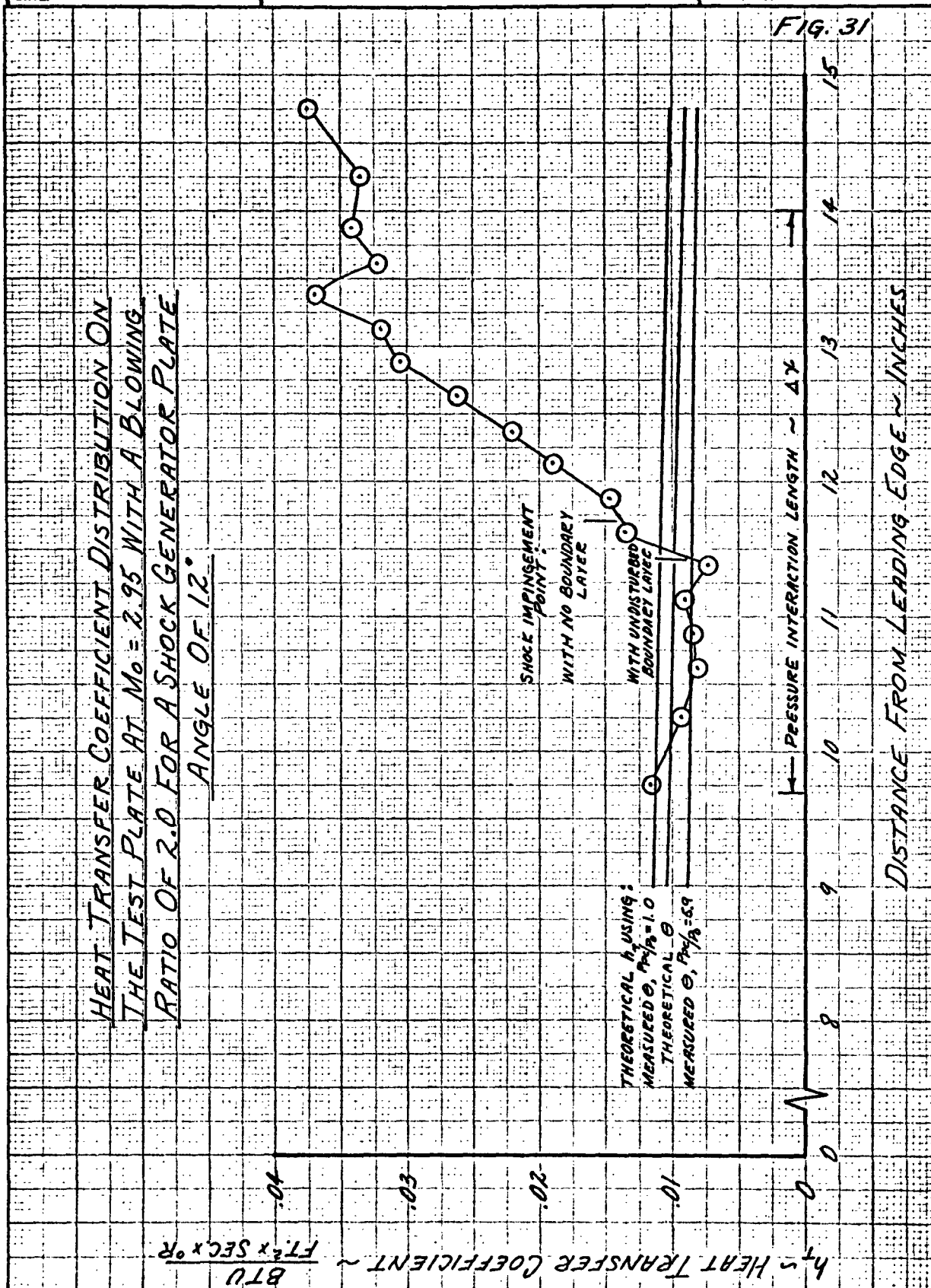
PAGE NO. 99 OF

CHECKED BY:

REPORT NO. NA 62H-795

DATE:

MODEL NO.



PREPARED BY:

REPORT NO. NA 62H-795

CHECKED BY:

MODEL NO.

DATE:

FIG. 32

HEAT TRANSFER COEFFICIENT DISTRIBUTION ON
THE TEST PLATE AT $M_0 = 2.95$ WITH A BLOWING
RATIO OF 5.9 FOR A SHOCK GENERATOR PLATE
ANGLE OF 12°

h HEAT TRANSFER COEFFICIENT $\sim \frac{BTU}{FT^2 \times SEC \times ^\circ R}$

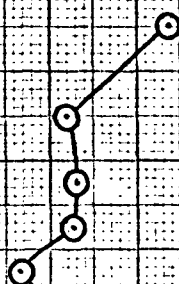
40

30

20

10

0



SHOCK IMPINGEMENT POINT

WITH NO BOUNDARY LAYER

WITH UNDISTURBED BOUNDARY LAYER

THEORETICAL h_t USING:MEASURED θ , $P_0/P_\infty = 1.0$ THEORETICAL θ MEASURED θ , $P_0/P_\infty = 1.0$ PRESSURE INTERACTION LENGTH $\sim \Delta x$

DISTANCE FROM LEADING EDGE - INCHES

15

14

13

12

11

10

9

8

7

6

5

4

3

2

1

0

PREPARED BY:

PAGE NO. 101 OF

CHECKED BY:

REPORT NO. NA 62H-795

DATE:

MODEL NO.

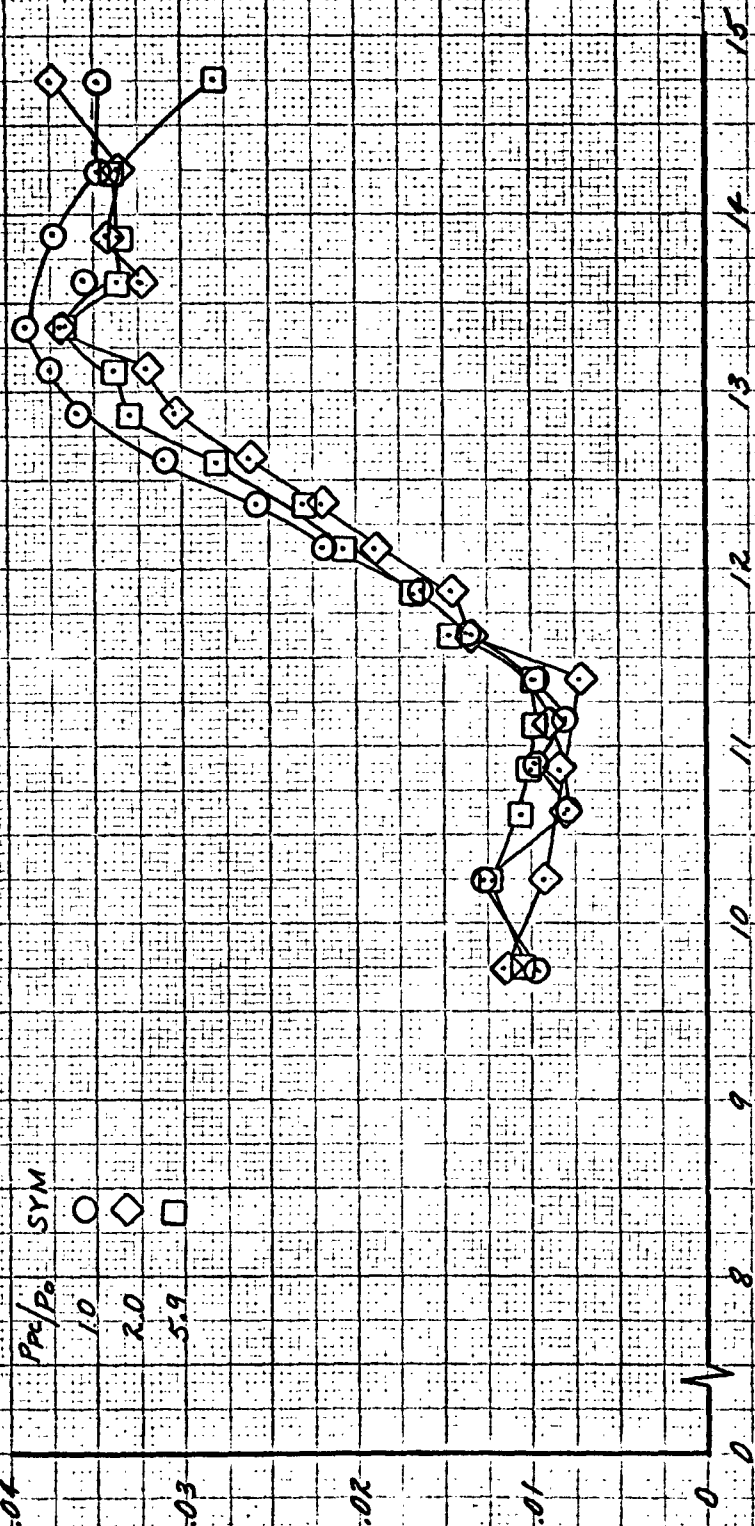
FIG. 33

EFFECT OF BOUNDARY LAYER BLOWING ON THE
HEAT TRANSFER COEFFICIENT DISTRIBUTION AT
 $M_0 = 2.95$ FOR A SHOCK GENERATOR PLATE
ANGLE OF 12°

h_T HEAT TRANSFER COEFFICIENT $\sim \frac{BTU}{FT^2 \times SEC. \times ^\circ R}$

P_c/P_0 SYN
1.0 \circ
2.0 \diamond
5.9 \square

DISTANCE FROM LEADING EDGE - INCHES



PREPARED BY:

CHECKED BY:

REPORT NO. NA 62H-795

DATE:

MODEL NO.

RECOVERY FACTOR DISTRIBUTION AT $M_0 = 2.95$ FOR
VARIOUS BLOWING RATIOS WITH A SHOCK GENERATOR
PLATE ANGLE OF 0°

P_{02}/P_0	SYM
1.0	—
2.6	—
13.7	—
18.0	—
7.5	—

RECOVERY FACTOR $\sim \eta$ 

FIG. 34

DISTANCE FROM LEADING EDGE - INCHES

PREPARED BY:	NORTH AMERICAN AVIATION, INC.	PAGE NO. 103 OF
CHECKED BY:		REPORT NO. NA 62H-795
DATE:		MODEL NO.

DISTRIBUTION OF EFFECTIVE RECOVERY FACTOR AT $M_0 = 2.95$
WITH THE SHOCK GENERATOR PLATE REMOVED

T_R = ISOTHERMAL TEMP. FOR LOCAL ZERO
 HEAT TRANSFER

$$\eta_R = \frac{T_R - T_1}{T_T - T_1} = \frac{(1 + 2M_1^2) \frac{T_R}{T_1} - 1}{2M_1^2}, M_1 = 2.98$$

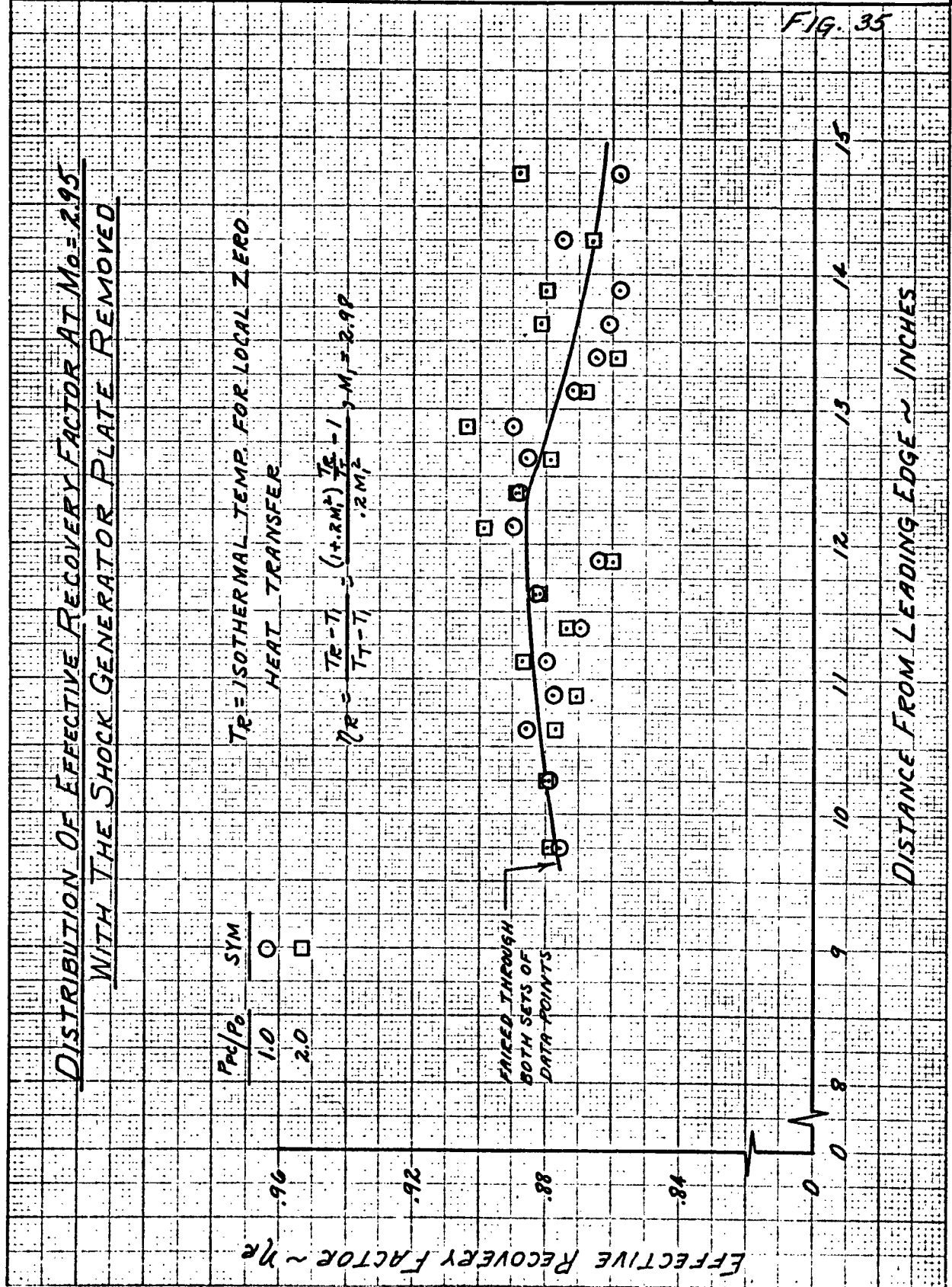
P_{01}/P_0 SYM
 1.0 ○
 2.0 □

EFFECTIVE RECOVERY FACTOR $\sim \eta_R$

PAIRED THROUGH
 BOTH SETS OF
 DATA POINTS

DISTANCE FROM LEADING EDGE ~ INCHES

FIG. 35



PREPARED BY:	NORTH AMERICAN AVIATION, INC.	PAGE NO. 104 OF
CHECKED BY:		REPORT NO. NA 62H-795
DATE:		MODEL NO.

FIG. 36

DISTRIBUTION OF EFFECTIVE RECOVERY FACTOR AT $M_0 = 2.95$
FOR A SHOCK GENERATOR PLATE ANGLE OF 0°

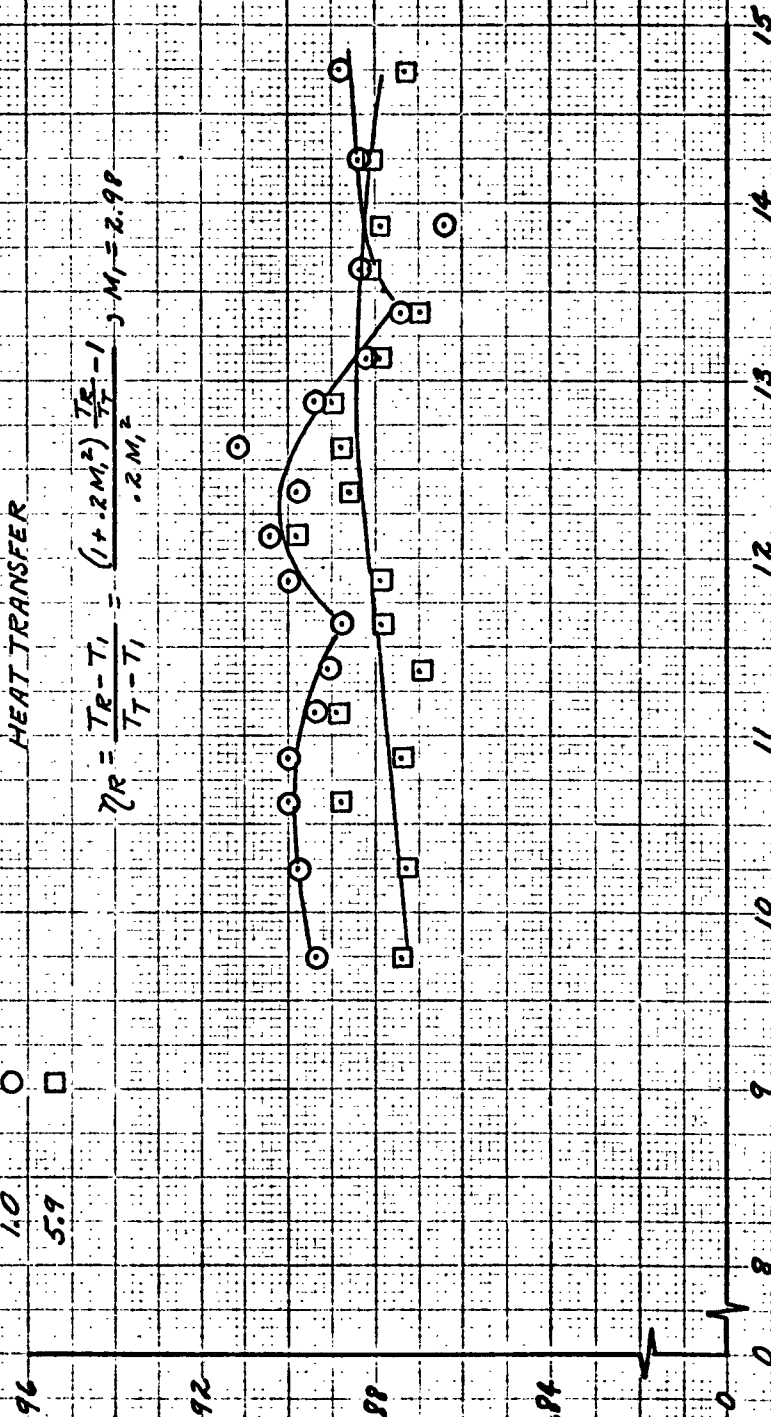
T_R = ISOTHERMAL TEMP. FOR LOCAL ZERO
HEAT TRANSFER

$$\eta_R = \frac{T_R - T_1}{T_T - T_1} = \frac{(1 + 2M_1^2) \frac{T_R}{T_1} - 1}{2M_1^2} \quad M_1 = 2.98$$

P_{02}/P_0 SYM
1.0 ○
5.9 □

EFFECTIVE RECOVERY FACTOR $\sim \eta_R$

DISTANCE FROM LEADING EDGE - INCHES



NORTH AMERICAN AVIATION, INC.

PREPARED BY:

PAGE NO. 105 OF

CHECKED BY:

REPORT NO. NA 62H-795

DATE:

MODEL NO.

COMPARISON OF RECOVERY FACTOR (η) AND EFFECTIVE RECOVERY FACTOR (η_R) AT $M_0 = 2.95$ WITH AND WITHOUT BOUNDARY LAYER BLOWING FOR A SHOCK GENERATOR PLATE ANGLE OF 0° .

$$\eta = \frac{T_{AW} - T_1}{T_T - T_1} = \frac{(1 + 2M_1^2) \frac{T_{AW}}{T_T} - 1}{2M_1^2}, M_1 = 2.98$$

$$\eta_R = \frac{T_R - T_1}{T_T - T_1} = \frac{(1 + 2M_1^2) \frac{T_R}{T_T} - 1}{2M_1^2}$$

SYM	P_{02}/P_0
η { \circ	1.0
η { \square	7.5
η_R { \circ	1.0
η_R { Δ	5.9

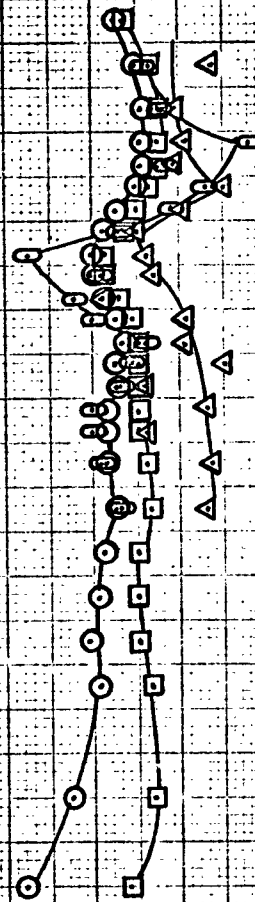
RECOVERY FACTOR $\sim \eta$ OR η_R 

FIG. 37

DISTANCE FROM LEADING EDGE ~ INCHES

DISTRIBUTION OF EFFECTIVE RECOVERY FACTOR AT $M_0 = 2.95$
FOR SHOCK GENERATOR PLATE ANGLE OF 6°

$$T_r = \text{ISOTHERMAL TEMP. FOR LOCAL ZERO HEAT TRANSFER}$$

$$\eta_R = \frac{T_r - T_f}{T_t - T_f} = \frac{(1 + 2 M_0^2) \frac{T_r}{T_f} - 1}{2 M_0^2}, M_0 = 2.99$$

P_r/P_0 $\frac{1}{2} M_0$ $\frac{1}{2} M_0$ $\frac{1}{2} M_0$

EFFECTIVE RECOVERY FACTOR η_R

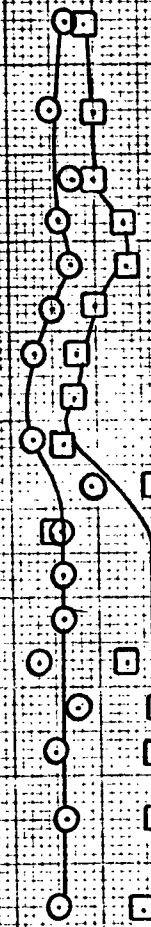


FIG. 38

DISTANCE FROM LEADING EDGE - INCHES

PREPARED BY:	NORTH AMERICAN AVIATION, INC.	PAGE NO. 107 OF
CHECKED BY:		REPORT NO. NA 62H-795
DATE:		MODEL NO.

FIG. 39

DISTRIBUTION OF EFFECTIVE RECOVERY FACTOR AT $M_0 = 2.95$
FOR A SHOCK GENERATOR PLATE ANGLE OF 9.5°

$T_R =$ ISOTHERMAL TEMP. FOR LOCAL ZERO
 HEAT TRANSFER

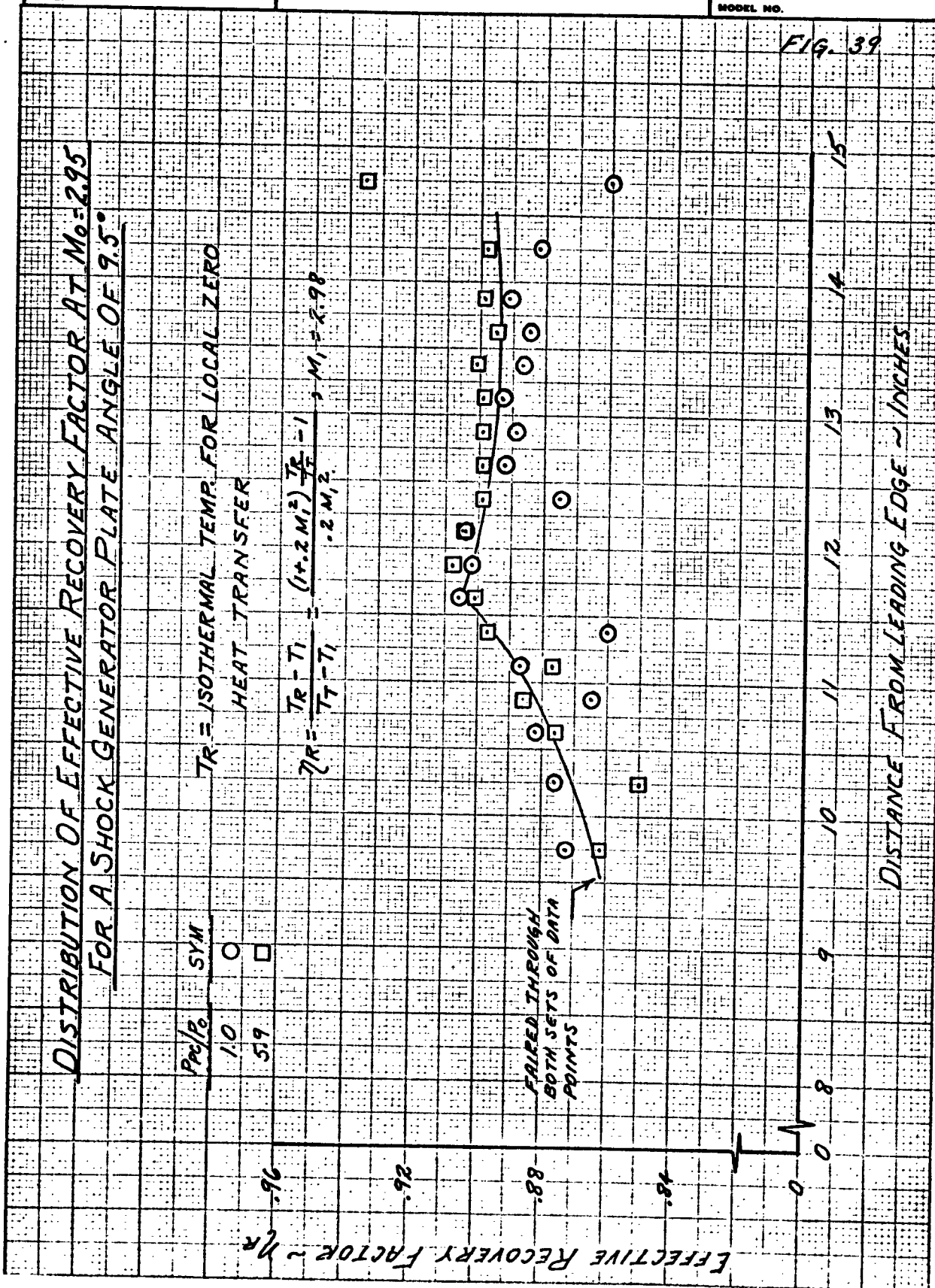
$$\eta_R = \frac{T_R - T_1}{T_1 - T_1} = \frac{(14.2 M_1^2) \frac{T_R}{T_1} - 1}{.2 M_1^2}, M_1 = 2.98$$

P_c/P_0 SYM
 1.0 \circ
 .59 \square

EFFECTIVE RECOVERY FACTOR $\sim \eta_R$

FAIRLED THROUGH
 BOTH SETS OF DATA
 POINTS

DISTANCE FROM LEADING EDGE ~ INCHES



PREPARED BY:

REPORT NO. NA 62H-795

CHECKED BY:

MODEL NO.

DATE:

Fig. 10

DISTRIBUTION OF EFFECTIVE RECOVERY FACTOR AT $M_0 = 2.95$
FOR A SHOCK GENERATOR PLATE ANGLE OF 12°

 $T_R = \text{ISOTHERMAL TEMP. FOR LOCAL ZERO}$
 HEAT TRANSFER

$$\eta_R = \frac{T_R - T_1}{T_T - T_1} = \frac{(+2.2M_1^2) \frac{T_R - 1}{T_1} - 1}{2.2M_1^2}, M_1 = 2.98$$

 P_{02}/P_0

SYM

1.0

O

2.0

□

5.9

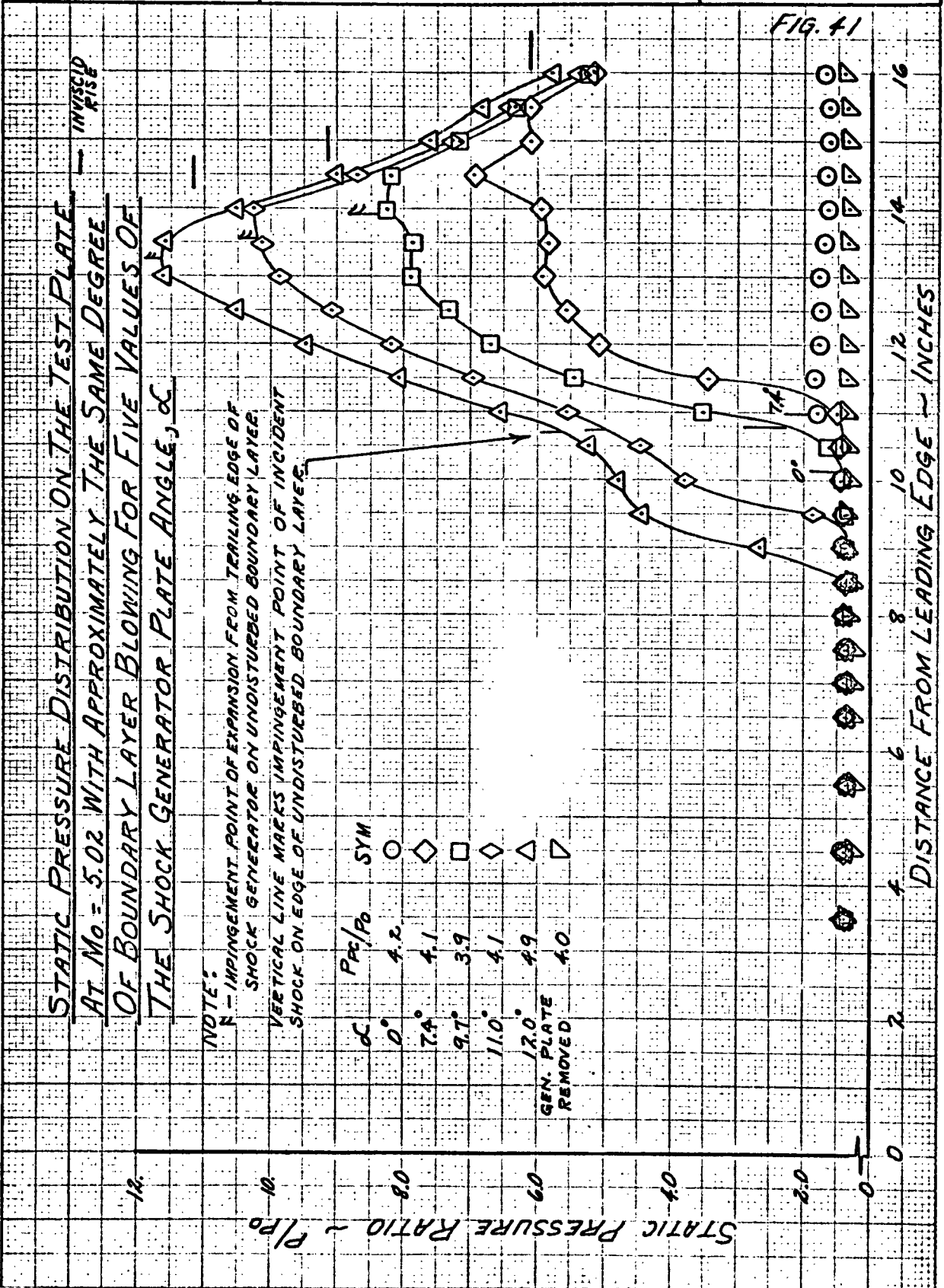
△

FAIRED THROUGH
ALL THREE SETS
OF DATA POINTS

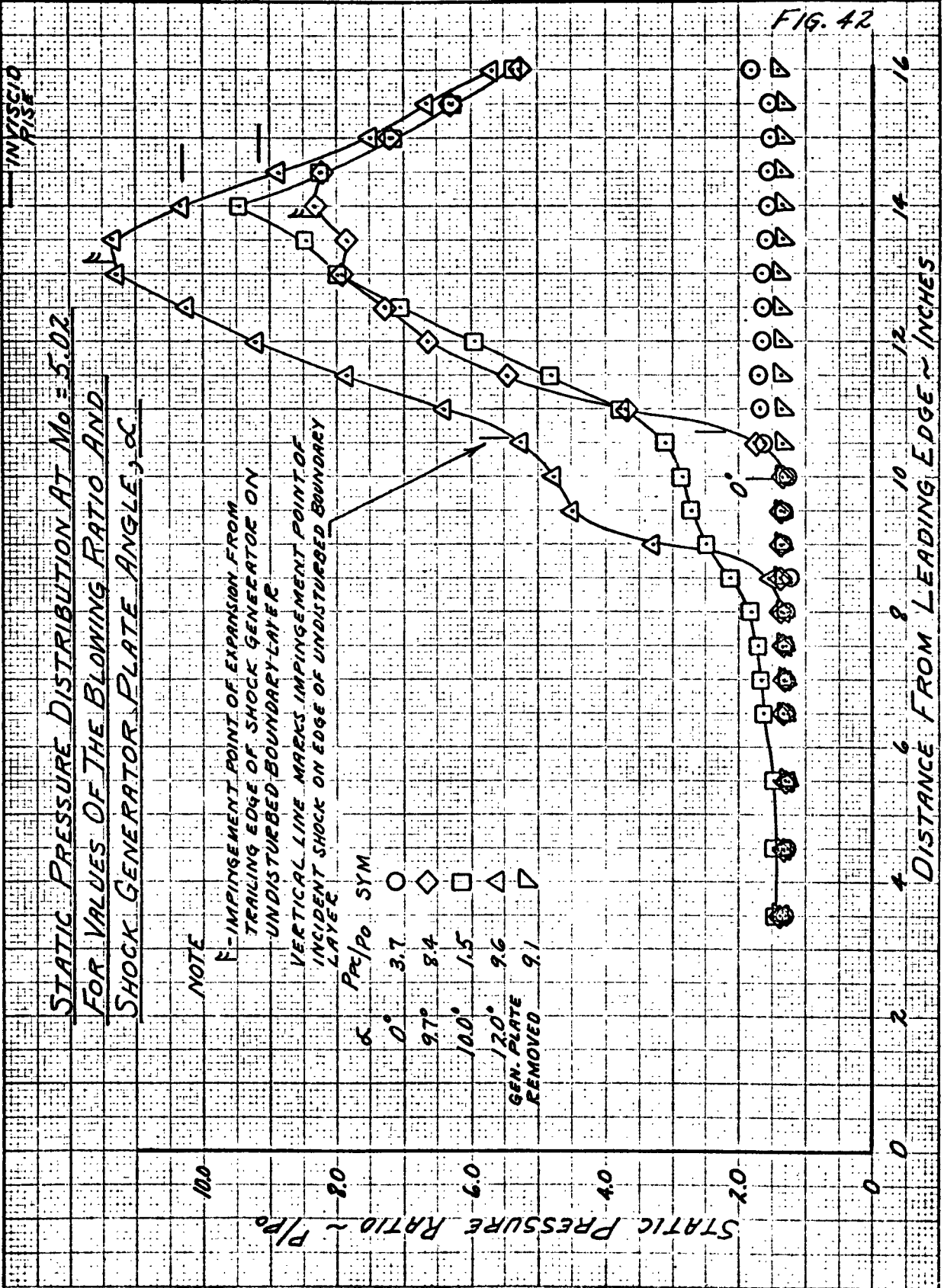
EFFECTIVE RECOVERY FACTOR $\sim \eta_R$ DISTANCE FROM LEADING EDGE \sim INCHES

0 0 8 9 10 11 12 13 14 15

PREPARED BY:	NORTH AMERICAN AVIATION, INC.	PAGE NO. 109 of
CHECKED BY:		REPORT NO. NA 62H-795
DATE:		MODEL NO.



PREPARED BY:	NORTH AMERICAN AVIATION, INC.	PAGE NO. 110 OF
CHECKED BY:		REPORT NO. NA 62H-795
DATE:		MODEL NO.



NORTH AMERICAN AVIATION, INC.

PREPARED BY:

PAGE NO. 111 OF

CHECKED BY:

REPORT NO. NA 62H-795

DATE:

MODEL NO.

FIG. 43

EFFECT OF BOUNDARY BLOWING ON THE STATIC
PRESSURE DISTRIBUTION AT $M_0 = 5.02$ FOR A SHOCK
GENERATOR PLATE ANGLE OF 11°

NOTE:

— IMPINGEMENT POINT OF EXPANSION FROM
TRAILING EDGE OF SHOCK GENERATOR ON
UNDISTURBED BOUNDARY LAYER

P/P_0 P_0 SYM

1.4

1.1

0.7

0.5

1.0

0.8

0.6

0.4

0.2

0.0

STATIC PRESSURE RATIO $\sim P/P_0$

DISTANCE FROM LEADING EDGE - INCHES

2

4

6

8

10

12

14

16

PREPARED BY:

NORTH AMERICAN AVIATION, INC.

PAGE NO. 112 OF

CHECKED BY:

REPORT NO. NA 62H-795

DATE:

MODEL NO.

BOUNDARY LAYER PROFILES AT $Mo = 5.02$

○ UPSTREAM RAKE $\sim X = 9.0$ INCHES
 □ DOWNSTREAM RAKE $\sim X = 15.0$ INCHES

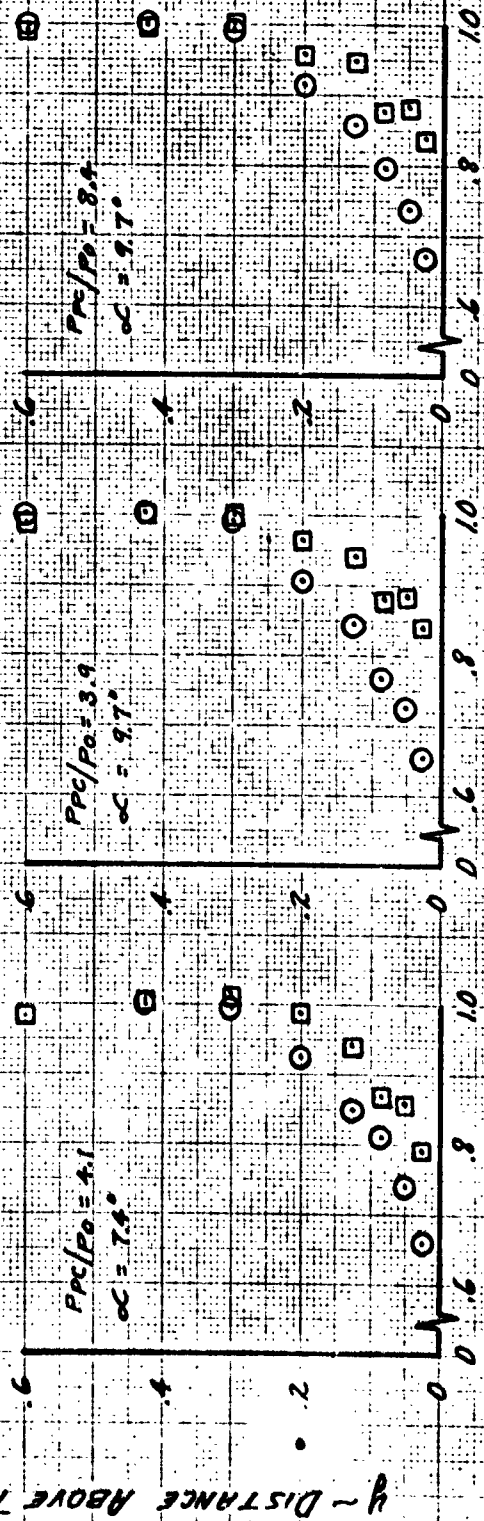
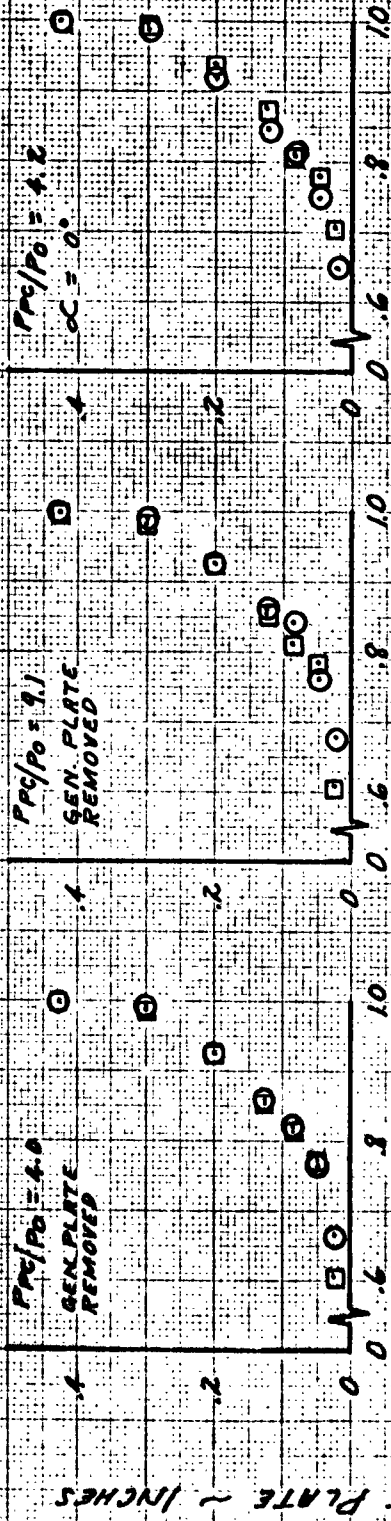


FIG. 44

$U/U_e \sim$ RATIO OF VELOCITY TO VELOCITY AT EDGE OF BOUNDARY LAYER

y ~ DISTANCE ABOVE TEST PLATE ~ INCHES

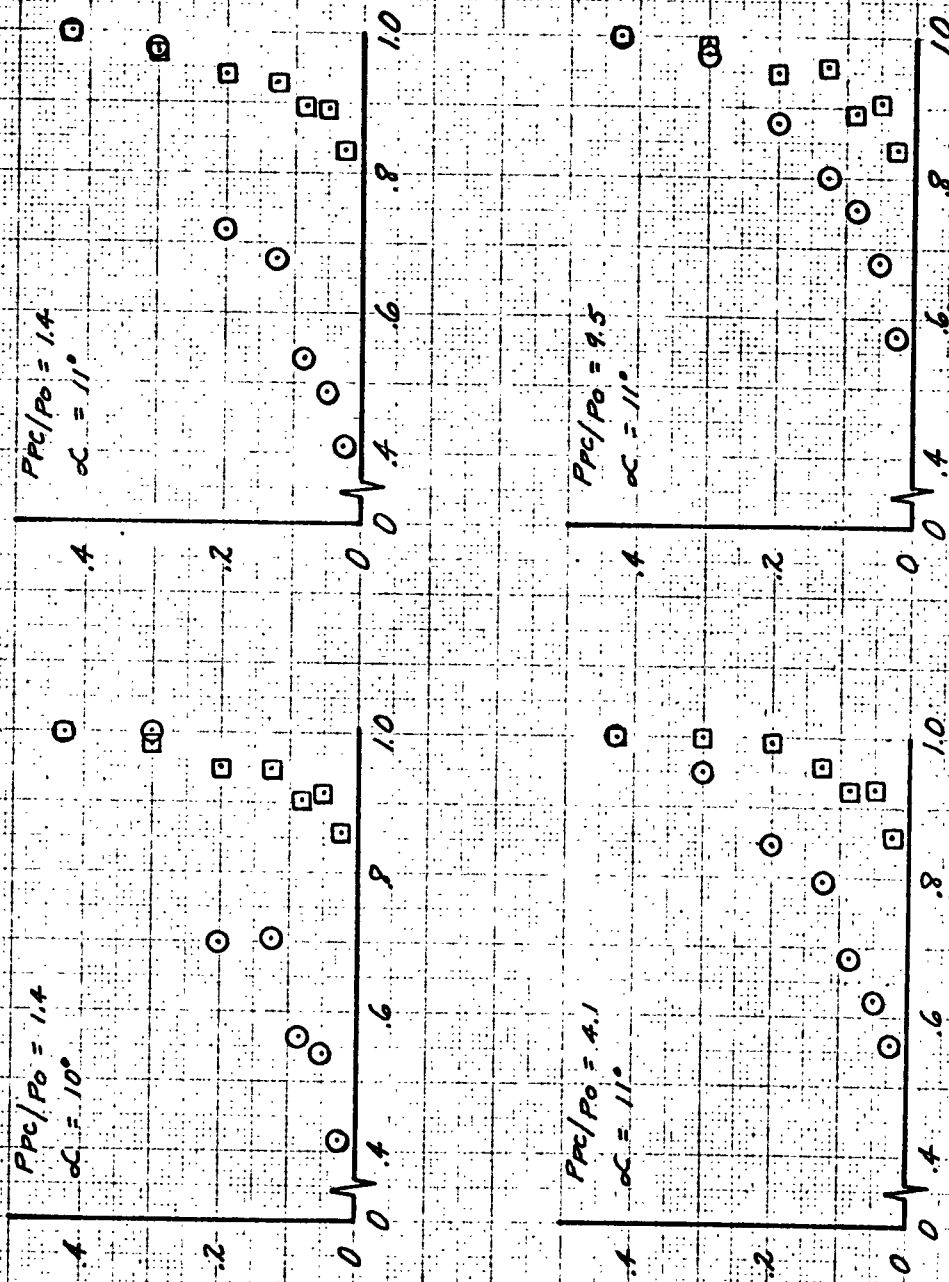
PREPARED BY:	NORTH AMERICAN AVIATION, INC.	PAGE NO. 113 OF
CHECKED BY:		REPORT NO. NA 62H-795
DATE:		MODEL NO.

FIG. 45

BOUNDARY LAYER PROFILES AT $M_0 = 5.02$

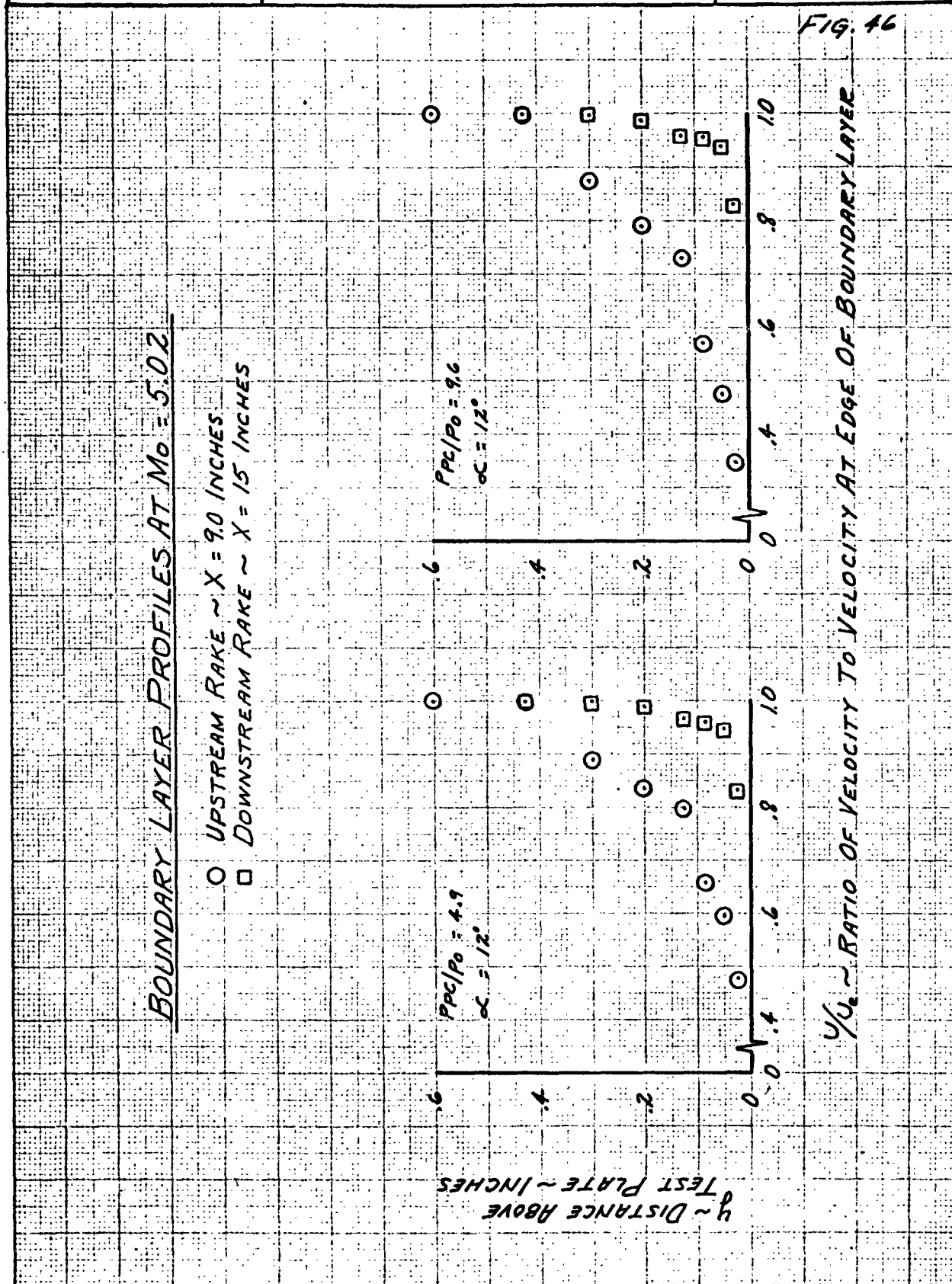
- UPSTREAM RAKE ~ $X = 9.0$ INCHES
- DOWNSTREAM RAKE ~ $X = 15$ INCHES

y ~ DISTANCE ABOVE TEST PLATE ~ INCHES



u/u_0 ~ RATIO OF VELOCITY TO VELOCITY AT EDGE OF BOUNDARY LAYER

PREPARED BY:		NORTH AMERICAN AVIATION, INC.	PAGE NO. 114 OF
CHECKED BY:			REPORT NO. NA 62H-795
DATE:			MODEL NO.



PREPARED BY:

NORTH AMERICAN AVIATION, INC.

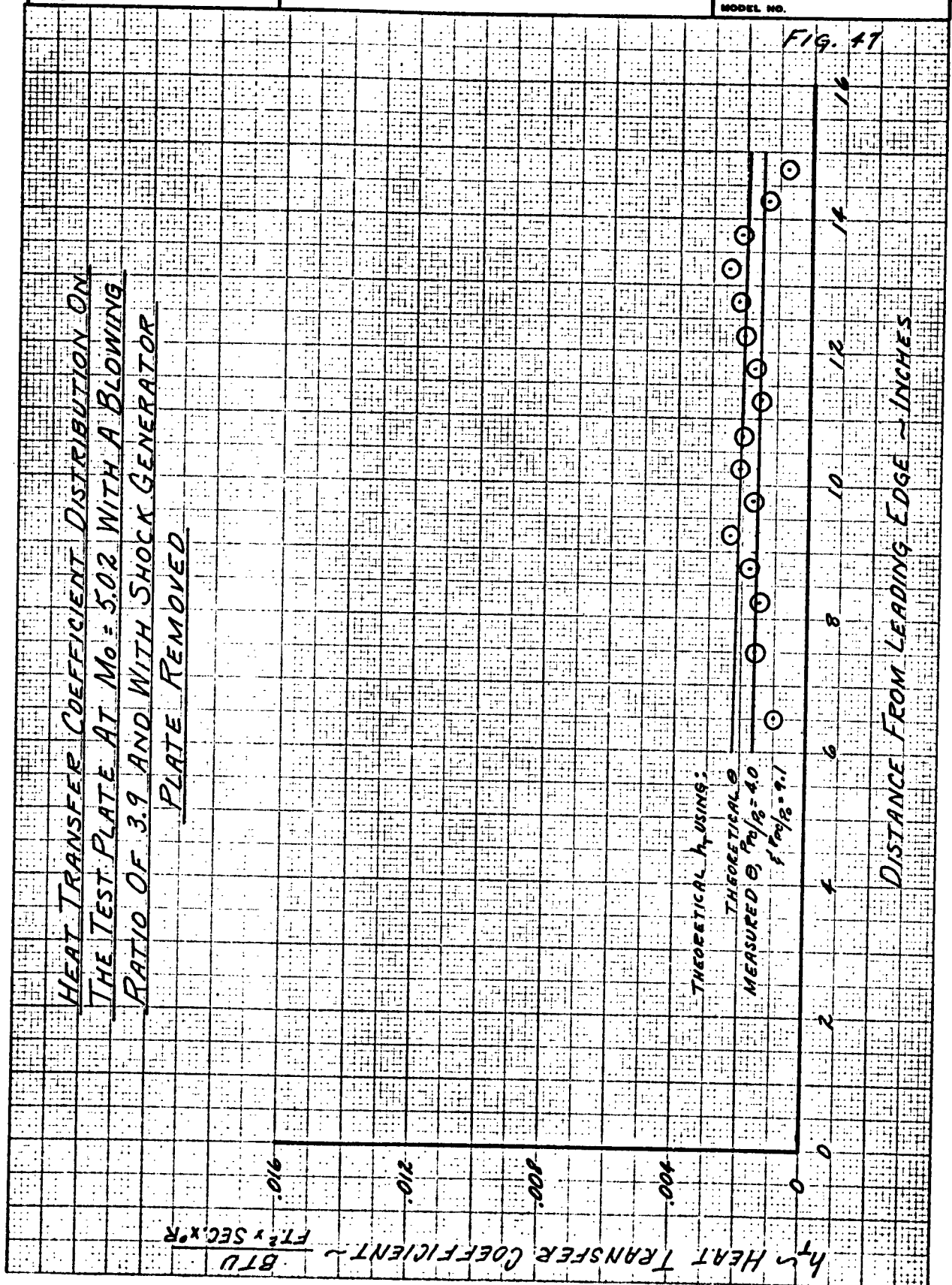
PAGE NO. 115 OF

CHECKED BY:

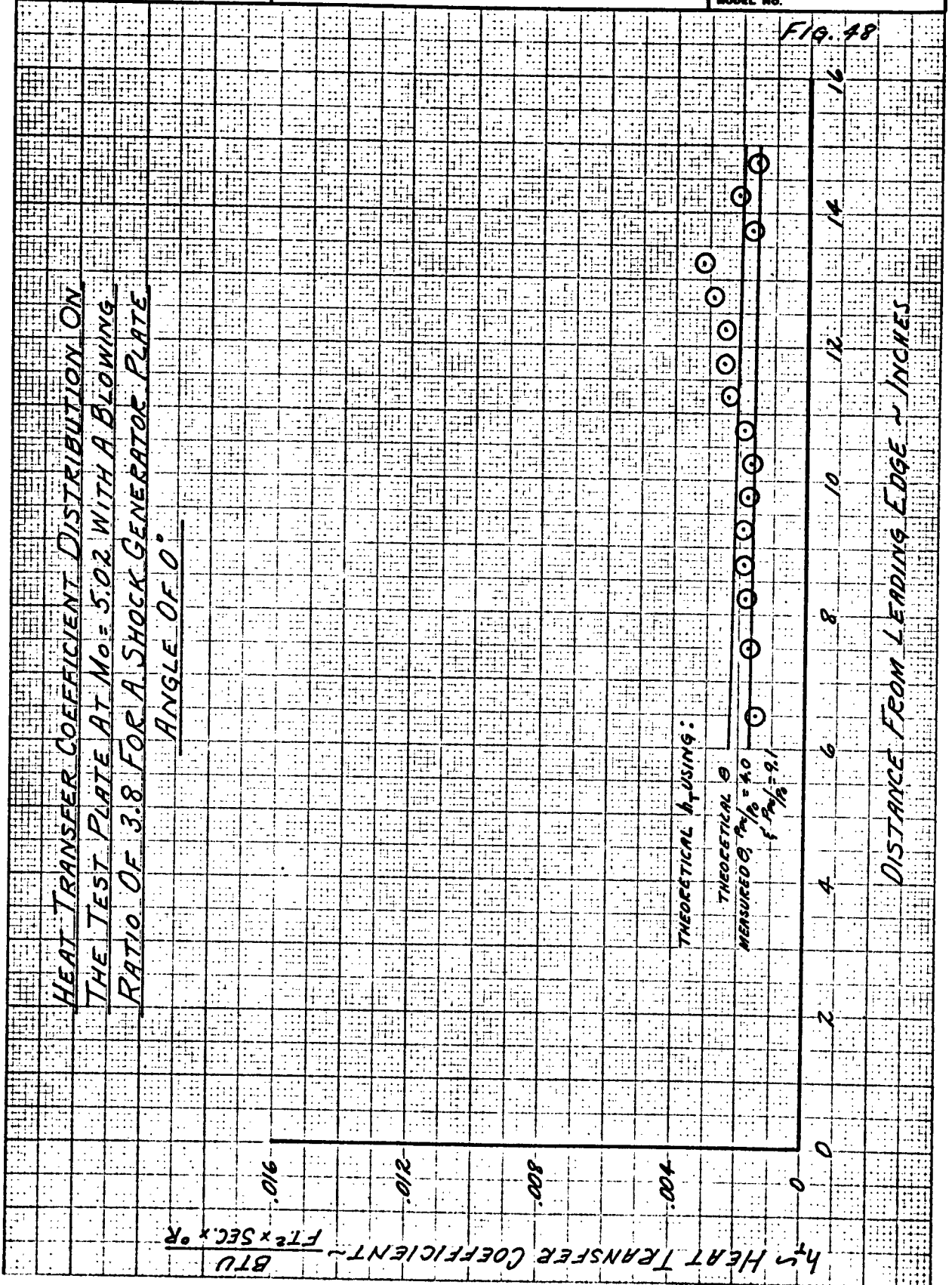
REPORT NO. NA 62H-795

DATE:

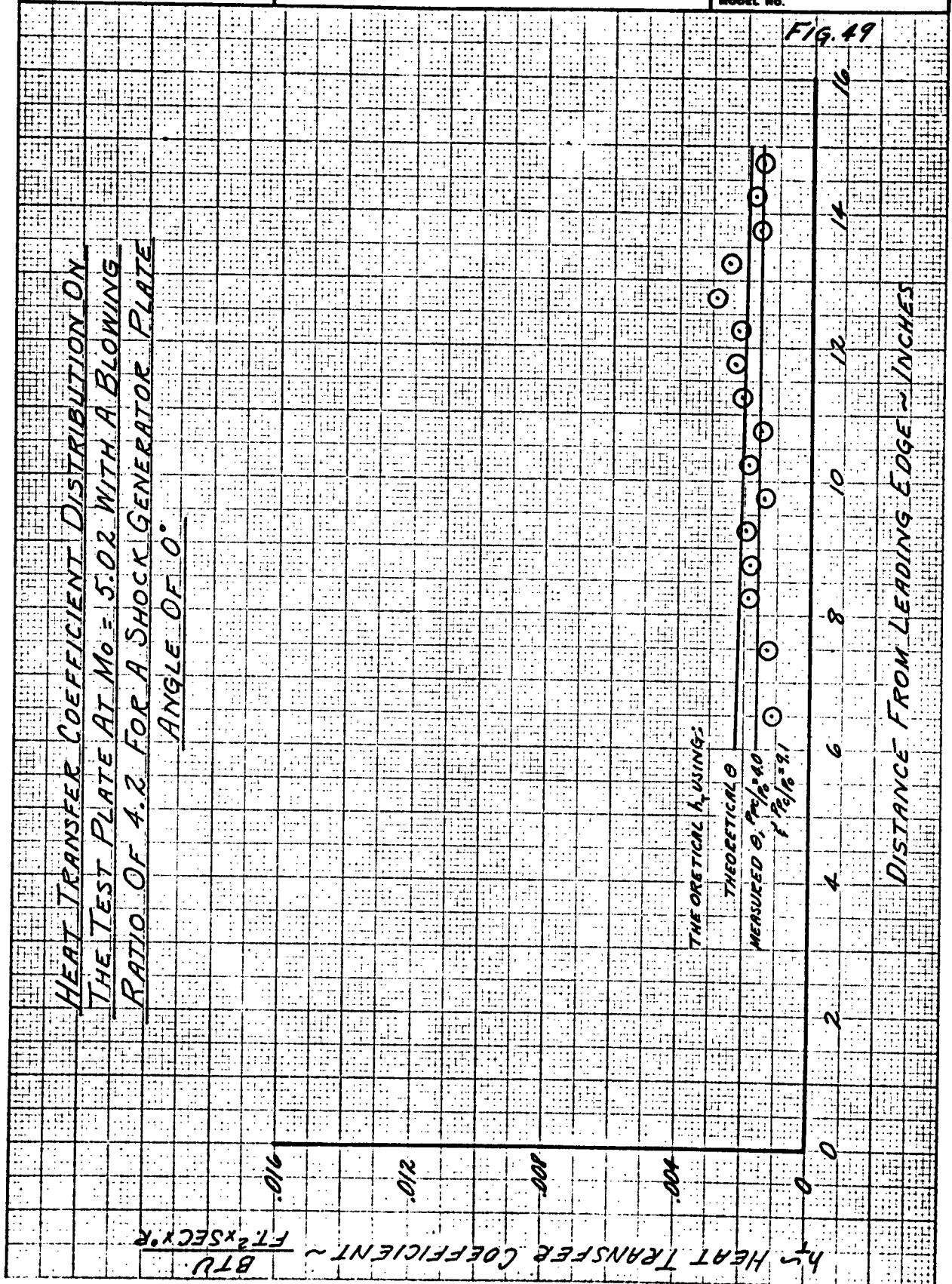
MODEL NO.



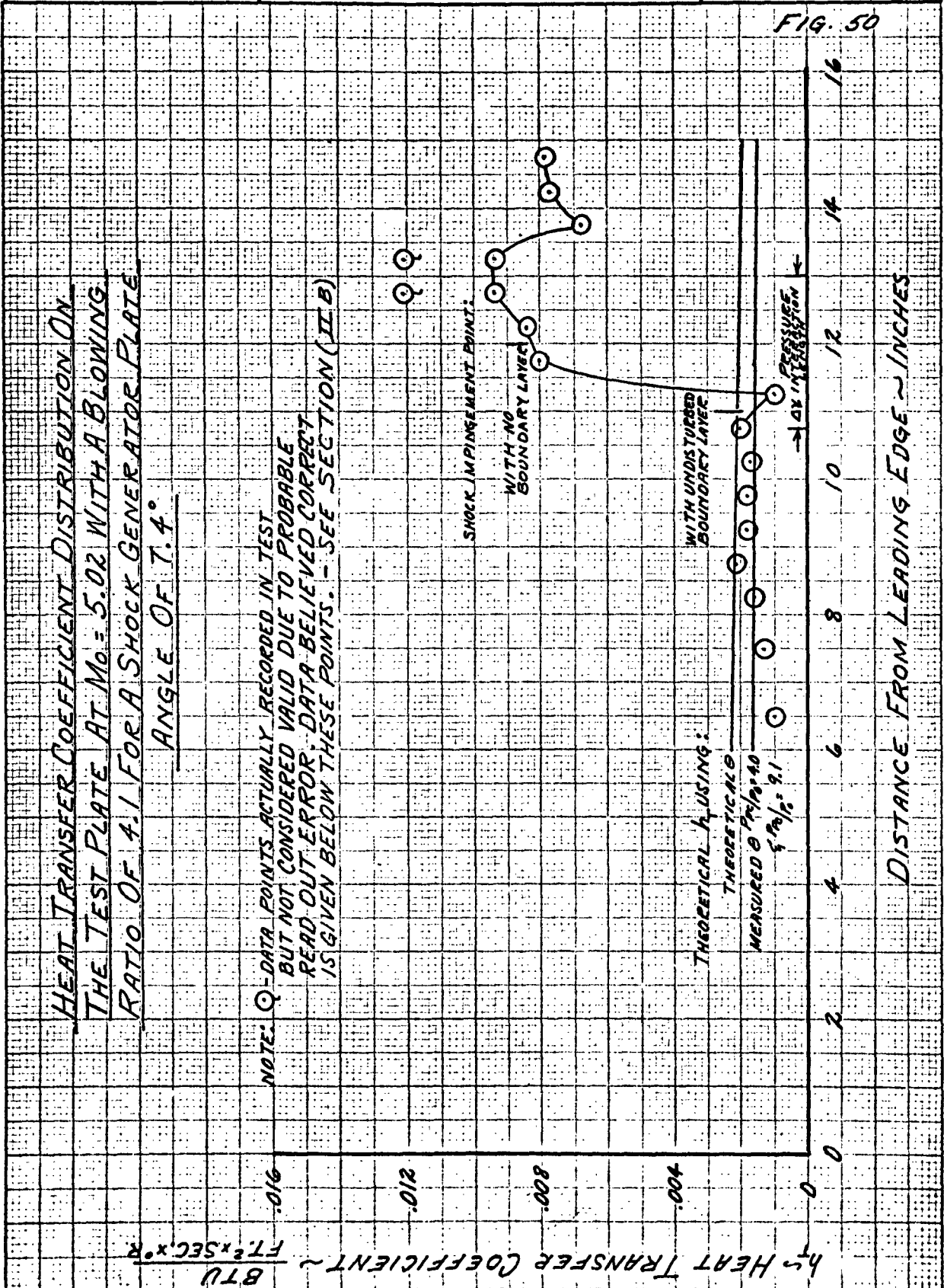
PREPARED BY:	NORTH AMERICAN AVIATION, INC.	PAGE NO. 116 OF
CHECKED BY:		REPORT NO. NA 62H-795
DATE:		MODEL NO.



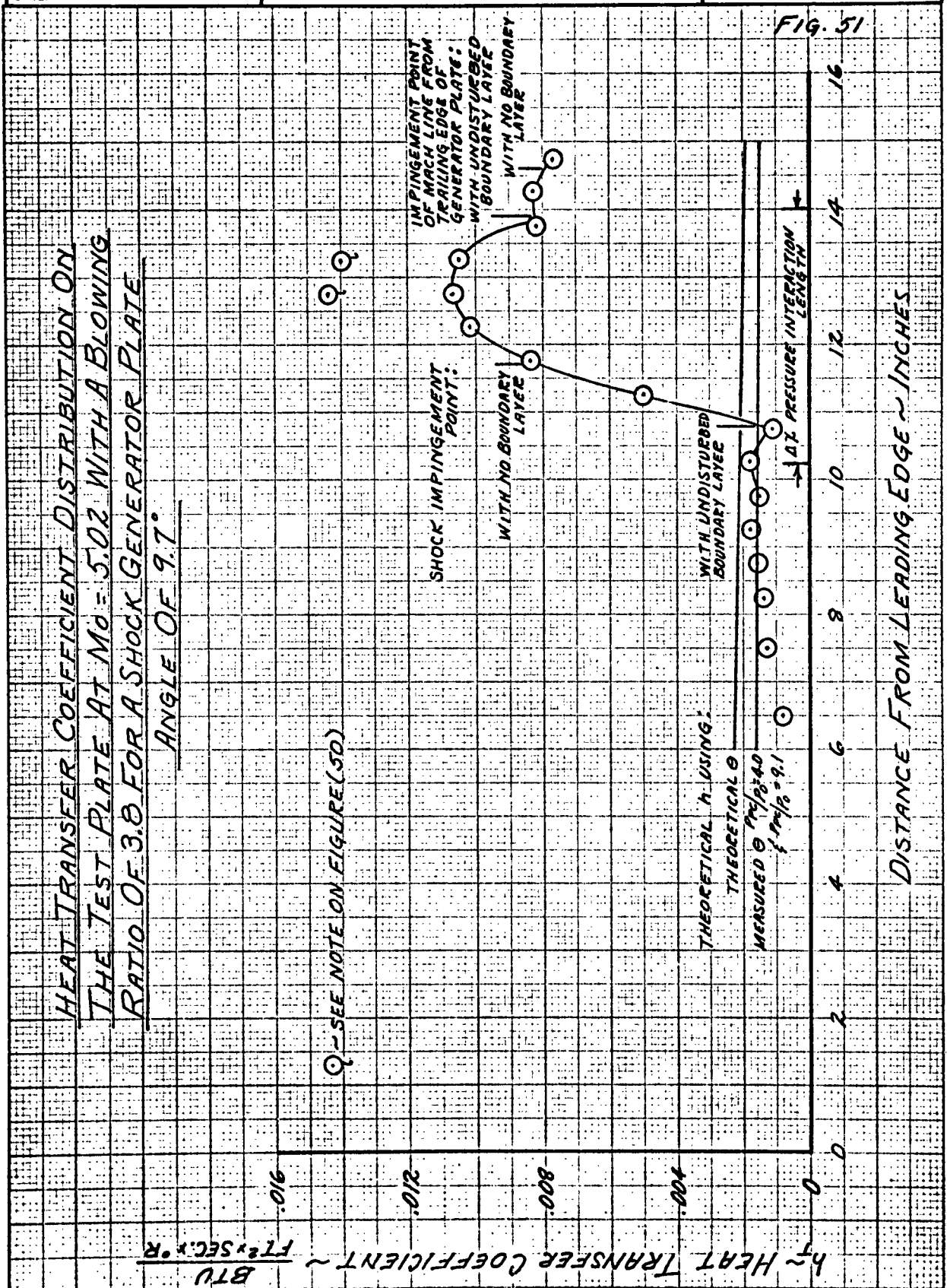
PREPARED BY:	NORTH AMERICAN AVIATION, INC.	PAGE NO. 117 of
CHECKED BY:		REPORT NO. NA 62H-795
DATE:		MODEL NO.



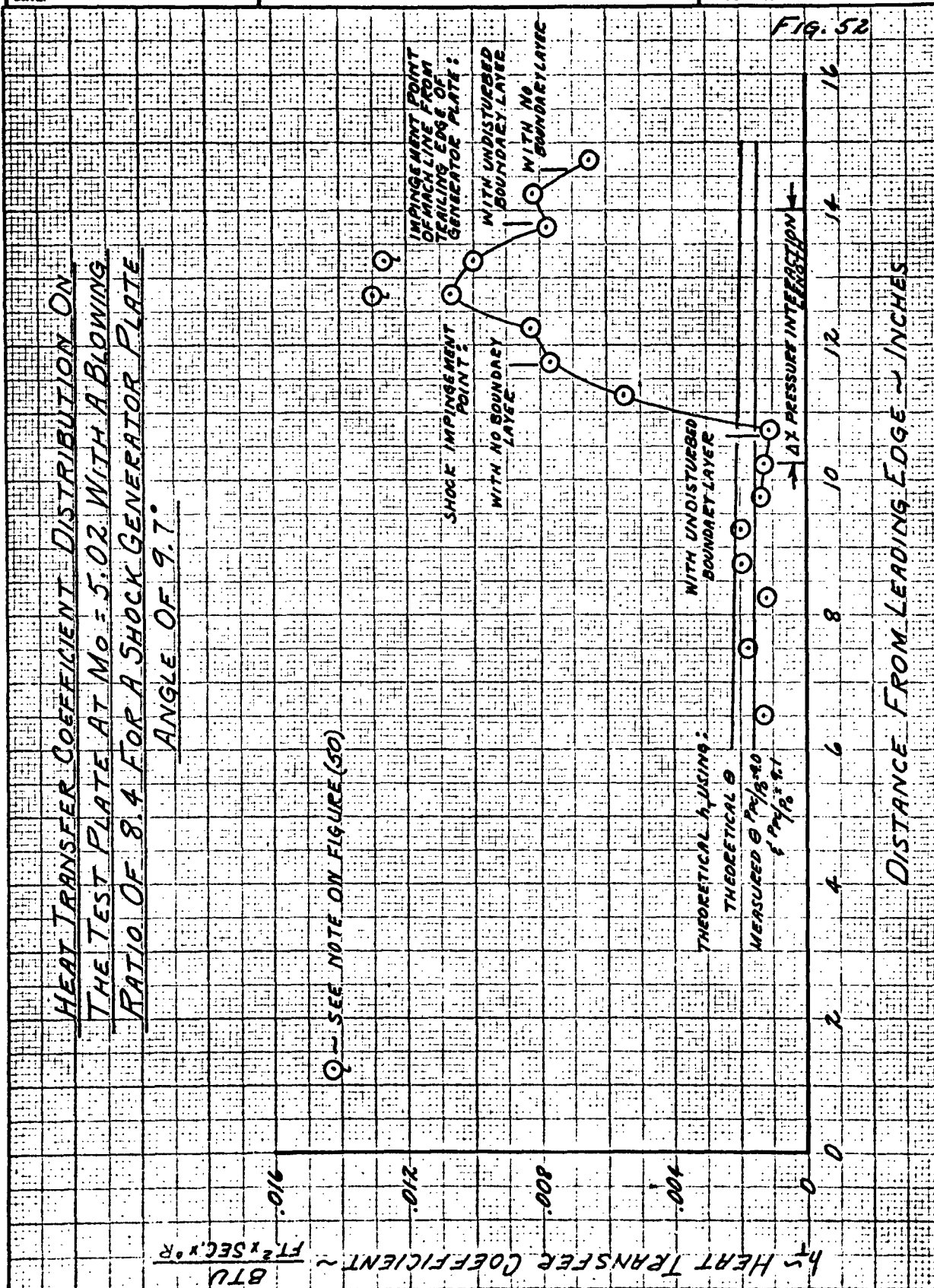
PREPARED BY:	NORTH AMERICAN AVIATION, INC.	PAGE NO. 118 ⁰⁷
CHECKED BY:		REPORT NO. NA 62H-795
DATE:		MODEL NO.



PREPARED BY:	NORTH AMERICAN AVIATION, INC.	PAGE NO. 119 of
CHECKED BY:		REPORT NO. NA 62H-795
DATE:		MODEL NO.



DATE:



NORTH AMERICAN AVIATION, INC.

PAGE NO. 121 OF

PREPARED BY:

CHECKED BY:

REPORT NO. NA 62H-795

DATE:

MODEL NO.

HEAT TRANSFER COEFFICIENT DISTRIBUTION ON
THE TEST PLATE AT $M_0 = 5.02$ WITH A BLOWING
RATIO OF 4.1 FOR A SHOCK GENERATOR PLATE

ANGLE OF 11°

$h \sim$ HEAT TRANSFER COEFFICIENT $\sim \frac{BTU}{FT^2 \cdot SEC \cdot ^\circ R}$

Q - SEE NOTE ON FIGURE (50)

IMPINGEMENT POINT
OF MACH LINE FROM
TRAILING EDGE OF
GENERATOR PLATE:

WITH UNDISTURBED
BOUNDARY LAYER

WITH NO
BOUNDARY LAYER

SHOCK IMPINGEMENT
POINT:
WITH NO BOUNDARY
LAYER

WITH UNDISTURBED
BOUNDARY
LAYER

THEORETICAL h USING:

THEORETICAL θ

MEASURED θ $\frac{P_2}{P_1} = 4.0$

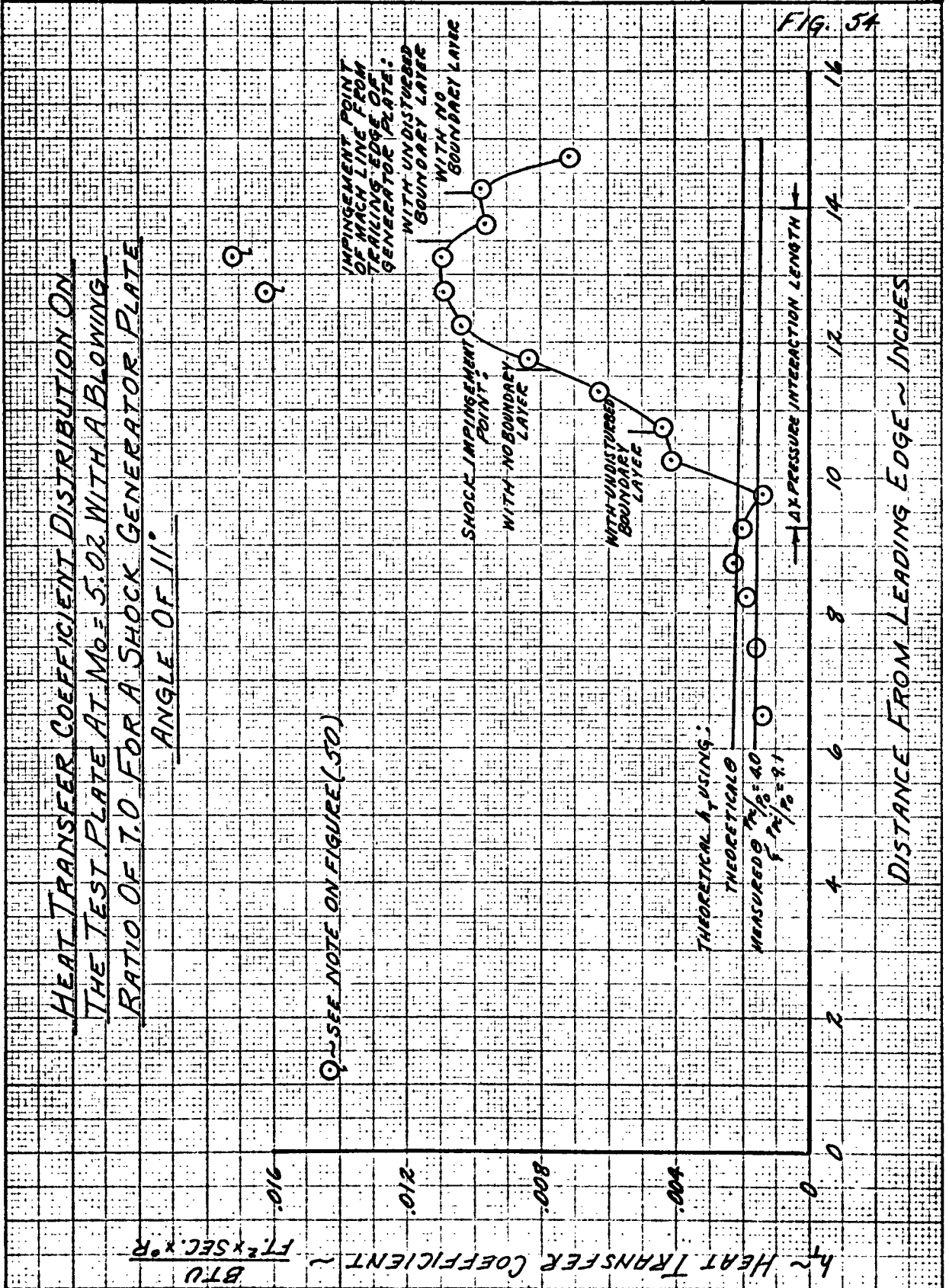
$\frac{f_1 P_2}{f_2 P_1} = 9.1$

Δx PRESSURE INTERACTION LENGTH

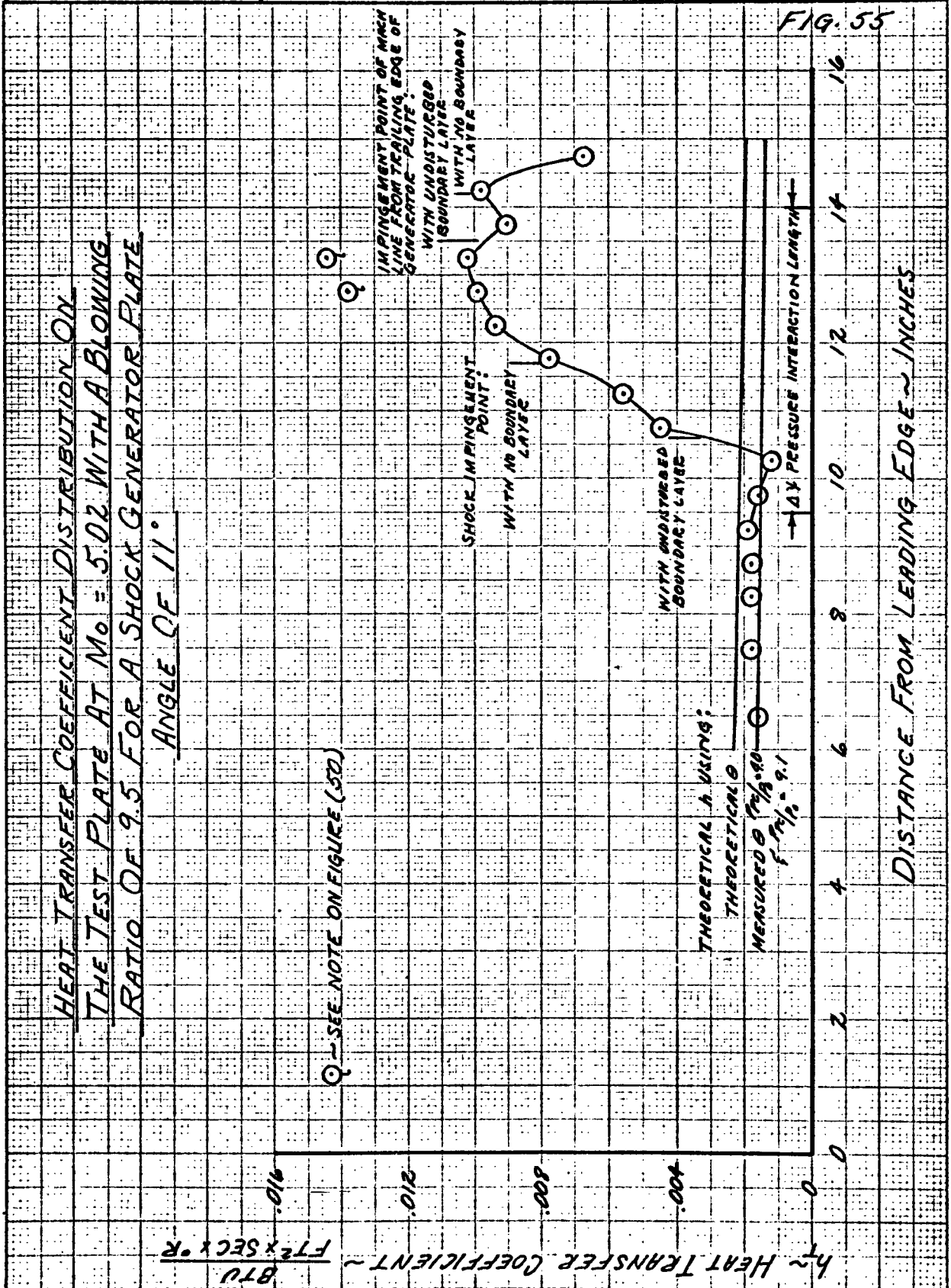
FIG. 53

DISTANCE FROM LEADING EDGE - INCHES

PREPARED BY:	NORTH AMERICAN AVIATION, INC.	PAGE NO. 122 OF
CHECKED BY:		REPORT NO. NA 62H-795
DATE:		MODEL NO.



PREPARED BY:	NORTH AMERICAN AVIATION, INC.	PAGE NO. 123 OF
CHECKED BY:		REPORT NO. NA 62H-795
DATE:		MODEL NO.



PREPARED BY:	NORTH AMERICAN AVIATION, INC.	PAGE NO. 124 OF
CHECKED BY:		REPORT NO. NA 62H-795
DATE:		MODEL NO.

HEAT TRANSFER COEFFICIENT DISTRIBUTION ON
THE TEST PLATE AT $M_0 = 5.02$ WITH A BLOWING
RATIO OF 4.9 FOR A SHOCK GENERATOR PLATE
ANGLE OF 12°

Q - SEE NOTE ON FIGURE (50)

$h \sim$ HEAT TRANSFER COEFFICIENT - $\frac{BTU}{FT^2 \cdot SEC \cdot R}$

IMPINGEMENT POINT OF HIGH
LINE FROM TRAILING EDGE
OF GENERATOR PLATE

WITH UNDISTURBED
BOUNDARY LAYER

WITH NO BOUNDARY
LAYER

SHOCK IMPINGEMENT
POINT:
WITH NO BOUNDARY
LAYER

WITH UNDISTURBED
BOUNDARY LAYER

THEORETICAL h USING:

THEORETICAL θ

MEASURED θ $P_0/P_\infty = 0.1$

$P_0/P_\infty = 0.1$

ΔX PRESSURE INTERACTION LENGTH

FIG. 56

DISTANCE FROM LEADING EDGE - INCHES

NORTH AMERICAN AVIATION, INC.

PAGE NO. 125 OF

PREPARED BY:

REPORT NO. NA 62H-795

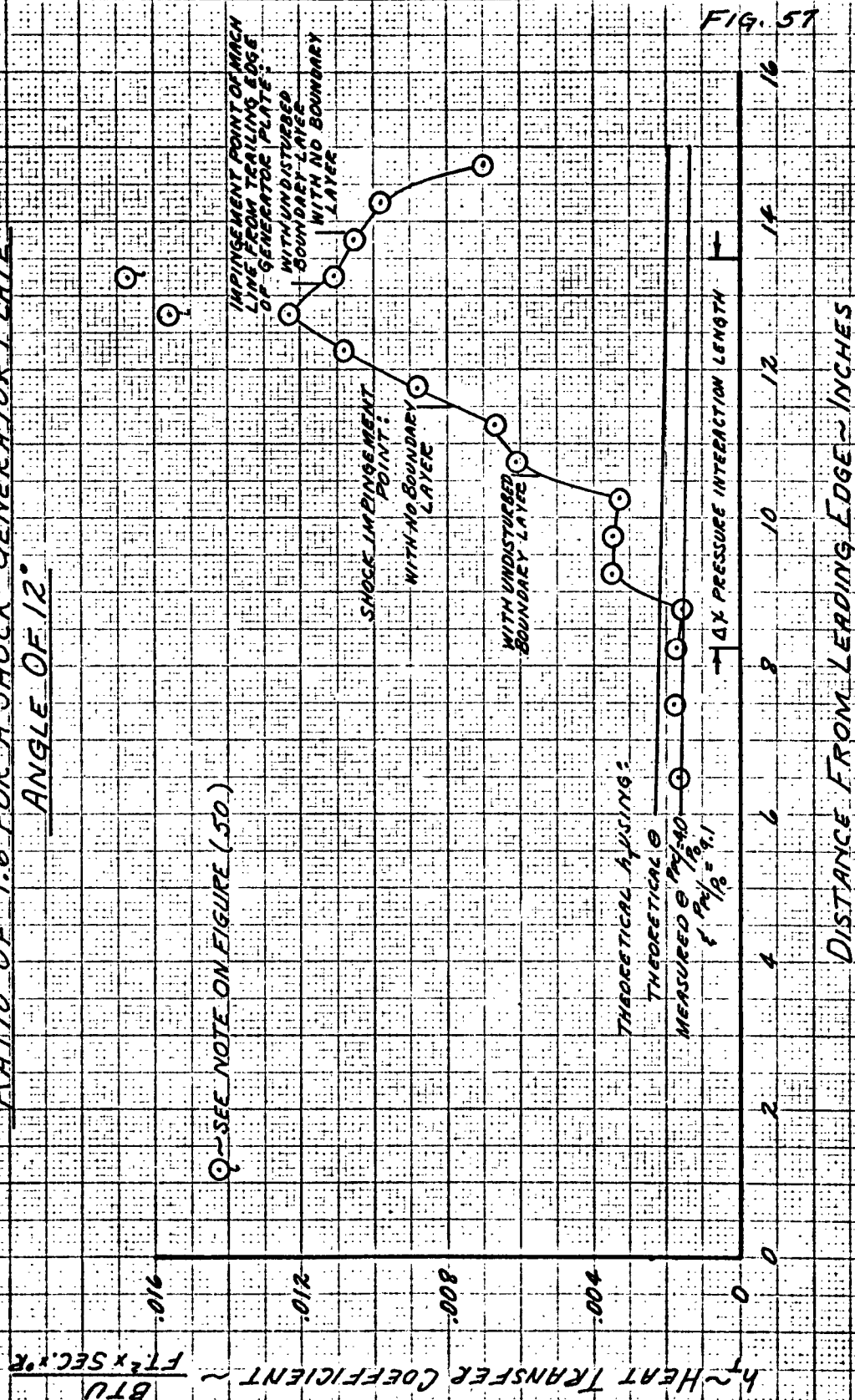
CHECKED BY:

DATE:

MODEL NO.

FIG. 57

HEAT TRANSFER COEFFICIENT DISTRIBUTION ON
THE TEST PLATE AT $M_0 = 5.02$ WITH A BLOWING
RATIO OF 9.6 FOR A SHOCK GENERATOR PLATE
ANGLE OF 12°



NORTH AMERICAN AVIATION, INC.

PREPARED BY:

PAGE NO. 126 OF

CHECKED BY:

REPORT NO. NA 62H-795

DATE:

MODEL NO.

FIG. 58

HEAT TRANSFER COEFFICIENT DISTRIBUTION ON THE
TEST PLATE AT $M_0 = 5.03$ WITH NO BOUNDARY LAYER
BLOWING FOR A SHOCK GENERATOR PLATE ANGLE OF 10°

Q~SEE NOTE ON FIGURE (50)

$h \sim$ HEAT TRANSFER COEFFICIENT $\sim \frac{BTU}{FT^2 \times SEC \times R}$

THEORETICAL h USING:

THEORETICAL θ

MEASURED θ $\frac{P_{01}}{P_0} = 0.40$

$\frac{P_{01}}{P_0} = 0.91$

DISTANCE FROM LEADING EDGE IN INCHES

0 2 4 6 8 10 12 14 16

910°

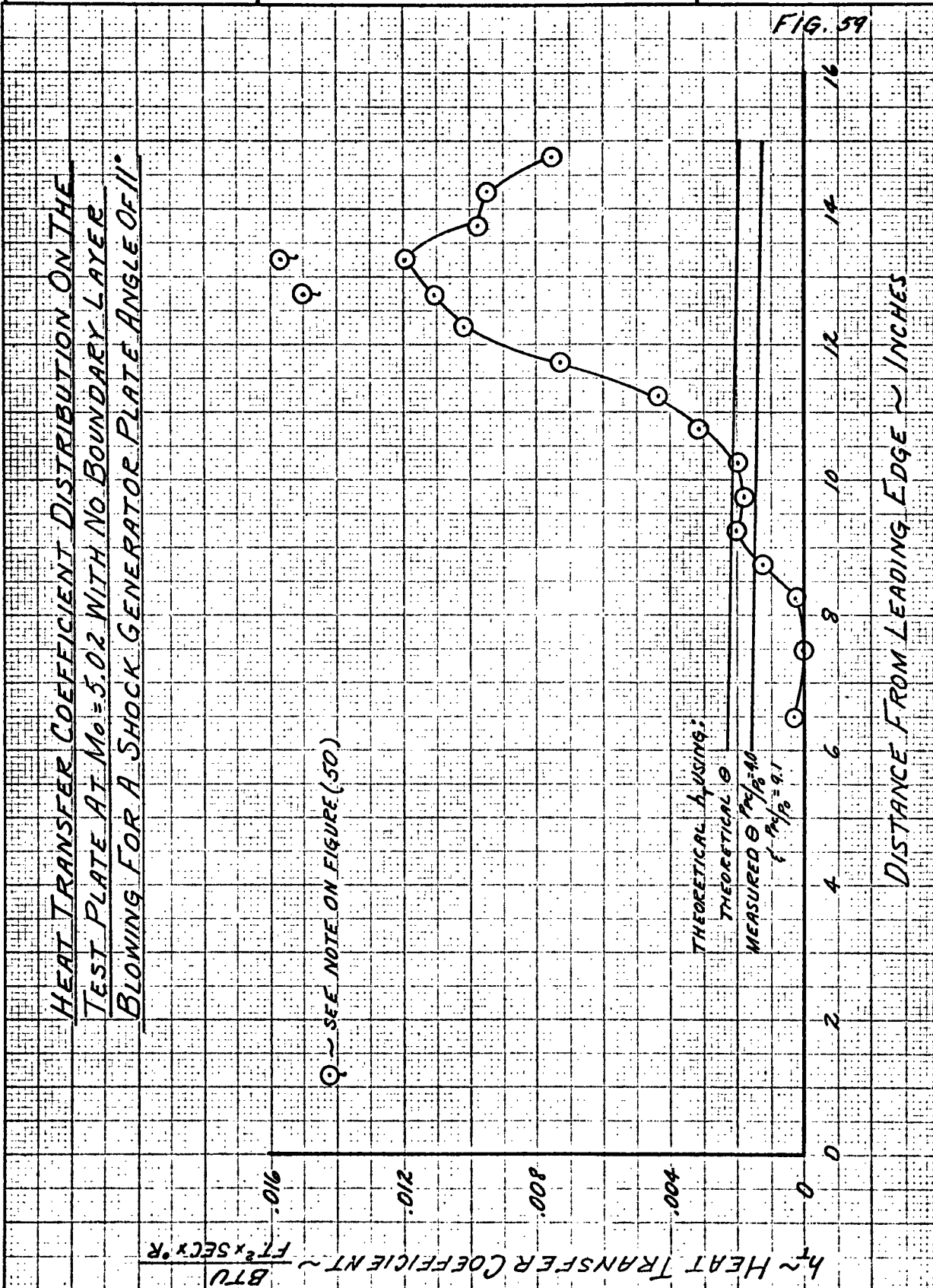
210°

800°

400°

0

PREPARED BY:	NORTH AMERICAN AVIATION, INC.	PAGE NO. 127 OF
CHECKED BY:		REPORT NO. NA 62H-795
DATE:		MODEL NO.



NORTH AMERICAN AVIATION, INC.

PAGE NO. 128 OF

PREPARED BY:

REPORT NO. NA 62H-795

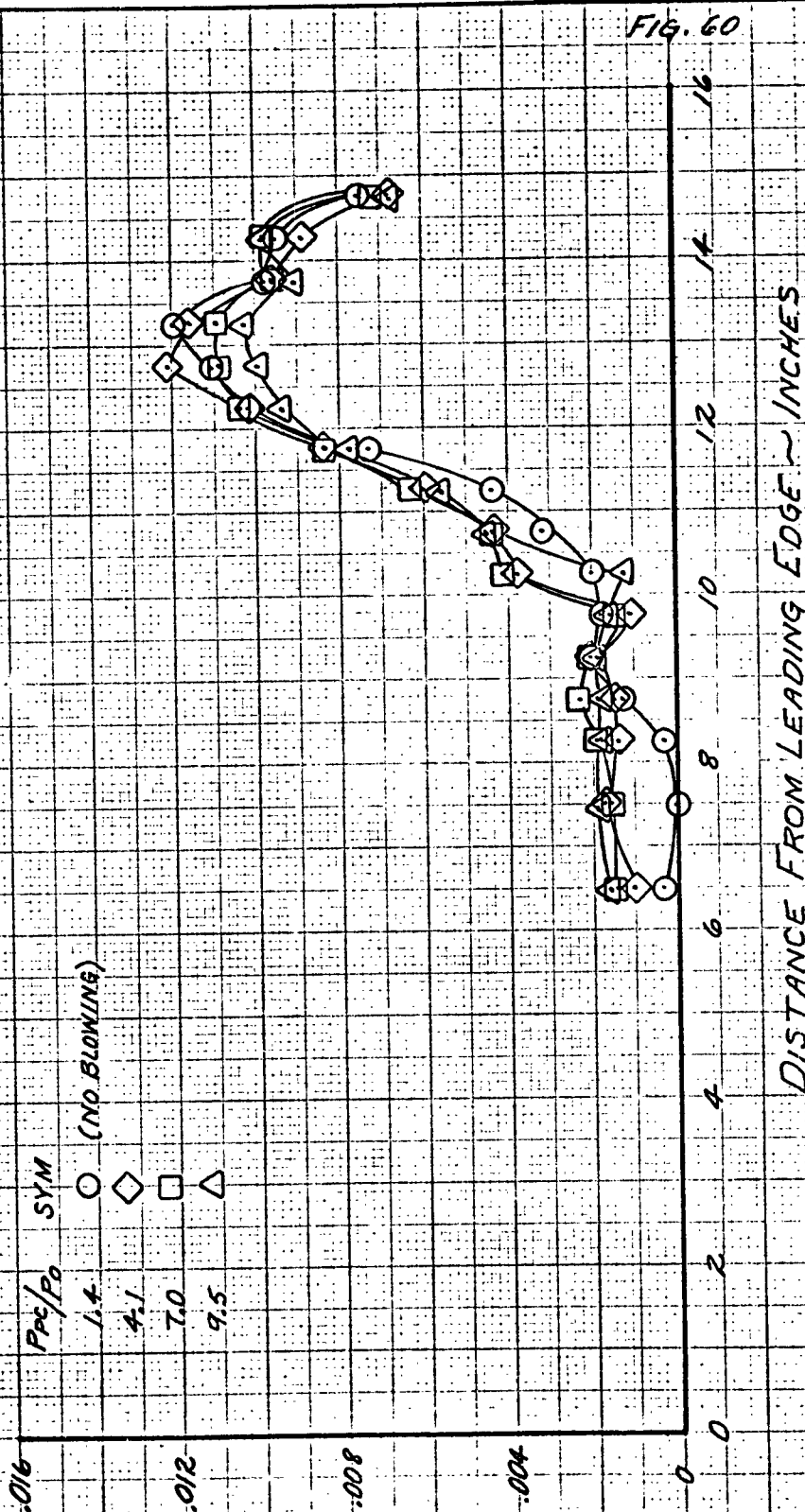
CHECKED BY:

MODEL NO.

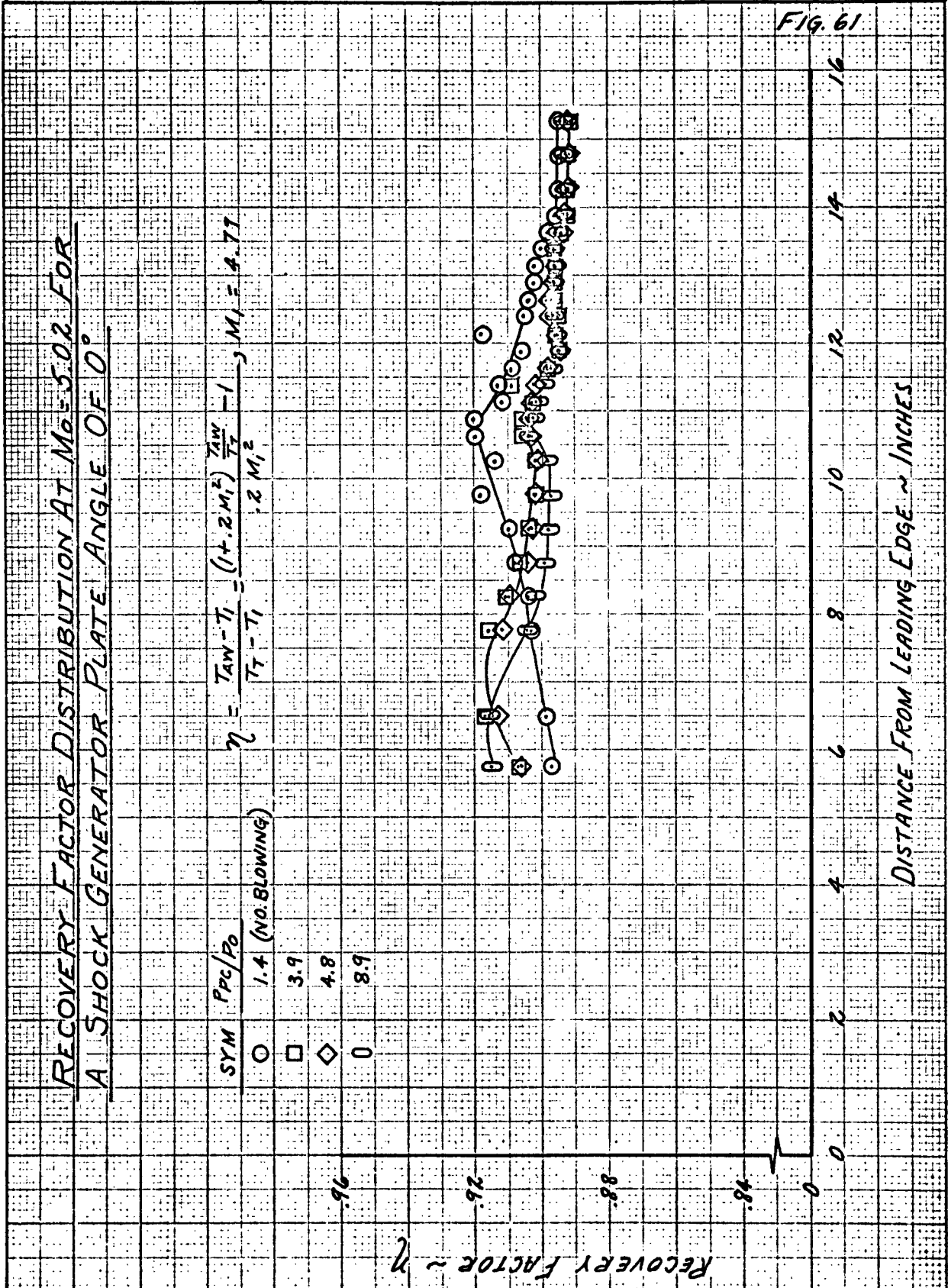
DATE:

EFFECT OF BOUNDARY LAYER BLOWING ON THE
HEAT TRANSFER COEFFICIENT DISTRIBUTION AT
 $M_o = 5.02$ FOR A SHOCK GENERATOR PLATE
ANGLE OF 11°

$h \sim$ HEAT TRANSFER COEFFICIENT $\sim \frac{BTU}{FT^2 \times SEC \times ^\circ F}$



PREPARED BY:		NORTH AMERICAN AVIATION, INC.	PAGE NO. 129 OF
CHECKED BY:			REPORT NO. NA 62H-795
DATE:			MODEL NO.

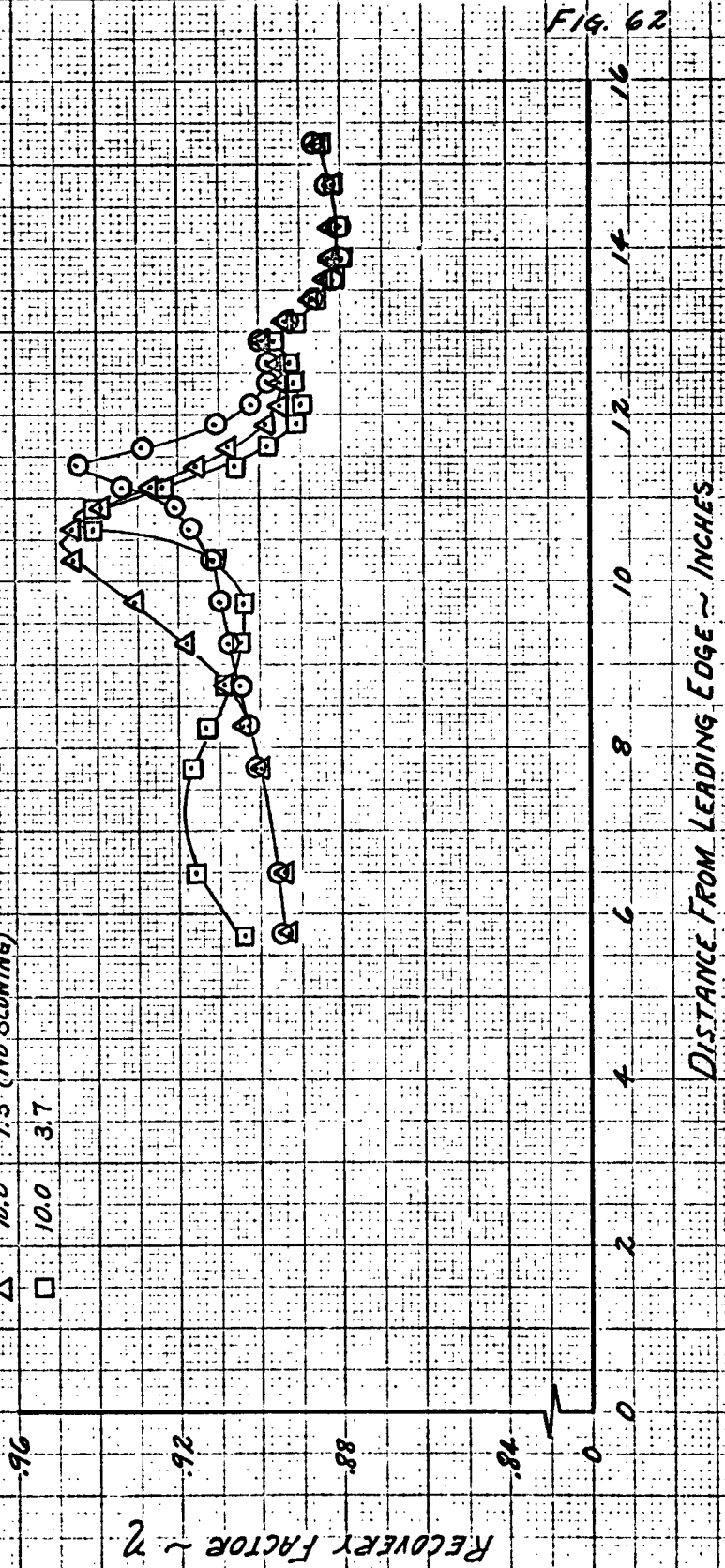


PREPARED BY:	NORTH AMERICAN AVIATION, INC.	PAGE NO. 130 OF
CHECKED BY:		REPORT NO. NA 62H-795
DATE:		MODEL NO.

RECOVERY FACTOR DISTRIBUTION AT $M_0 = 5.02$ FOR
SHOCK GENERATOR PLATE ANGLES OF 7.4° AND 10.0°

$$\eta = \frac{T_{AW} - T_1}{T_T - T_1} = \frac{(14.2 M_1^2) T_T - 1}{2 M_1^2} \quad , \quad M_1 = 4.77$$

SYM	α	P_{02}/P_0
○	7.4°	1.4 (NO BLOWING)
△	10.0°	1.5 (NO BLOWING)
□	10.0°	3.7



NORTH AMERICAN AVIATION, INC.

PREPARED BY:

PAGE NO. 131 OF

CHECKED BY:

REPORT NO. NA 62H-795

DATE:

MODEL NO.

RECOVERY FACTOR DISTRIBUTION AT $M_0 = 5.02$ FOR
A SHOCK GENERATOR PLATE ANGLE OF 12°

$$\eta = \frac{T_{AW} - T_1}{T_1 - T_1} = \frac{(1 + 2M_1^2) \frac{T_{AW}}{T_1} - 1}{2M_1^2}, M_1 = 4.77$$

SYM P_{01}/P_0
O 1.6 (NO BLOWING)
□ 3.9

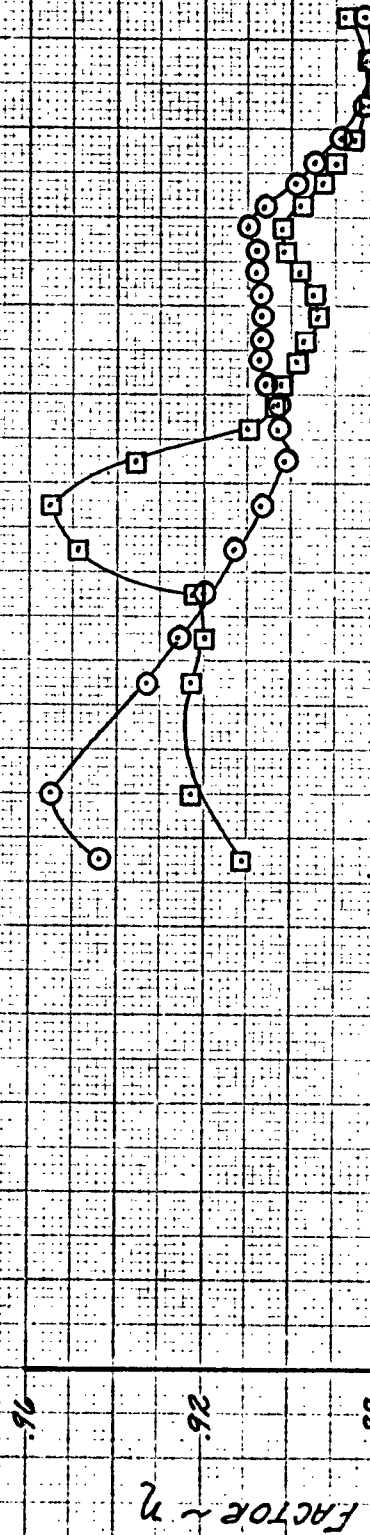


FIG. 63

DISTANCE FROM LEADING EDGE ~ INCHES

RECOVERY FACTOR $\sim \eta$

NORTH AMERICAN AVIATION, INC.

PREPARED BY:

PAGE NO.

132 of

CHECKED BY:

REPORT NO.

NA 62H-795

DATE:

MODEL NO.

FIG. 64

DISTRIBUTION OF EFFECTIVE RECOVERY FACTOR AT $M_0 = 5.02$
FOR A SHOCK GENERATOR PLATE ANGLE OF 0° AND ALSO WITH
THE PLATE REMOVED

T_R = ISOTHERMAL TEMP. FOR LOCAL ZERO
 HEAT TRANSFER

$$\eta_R = \frac{T_R - T_i}{T_T - T_i} = \frac{(1 + 2M_0^2) \frac{T_R}{T_i} - 1}{2M_0^2}, M_0 = 4.77$$

P_{0c}/P_0 & SYM

4.0 GEN PLATE
 REMOVED

3.7 0°

4.2 0°

EFFECTIVE RECOVERY FACTOR $\sim \eta_R$

FAKED CURVE

DISTANCE FROM LEADING EDGE ~ INCHES

NORTH AMERICAN AVIATION, INC.

PREPARED BY:

PAGE NO. 133 of

CHECKED BY:

REPORT NO. NA 62H-795

DATE:

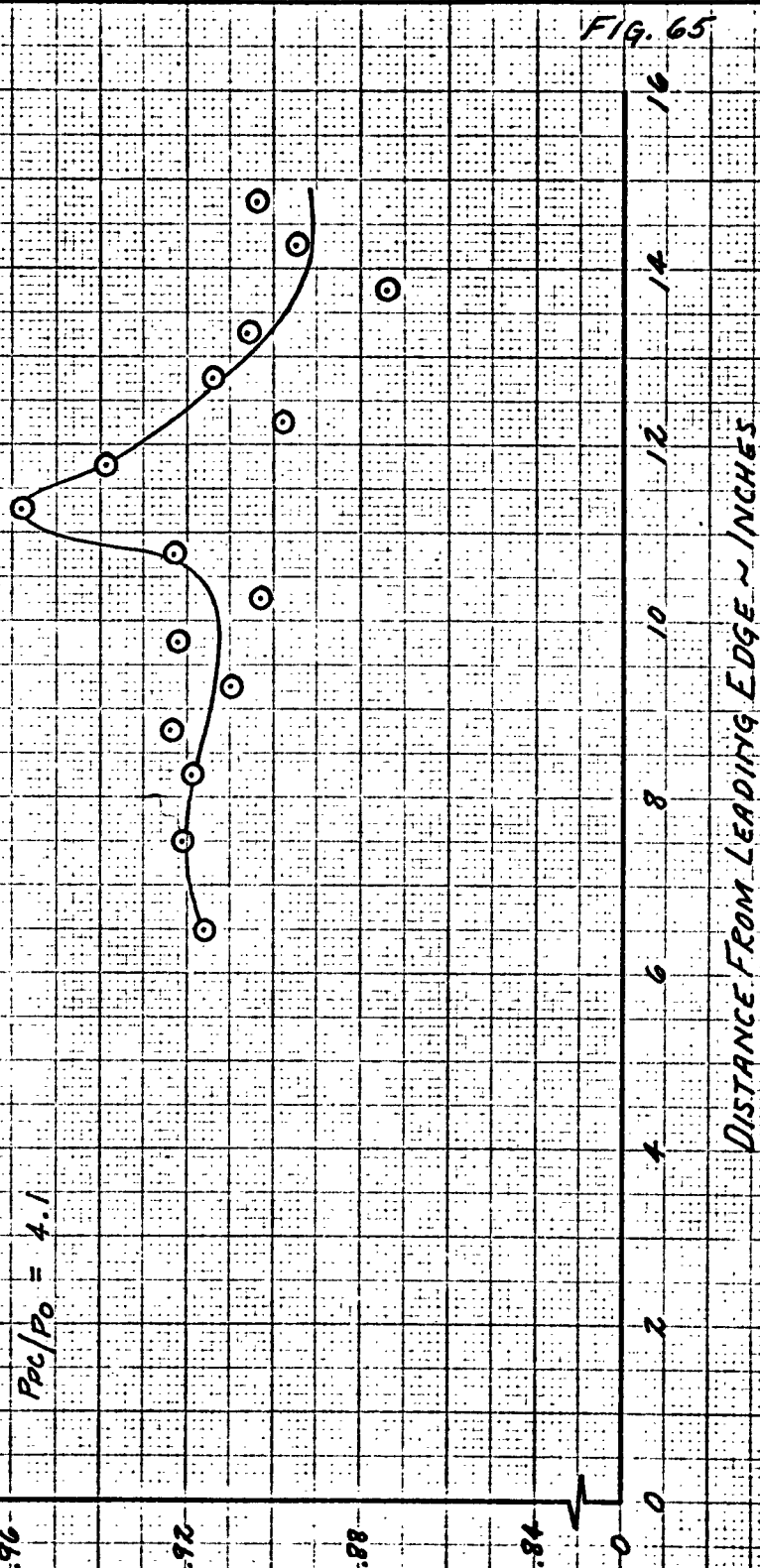
MODEL NO.

DISTRIBUTION OF EFFECTIVE RECOVERY FACTOR AT $M_0 = 5.02$
 FOR A SHOCK GENERATOR PLATE ANGLE OF 7.4°

$T_r =$ ISOTHERMAL TEMP FOR LOCAL ZERO
 HEAT TRANSFER

$$\eta_R = \frac{T_r - T_i}{T_f - T_i} = \frac{(1 + 2M_1^2) \frac{T_r}{T_f} - 1}{.8M_1^2}, M_1 = 4.77$$

$$P_{0C}/P_0 = 4.1$$

EFFECTIVE RECOVERY FACTOR $\sim \eta_R$ 

PREPARED BY:	NORTH AMERICAN AVIATION, INC.	PAGE NO. 134 OF
CHECKED BY:		REPORT NO. NA 62H-795
DATE:		MODEL NO.

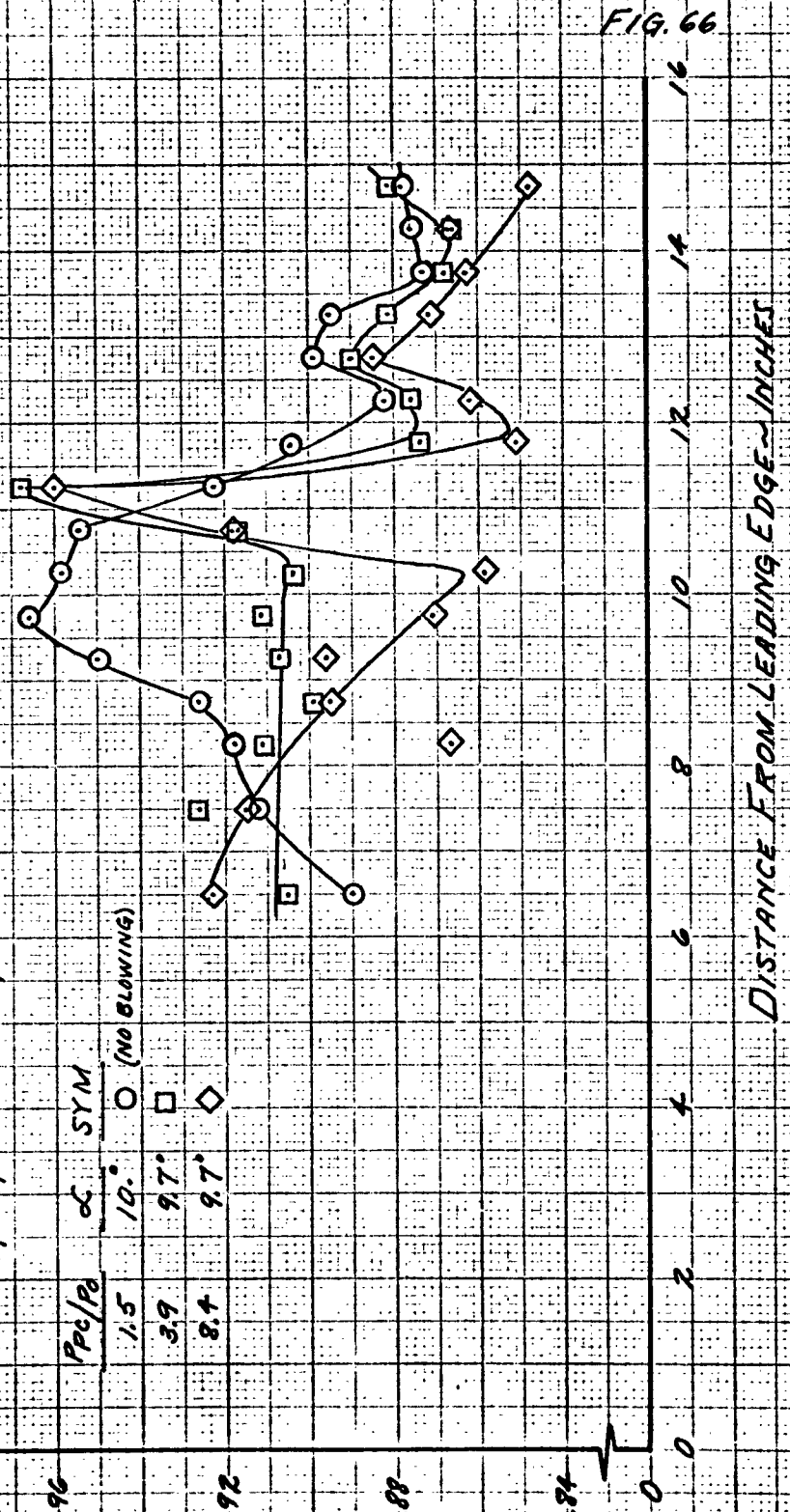
DISTRIBUTION OF EFFECTIVE RECOVERY FACTOR AT $M_0 = 5.02$
FOR A SHOCK GENERATOR PLATE ANGLE OF APPROXIMATELY 10°

T_R = ISOTHERMAL TEMP FOR LOCAL ZERO
 HEAT TRANSFER

$$\eta_R = \frac{T_R - T_L}{T_f - T_L} = \frac{(1 + 2M_1^2) \frac{T_R}{T_f} - 1}{2M_1^2}, M_1 = 4.77$$

EFFECTIVE RECOVERY FACTOR $\sim \eta_R$

P_{02}/P_0	α	SYM.
1.5	10°	O (NO BLOWING)
3.9	9.7°	□
8.4	9.7°	◇



PREPARED BY:

NORTH AMERICAN AVIATION, INC.

PAGE NO. 135 OF

CHECKED BY:

REPORT NO. NA 62H-795

DATE:

MODEL NO.

FIG. 67

DISTRIBUTION OF EFFECTIVE RECOVERY FACTOR AT $M_o = 5.02$
FOR A SHOCK GENERATOR PLATE ANGLE OF 11°

T_r = ISOTHERMAL TEMP. FOR LOCAL ZERO
HEAT TRANSFER

$\eta_E = \frac{T_r - T_1}{T_T - T_1} = \frac{(1 + 2M_1^2) \frac{T_r}{T_1} - 1}{2M_1^2}$, $M_1 = 4.77$

P/P_o P_o SYM

4.1 ○

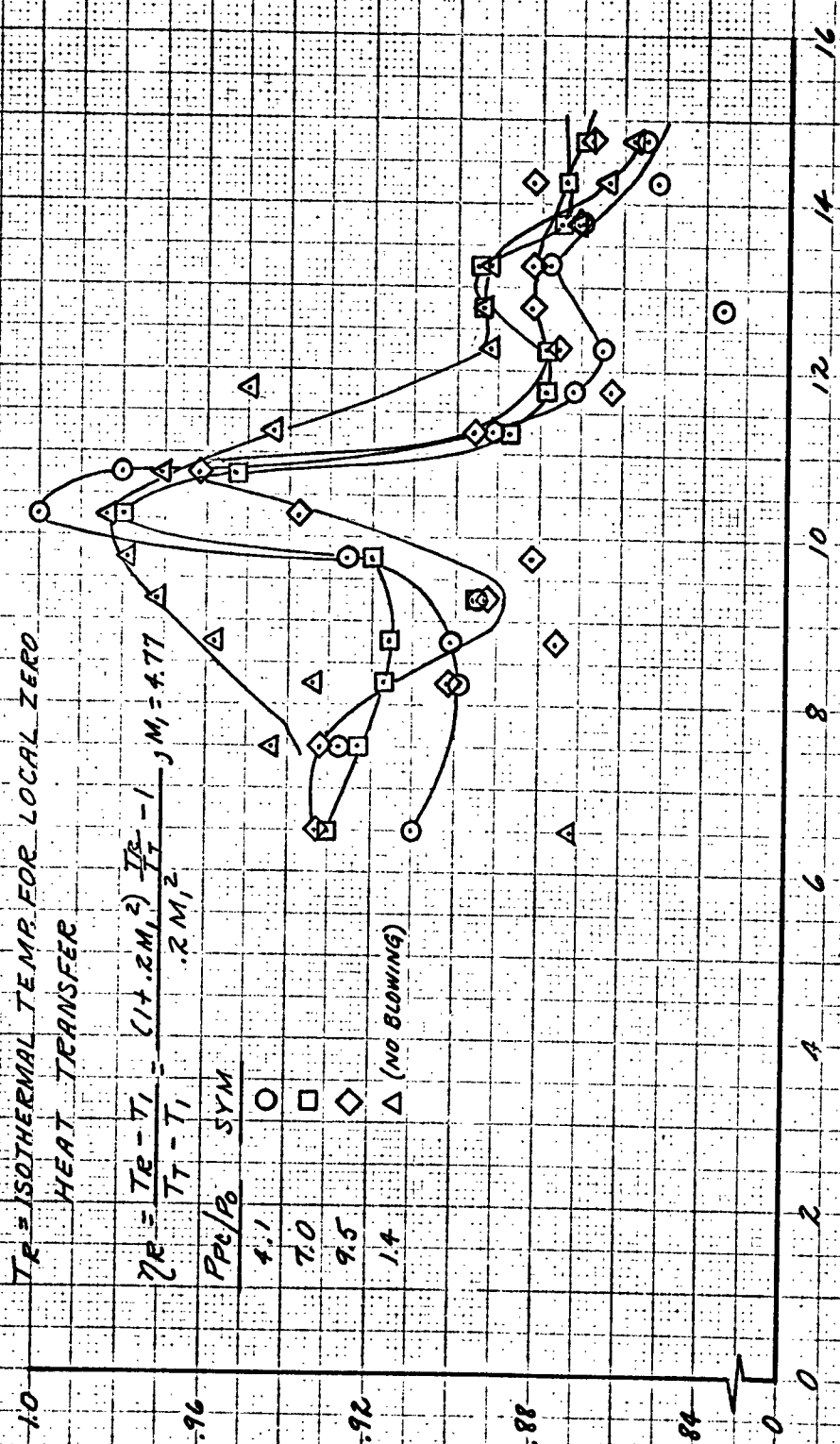
7.0 □

9.5 ◇

1.4 △ (NO BLOWING)

EFFECTIVE RECOVERY FACTOR $\sim \eta_E$

DISTANCE FROM LEADING EDGE ~ INCHES



NORTH AMERICAN AVIATION, INC.

PREPARED BY:

PAGE NO. 136 of

CHECKED BY:

REPORT NO. NA 62H-795

DATE:

MODEL NO.

DISTRIBUTION OF EFFECTIVE RECOVERY FACTOR AT $M_0 = 5.02$
FOR A SHOCK GENERATOR PLATE ANGLE OF 12°

T_R = ISOTHERMAL TEMP FOR LOCAL ZERO
HEAT TRANSFER

$$\eta_R = \frac{T_R - T_1}{T_T - T_1} = \frac{(1 + 2 M_1^2) \frac{T_R}{T_1} - 1}{2 M_1^2}, M_1 = 4.77$$

P_{R0}/P_0 SYM

4.9 ○

9.6 □

EFFECTIVE RECOVERY FACTOR $\sim \eta_R$

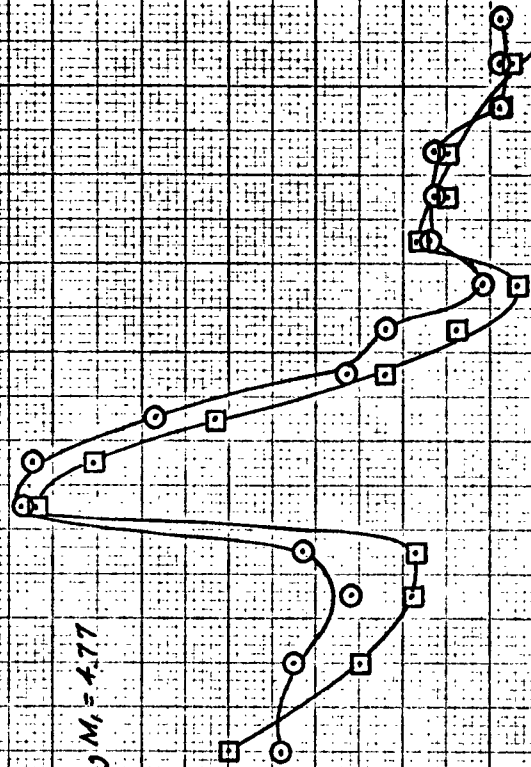


FIG. 68

DISTANCE FROM LEADING EDGE ~ INCHES

NORTH AMERICAN AVIATION, INC.

PAGE NO. 137 OF

REPORT NO. NA 62H-795

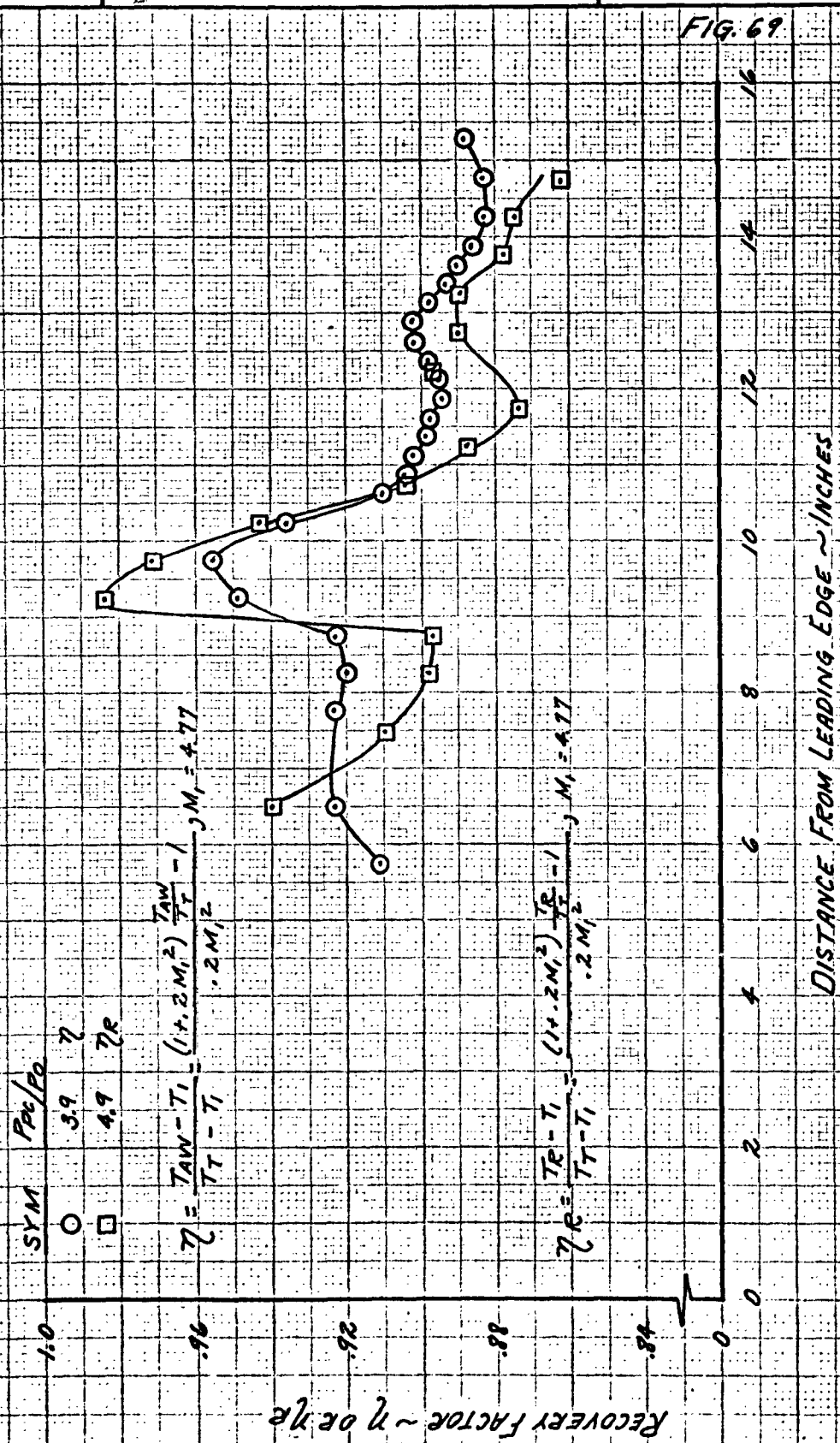
PREPARED BY:

CHECKED BY:

DATE:

MODEL NO.

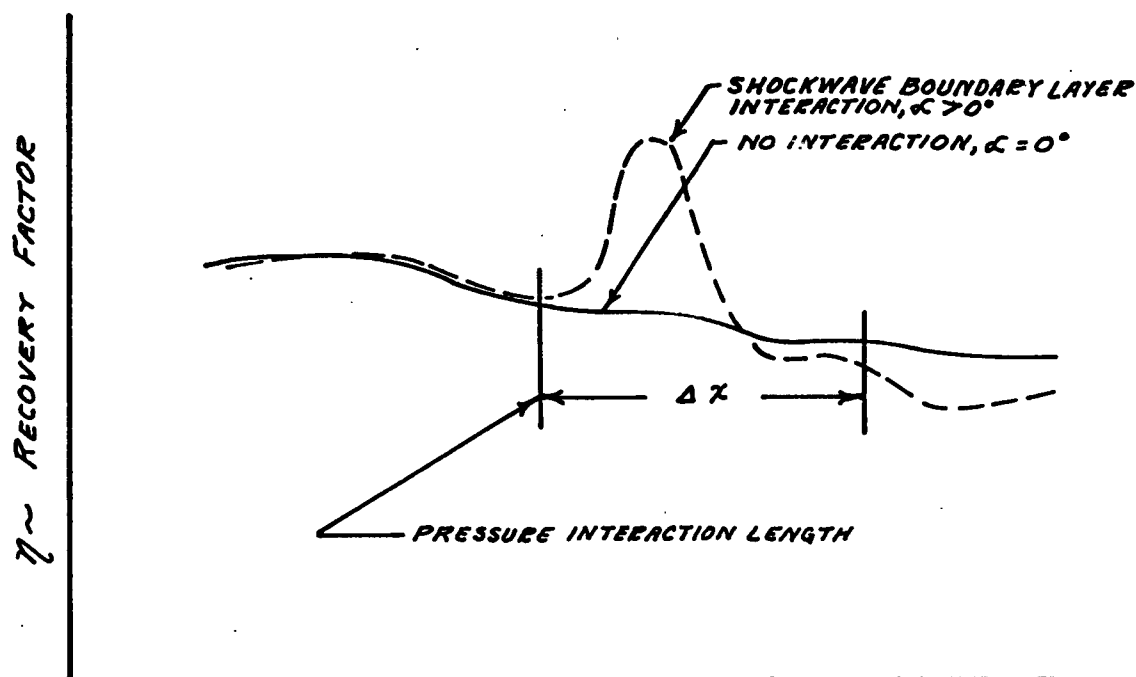
COMPARISON OF RECOVERY FACTOR (η) AND EFFECTIVE RECOVERY FACTOR (η_R) AT $M_0 = 5.02$ WITH MODERATE BOUNDARY LAYER BLOWING FOR A SHOCK GENERATOR PLATE ANGLE OF 12°



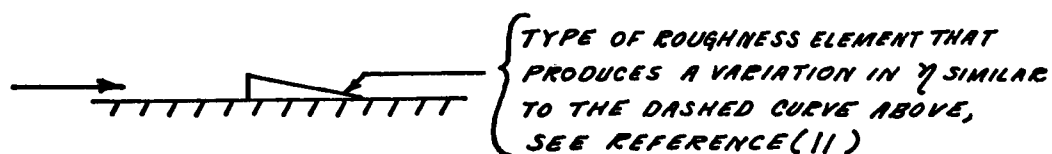
PREPARED BY:	NORTH AMERICAN AVIATION, INC. COLUMBUS DIVISION COLUMBUS 16, OHIO	PAGE NO. 138 OF
CHECKED BY:		REPORT NO. NA 62H-795
DATE:		MODEL NO.

FIG. 70

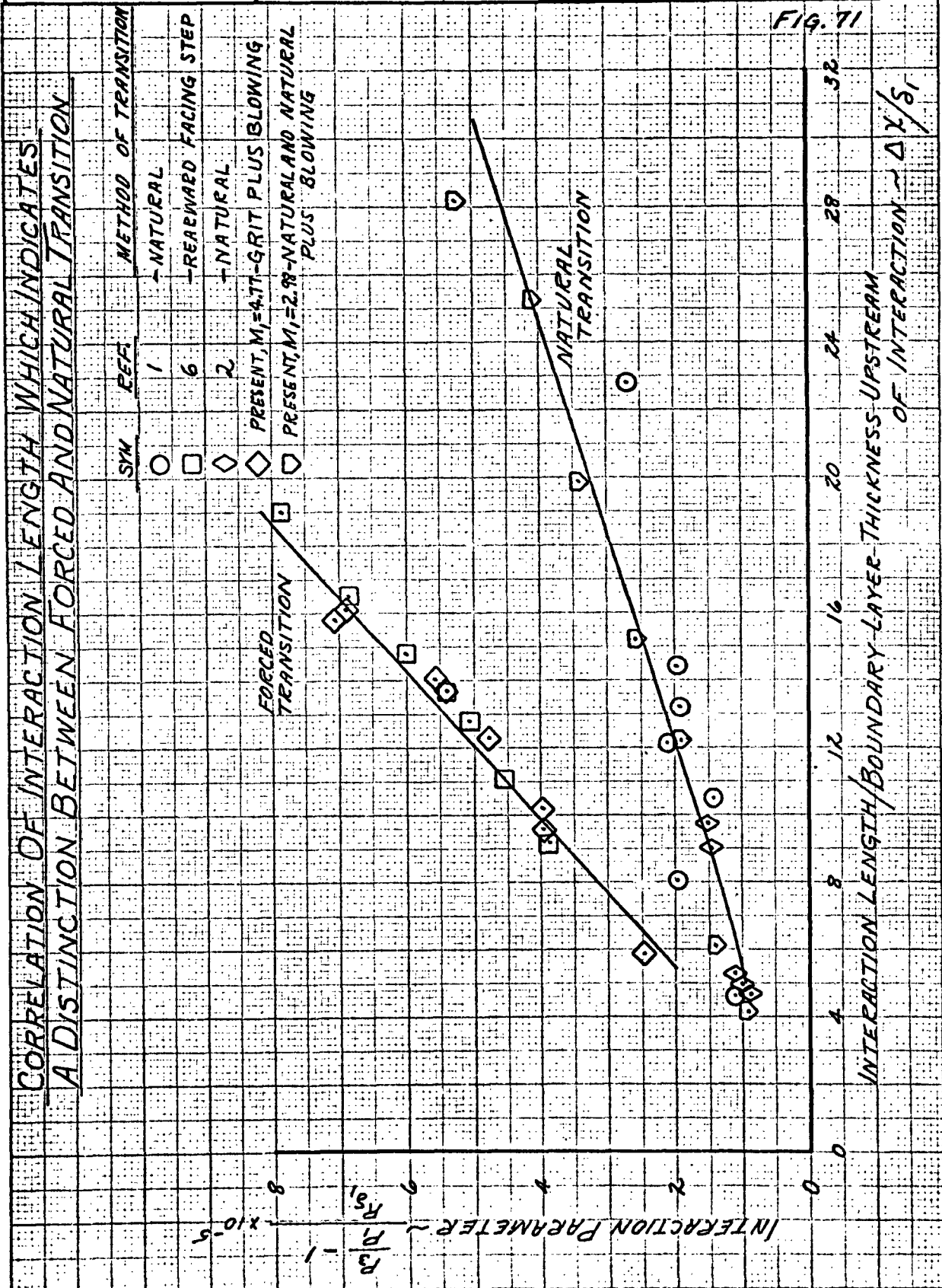
QUALITATIVE EFFECT OF SHOCKWAVE
BOUNDARY LAYER INTERACTION ON RECOVERY
FACTOR DISTRIBUTION AT $M_0 = 5.02$



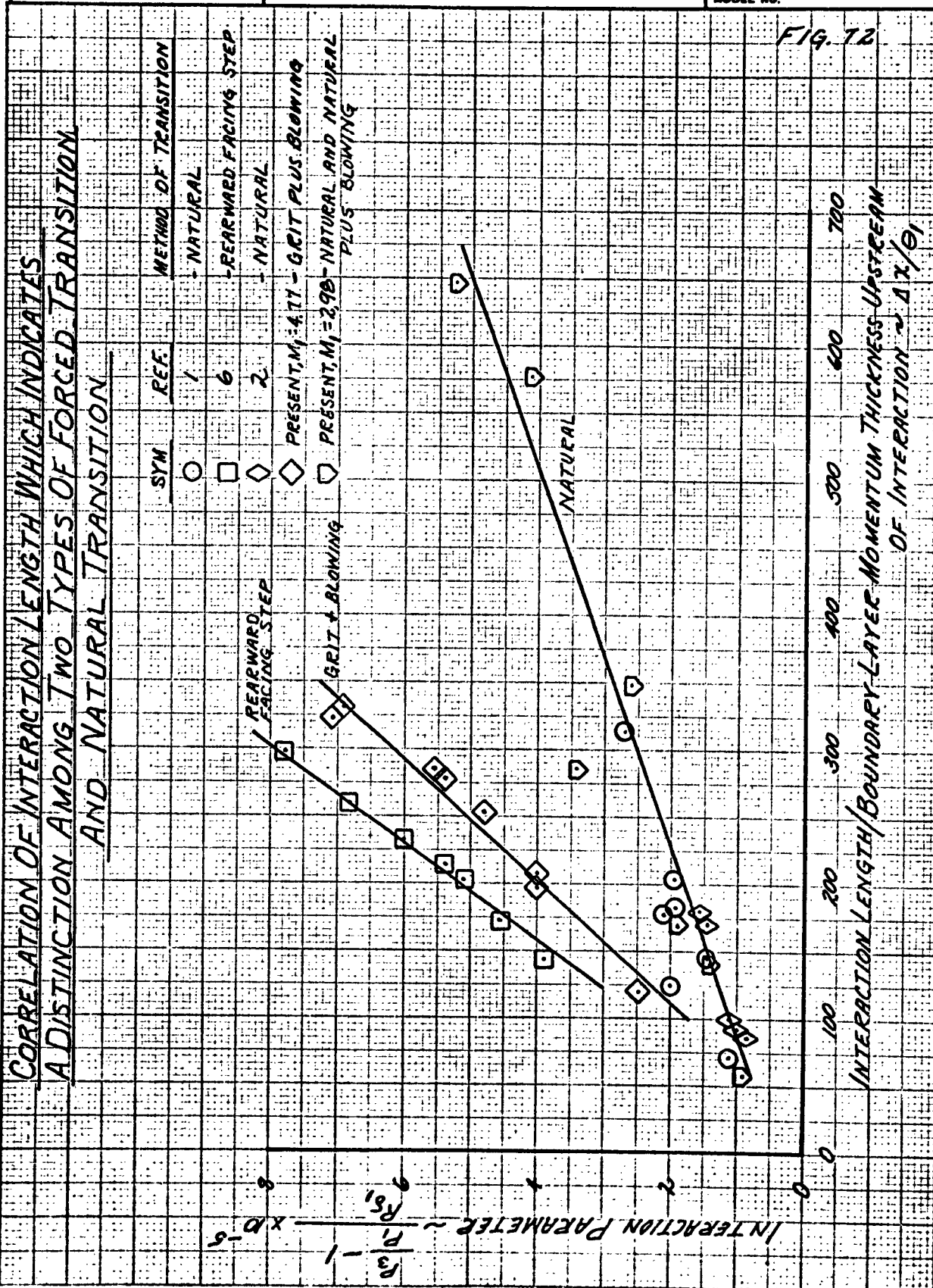
$x \sim$ DISTANCE FROM LEADING EDGE



PREPARED BY:	NORTH AMERICAN AVIATION, INC.	PAGE NO. 139 of
CHECKED BY:		REPORT NO. NA 62H-795
DATE:		MODEL NO.



PREPARED BY:	NORTH AMERICAN AVIATION, INC.	PAGE NO. 140 OF
CHECKED BY:		REPORT NO. NA 62H-795
DATE:		MODEL NO.



PREPARED BY:

NORTH AMERICAN AVIATION, INC.

PAGE NO. 141 of

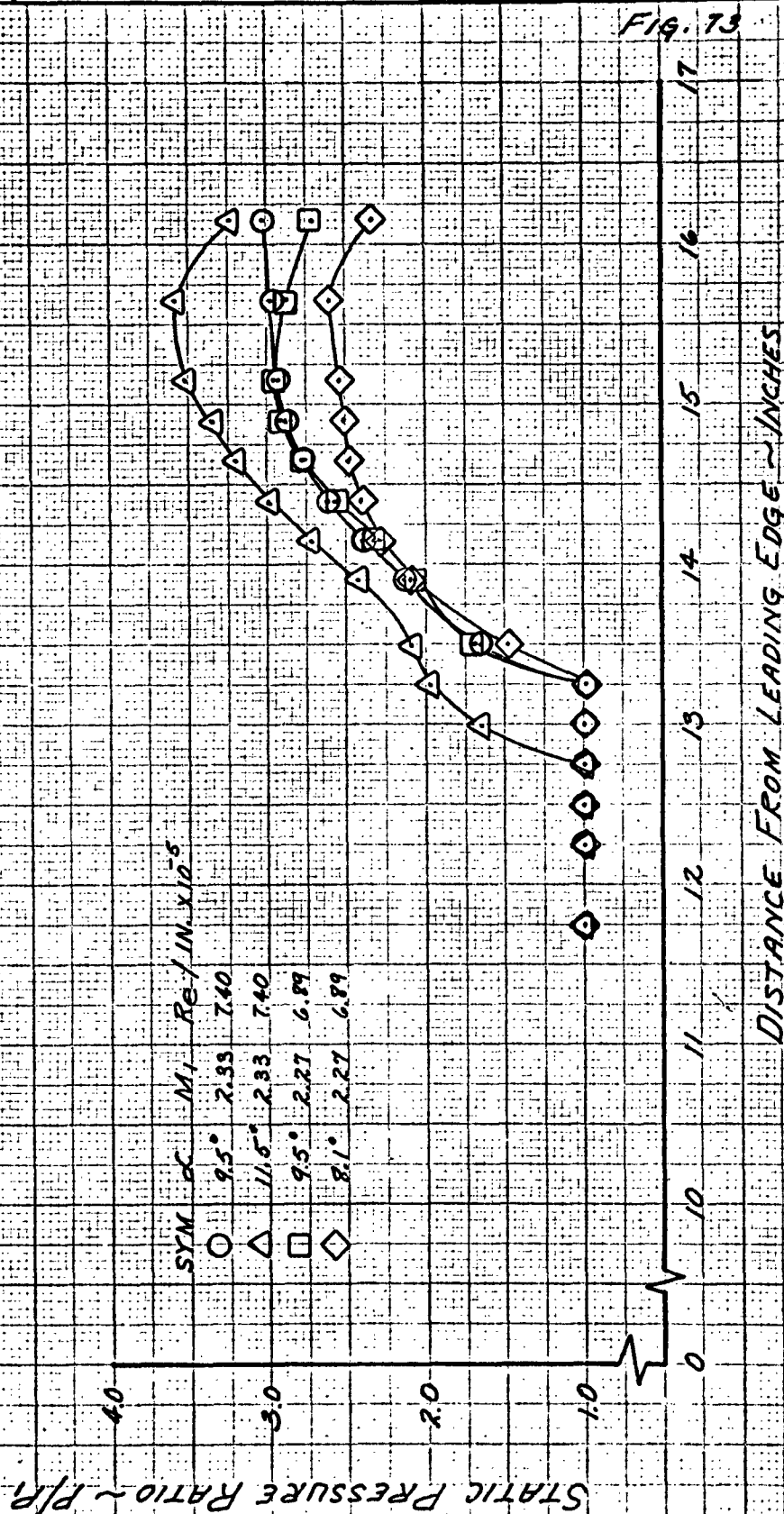
CHECKED BY:

REPORT NO. NA 62H-795

DATE:

MODEL NO.

PRESSURE DISTRIBUTIONS FROM REFERENCE (1),
APPENDIX III, FOR THOSE DATA RUNS WHICH WERE
USED IN THIS REPORT



PREPARED BY:

NORTH AMERICAN AVIATION, INC.

PAGE NO. 142 OF

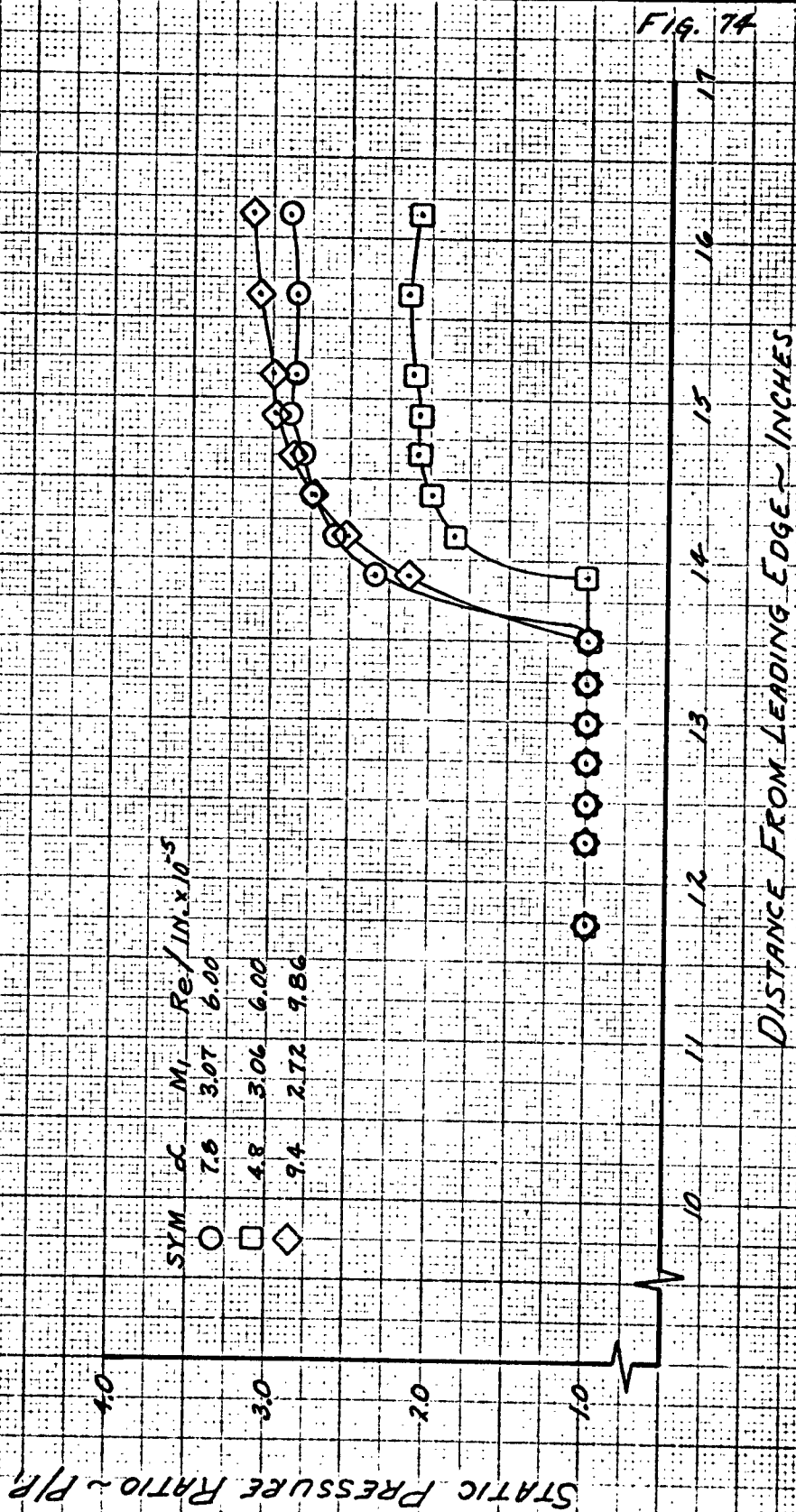
CHECKED BY:

REPORT NO. NA 62H-795

DATE:

MODEL NO.

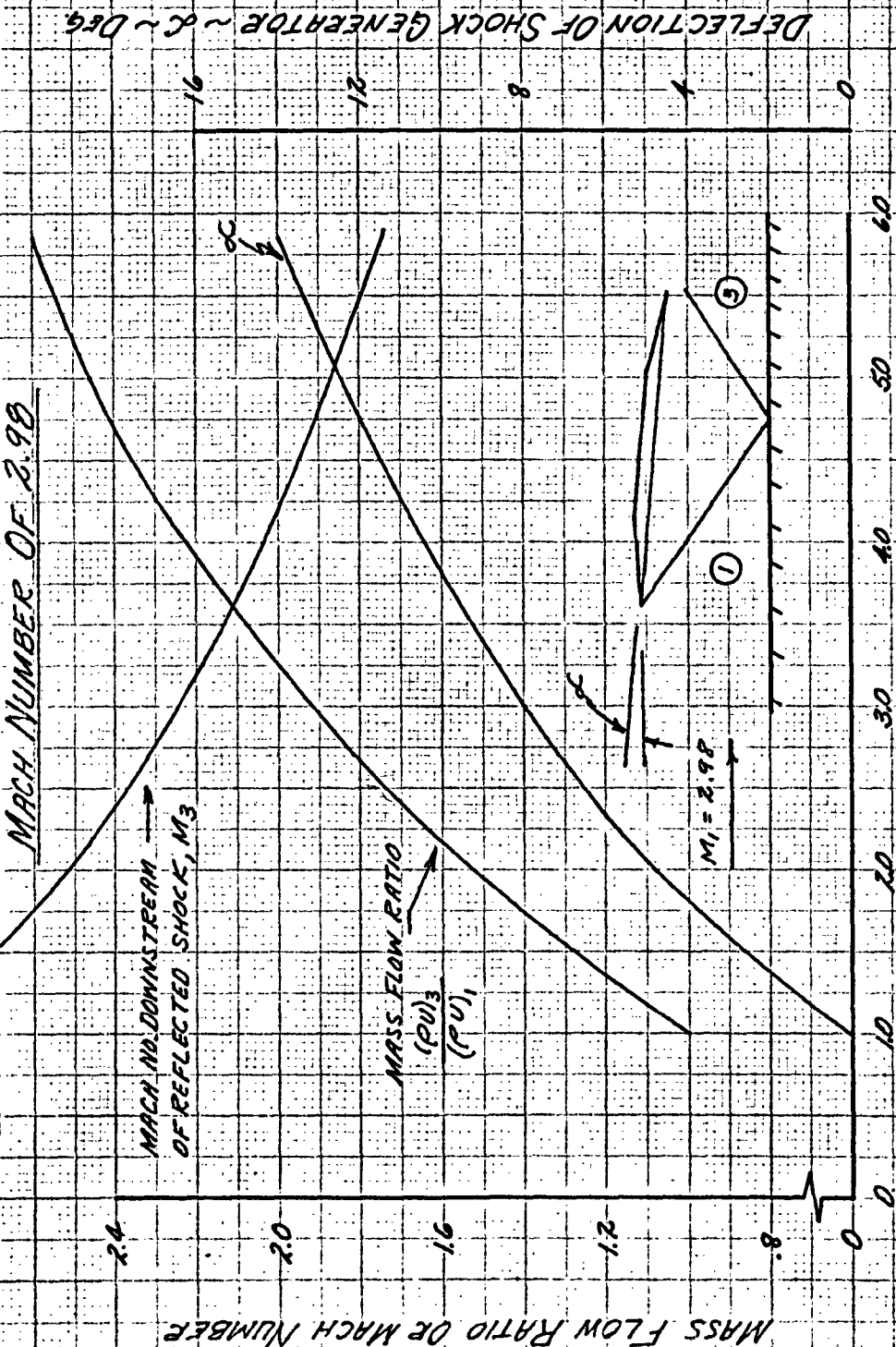
PRESSURE DISTRIBUTIONS FROM REFERENCE (1),
APPENDIX III, FOR THOSE DATA RUNS WHICH WERE
USED IN THIS REPORT



PREPARED BY:	NORTH AMERICAN AVIATION, INC.	PAGE NO. 143 OF
CHECKED BY:		REPORT NO. NA 62H-795
DATE:		MODEL NO.

FIG. 75

MACH NUMBER, MASS FLOW RATIO AND SHOCK GENERATOR PLATE
ANGLE VERSUS STATIC PRESSURE RATIO ACROSS A REFLECTED
SHOCK FOR TWO-DIMENSIONAL INVISCID FLOW WITH AN UPSTREAM
MACH NUMBER OF 2.98



P_3/P_1

MASS FLOW RATIO OF MACH NUMBER

MACH NO. DOWNSTREAM
OF REFLECTED SHOCK, M_3

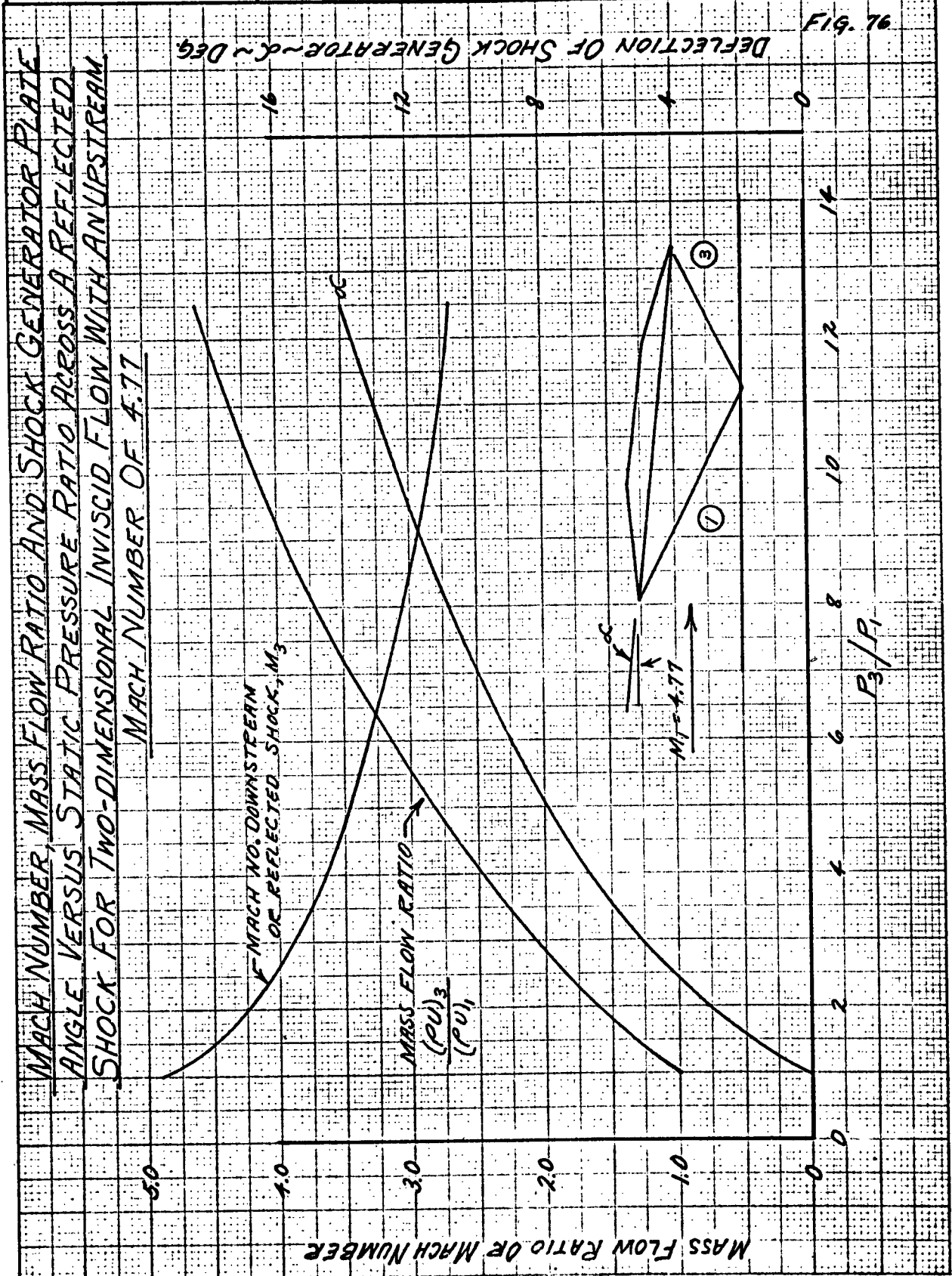
MASS FLOW RATIO
 $(P_{03})/(P_{01})$

$M_1 = 2.98$

δ

DEFLECTION OF SHOCK GENERATOR $\sim \delta \sim \text{Deg}$

PREPARED BY:	NORTH AMERICAN AVIATION, INC.	PAGE NO. 144 OF
CHECKED BY:		REPORT NO. NA 62H-795
DATE:		MODEL NO.

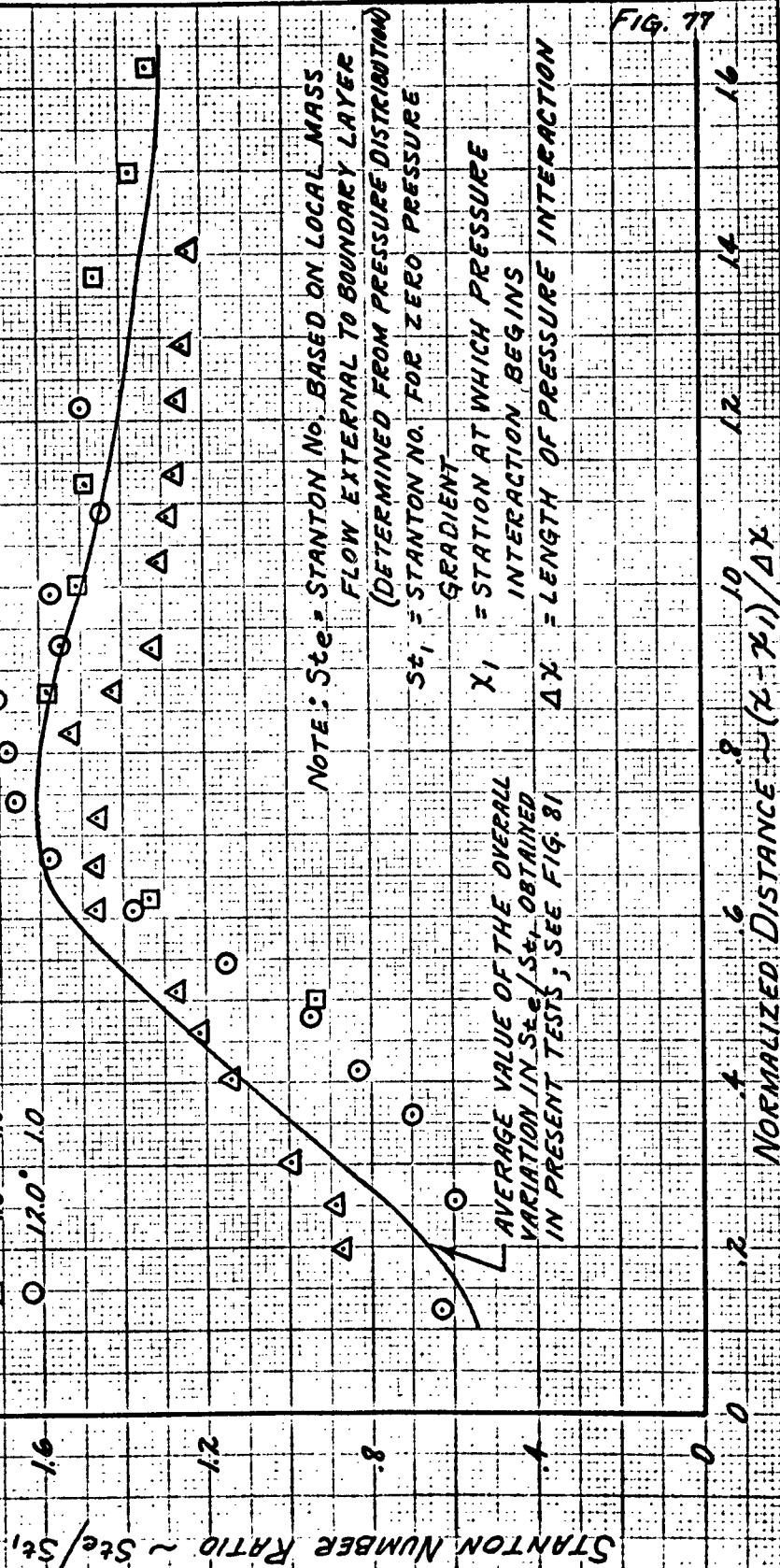


PREPARED BY:	NORTH AMERICAN AVIATION, INC.	PAGE NO. 145 OF
CHECKED BY:		REPORT NO. NA 62H-795
DATE:		MODEL NO.

EFFECT OF THE SHOCKWAVE BOUNDARY LAYER INTERACTION
ON THE LOCAL STANTON NUMBER RATIO AT $Mo = 2.95$ WITH
NO BOUNDARY LAYER BLOWING

SYM	α	P_0/P_2
□	6.0°	1.0
△	7.5°	1.0
○	12.0°	1.0

STANTON NUMBER RATIO $\sim St_e/St_1$



PREPARED BY:

NORTH AMERICAN AVIATION, INC.

PAGE NO. 146 OF

CHECKED BY:

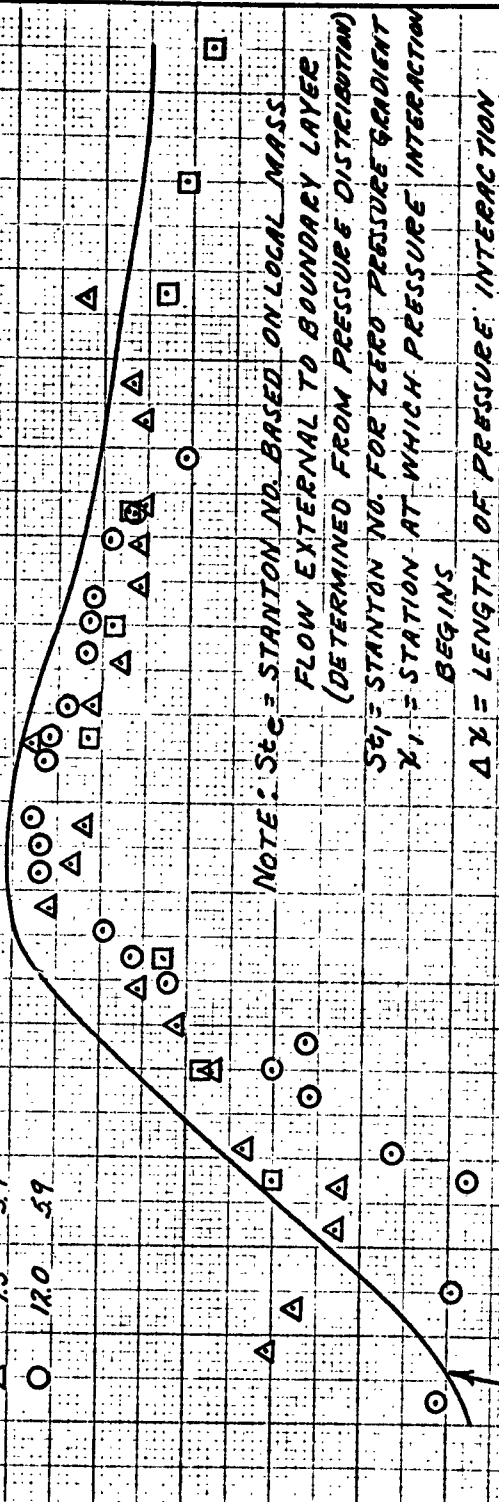
REPORT NO. NA 62H-795

DATE:

MODEL NO.

EFFECT OF THE SHOCKWAVE BOUNDARY LAYER INTERACTION ON THE LOCAL STANTON NUMBER RATIO AT $M_0 = 2.95$ WITH BOUNDARY LAYER BLOWING

SYM	α	P_{01}/P_0
□	6.0	5.9
△	9.5	5.9
○	12.0	

STANTON NUMBER RATIO $\sim St_e/St_1$ 

AVERAGE VALUE OF THE
OVERALL VARIATION IN St_e/St_1
OBTAINED IN PRESENT TESTS,
SEE FIG. 81

FIG. 78

NORMALIZED DISTANCE $\sim (x - x_1)/\Delta x$

PREPARED BY:

NORTH AMERICAN AVIATION, INC.

PAGE NO. 147 OF

CHECKED BY:

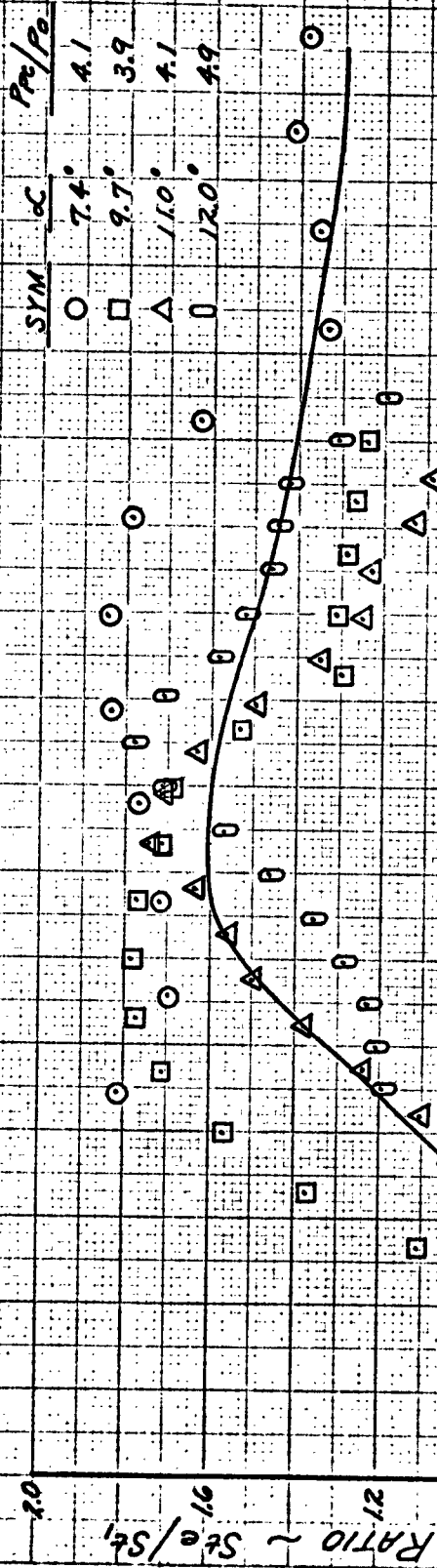
REPORT NO. NA 62H-795

DATE:

MODEL NO.

FIG. 79

EFFECT OF THE SHOCKWAVE BOUNDARY LAYER INTERACTION
ON THE LOCAL STANTON NUMBER RATIO AT $Mo = 5.02$ FOR
BOUNDARY LAYER BLOWING RATIOS FROM 3.9 TO 4.9



NOTE: St_e = STANTON NO. BASED ON LOCAL MASS FLOW
EXTERNAL TO BOUNDARY LAYER
(DETERMINED FROM PRESSURE DISTRIBUTION)

St_1 = STANTON NO. FOR ZERO PRESSURE GRADIENT
 x_1 = STATION AT WHICH PRESSURE INTERACTION
BEGINS

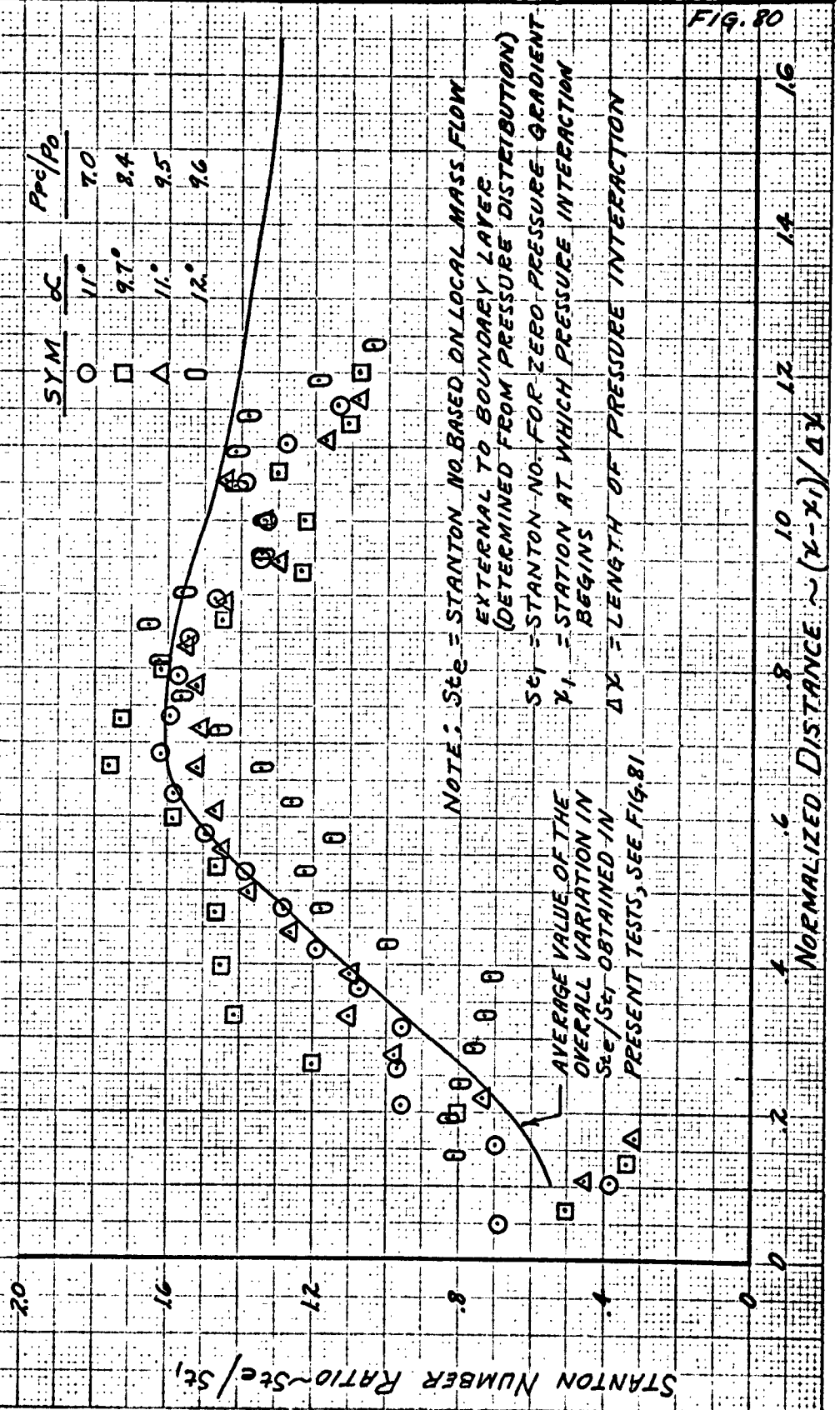
Δx = LENGTH OF PRESSURE INTERACTION

AVERAGE VALUE OF THE
OVERALL VARIATION IN
 St_e/St_1 OBTAINED IN
PRESENT TESTS,
SEE FIG. 81

NORMALIZED DISTANCE $\sim (x-x_1)/\Delta x$

PREPARED BY:	NORTH AMERICAN AVIATION, INC.	PAGE NO. 148 of
CHECKED BY:		REPORT NO. NA 62H-795
DATE:		MODEL NO.

EFFECT OF THE SHOCKWAVE BOUNDARY LAYER INTERACTION
ON THE LOCAL STANTON NUMBER RATIO AT $Mo = 5.02$
FOR BOUNDARY LAYER BLOWING RATIOS FROM 7.0 TO 9.6



PREPARED BY:

NORTH AMERICAN AVIATION, INC.

PAGE NO. 149 OF

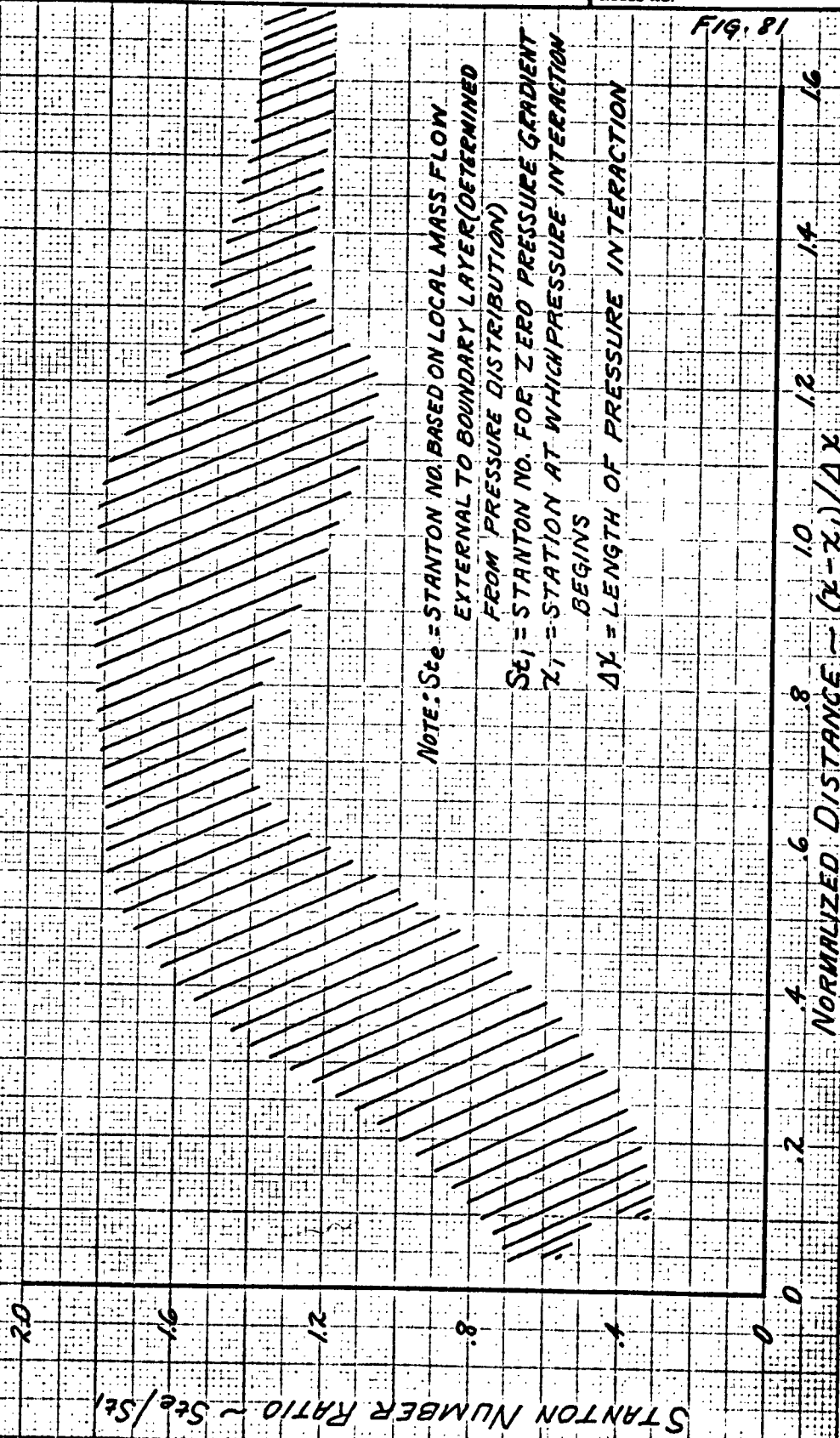
CHECKED BY:

REPORT NO. NA 62H-795

DATE:

MODEL NO.

OVERALL VARIATION OF STANTON NUMBER RATIO OBTAINED IN THE PRESENT TESTS



PREPARED BY:

NORTH AMERICAN AVIATION, INC.

PAGE NO. 150 OF

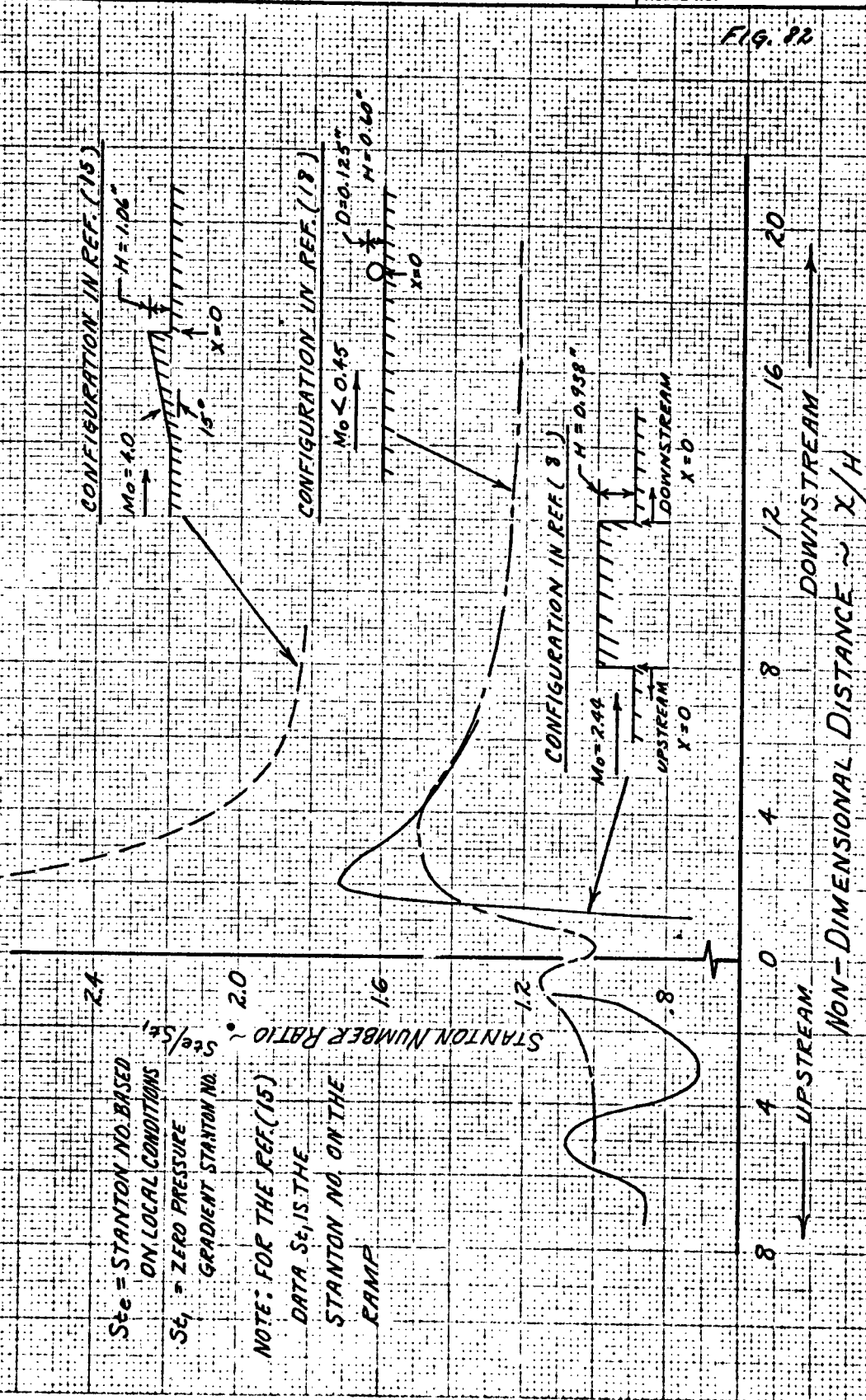
CHECKED BY:

REPORT NO. NA 62H-795

DATE:

MODEL NO.

STANTON NUMBER RATIO DISTRIBUTION FOUND IN OTHER TWO-DIMENSIONAL TURBULENT FLOW INVESTIGATIONS



PREPARED BY:

NORTH AMERICAN AVIATION, INC.

PAGE NO. 151 OF

CHECKED BY:

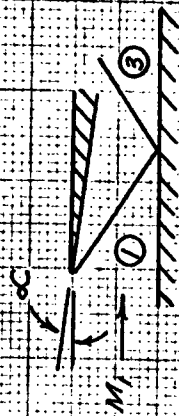
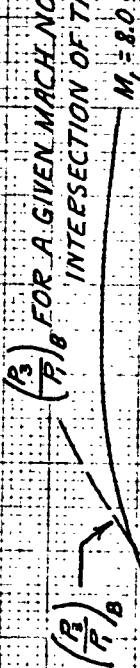
REPORT NO. NA 62H-795

DATE:

MODEL NO.

INVISCID STATIC PRESSURE RATIO ACROSS A REFLECTED SHOCK

FOR A GIVEN MACH NO. IS THE VALUE OF $\frac{P_3}{P_1}$ AT THE INTERSECTION OF THE DASHED LINE AND A SOLID LINE



IN THE DESIGN PROCEDURE (SEE SECTION IV) THE PEAK STANTON NO. RATIO IS:

TO THE LEFT OF THE DASHED LINE TO THE RIGHT OF THE DASHED LINE

$$\frac{St_2}{St_1} = K_1$$

$$\frac{St_2}{St_1} = K_1 + 1.43 \left[\frac{P_3}{P_1} - \left(\frac{P_3}{P_1} \right)_B \right]$$

CONSERVATIVE ESTIMATE: $K_1 = 1.8$

AVERAGE VALUE ESTIMATE: $K_1 = 1.6$

FIG. 13

STATIC PRESSURE RATIO $\sim \frac{P_2}{P_1}$

NORTH AMERICAN AVIATION, INC.

PREPARED BY:

PAGE NO. 152 OF

CHECKED BY:

REPORT NO. NA 62H-795

DATE:

MODEL NO.

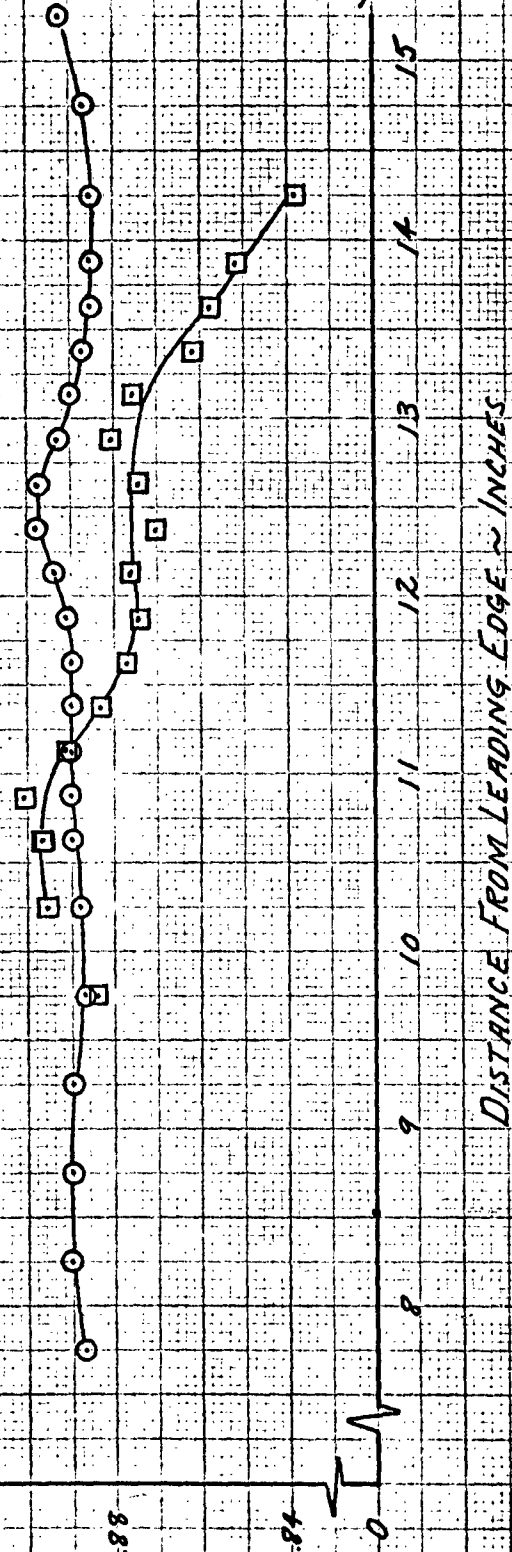
EFFECT OF SHOCKWAVE BOUNDARY LAYER INTERACTION AT $M_0 = 2.95$ ON LOCAL RECOVERY FACTOR

$$\eta_e = \frac{T_{AW} - T_e}{T_t - T_e} = \frac{(1 + 2 M_e^2) \frac{T_{AW}}{T_t} - 1}{2 M_e^2}$$

M_e = LOCAL MACH NO.
DETERMINED FROM
STATIC PRESSURE
DISTRIBUTION

SYM	α	P_{t0}/P_0
○	0°	7.5
□	12°	5.9

NOTE: FOR $\alpha = 0^\circ$, $\eta_e = \eta_e$
FOR $\alpha = 12^\circ$ SUBSTITUTE T_e FOR T_{AW} IN THE
 η_e EQUATION, SINCE T_{AW} WAS NOT OBTAINED
FOR $\alpha > 0$ AT $M_0 = 2.95$

LOCAL RECOVERY FACTOR η_e 

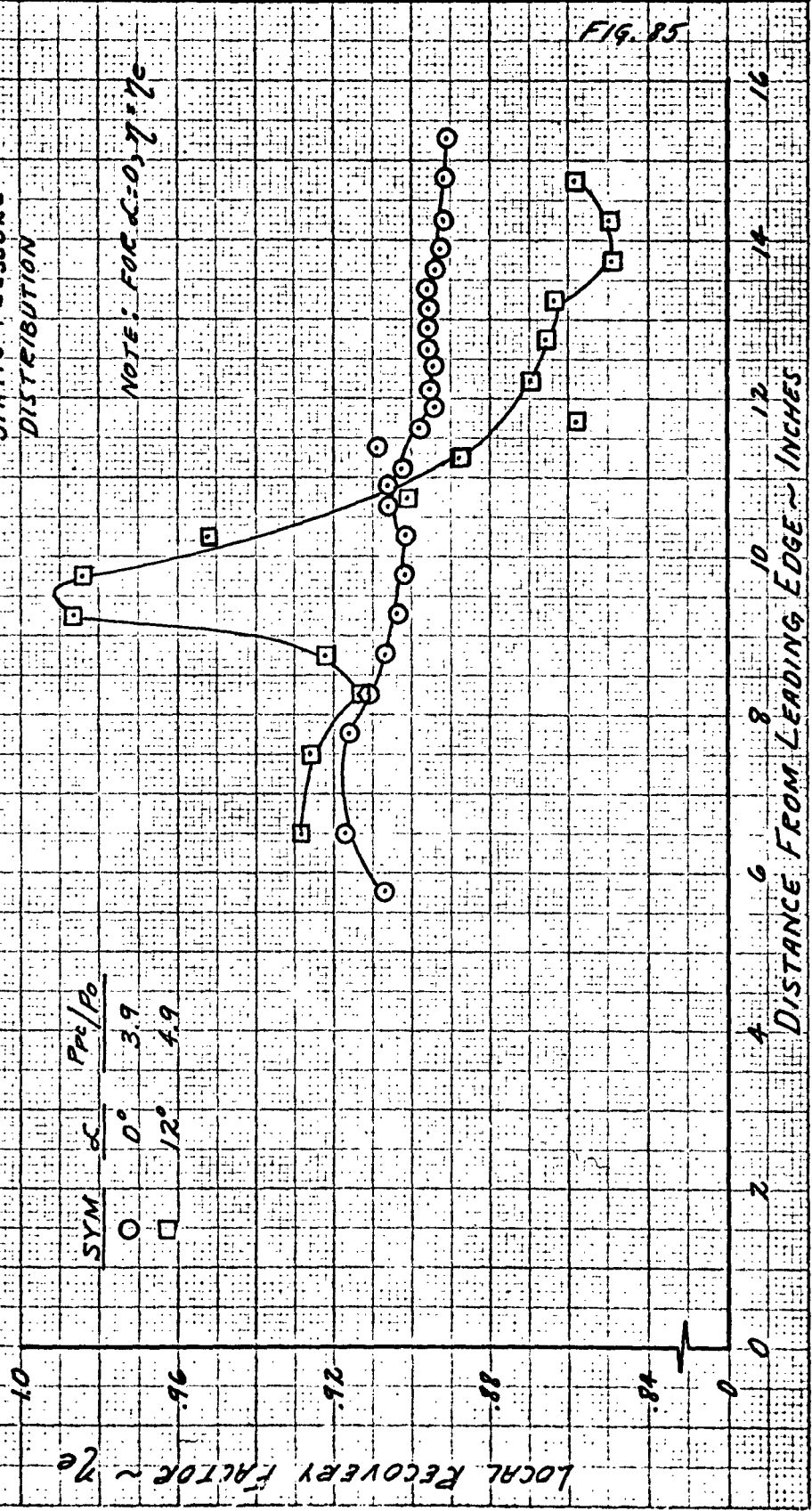
PREPARED BY:		NORTH AMERICAN AVIATION, INC.	PAGE NO. 153 OF
CHECKED BY:			REPORT NO. NA 62H-795
DATE:			MODEL NO.

EFFECT OF SHOCKWAVE BOUNDARY LAYER INTERACTION
AT Mo = 5.02 ON LOCAL RECOVERY FACTOR

$$\eta_e = \frac{T_{aw} - T_e}{T_t - T_e} = \frac{(1 + 2M_e^2) \frac{T_{aw}}{T_t} - 1}{2M_e^2}, \quad M_e = \text{LOCAL MACH NO. DETERMINED FROM STATIC PRESSURE DISTRIBUTION}$$

NOTE: FOR $\alpha = 0, \eta = \eta_e$

SYM	α	P_{re}/P_0
○	0°	3.9
□	12°	4.9



PREPARED BY:

NORTH AMERICAN AVIATION, INC.

PAGE NO. 154 OF

CHECKED BY:

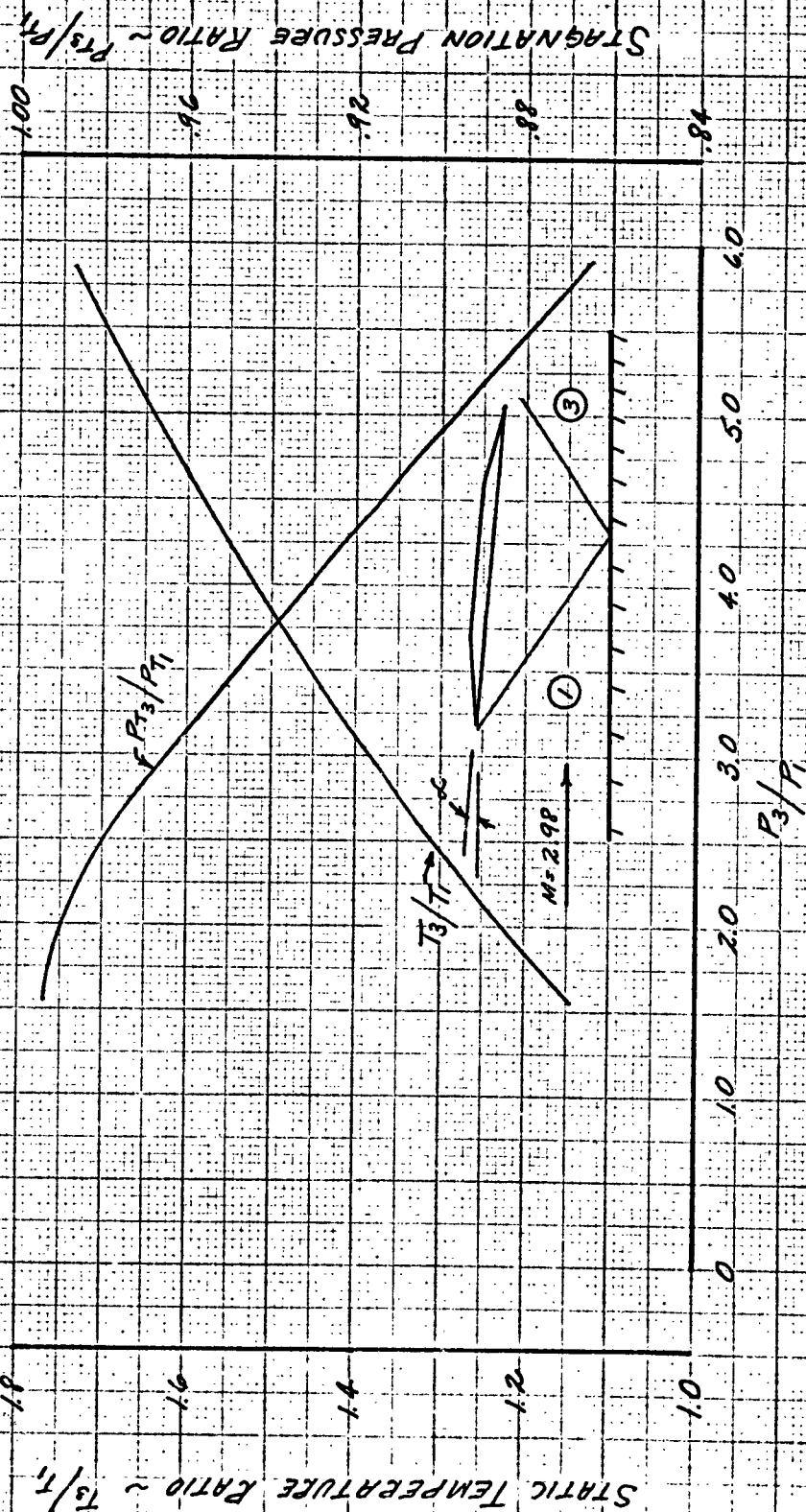
REPORT NO. NA 62H-795

DATE:

MODEL NO.

FIG. 86

STAGNATION PRESSURE RATIO AND STATIC TEMPERATURE
RATIO VERSUS STATIC PRESSURE RATIO ACROSS A REFLECTED
SHOCK FOR TWO-DIMENSIONAL INVISCID FLOW WITH AN
UPSTREAM MACH NUMBER OF 2.98



NORTH AMERICAN AVIATION, INC.

PREPARED BY:

PAGE NO. 155 OF

CHECKED BY:

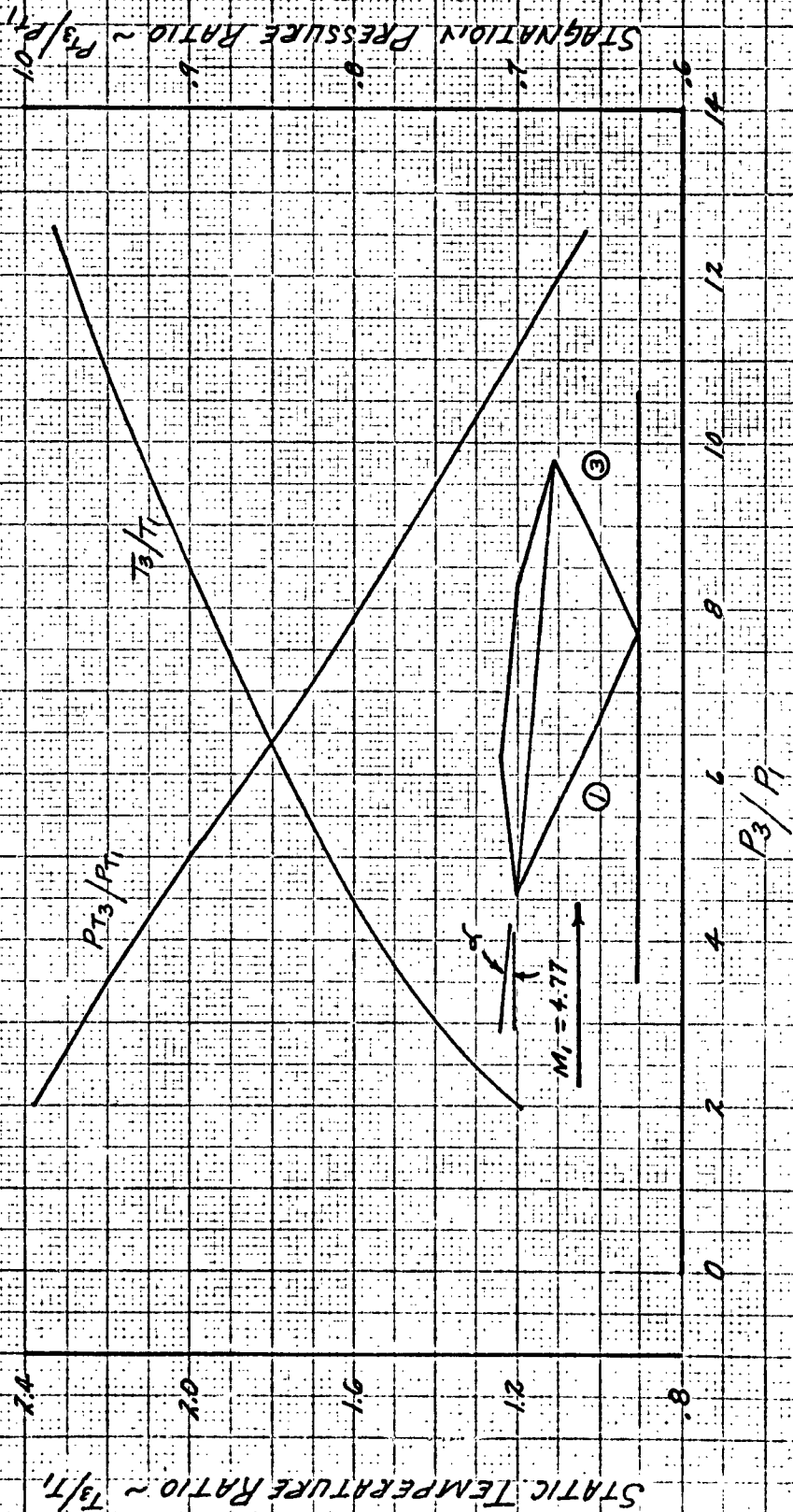
REPORT NO. NA 62H-795

DATE:

MODEL NO.

FIG. 87

STAGNATION PRESSURE RATIO AND STATIC TEMPERATURE
RATIO VERSUS STATIC PRESSURE RATIO ACROSS A REFLECTED
SHOCK FOR TWO-DIMENSIONAL INVISCID FLOW WITH AN
UPSTREAM MACH NUMBER OF 4.77



PREPARED BY:	NORTH AMERICAN AVIATION, INC.	PAGE NO.	156 OF
CHECKED BY:		REPORT NO.	NA 62H-795
DATE:		MODEL NO.	

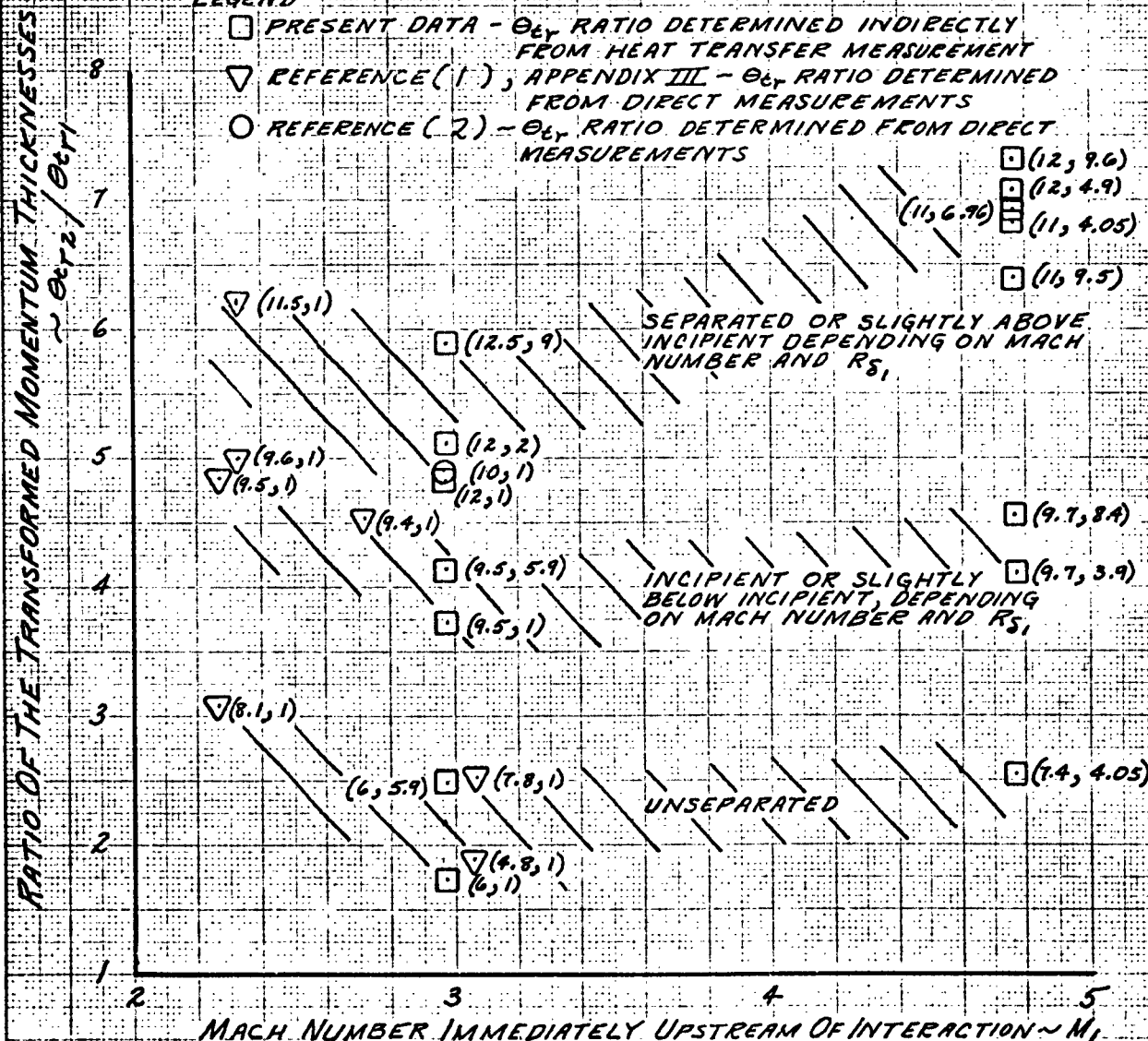
FIG. 88

VARIATION OF THE TRANSFORMED MOMENTUM THICKNESS RATIO (Θ_{tr} AT PEAK HEAT TRANSFER LOCATION TO Θ_{tr} AT THE BEGINNING OF THE PRESSURE INTERACTION) WITH MACH NUMBER

NOTE: (1) THE PARAMETERS ASSOCIATED WITH EACH POINT ARE (α , P_{pc}/P_0) WHERE α IS THE FLOW TURNING ANGLE AND P_{pc}/P_0 IS THE RATIO OF PLENUM CHAMBER PRESSURE TO THE FREE STREAM STATIC PRESSURE UPSTREAM OF THE PLATE.
 (2) IN THIS GRAPH: $8.57 \times 10^{-4} \leq R_{S_1} \leq 19.9 \times 10^{-4}$

LEGEND

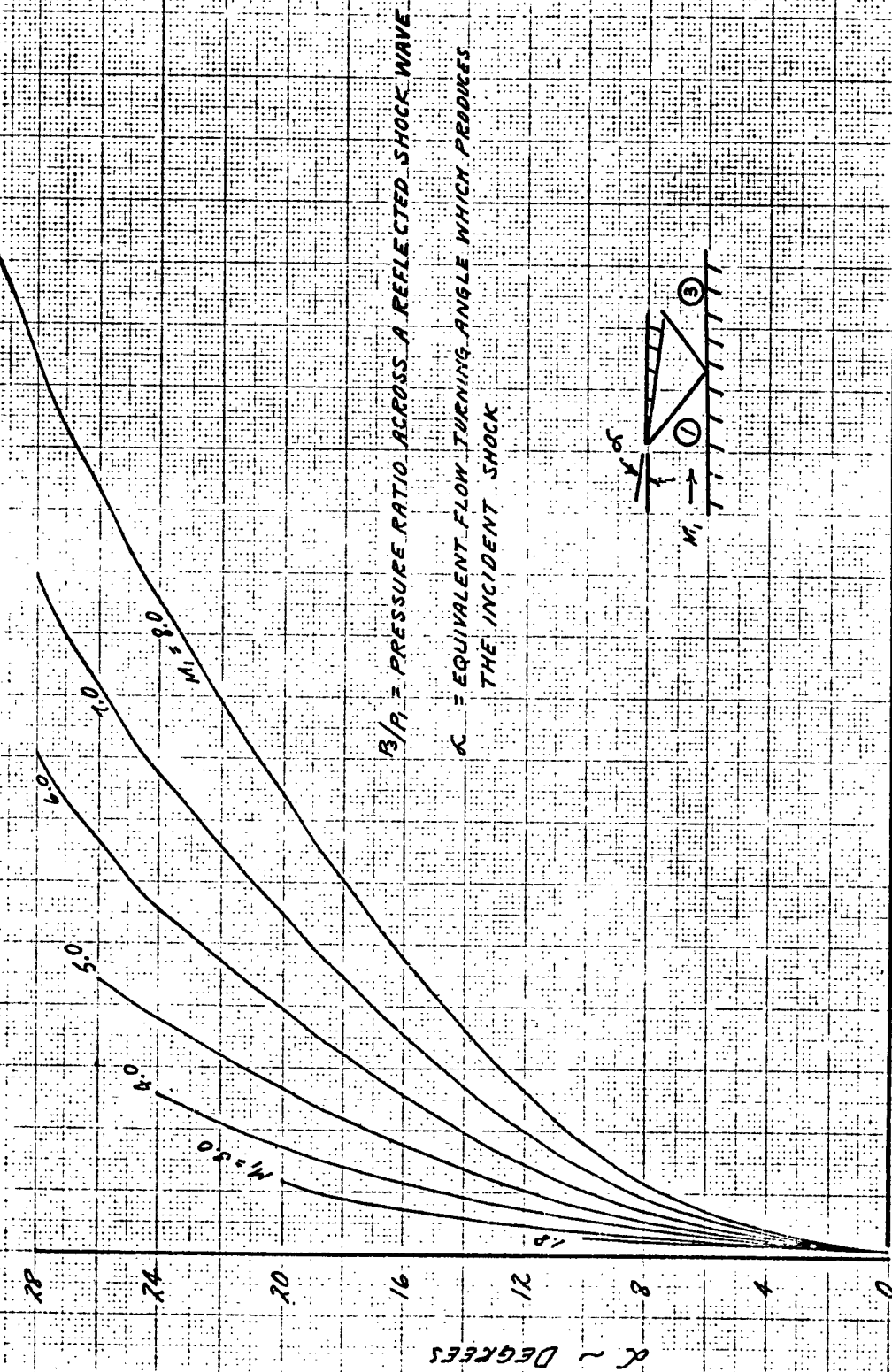
- \square PRESENT DATA - Θ_{tr} RATIO DETERMINED INDIRECTLY FROM HEAT TRANSFER MEASUREMENT
- ∇ REFERENCE (1), APPENDIX III - Θ_{tr} RATIO DETERMINED FROM DIRECT MEASUREMENTS
- \circ REFERENCE (2) - Θ_{tr} RATIO DETERMINED FROM DIRECT MEASUREMENTS



PREPARED BY:	NORTH AMERICAN AVIATION, INC.	PAGE NO. 157 OF
CHECKED BY:		REPORT NO. NA 62H-795
DATE:		MODEL NO.

FIG. 89

PRESSURE RATIO ACROSS A REFLECTED SHOCK PATTERN AS A FUNCTION OF THE INITIAL FLOW DEFLECTION ANGLE



P_3/P_1 = PRESSURE RATIO ACROSS A REFLECTED SHOCK WAVE
 α = EQUIVALENT FLOW TURNING ANGLE WHICH PRODUCES THE INCIDENT SHOCK



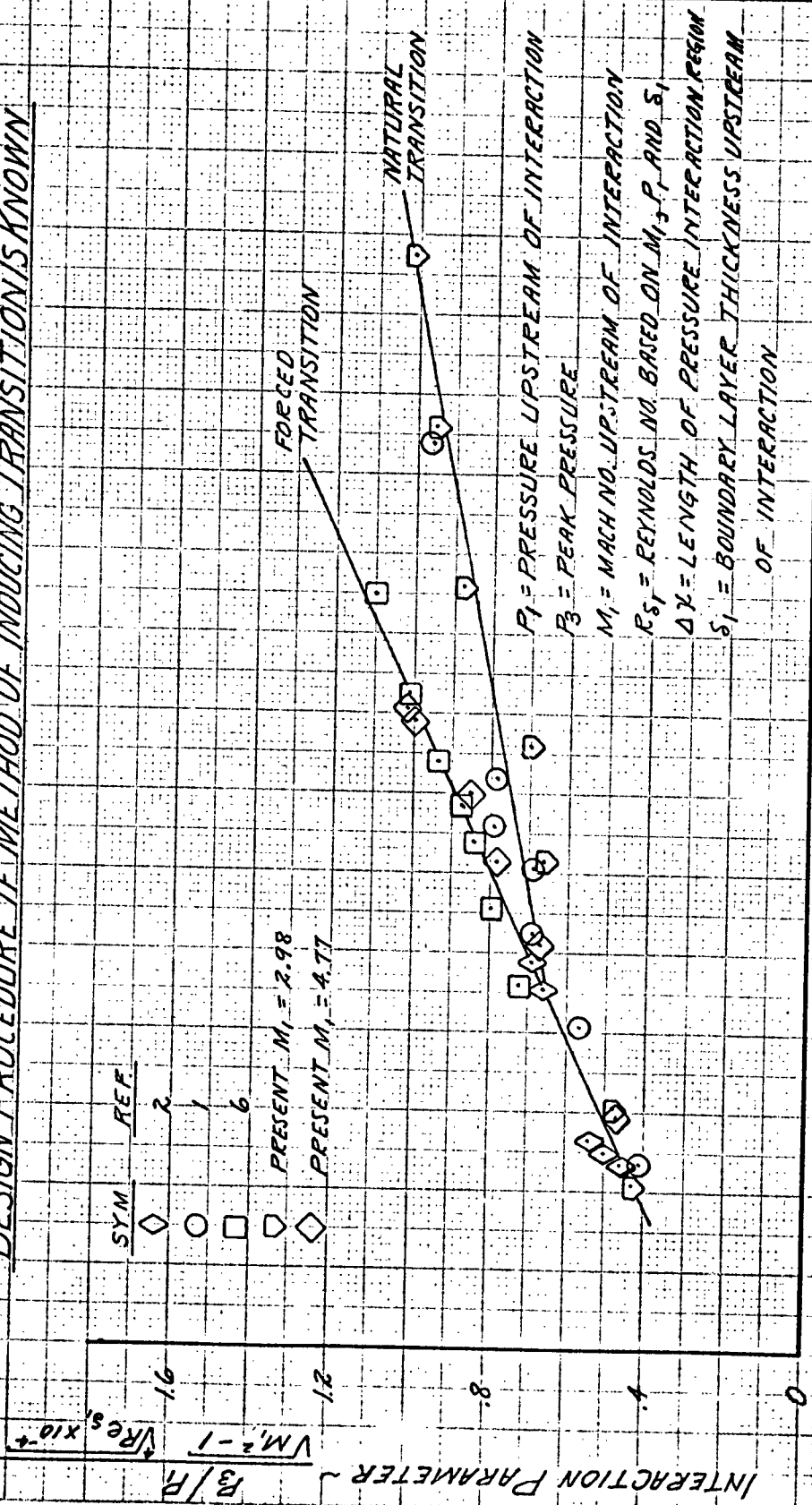
P_3/P_1

PREPARED BY:	NORTH AMERICAN AVIATION, INC.	PAGE NO. 158 OF
CHECKED BY:		REPORT NO. NA 62H-795
DATE:		MODEL NO.

CORRELATION OF PRESSURE INTERACTION LENGTH TO BE USED IN

DESIGN PROCEDURE IF METHOD OF INDUCING TRANSITION IS KNOWN

SYM	REF
◇	2
○	1
□	6
▽	PRESENT $M_1 = 2.98$
◇	PRESENT $M_1 = 4.77$



P_1 = PRESSURE UPSTREAM OF INTERACTION
 P_3 = PEAK PRESSURE
 M_1 = MACH NO. UPSTREAM OF INTERACTION
 Re_s = REYNOLDS NO. BASED ON M_1, P_1 AND δ_1
 ΔX = LENGTH OF PRESSURE INTERACTION REGION
 δ_1 = BOUNDARY LAYER THICKNESS UPSTREAM OF INTERACTION

FIG. 90

$\frac{\Delta X}{\delta_1}$
 0 4 8 12 16 20 24 28 32

PREPARED BY:

NORTH AMERICAN AVIATION, INC.

PAGE NO. 159 OF

CHECKED BY:

REPORT NO. NA 62H-795

DATE:

MODEL NO.

CORRELATION OF PRESSURE INTERACTION LENGTH TO BE USED IN
DESIGN PROCEDURE IF METHOD OF INDUCING TRANSITION IS NOT KNOWN

NOTE: CORRELATION IS NOT USEFUL FOR VALUES
 OF THE INTERACTION PARAMETER GREATER
 THAN 1.34

SYM REF

2

1

6

PRESENT $M_1 = 2.99$ PRESENT $M_1 = 4.77$

INTERACTION PARAMETER $\sim \frac{P_3/P_1}{\sqrt{M_1^2 - 1}} \sqrt{R_{S1}} \times 10^{-4}$

P_1 = PRESSURE UPSTREAM OF INTERACTION
 P_3 = PEAK PRESSURE
 M_1 = MACH NO. UPSTREAM OF INTERACTION
 R_{S1} = REYNOLDS NO. BASED ON M_1 , P_1 AND S_1
 ΔX = LENGTH OF PRESSURE INTERACTION REGION
 S_1 = BOUNDARY LAYER THICKNESS UPSTREAM
 OF INTERACTION

FIG. 91

32

28

24

20

16

12

8

4

0

 ΔX S_1

0

4

8

12

16

20

24

28

32

PREPARED BY:

CHECKED BY:

DATE:

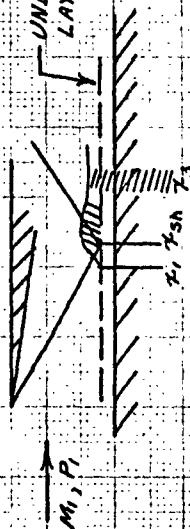
NORTH AMERICAN AVIATION, INC.

PAGE NO. 160 OF

REPORT NO. NA 62H-795

MODEL NO.

CORRELATION OF LOCATION OF BEGINNING OF PRESSURE INTERACTION REGION IN TERMS OF KNOWN PARAMETERS



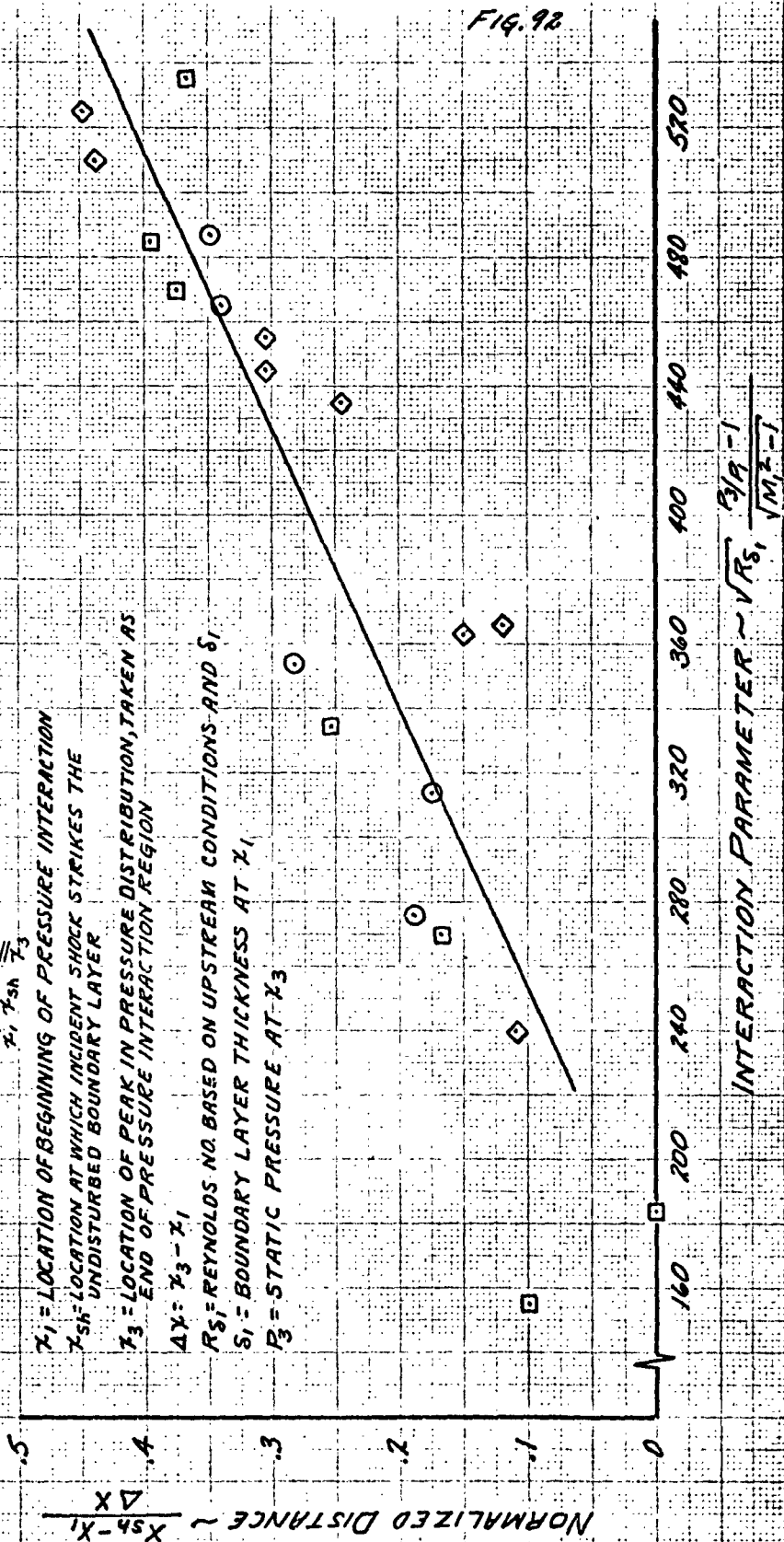
x_1 = LOCATION OF BEGINNING OF PRESSURE INTERACTION
 x_{sh} = LOCATION AT WHICH INCIDENT SHOCK STRIKES THE UNDISTURBED BOUNDARY LAYER
 x_3 = LOCATION OF PEAK IN PRESSURE DISTRIBUTION, TAKEN AS END OF PRESSURE INTERACTION REGION

$$\Delta x = x_3 - x_1$$

Re_s = REYNOLDS NO. BASED ON UPSTREAM CONDITIONS AND δ_1

δ_1 = BOUNDARY LAYER THICKNESS AT x_1

P_3 = STATIC PRESSURE AT x_3



PREPARED BY:

NORTH AMERICAN AVIATION, INC.

PAGE NO. 161 OF

CHECKED BY:

REPORT NO. NA 62H-795

DATE:

MODEL NO.

FIG. 93

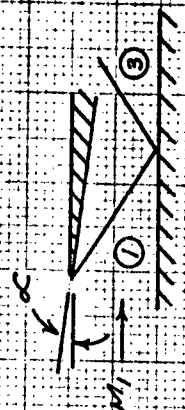
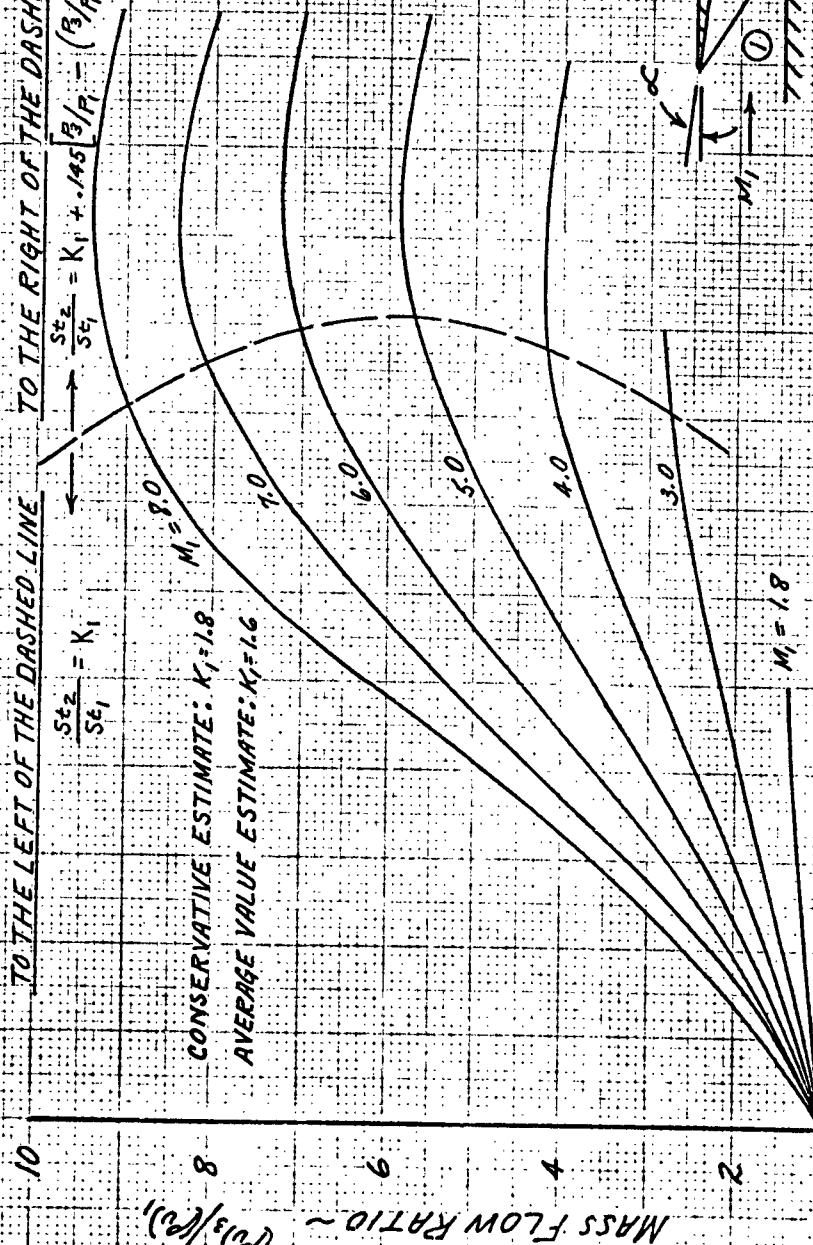
INVISCID MASS FLOW RATIO ACROSS A REFLECTED SHOCK

IN THE DESIGN PROCEDURE THE PEAK STANTON NO. RATIO IS:

TO THE LEFT OF THE DASHED LINE TO THE RIGHT OF THE DASHED LINE

$$\frac{St_2}{St_1} = K_1 \quad \frac{St_2}{St_1} = K_1 + .145 \left[\frac{B}{R} - \left(\frac{B}{R} \right)_B \right] \cdot \left(\frac{P_3}{P_1} \right)$$

AT A GIVEN MACH NO. CORRESPONDS TO THE INTERSECTION OF THE SOLID AND DASHED LINES



INITIAL FLOW DEFLECTION ANGLE $\sim \alpha \sim \text{DEG}$

PREPARED BY:	NORTH AMERICAN AVIATION, INC. COLUMBUS DIVISION	PAGE NO. 162 OF
CHECKED BY:		REPORT NO. NA 62H-795
DATE:		MODEL NO.

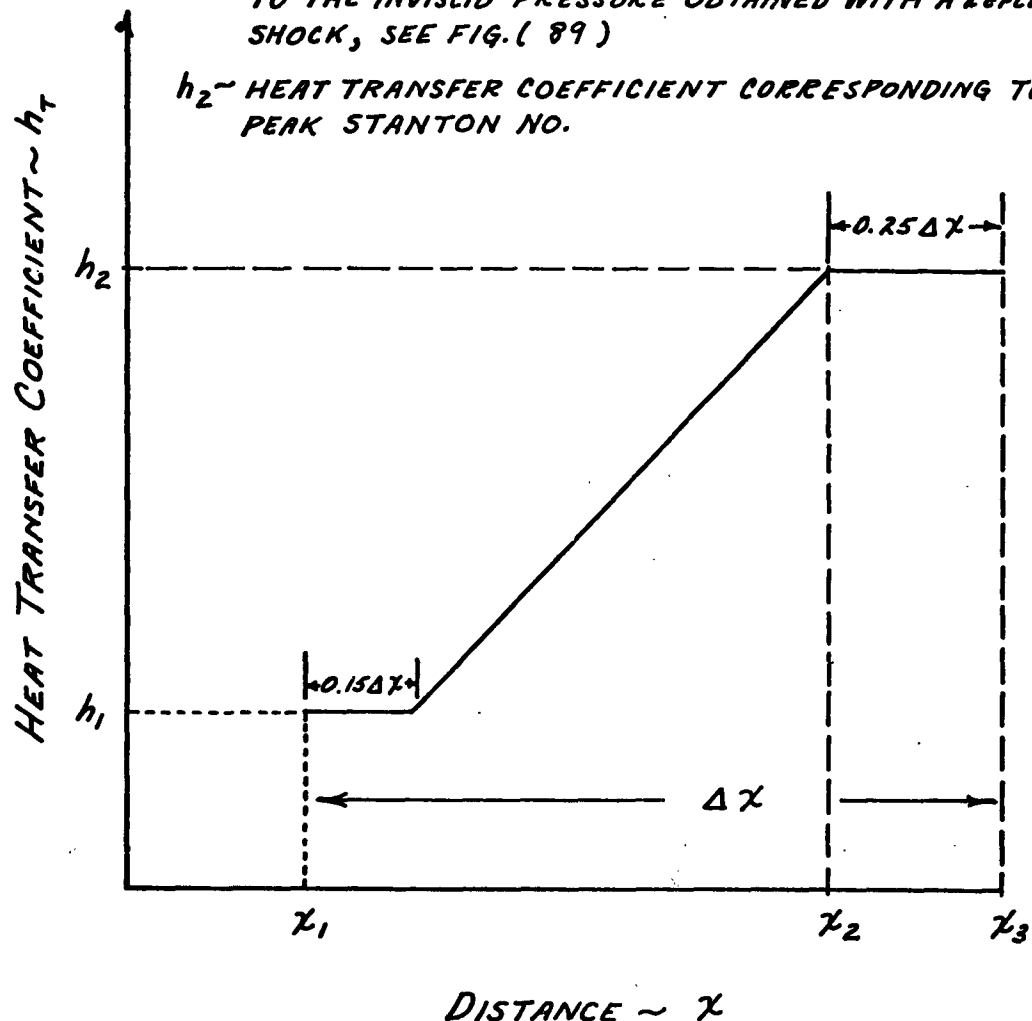
FIG. 94

DISTRIBUTION OF HEAT TRANSFER COEFFICIENT EMPLOYED IN DESIGN PROCEDURE

χ_1 ~ STATION AT WHICH PRESSURE INTERACTION BEGINS

χ_3 ~ DOWNSTREAM END OF PRESSURE INTERACTION, PRESSURE AT AND DOWNSTREAM OF THIS STATION IS ASSUMED EQUAL TO THE INVISCID PRESSURE OBTAINED WITH A REFLECTED SHOCK, SEE FIG. (89)

h_2 ~ HEAT TRANSFER COEFFICIENT CORRESPONDING TO PEAK STANTON NO.



PREPARED BY:

NORTH AMERICAN AVIATION, INC.

PAGE NO. 163 OF

CHECKED BY:

REPORT NO. NA 62H-795

DATE:

MODEL NO.

FIG. 95

SUGGESTED VARIATION IN STANTON NUMBER DOWNSTREAM OF END OF PRESSURE INTERACTION

x_1 ~ STATION AT WHICH PRESSURE INTERACTION BEGINS

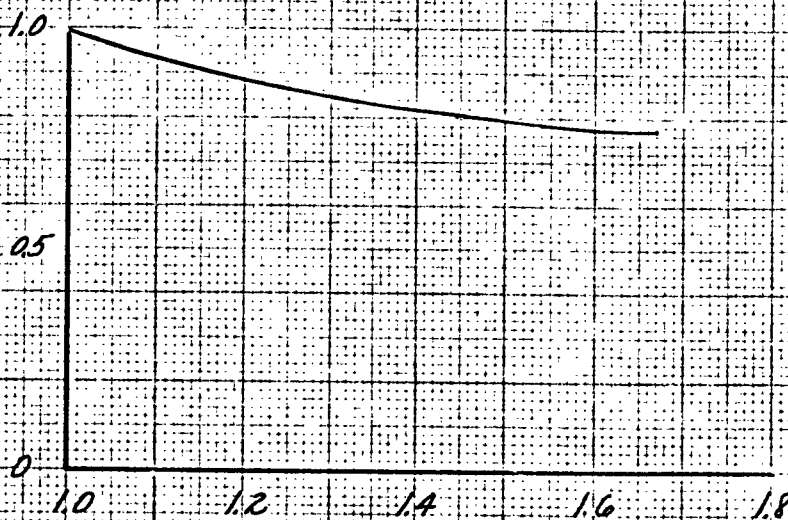
x_3 ~ DOWNSTREAM END OF PRESSURE INTERACTION

$\Delta x \sim x_3 - x_1$

St_2 ~ PEAK STANTON NO.

St_e ~ LOCAL STANTON NO. DOWNSTREAM OF x_3

LOCAL STANTON NUMBER
 RATIO ~ St_e / St_2



DIMENSIONLESS DISTANCE ~ $\frac{x - x_1}{\Delta x}$, $x > x_3$

PREPARED BY:	NORTH AMERICAN AVIATION, INC.	PAGE NO. 164 OF
CHECKED BY:		REPORT NO. NA 62H-795
DATE:		MODEL NO.

COMPARISON OF EXPERIMENTAL HEAT TRANSFER COEFFICIENT DISTRIBUTION WITH THAT CALCULATED ACCORDING TO THE DESIGN PROCEDURE

